

International Journal on Advances in Networks and Services



The *International Journal on Advances in Networks and Services* is Published by IARIA.

ISSN: 1942-2644

journals site: <http://www.ariajournals.org>

contact: petre@aria.org

Responsibility for the contents rests upon the authors and not upon IARIA, nor on IARIA volunteers, staff, or contractors.

IARIA is the owner of the publication and of editorial aspects. IARIA reserves the right to update the content for quality improvements.

Abstracting is permitted with credit to the source. Libraries are permitted to photocopy or print, providing the reference is mentioned and that the resulting material is made available at no cost.

Reference should mention:

International Journal on Advances in Networks and Services, issn 1942-2644
vol. 2, no. 2&3, year 2009, http://www.ariajournals.org/networks_and_services/

The copyright for each included paper belongs to the authors. Republishing of same material, by authors or persons or organizations, is not allowed. Reprint rights can be granted by IARIA or by the authors, and must include proper reference.

Reference to an article in the journal is as follows:

<Author list>, "<Article title>"
International Journal on Advances in Networks and Services, issn 1942-2644
vol. 2, no. 2&3, year 2009,<start page>:<end page> , http://www.ariajournals.org/networks_and_services/

IARIA journals are made available for free, proving the appropriate references are made when their content is used.

Sponsored by IARIA

www.aria.org

Copyright © 2009 IARIA

Editor-in-Chief

Tibor Gyires, Illinois State University, USA

Editorial Advisory Board

- Jun Bi, Tsinghua University, China
- Mario Freire, University of Beira Interior, Portugal
- Jens Martin Hovem, Norwegian University of Science and Technology, Norway
- Vitaly Klyuev, University of Aizu, Japan
- Noel Crespi, Institut TELECOM SudParis-Evry, France

Networking

- Adrian Andronache, University of Luxembourg, Luxembourg
- Robert Bestak, Czech Technical University in Prague, Czech Republic
- Jun Bi, Tsinghua University, China
- Tibor Gyires, Illinois State University, USA
- Go-Hasegawa, Osaka University, Japan
- Dan Komosny, Brno University of Technology, Czech Republic
- Birger Lantow, University of Rostock, Germany
- Pascal Lorenz, University of Haute Alsace, France
- Iwona Pozniak-Koszalka, Wroclaw University of Technology, Poland
- Yingzhen Qu, Cisco Systems, Inc., USA
- Karim Mohammed Rezaul, Centre for Applied Internet Research (CAIR) / University of Wales, UK
- Thomas C. Schmidt, HAW Hamburg, Germany
- Hans Scholten, University of Twente – Enschede, The Netherlands

Networks and Services

- Claude Chaudet, ENST, France
- Michel Diaz, LAAS, France
- Geoffrey Fox, Indiana University, USA
- Francisco Javier Sanchez, Administrador de Infraestructuras Ferroviarias (ADIF), Spain
- Bernhard Neumair, University of Gottingen, Germany
- Gerard Parr, University of Ulster in Northern Ireland, UK
- Maurizio Pignolo, ITALTEL, Italy
- Carlos Becker Westphall, Federal University of Santa Catarina, Brazil
- Feng Xia, Dalian University of Technology, China

Internet and Web Services

- Thomas Michael Bohnert, SAP Research, Switzerland
- Serge Chaumette, LaBRI, University Bordeaux 1, France
- Dickson K.W. Chiu, Dickson Computer Systems, Hong Kong
- Matthias Ehmann, University of Bayreuth, Germany
- Christian Emig, University of Karlsruhe, Germany
- Geoffrey Fox, Indiana University, USA
- Mario Freire, University of Beira Interior, Portugal
- Thomas Y Kwok, IBM T.J. Watson Research Center, USA
- Zoubir Mammeri, IRIT – Toulouse, France
- Bertrand Mathieu, Orange-ftgroup, France
- Mihhail Matskin, NTNU, Norway
- Guadalupe Ortiz Bellot, University of Extremadura Spain
- Dumitru Roman, STI, Austria
- Monika Solanki, Imperial College London, UK
- Vladimir Stantchev, Berlin Institute of Technology, Germany
- Pierre F. Tiako, Langston University, USA
- Weiliang Zhao, Macquarie University, Australia

Wireless and Mobile Communications

- Habib M. Ammari, Hofstra University - Hempstead, USA
- Thomas Michael Bohnert, SAP Research, Switzerland
- David Boyle, University of Limerick, Ireland
- Xiang Gui, Massey University-Palmerston North, New Zealand
- Qilian Liang, University of Texas at Arlington, USA
- Yves Louet, SUPELEC, France
- David Lozano, Telefonica Investigacion y Desarrollo (R&D), Spain
- D. Manivannan (Mani), University of Kentucky - Lexington, USA
- Jyrki Penttinen, Nokia Siemens Networks - Madrid, Spain / Helsinki University of Technology, Finland
- Radu Stoleru, Texas A&M University, USA
- Jose Villalon, University of Castilla La Mancha, Spain
- Natalija Vlajic, York University, Canada
- Xinbing Wang, Shanghai Jiaotong University, China
- Qishi Wu, University of Memphis, USA
- Ossama Younis, Telcordia Technologies, USA

Sensors

- Saied Abedi, Fujitsu Laboratories of Europe LTD. (FLE)-Middlesex, UK
- Habib M. Ammari, Hofstra University, USA
- Steven Corroy, University of Aachen, Germany
- Zhen Liu, Nokia Research – Palo Alto, USA

- Winston KG Seah, Institute for Infocomm Research (Member of A*STAR), Singapore
- Peter Soreanu, Braude College of Engineering - Karmiel, Israel
- Masashi Sugano, Osaka Prefecture University, Japan
- Athanasios Vasilakos, University of Western Macedonia, Greece
- You-Chiun Wang, National Chiao-Tung University, Taiwan
- Hongyi Wu, University of Louisiana at Lafayette, USA
- Dongfang Yang, National Research Council Canada – London, Canada

Underwater Technologies

- Miguel Ardid Ramirez, Polytechnic University of Valencia, Spain
- Fernando Boronat, Integrated Management Coastal Research Institute, Spain
- Mari Carmen Domingo, Technical University of Catalonia - Barcelona, Spain
- Jens Martin Hovem, Norwegian University of Science and Technology, Norway

Energy Optimization

- Huei-Wen Ferng, National Taiwan University of Science and Technology - Taipei, Taiwan
- Qilian Liang, University of Texas at Arlington, USA
- Weifa Liang, Australian National University-Canberra, Australia
- Min Song, Old Dominion University, USA

Mesh Networks

- Habib M. Ammari, Hofstra University, USA
- Stefano Avallone, University of Napoli, Italy
- Mathilde Benveniste, Wireless Systems Research/En-aerion, USA
- Andreas J Kassler, Karlstad University, Sweden
- Ilker Korkmaz, Izmir University of Economics, Turkey

Centric Technologies

- Kong Cheng, Telcordia Research, USA
- Vitaly Klyuev, University of Aizu, Japan
- Arun Kumar, IBM, India
- Juong-Sik Lee, Nokia Research Center, USA
- Josef Noll, ConnectedLife@UNIK / UiO- Kjeller, Norway
- Willy Picard, The Poznan University of Economics, Poland
- Roman Y. Shtykh, Waseda University, Japan
- Weilian Su, Naval Postgraduate School - Monterey, USA

Multimedia

- Laszlo Boszormenyi, Klagenfurt University, Austria
- Dumitru Dan Burdescu, University of Craiova, Romania
- Noel Crespi, Institut TELECOM SudParis-Evry, France
- Mislav Grgic, University of Zagreb, Croatia

- Hermann Hellwagner, Klagenfurt University, Austria
- Polychronis Koutsakis, McMaster University, Canada
- Atsushi Koike, KDDI R&D Labs, Japan
- Chung-Sheng Li, IBM Thomas J. Watson Research Center, USA
- Parag S. Mogre, Technische Universität Darmstadt, Germany
- Eric Pardede, La Trobe University, Australia
- Justin Zhan, Carnegie Mellon University, USA

Additional reviews by:

- Yongning Tang, Illinois State University, USA

Foreword

The papers selected for publication in this volume represent a wide spectrum of networking and network services research. The papers range from the presentation of theoretical problems to the description of the implementation of test beds. The papers represent research results in the areas of quality of video transmissions, quality of service in voice over IP, radio resource management, validation of integrated end to end Quality of Service (QoS) management system, and diffusion approximation modeling applied to investigate the behavior of priority queues.

The current trends in the development and convergence of wireless Internet applications and mobile systems are seen as the next step in the mobile wireless broadband evolution. The use of multimedia streaming services and applications across different, converging wireless transmission technologies are becoming more and more prevalent. The quality of streaming video is very much dependent on the attributes of the content. The primary goal of the paper "Video Quality Assessment as Impacted by Video Content over Wireless Networks" is to assess video quality for all content types as affected by the QoS parameters both in the application and network layer. The authors classify video sequences into groups representing different content types. Using cluster analysis they investigate the impact of packet loss on video content in order to find the threshold in terms of upper, medium, and lower quality boundaries at which users' perception of service quality is acceptable. The paper also identifies the minimum "send bit rate" to meet QoS requirements for the different content types. Overall, the paper can help optimizing bandwidth allocation for specific content in content delivery networks.

The paper "Dynamic Adaptation of Quality of Service for VoIP Communications" proposes an adaptive QoS strategy to solve the problem of momentary drop of voice quality and improve the overall quality of service. The authors provide three different approaches to achieve higher quality in voice communications. The first two approaches change the codec and the transport protocol in real-time during a conversation; the third one applies a Forward Error Correction mechanism to recover from loss packets. Simulation results demonstrate that the proposed solutions significantly increase the voice quality of VoIP communication.

A novel IPTV channel switching technique is presented in the paper "Enhancement of channel switching scenario and IGMPv3 Protocol Implementation in Multicast IPTV Networks." Unlike the standard approach used to switch between two channels, the recommended solution consists of sending an IGMP-Join message for the requested channel before leaving the currently watched channel by sending an IGMP-Leave message. It is demonstrated through measurements and simulation that if channels overlap during the switching process, the proposed solution increases the maximum number of the requested channels at least by eight percent and can also reduce the blackout time during the channel surfing.

The potential of advanced multiuser packet scheduling algorithms in OFDMA type radio systems is analyzed in the paper "Efficient Packet Scheduling Schemes with Built-in Fairness Control for Multiantenna Packet Radio Systems." The authors propose a new multistream, proportional fair scheduler metric covering time-, frequency- and spatial domains. The metric takes into account both the instantaneous channel qualities (CQI's) as well as resource allocation fairness. The

achieved throughput of the proposed metric is evaluated through extensive radio system simulations.

Today's real time multimedia services raise new challenges for networks regarding the QoS control in order to ensure the proper delivery of the services from content provider to content consumer. The creation of an integrated management system is needed to manage the high level services with end to end QoS guarantees while preserving the independency of each network domain to be administrated autonomously. An integrated end to end QoS management system has been designed, implemented, and validated in the framework of the European ENTHRONE project. In the paper "SLS management validation for end to end QoS management in a multidomain test-bed environment" the authors present the implementation and infrastructure of a complex, multiple domain test-bed developed at the Polytechnic University of Bucharest based on the ENTHRONE architecture.

The paper "Diffusion Approximation Models for Transient States and their Application to Priority Queues" presents a diffusion approximation model applied to investigate the behavior of priority queues. The model may be applied in performance evaluation of mechanisms to differentiate QoS in IP routers, WiMAX, metro networks, etc.

A policy based vertical handover controller system for heterogeneous multi-access environments is proposed in the paper "The VERHO Mobility Management System for Heterogeneous Network Environments." The paper presents the VERHO architecture and discusses its possible benefits in 4th generation mobile communication systems.

The paper "Function Modulation – the Theory for Green Modem" considers the bandwidth of a digital communication channel a valuable natural resource. The authors stress that it is important to design digital modems that can minimize the use of this resource. The paper presents a new modulation scheme that satisfies the Shannon's model and can help to save bandwidth by creating a green modem. It is also stated that existing modulation methods based on sinusoidal functions do not meet the requirements of the Shannon's model and therefore have lower capacity for a given bandwidth.

We hope that the current volume will highlight recent research achievements for the readers and present both practical and theoretical perspectives of issues related to the networking research. We would like to thank the authors for their quality submissions, and the reviewers for devoting their time and effort that made the publishing of this issue possible. We are also grateful to Professor Petre Dini for his time and continual coordination between the authors and reviewers.

Tibor Gyires, Editor-in-Chief

CONTENTS

The VERHO Mobility Management System for Heterogeneous Network Environments	110 - 120
Tapio Väärämäki, Department of Mathematical Information Technology, University of Jyväskylä, Finland	
Function Modulation - the Theory for Green Modem	121 - 143
Subhendu Das, CCSI, California, USA Nirode Mohanty, Fellow-IEEE, CCSI, California, USA Avtar Singh, San Jose State University, California, USA	
Video Quality Assessment as Impacted by Video Content over Wireless Networks	144 - 154
Asiya Khan, School of Computing, Communications and Electronics, University of Plymouth, UK Lingfen Sun, School of Computing, Communications and Electronics, University of Plymouth, UK Emmanuel Ifeakor, School of Computing, Communications and Electronics, University of Plymouth, UK	
Dynamic Adaptation of Quality of Service for VoIP Communications	155 - 166
Nelson Costa, Instituto Superior Técnico Lisbon, Portugal Mário Serafim Nunes, IST, INESC-ID, Portugal	
Enhancement of channel switching scenario and IGMPv3 Protocol Implementation in Multicast IPTV Networks	167 - 181
Benoit Hilt, Université de Haute Alsace, France Mounir Sarni, Vialis & Université de Haute Alsace, France Pascal Lorenz, Université de Haute Alsace, France	
Efficient Packet Scheduling Schemes with Built-in Fairness Control for Multiantenna Packet Radio Systems	182 - 194
Stanislav Nonchev, Tampere University of Technology, Finland Mikko Valkama, Tampere University of Technology, Finland	
SLS Management Validation for End to End QoS Management in a Multidomain Testbed Environment	195 - 204
Serban Georgica Obreja, University Politehnica Bucharest, Romania Eugen Borcoci, University Politehnica Bucharest, Romania Radu Lupu, University Politehnica Bucharest, Romania Silviu Ciocina, University Politehnica Bucharest, Romania	
Diffusion Approximation Models for Transient States and their Application to Priority	205 - 217

Queues

Tadeusz Czachórski, IITIS PAN, Polish Academy of Sciences, Poland

Tomasz Nycz, Centrum Komputerowe, Politechnika Slaska, Poland

Ferhan Pekergin, LIPN, Université Paris-Nord, France

The VERHO Mobility Management System for Heterogeneous Network Environments

Tapio Väärämäki

Department of Mathematical Information Technology
University of Jyväskylä
Jyväskylä, Finland

Abstract— In this paper we present our solution for intelligent network interface selection and (vertical) handover control for heterogeneous multi-access environments. The 4th generation mobile communication system is seen here as a combination of several access technologies optimized for different purposes. A combination of these access technologies can constitute, with intelligent control, a 4G access with capabilities to support various application and user requirements and preferences. A policy based vertical handover controller system, called VERHO, utilizes input from several cross-layer sources, the Mobile IPv6 protocol and network interface selection to achieve both proactive and intelligent vertical handovers between a variety of access interfaces. Real-time link status information, access point scanning support, user profiles, policies and Multiple Attribute Decision Making algorithms provide flexibility in interface selection and result in an Always-Best-Connected access for the user. We present the VERHO architecture, discussing and showing the possible benefits of the system for the future.

Index Terms — Multihoming, Wireless, Heterogeneous, Interface Selection, 802.21, Media Independent Handover

1 INTRODUCTION

In the last few years the number of mobile devices, as well as access technologies, have increased and this tendency is expected to continue. The number of cellular subscribers has increased exponentially since the beginning of the 1990's, and even more accelerated growth is expected with the advent of 3rd generations networks (3G). Also, the development of mobile devices is now leading us to a direction where we can have multiple access interfaces on a single device enabling a variety of network services. Even today, advanced cellular phones can support multiple access technologies in addition to traditional cellular ones, e.g. Wi-Fi, and Bluetooth.

The deployment of current wireless technologies is rapid and on-going. The properties of wireless technologies differ in several attributes. The access technologies can be divided into Wireless Wide Area Networks (WWAN), Wireless Local Area Networks (WLAN) and Wireless Personal Area Networks (WPAN), mainly according to their offered

coverage area. In [1] the authors introduce the term *wireless overlay networks*, which reflects the fact that several access technologies will co-exist in the future and their coverage area will overlap. The term *overlay* refers to overlapping networks, where WWAN, WLAN and WPAN networks constitute the different layers of access technologies. Also, the access technologies will have different characteristics related to several technology-specific parameters, such as Quality-of-Service (e.g. delay, jitter), bandwidth, coverage area, cost, power consumption and security [2].

In considering several of the technology parameters and users and applications with different needs and requirements, it is generally thought that no access technology will or even can be superior to other technologies. Due to their partly conflicting characteristics, as well as physical restrictions, maintenance, deployment costs, etc. none of the access technologies meet all the demands of modern communication. On the contrary, access technologies of different characteristics are converging into one heterogeneous, but ubiquitous access network, where different access technologies with different parameters complement each other. We refer to these kinds of networks as 4th generation networks (4G).

1.1. Fourth generation communication system

A fourth generation communication system can be thought of as a combination of network technologies with different characteristics. References [3] and [4] discuss related visions and research challenges. The key features of 4G networks are

- High usability – access anywhere, anytime and with any technology
- Support for multimedia services at low cost - access and communication speed
- Personalization – Always-Best-Connected concept
- Integrated services – Quality of Service 4G networks will be entirely packet based.

For this reason, the core networks (CN) of cellular systems are evolving into packet switched networks based on the Internet Protocol (IP). IP is generally thought of being the integration layer for all the access technologies and applications [4]. The term All-IP (i.e. Native IP) refers to the integrating nature of the Internet Protocol [5]. Also, with the success of Voice over IP (VoIP) technologies, voice

communication is evolving towards IP connectivity, and Session Initiation Protocol (SIP) is seen as the most likely enabling technology. Every kind of content has to be accessible with good quality (or diverse set of qualities) and at a reasonable cost anywhere, anytime and with any technology, without compromising service security.

The vision discussed above creates many research challenges. Here we focus mainly on the above 3rd layer challenges, link technology specific technology challenges (such as adaptive coding/modulation, multiple antenna technologies) being out of scope. For example, [3] divides the research challenges into mobile station, system and service categories.

Terminals need to be capable of discovering different wireless systems by scanning. Traditional technology specific (Layer 2) scanning techniques might not be enough for selecting the best usable link at each point in time. The decision of the best link is dependent on many parameters, but taking into account multiple different parameters can render the decision making complex. Thus the question arises: What is the sufficient level of complexity to come up with optimal decisions? The aim is towards Always-Best-Connected (ABC) access [6]. Reference [7] discusses different enabling technologies, such as different protocol stack enhancements, mobility support and End-to-End QoS support, to provide ABC.

From the system point of view, efficient mobility and location management of mobile devices is important. Mobile IPv6 [8] is quite successful in trying to solve this problem, but the handover processes cause an increase in system load, high handover latency and packet losses, and require some improvements. Also, heterogeneous networks induce some additional problems related to interface selection and simultaneous access. Moving networks (NEMO) create some additional research challenges to mobility management protocols. To provide End-to-End Quality-of-Service (QoS) requires access technology independent QoS procedures. Basically IP or higher layer QoS architectures (e.g. differentiated or integrated services) or possibly mapping procedures with different QoS mechanisms [7] are needed. Security and privacy solutions need to be flexible due to various technologies and devices (varied capabilities, processing powers, security needs, etc) in use. Technology dependent solutions might not be the most suitable ones, but some upper layer solutions could be feasible. Single sign-on to the network is needed. At system level, also fault tolerance must be solved (e.g. hierarchical system or overlapping network) to provide users sufficient QoS [3].

In the future a consumer is no more dependent on any single provider, thus he/she might be a customer to several of them, possibly using their services simultaneously. For these new business architectures, accounting procedures and accounting data maintenance is needed. For the operator, new ways of gathering the surplus is needed because of the increasing usage of unlicensed networks. New challenges include also an open access model, where a municipal

network is seen as a part of the general infrastructure and is built without a profit making operator [21]. Service based approaches seem to be the current view. Traditional billing systems (technology and transaction dependent) might go out of fashion altogether. In this paper we concentrate on technical issues related to mobility management with interface selection in heterogeneous environments. Even though we do not depend on Mobile IPv6, we consider it to be the most likely choice for forming the foundation for IP mobility management.

There exist several related projects, both within and outside the standardization bodies, which study the field of IP mobility management to fulfill the needs of users and applications in upcoming heterogeneous wireless environments.

1.2. Related research

Internet Engineering Task Force (IETF) standardized the Mobile IPv6 (MIPv6) protocol in its Mobility for IPv6 (mip6) charter, in June 2004. Since then, several other charters have been working on enhancing the MIPv6 functionality, with performance, reliability, multihoming, etc. in mind. For example

- MIPv6 signaling and Handoff Optimization (mipshop),
- Mobility EXTensions (MEXT) [18] working group for IPv6. Among others, it includes multihoming and firewall issues, mobile node (MN) bootstrapping with Authentication, Authorization & Accounting (AAA) and IPv4-IPv6 dual stack solutions,
- Proxy Mobile IPv6 (PMIP) [19] for network based mobility management,
- Shim6 [20] is a network layer approach for providing the split of locator/identifier of the IP address, so that multihoming can be provided for IPv6 with transport-layer survivability

The Institute of Electrical and Electronics Engineers (IEEE) 802 working groups have traditionally focused on different access technologies, but in IEEE 802.21 [9] the researchers have worked on Media Independent Handover (MIH) services focusing not only on one specific access technology but on handovers and interoperability between different access technologies, including both 802 and non-802. It is introduced in more detail in Section 3.

In [10, 11, 12] the authors of these papers present policy-based interface selection procedures and architectures to support multiple access interfaces. They aim to provide mechanisms to make dynamic interface selection decisions.

1.3. Problem statement

Mobile IPv6 [8] handles the IP mobility management in an application transparent way. The applications are unaware of the links in use and about possible handovers taking place. The application flows (and possible transport layer

connections) do not break even though the MN is moving between IP subnets. But the procedures related to the handovers result in a period of time when the MN cannot send nor receive data. This handover (or handoff) delay time causes packet loss and possibly packet retransmissions (in case of reliable transport protocols). The objective is to minimize the delay to offer the applications seamless connections in addition to non-breaking ones.

In case where the MN has multiple active interfaces (and links), one has to choose which interface to use. Pure MIPv6 implementations usually have some static priority for each interface, and the interface with the biggest priority is chosen for use. However, static priority based interface selection may not be sufficient for users with different preferences nor for applications with different demands in heterogeneous environments [13].

The objective is to find ways to provide Always-Best-Connected access for different users with a minimum user intervention.

1.4. Paper outline

In Section 1 we presented previous and on-going research work related to the challenges of 4G systems. Section 2 presents the VERHO system architecture. Section 3 amends the VERHO system with the IEEE 802.21 standard, and Section 4 introduces two prototype applications that can benefit from VERHO's knowledge of the link and handover information. Section 5 discusses the VERHO architecture and its benefits in a heterogeneous environment. Section 6 concludes the paper and presents some ideas for future work.

2 VERHO CONTROLLED MOBILITY

2.1. Overview

The VERHO system is designed to manage available interfaces, links and access points in a multi-interfaced mobile IP-networked device. Basically, the system gathers information about available interfaces (link types, access points, etc.), decides dynamically during run-time about how the interfaces could be utilized best and performs IP handovers using Mobile IPv6.

The system has a cross-layer design, since the goal is to provide link information to interested layers. Figure 1 shows which layers VERHO interacts with.

- Link Information Provider (LIP) extracts link information from network interfaces (Link Layer),
- Link Access Controller (LAC) gets information from LIP and controls MIPv6 handovers (Network Layer),
- Applications can utilize information provided by LIP and LAC (Application Layer),
- Users can set their profiles through a Graphical User Interface (GUI) and see some statistics from the underlying system.

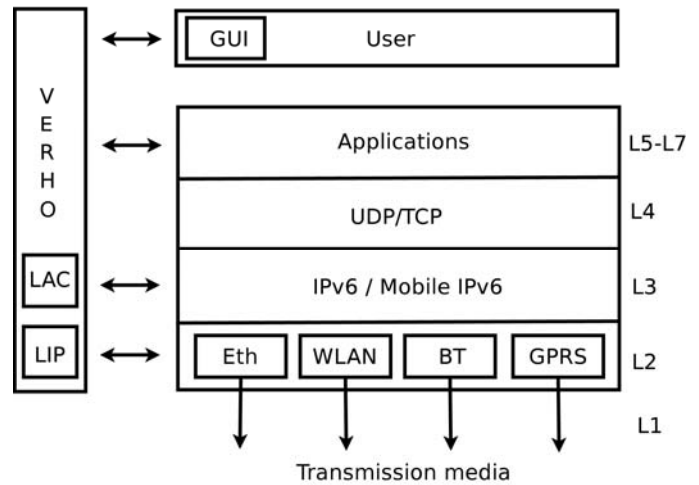


Figure 1. VERHO cross-layer interaction

2.2. System architecture

The system consists of several modules, each with a dedicated purpose. The following chapters revisit all of them. Figure 2 shows a high level overview of the architecture. The components communicate with each other over Desktop Bus (D-BUS). D-BUS is a messaging bus mainly for local inter-process communication (IPC) and remote procedure call (RPC) on a single host.

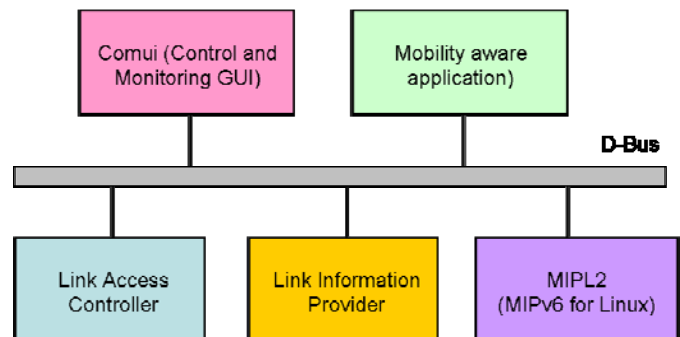


Figure 2. VERHO D-Bus architecture

The core VERHO system consists of the Link Information Provider (LIP) and the Link Access Controller (LAC). The task of LIP is to keep an up-to-date information database about the available links and provide some control functions (e.g. connecting to Access Points). LAC gathers link information from LIP and makes decisions regarding the usage of available links; moreover, it controls Mobile IPv6 when IP layer handovers are needed to be accomplished.

The system has a GUI for controlling and monitoring purposes and it uses D-BUS to get link information from LIP and to control the system via LAC. Just like the GUI, other applications can utilize the features of LIP and LAC. For example, all of the developed mobility aware demonstration applications use LIP and LAC over D-BUS.

From a more technical point of view, the whole system is implemented in a Linux environment. Mobile IPv6 for Linux v2 (MIPL2) is used as the MIPv6 implementation with some D-BUS interface additions. The whole system is developed in user space. The GUI and the demonstration applications are

written using GIMP Toolkit, G-Streamer, and Java Media Framework.

2.3. Link Information Provider

The task of LIP is to extract information about the available network interfaces and links [15]. This information is then made available over D-BUS for consumption. LIP consists of two main parts, the Link Module (LM) and the Access Point Module (APM). Figure 3 shows a high level architecture overview of LIP.

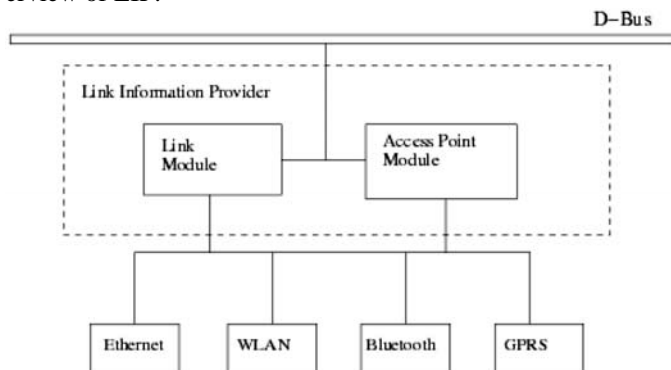


Figure. 3. High level LIP architecture

2.3.1. The Link Module

LM extracts information from interfaces. It supports IEEE 802.11 WLAN, Bluetooth, General Packet Radio Service (GPRS) / Universal Mobile Telecommunication System (UMTS) and wired IEEE 802.3 Ethernet interfaces. Each technology is managed by a separate technology-specific submodule and these submodules export a common interface. In this way it is easy to extend the system with new access technologies.

Link information is provided by two means. Whenever an event takes place in a monitored interface that the LM is capable of listening to or when a new interface appears, a signal is sent over D-BUS carrying the new link information. Also, consumers can ask LIP (using RMI over D-BUS) for information about a specific interface or about all the interfaces.

The information provided by each access technology is quite heterogeneous. Even if the same information can be extracted from two different technologies, conversion to a common dimension may be necessary. For this reason LM, in addition to providing raw link information, provides unified link information for link parameters whenever that makes sense. Table I shows some of the link parameters that are unified by LM. The Parameter Name column shows the name of the parameter after unification.

Signal Strength is somewhat special among the information provided by LM. Its value is the source for the Link Going Down and Link Coming Up indications.

Signal Strength dimension value is a dynamically calculated unified value. For WLAN it originates from Signal to Noise Ratio (SNR), for Bluetooth from Link Quality and for GPRS from Signal Quality. Its range is from 1 to 5 and is calculated by dividing the technology specific value (e.g. SNR in the

TABLE I
UNIFIED LINK PARAMETERS

Parameter name	Dimension
Signal Strength	Integer value between 1 and 5
Tx Power level	Converted to dBm
Bitrate	Converted to kbps

case of WLAN) into five ranges using hysteresis. For more specific information on the classification of the signal quality, refer to [15].

Besides providing information, LM helps consumers by indicating the actual cause of the signaling of link information. Some of these indications can be seen in Table II.

2.3.2. The AP Module

The AP Module (APM) provides information and controlling facilities for Access Point management. It supports

TABLE II
LIP LINK INFO INDICATIONS

Indication	Description
Common	
NewIface	A new interface or interface change
Dellface	Interface disappeared (i.e. removed from the computer)
NewLink	Link established on interface
DelLink	Link deleted on interface
IfUp	Interface administratively enabled
IfDown	Interface administratively disabled
LinkComingUp	The link on the interface is becoming available
LinkGoingDown	The link on the interface is becoming unavailable
ChgIfName	Interface name changed
ChgTPL	Tx power level changed
ChgSigStr	Signal strength changed
ChgBitrate	Bitrate changed
ChgRMAC	Remote MAC changed (i.e. AP change)
WLAN	
ChgWLANName	WLAN name of interface changed
ChgSNR	SNR changed
ChgEnc	Encryption got enabled or disabled
ChgESSID	ESSID changed
Bluetooth	
ChgDevID	Device ID changed
ChgLQ	Link Quality changed
GPRS	
ChgSQ	Signal quality changed
ChgBER	Bit error rate changed
ChgPC	Power consumption changed

802.11 WLAN, Bluetooth and GPRS/UMTS access technologies. Just like LM, APM supports these access technologies via specific submodules in order to make the

system easily extensible. Also, the technologies to access the link layer are the same as with LIP. AP information is also heterogeneous and varies between access technologies. Table III shows various information provided by APM.

APM manages an AP list for each supported access technology. AP information is sent to consumers in the same two ways as for LM. On events affecting APs, signals are sent to D-BUS about the change. Such changes can be

- New AP appeared
- AP disappeared
- AP state changed

TABLE III
AP INFORMATION

Access technology	AP Information
WLAN	ESSID, MAC addr, channel, bitrate, noise, signal quality
Bluetooth	AP name, MAC addr, Link quality, TX Power level
GPRS	AP name, IP protocol

2.4. Link Access Controller

The logic of the VERHO system resides in the Link Access Controller (LAC). LAC consumes LIP (LM and APM) information and controls MIPv6 handovers. The modifications to the MIPL implementation have been kept at a minimum level to support easy code portability to other implementations and protocols.

LAC manages a single list of all the interfaces. Each interface is assigned a flag and a preference value. The flag can indicate

- The interface state: Enabled or disabled.
- Preference Value calculation: Automatic or Manual.
- Interface state management: Automatic or Manual.

If the interface state is Disabled, the interface is not allowed to be used by MIPv6, i.e., no Care of Address (CoA) on the interface can be registered with the Home Agent (HA) or Corresponding Nodes (CN). By default, LAC manages the interface state automatically, that is, it enables and disables according to specific events (information received from LIP). The interface state can also be managed manually, in which case it is the responsibility of an outside party (e.g. an external application).

Preference values for interfaces are calculated by LAC dynamically and they change due to changing link information. Just like interface state management, preference value calculation can also be managed manually by some outside party, e.g. an operator, for load balancing purposes.

At any point in time, the interface in an Enabled state and with the highest preference value is chosen to be used. In case where there are several available connections with similar properties, a hysteresis or extra interface specific priorities might help in avoiding ping-ponging.

2.4.1. Preference Value Calculation

Preference values are calculated using the Simple Additive Weighting Multiple Attribute Decision Making (MADM) method. This method fits very well for the purpose of choosing among interfaces by taking into account multiple interface characteristics.

LAC uses the unified link information provided by LIP (shown in Table 1) to make its decisions. Each link characteristic is assigned a weight, which describes the importance of the given characteristic. A weight vector consists of a weight for each characteristic and defines a Profile. An outside party can supply or change profiles on-the-fly. Profiles can represent, for example, user demands, in which case the outside party is the user. The controlling interface (see Subsection 2.5) is used to define and activate user profiles.

The weighted average is calculated by Formula 1.

$$pv_i = \frac{\sum_{j=1}^p w_j * r_{i,j}}{\sum_{j=1}^p w_j} \quad (1)$$

pv_i is the preference value of interface i , w_j is the weight of characteristic j , $r_{i,j}$ is the value of characteristic j for interface i . In [16] different multiple attribute decision making algorithms with simulations are analyzed in more detail. MADM methods provided good flexibility due to the possibility of several affecting parameters. We also proposed an algorithm combining MADM algorithms aiming at the shortest distance from the optimal solution.

2.5. Controlling and monitoring GUI

Comui is the controlling and monitoring interface for the VERHO system. It is a graphical interface developed with the GTK+ toolkit and is available for the Linux based Maemo platform. Comui allows users to monitor and control the system and choose how much they want to participate in the link selection decisions. In addition to regular Linux PC, the VERHO prototype is developed for Nokia N770 Internet Tablet running the Linux based Maemo operating system. The screenshots are from the Maemo version.

A screenshot from the main screen can be seen in Figure 4. The user can see a list of different available network devices in the Type column (mobile phone, cable link and WLAN). The E/D column indicates whether the device is enabled or not, and the Rank column shows the calculated ranking value for each network device. Currently WLAN has the highest ranking (Active profile is Prefer Bandwidth) and thus it is the active device.

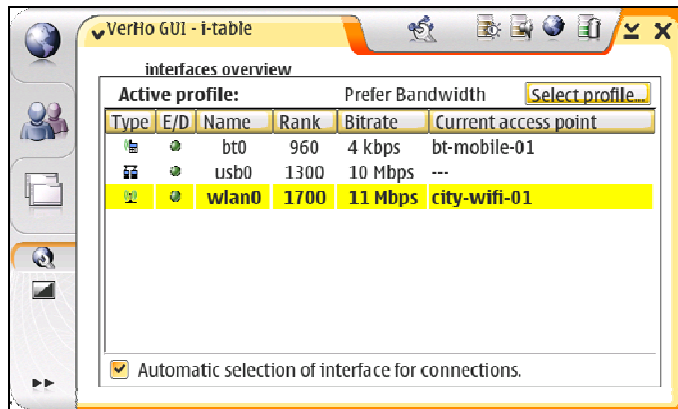


Figure 4. VERHO GUI main screen

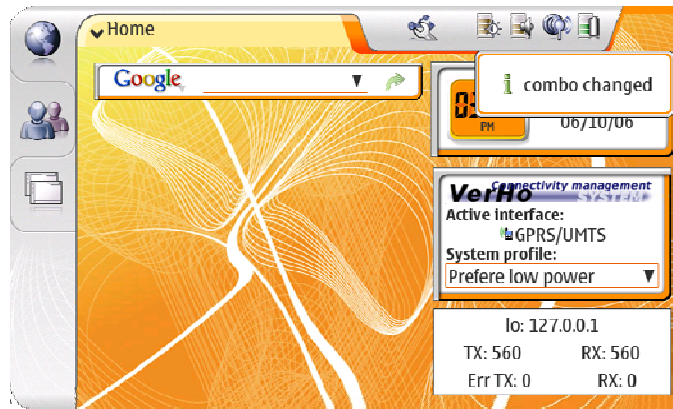


Figure 6. VERHO desktop applet with profile changer

The profile management screen is presented in Figure 5. The user can define different profiles according to his/her needs and preferences. For example, in the situation depicted in Figure 5, the user prefers bandwidth and thus the profile has a high weight and parameters on bitrate, some weight on the signal strength to have a good quality connection and no weight on power consumption.

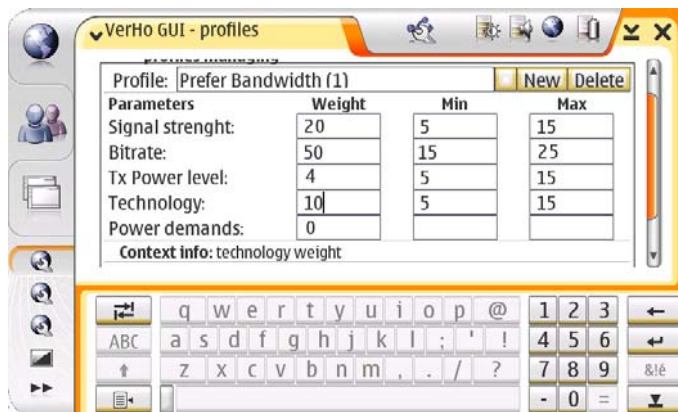


Figure 5. VERHO profile definition screen

Figure 6 shows the desktop applet, where the user can choose the best profile according to current needs. The applet shows also the currently used network interface. The operational principle is similar to mobile phones or laptops, where the user can define sound and battery profiles, e.g. “no sounds” or “beeping” on mobile phones and “maximum performance” or “stretch battery” on laptops.

3 IEEE 802.21 AND INTEGRATION WITH VERHO

3.1. IEEE 802.21 Media Independent Handover overview

The IEEE 802.21 standard introduces a MIH Function, which is located between L2 and upper layers, i.e. IP or MIP. It defines generic SAPs and primitives for both upper and lower layers. The MIH function consists of three services:

The Media Independent Event Service (MIES) signals the state changes of lower layers, the Media Independent Command Service (MICS) provides control for higher layers, and Media Independent Information Service (MIIS) serves information about the current and neighboring access networks. The functionality is introduced in Figure 7.

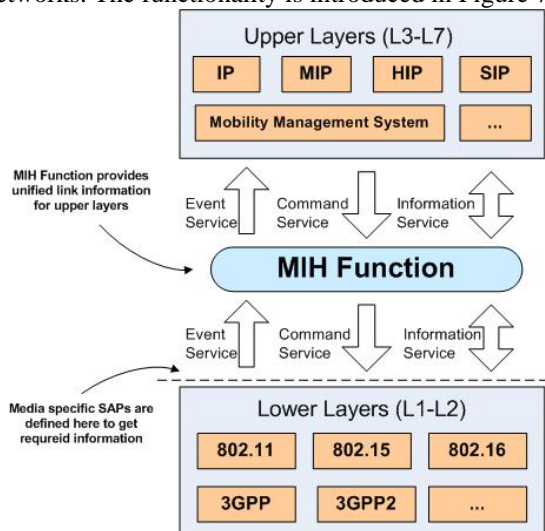


Figure 7. The MIH Function is located Between Layer 2 and Layer 3, defining a so called Layer 2.5.

MIH Function works as a generic link layer instance for upper and lower layers. It makes it possible to transmit unified information from lower layers to upper layers, regardless of the access technology used. To be able to acquire all required information, access technologies must be amended by technology specific Service Access Points (SAP). They are to be defined in IEEE standardization bodies such as 802.11u (SAPs for Wi-Fi) [22] and 802.16g (SAPs for WiMAX) [23] and in 3GPP/2 .

For the mobility management system, MIH Function works as an information unifier which collects information from networks, but does not decide anything. Thus handover policies are out of the scope of the standard, and it requires a mobility management system to work with.

3.2. Integration with the VERHO mobility management system

After following the development of 802.21 for a while, there was a decision to study how an integration of MIH Function and the VERHO system could be implemented. The functionality of MIH Function is pretty much similar to the LIP module, even though there are several advantages MIH Function has.

The biggest challenges regarding link information collecting can be identified to three categories. 1) The amount of information the LIP module collects is limited to a number of parameters supported in each access technology. Also, the provided information is not unified, so the name of parameters and parameter values must be converted to a common scale. Also, all the parameters are not supported in every technology. 2) Currently, scanning is the only way the LIP module can collect the information. Every time that information needs to be collected, the specific access interface must be activated and power intense activities performed. 3) Finally, probably the biggest challenge with LIP is the lack of standardization. It is our own proprietary implementation.

MIH Function can more or less solve the above mentioned challenges and limitations: 1) Standard amendments, i.e. SAPs, for each technology are used to provide unified link layer information. Information is stored in Information Elements (IE) which provide all information that is essential to make intelligent handover decisions. IEs specified in the standard support a wide range of parameters, and there is space reserved for future extensions and vendor specific implementations. 2) The exchange of IEs is based on request and response messages which make the information gathering effective. The mobile node can acquire information from all interesting networks via the active network interface, so there is no need to activate and burden other radios. In terms of power consumption this is extremely important. 3) Obviously the biggest benefit IEEE 802.21 can provide for the VERHO system is a standardized implementation. With a wide support of IEEE 802.21, the VERHO system can focus on decision making and managing the user mobility.

MIH Function is not, however, limited only to network information collecting, but it also provides Command Service for controlling network interfaces. As with information collecting, the benefit is a unified interface between the mobility management system and different network interfaces so that operating system dependent implementations are not needed. Command Service also introduces the possibility of network originated handovers that can be an important feature if there is a need to implement the network controlled or originated mobility management.

The hierarchy and structure of MIH Function and VERHO

is introduced in Figure 8. MIH Function works now as so called Layer 2.5 between network and link layers. VERHO commands network interfaces and gathers network information over MIH Function. By utilizing the collected information, VERHO makes the mobility management decisions on the IP level.

The communication between different MIH Functions (e.g. MIH Function of MN and AP or AP to AP) relies on MIH Protocol which is defined in the standard.

The VERHO system is connected to MIH Function with SAPs which are defined in the standard. In addition to lower layers, VERHO is connected to Application Layer (L7) and the user – as was also done in the LIP implementation shown in Figure 1. The integration of VERHO with MIH Function does not change this part of the architecture, because a user and application interaction with the mobility management system is still needed.

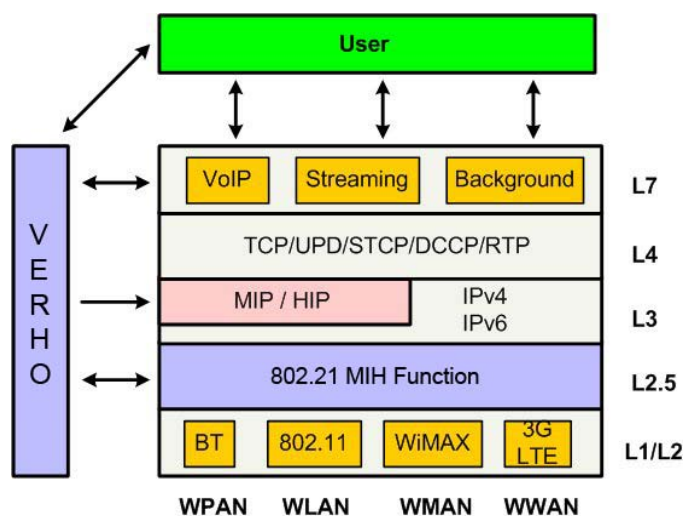


Figure 8. Integration of VERHO and IEEE 802.21 MIH Function

4 PROTOTYPE APPLICATIONS

The VERHO system can be used to develop mobility aware applications. A mobility aware application can use the provided information for example to adapt to the current link characteristics (e.g. a media player). Information provided by VERHO includes

- Link information from LIP (LM),
- Access point information from LIP (APM),
- Handover indications from LAC.

In the following sections we look at some of the prototype mobility aware applications developed within the VERHO project.

4.1. Multimedia streamer

Multimedia Streamer (MS) consists of a client and a server. It supports streaming of images, audio and video. Both the client and the server are written in Java. The client integrates image, audio and video playing functionalities. The server supports audio and video streaming. For the camera stream, a

dedicated webcam acts as the server.

Streaming of multimedia content is done by using Real-time Transport Protocol (RTP) and RTP Control Protocol (RTCP), and Real Time Streaming Protocol (RTSP) is used for controlling the playing process (e.g. requesting the proper stream quality during adaptation).

4.1.1. Adaptation

The player runs on the MN and it is made mobility aware by listening to LIP and LAC information. Information about the active interface is available to the player. The player, based on the capabilities of the active interface, requests proper stream quality from the server. Whenever the player receives information from LIP and LAC, it checks whether the current stream quality is still valid with regards to the active interface. If it is not valid, the player requests the proper quality from the server.

4.1.2. Camera streamer

The camera used for the camera streamer is Axis 2100 and it supports only IPv4 networks. Due to the fact that the VERHO system operates only in IPv6, we needed to develop an IPv6-IPv4 proxy. The proxy is written in Java and its sole purpose is to relay the camera stream between IPv6 and IPv4 realms.

The camera uses HTTP to transfer images and it can transmit motion JPEG and still images in various image qualities. The different image types and qualities are accessible by using CGI requests via HTML GET destined for the web server running on the camera itself. The camera itself served as the streaming server and no separate server code was needed. During adaptation the client requests proper image quality from the camera using CGI and HTML GET method.

4.1.3. Audio streamer

The audio streamer server contains several audio files that can be requested by the client. Each audio file can be delivered with various qualities. During adaptation, the client requests a given quality and the server maps this request to a class and starts streaming the selected video file. During adaptation, the newly selected video file starts streaming from the position where the previous video stream left off.

4.1.4. Video streamer

Unlike the audio streamer, the video streamer server supports pre-defined classes of qualities. A video content is prepared for all the supported classes as a separate video file. When the client requests a specific quality the server maps this request to a class and starts streaming the selected video file. During adaptation, the newly selected video file starts streaming from the position where the previous video stream left off.

4.2. IP-TV

The IP-TV is similar to the Media Streamer. Figure 9 shows

the topology of the client/server model of the IP-TV. We have divided the operations into content, network, access and end-devices. Content providers provide only content with good quality to the customers. Network operators provide the adaptation services as well as digital rights management, etc. Access operators provide accesses to different technologies for the consumers. The VERHO device is just one of the devices consuming the IP-TV services tailored for the device's physical restrictions as well as for its software and access requirements and end users' preferences.

The TV stream is received from a terrestrial digital TV broadcast network. This stream is then made available on an IP network via multicast (one multicast channel per TV channel). In the network a node acts as an Adaptation Proxy (APr). The APr, on joining the multicast IP-TV stream, can provide different MPEG4 quality classes of the TV stream. In addition to adaptation, APr performs the conversion from IPv4 to IPv6 and from multicast to unicast for the clients. Mobile clients request the stream from the APr by indicating their quality requirements, which are provided by VERHO.

When a mobile client needs a different quality (e.g. due to moving to a different access technology), it informs the APr about its new requirements. The APr, upon receiving the request, maps the request of the client to a supported quality class and starts streaming the adapted content to the client.

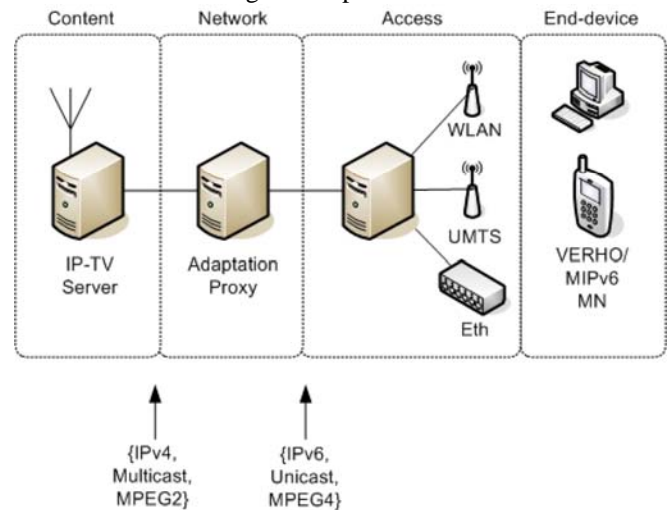


Figure 9. The IP-TV network

5 DISCUSSION

We did not discuss the design principles and benefits of the presented architecture of VERHO in Section 2 and 3. Now we consider some of these and refer to some earlier work. Also mobility management related challenges will be discussed here.

The use of link layer has been researched to some extent in the context of speeding up horizontal handover processes. For example, [17] defines triggers and hints to assist in fast triggering of handovers and proactiveness. In [15] there is a discussion on the use of link layer information in the context of heterogeneous networks with multi-interfaced terminals. Link layer triggers, hints based on signal strength and

parameter unification are considered and their benefits presented. Link layer hints, such as Link-Going-Down, can be utilized to achieve a proactive behavior in the system. Moreover, pure link layer parameters can also be utilized as parameters in the multiple attribute interface and link selection. We can achieve seamless handovers by doing the handovers proactively, partly or entirely, while still connected to the old access router or by utilizing two links simultaneously resulting in soft handovers. The proactive handover preparation allows flexible handover delays. Currently, the handover delay correlates directly with the signalization delays of MIPv6.

Horizontal handovers have been affected traditionally by using signal strength and some hysteresis values. However, this is not suitable for multiple interface management. In [16] there are simulations of various Multiple Attribute Decision Making (MADM) based interface selection algorithms. The benefit of MADM methods is their flexibility due to several affecting parameters. But the intelligence of most of the MADM algorithms lies in the weight assignments. Weights determine how the algorithm utilizes the input parameters in the preference value calculation. This brings a lot of flexibility for users with different preferences for link characteristics. Currently, the weights are specified by user defined profiles, but they can be extended to other sources as well. For example, operators' viewpoint could be provided by introducing their profiles and policies to the interface selection. The weights have always a priority order, so there can never occur a situation where the network interface could not be selected. Also, the lack of some parameters does not prevent decision making, but will just hamper it. The weights can be modified to override the usual behavior, e.g. disable GPRS/UMTS while being abroad. The reader can refer to Figure 5 to see better how the weights are adjusted in the VERHO prototype.

VERHO, with the knowledge of multiple link status and handover timing and targets, can assist other applications as well. VERHO can provide, for example, realtime unified bandwidth information to applications (lets say ranging from 0-10), which can adjust their stream qualities appropriately. Adaptive mobility and link aware applications are seen as one of the research challenges of the 4G networks [4]. For example, LAC can be the source of information for MPEG-21 based adaptive multimedia terminals. The access network technology might also affect some internal states of an application. For example, an application could be designed to avoid fetching new emails when connected to an expensive network, or to sleep when the current network is insecure, etc.

From the perspective of the VERHO system, IEEE 802.21 is a highly welcome standard. It offers much the same functionality as VERHO, but also a significant number of new functionalities. The best performance is achieved by replacing LIP with the 802.21 advanced information framework and utilizing 802.21 Command Service for network interface management. In terms of power consumption, such design provides more feasible and permanent solutions than our

technology dependent scanning mechanisms in LIP. It is extremely power consuming to try to scan network information frequently with all interfaces. However, without being aware of the surrounding networks, also the potential benefits of heterogeneous networking might not be achieved. IEEE 802.21 mechanisms to acquire information about surrounding networks via an active interface are an effective way to implement information collecting. IEEE 802.21 can provide handover candidate information, e.g. neighbor base stations, and it can be even supported with geographical location information. This helps in avoiding ping-ponging between networks as the handovers can be planned better.

The benefits of IEEE 802.21 will be strongly dependent on the scale of the implementation of the standard. If, for example, IEEE would implement 802.21 in 802-technologies, but 3GPP would not use it, the benefits would remain small. The issue is not technical but rather political. The convergence of networks and the development towards Internet based services is leading to a situation where clear boundaries between 3GPP, IETF and IEEE working groups are going to disappear. 3GPP based networks have been considered strictly operator controlled, while the IEEE technologies are merely used for implementation of non-operator controlled networks. This can be seen also in the architecture of technologies from both organizations. Now these two organizations with totally different backgrounds should start to work together to reach the next step in the convergence. Especially for 3GPP the motives might be questionable, because they co-operate with the GSM Association which is ruled by operators. A current business model for the operators is to have the users' traffic in their network while placing charge for it. IEEE 802.21 might lead this development to an opposite direction, depending partially on who will implement the decision making policies. The alluring opportunity for 3GPP in 802.21 might be in traffic sharing with other technologies. For example, the user's traffic could be routed always via a WLAN access point when such is available. Easing the load of cellular networks is necessary, because the current cost structure is too high to support quickly growing amounts of mobile data. However, there are other potential solutions to handle this issue, e.g. femtocell, which would also support the operators' business model better than by directing users to non-operator controlled networks.

An interesting topic in policy development and power management will be multihoming. Increasing the bitrate by improving coding or modulation has brought the performance of new wireless technologies such as WiMAX and LTE near to the limits of the Shannon's law. Combining the capacity of several network interfaces can increase the performance of the terminal. Multihoming can increase the system performance also in terms of reliability when the traffic of critical applications is routed via reliable networks and is secured to use another interface if the current one malfunctions. The obvious con with multihoming is more complex policy creation. The power consumption will increase, but so will the performance. One should point out that VERHO consumes

very little power and resources itself; most of the power consumption originates from the network interfaces and terminal applications. In addition to power consumption, also signaling traffic will increase significantly with multihoming. There is plenty of development work going on in MEXT working group, and promising solutions can be tested thanks to the modular design of VERHO.

Designing the GUI for VERHO poses challenges. The current version allows detailed adjustments of profiles, but for many users the desktop applet alone can be confusing. How does the user know whether he should prefer bandwidth or network reliability? Power consumption and bitrate may be parameters that can be visualized clearly enough by the users, but some other parameters such as network reliability or latency are probably better suited for interaction between applications and QoS mappings. In the GUI design we had usability tests for test subjects, and the results were used to improve the GUI. The tested persons, were, however technology oriented students, so the results cannot be generalized. On the other hand, in this phase we did not want to go further in testing, and results were satisfying for a prototype. The GUI could be improved by providing statistical data information based on a usage history. It might help the users in understanding better the behavior of the device and also in adjusting better the settings to support their preferences.

6 CONCLUSIONS

In this paper we have presented the VERHO system, which utilizes information from different sources to calculate the best link to be used in a multihomed or mobile node. We have presented the VERHO architecture and discussed the possible benefits of the system in question. Link layer modules have a real-time status and quality information about the current interfaces. Access point management (scanning, connection, disconnection) enables automatic network and access point selection. User requirements are taken into account by using profiles, which map the interface selection algorithm executed by the Link Access Controller into a set of weights. LAC comes with the ABC selection and utilizes the Mobile IPv6 protocol to trigger the actual handovers.

Since VERHO has real-time knowledge of link status and handover timing, mobility aware applications can utilize the information provided by VERHO for different purposes, such as setting up a proper streaming quality to support the change in access technologies while moving. We presented two prototype multimedia streaming applications, which have been implemented to verify the concept.

The current system functions as a prototype for future generation mobile terminals with an All-IP access and ABC connections. As future work, the current interface management can be extended to support multihoming and simultaneous access based on application preferences, i.e. multihoming management. This, however, require that the work of the IETF MEXT working group will be finished, so

that MIPv6 will support multihoming.

We are also looking forward to see how the IEEE 802.21 standard will be perceived among IEEE and 3GPP groups. For VERHO it would be a perfect amendment to network information collecting, but without wide implementation it will not provide real benefits.

The focus of the VERHO system is to provide an optimal connectivity for a single user. However, in the future the research could be extended to a simulator environment with a goal to optimize connectivity for multiple users, including some network load balancing functions.

As a future work, also the development of prototype application for Linux based devices should be continued and new features introduced. Especially, user centric design and power consumption are interesting topics to study.

ACKNOWLEDGMENT

Part of this work was published earlier in [24]; we highly appreciate the invitation to submit this extended version. The author would like to thank Gábor Fekete and Jani Puttonen for work related to VERHO, Martin Spurek for work related to Comui on Maemo platform, Lukas Lukowsky for work related to streamer application and Michael Chukwu for work related to the IP-TV proxy. Also, our acknowledgments to Jukka Mäkelä from VTT Technical Research Centre of Finland, to Henry Haverinen from Nokia Enterprise Solutions as well as to Petteri Weckström and Jorma Narikka from the Jyväskylä University of Applied Sciences for their valuable comments and feedback.

REFERENCES

- [1] Katz, R. H.; Brewer, E. A.: The case for wireless overlay networks. *Mobile Computing* (1996), 621–650.
- [2] Frodigh, M.; Parkvall, S.; Roobol, C.; Johansson, P.; Larsson, P.: Future-Generation Wireless Networks. *IEEE Personal Communications* 8 (2001), 10–17.
- [3] Hui, S. Y.; Yeung, K. H.: Challenges in the Migration to 4G Mobile Systems. *IEEE Communications Magazine* 41 (December 2003), 54–59.
- [4] Berezdivin, R.; Brenig, R.; Topp, R.: Next Generation Wireless Communications Concepts and Technologies. *IEEE Communications Magazine* 40 (2002), 49–55.
- [5] Newman, P.: In Search of the All-IP Mobile Network. *IEEE Communications Magazine* 42 (December 2004), S3–S8.
- [6] Gustafsson, E.; Jonsson, A.: Always Best Connected. *IEEE Wireless Communications* 10 (2003), 49–55.
- [7] Passas, N.; Paskalis, S.; Kaloxylas, A.; Bader, F.; Narcisi, R.; Tsontsis, E.; Jahan, A. S.; Aghvami, H.: Enabling Technologies for the 'Always Best Connected' Concept. *Wiley Wireless Communications and Mobile Computing* 5 (March 2005), 175–191.
- [8] Johnson, D.; Perkins, C.; Arkko, J.: Mobility Support in IPv6. *IETF RFC* 3775, June 2004.
- [9] IEEE Std. 802.21-2008, "IEEE standard for local and metropolitan area networks: Media independent handover services," IEEE Standard, January 2009.

- [10] Ylitalo, J.; Jokikyyny, T.; Kauppinen, T.; Tuominen, A. J.; Laine, J.: Dynamic Network Interface Selection in Multihomed Mobile Hosts. Proceedings of the 36th Hawai'i International conference on System Sciences (HICSS-36), Jan 2003.
- [11] Andre, F.; Bonnin, J.-M.; Deniaud, B.; Guilloard, K.; Montavont, N.; Noel, T.; Suciuc, L.: Optimized Support of Multiple Wireless Interfaces within an IPv6 Terminal. Proceedings of the Smart Objects Conference (SOC'2003), May 2003.
- [12] Vidales, P.; Baliosian, J.; Serrat, J.; Mapp, G.; Stajano, F.; Hopper, A.: Autonomic System for Mobility Management in 4G Networks. IEEE Journal on Selected Areas in Communications 23 (December 2005), 2288–2304.
- [13] Puttonen, J.; Fekete, G.; Rybczyk, P.; Narikka, J.: Practical Experimentation on Mobile IPv6 in Heterogeneous Environment. Acta Electrotechnica et Informatica 6 (2006).
- [14] Mäkelä, J.; Hämäläinen, T.; Fekete, G.; Narikka, J.: Intelligent Vertical Handover System for Mobile Clients. Proceedings of the 3rd International Conference on Emerging Telecommunications Technologies and Applications (ICETA 2004), September 2004. 151–155.
- [15] Puttonen, J.; Fekete, G.; Mäkelä, J.; Hämäläinen, T.; Narikka, J.: Using Link Layer Information for Improving Vertical Handovers. Proceedings of the 16th Annual IEEE International Symposium on Personal Indoor and Mobile Radio Communications (PIMRC'06), September 2005.
- [16] Puttonen, J.; Fekete, G.: Interface Selection for Multihomed Mobile Hosts. Proceedings of the 17th Annual IEEE International Symposium on Personal Indoor and Mobile Radio Communications (PIMRC'06), September 2006.
- [17] (ed.), A. Y.: Link-layer Event Notifications for Detecting Network Attachments. IETF Draft, October 2005.
- [18] IETF MEXT, "Mobile EXTensions for IPv6 (mext)" <http://www.ietf.org/html.charters/mext-charter.html>. Accessed: 25.5.2009.
- [19] S. Gundavelli, K. Leung, V. Devarapalli, K. Chowdhury, and B. Patil; Proxy Mobile IPv6. IETF RFC 5213, August 2008.
- [20] E. Nordmark and M. Bagnulo; Level 3 Multihoming Shim Protocol for IPv6. Internet-Draft (work in progress), draft-ietf-shim6-proto-09, October 2007.
- [21] Karila, A., Korhonen, T., Salminen, R and Väärämäki, T.; Broadband in Public Transportation Vehicles – Technology Study. ÄLLI Publications 1/2008.
- [22] IEEE P802.11 – Task Group U; "Interworking with external networks," IEEE, May 2009.
- [23] IEEE 802.16 Network Management Task Group; "Amendment to IEEE Standard for Local and Metropolitan Area Networks - Part 16: Air Interface for Fixed Broadband Wireless Access Systems - Management Plane Procedures and Services," IEEE Standard, May 2007.
- [24] Puttonen, J.; Fekete, G.; Väärämäki, T.; Hämäläinen, T.: " Multiple Interface Management of Multihomed Mobile Hosts in Heterogeneous Wireless Environments", The Eight International Conference on Networks (ICN 2009), March 2009.

Function Modulation – the Theory for Green Modem

Subhendu Das, CCSI, California, USA, subhendu.das@ccsi-ca.com

Nirode Mohanty, Fellow-IEEE, CCSI, California, USA, nirode.mohanty@ccsi-ca.com

Avtar Singh, San Jose State University, California, USA, avtar.singh@sjsu.edu

Abstract - Bandwidth of a digital communication channel is a valuable natural resource. Therefore it is important that the usage of this resource is minimized by carefully designing the digital modems. In this paper a new modulation scheme, called function modulation, is discussed that satisfies the Shannon's model and therefore can help to save bandwidth by creating a green modem. It is also shown that all existing modulation methods based on sinusoidal functions do not meet the requirements of Shannon's model and therefore have lower capacity for a given bandwidth.

In addition, the paper shows that Shannon's capacity is also not the limit. This capacity was derived under the assumption that the symbol duration is infinity. By relaxing this infinite time requirement much higher capacity is achieved. In order to derive this new capacity result a powerful and very well known mathematical concept, the infinite dimensionality of function space is used. It is shown that this concept can be the foundation of the digital communication as well as digital signal processing engineering.

Keywords - information rates; sampling methods; orthogonal functions; communication; modulation.

I. INTRODUCTION

This paper is the extended version of [1]. Here all the relevant research work is integrated to present in details the function modulation (fm) concept and its capacity.

In the derivation of capacity theorem Shannon used general functions as digital communication symbols. It is shown in [1] that if sinusoidal functions are used then Shannon's conditions cannot be satisfied and therefore it will not be possible to achieve the capacity results derived in Shannon's paper [2]. The fm method uses this general class of functions and it is shown that this method can achieve the Shannon's capacity result.

Another very important assumption in the derivation of the original capacity theorem was that all symbols must be of infinite time durations. This infinite time for symbols is not feasible in engineering. By relaxing this condition it is shown that even higher capacity can be achieved, under the same channel bandwidth requirement, giving an opportunity to design a green modem.

Thus two major changes are introduced. First, the sinusoidal functions are replaced by the general class of functions to create the fm modems. This fm model is called the Shannon's model, because we show that his geometric proof is based on this general class of functions. Second, the

infinite time assumption is replaced by the finite time assumption to derive a new high rate sampling theorem. The above two ideas are integrated in the fm system using a Software Radio (SWR) approach. This fm design is the green modem. This system gives a method for implementing Shannon's capacity theorem, which was missing from the communication literature.

A detailed discussion of a very well known mathematical theory of infinite dimensionality of function space is presented. Then this concept is used to derive the new sampling theorem. This theorem shows that [3] for finite duration signals more we sample more information we get from the signal, thus theoretically validating the common engineering practice. Like in the original paper [2], this new sampling theorem is used to derive the new capacity theorem. The new theorem shows that the capacity depends on the sample rate, and therefore can be much higher, theoretically unbounded, but practically bounded by the technology.

Shannon's original theory was derived using a geometric concept of n-dimensional Cartesian space where n approaches infinity. In this paper we use an apparently different geometric approach using infinite dimensional function space. We say it apparently, because on the face of it they are completely different, but their underlying concepts are linked together. We use our geometric approach to first derive the original result over finite time and then extend it to new result, also over finite time.

The paper is organized in several sections and their subsections. The major sections are Fundamentals, Sampling Theorem, Function Modulation, and Capacity Theorem. In the Fundamentals section we put the original thoughts that triggered this research. These thoughts were provided by various reviewers. The Sampling Theorem section answers – how many samples we need to describe a finite duration signal. The Function Modulation section describes the transmitter and the receiver. The Capacity Theorem section shows that the Shannon's theorem can be extended if we use finite duration symbols.

II. FUNDAMENTALS

In this section we collect all the fundamental ideas that will be used in the rest of the paper. They are related to infinite time assumption of classical theories, infinite dimensionality of function space, finite duration sampling needs, and the software radio concepts that are considered

crucial to the understanding of the thoughts that integrate all the research work presented in this paper.

A. Infinite Time Assumption

In this section we show that the assumption of infinite time duration for signals is not practical and is not necessary for our theories. In real life and in all our engineering systems we use signals of finite time durations only. Intuitively this finite duration concept may not be quite obvious though. Ordinarily we know that all our engineering systems run continuously for days, months, and years. Traffic light signaling systems, Global Positioning Systems (GPS) satellite transmitters, long distance airplane flights etc. are some common examples of systems of infinite time durations. Then why do we talk about finite duration signals? The confusions will be cleared when we think little bit and examine the internal design principles, the architecture of our technology, and the theory behind our algorithms. Originally we never thought that this question will be asked, but it was, and therefore we look here, at the implementations, for an explanation.

The computer based embedded engineering applications run under basically two kinds of Operating Systems (OS). One of these OS uses periodic approaches. In these systems the OS has only one interrupt that is produced at a fixed rate by a timer counter. Here the same application runs periodically, at the rate of this interrupt, and executes a fixed algorithm over and over again on input signals of fixed and finite time duration. As an example, in digital communication engineering, these signals are usually the symbols of same fixed duration representing the digital data and the algorithm is the bit recovery process. Every time a analog symbol comes, the algorithm recovers the bits from the symbol and then goes back to process the next arriving symbol.

Many core devices of an airplane, carrying passengers, are called flight critical systems. Similarly there are life critical systems, like pacemaker implanted inside human body. It is a very strict requirement that all flight critical and life critical systems have only one interrupt. This requirement is mainly used to keep the software simple and very deterministic. They all, as explained before, repeat the same periodic process of finite duration, but run practically for infinite time.

The other kind of applications is based on the Real Time multi-tasking Operating Systems (RTOS). This OS is required for systems with more than one interrupts which normally appear at asynchronous and non-periodic rate. When you have more than one interrupts, you need to decide which one to process first. This leads to the concept of priority or assignment of some kind of importance to each interrupt and an algorithm to select them. The software that does this work is nothing but the RTOS. Thus RTOS is essentially an efficient interrupt handling algorithm. Thus RTOS is not unique and can be designed in your way.

These RTOS based embedded applications are designed as a finite state machine. We are not going to present a theory of RTOS here. So to avoid confusions we do not try to distinguish among threads, tasks, processes, memory management, and states etc. We refer to all of these concepts as tasks, that is, we ignore all the details below the level of tasks, in this paper. These tasks are executed according to the arrival of interrupts and the design of the application software. The total application algorithm is still fixed and finite but the work load is distributed among these finite numbers of tasks. The execution time of each task is finite also. These tasks process the incoming signals of finite time and produce the required output of finite size.

An example will illustrate it better. A digital communication receiver can be designed to have many tasks – signal processing task, bit recovery task, error correcting task etc. They can be interconnected by data buffers, operating system calls, and application functions. All these tasks together, implement a finite state machine, execute a finite duration algorithm, and process a finite size data buffer. These data buffers are originated from the samples of the finite duration signals representing the symbols. The transmitter of a digital communication system can also be implemented using similar principles.

We should point out that it is possible to design application systems which are combinations or variants of these two basic concepts. Most commercial RTOS provide many or all of these capabilities. Thus although all of the engineering systems run continuously for all time, all of them are run under the above two basic OS environment. Or in other words for all practical engineering designs the signal availability windows, the measurement windows, and the processing windows are all of finite time. For more details of real time embedded system design principles see many standard text books, for example [4, pp. 73-88].

The signals may exist theoretically or mathematically for infinite time but in this paper none of our theories, derivations, and assumptions will use that infinite time interval assumption. However, interestingly enough, to deal with the finite duration problem we have to use the well known mathematical concept of infinite dimensionality of function space. Thus somehow infinity appears to be inescapable. In the next subsection we explain this infinite dimensionality idea in details.

B. Infinite Dimensionality

We will use the following basic notations and definitions in our paper. Consider the class of all real valued measurable functions in $L_2[a,b]$, defined over the finite time interval $[a,b]$. We assume that the following Lebesgue integral (1) is bounded, i.e.

$$\int_a^b |f(t)|^2 dt < \infty, \quad \forall f \in L_2[a, b] \quad (1)$$

Then we define the L_2 norm as in (2):

$$\|f\| = \left[\int_a^b |f(t)|^2 dt \right]^{1/2}, \forall f \in L_2[a, b] \quad (2)$$

Then the following (3) definition can be used for metric d

$$d(f, g) = \|f - g\| = \left[\int_a^b |f(t) - g(t)|^2 dt \right]^{1/2} \quad (3)$$

In addition (4) defines the inner product as

$$\langle f, g \rangle = \int_a^b f(t)g(t)dt \quad \forall f, g \in L_2[a, b] \quad (4)$$

Under the above conditions the function space, $L_2 [a,b]$, is a Hilbert space. One very important property of the Hilbert space [5, pp. 31-32], related to the communication theory, is that it contains a countable set of orthonormal basis functions. Let $\{\varphi_n, n = 1, 2, \dots\}$ be such a set of basis functions. Then the following (5) holds:

$$\langle \varphi_i, \varphi_j \rangle = \delta_{ij} = \begin{cases} 0 & \text{if } i \neq j \\ 1 & \text{if } i = j \end{cases} \quad (5)$$

And for any $f \in L_2[a, b]$ the Fourier series (6) can be written using (5) as:

$$f(t) = \sum_{i=1}^{\infty} a_i \varphi_i(t), \quad \forall t \in [a, b] \quad (6)$$

The expression (6) really means that for any given $\varepsilon > 0$ there exists an N such that

$$\|f(t) - \sum_{i=1}^n a_i \varphi_i(t)\| < \varepsilon, \quad \forall n > N \quad (7)$$

Since the functions in (5) are orthogonal, the Fourier series coefficients in (6) can be obtained using the Lebesgue integral (8) as shown below:

$$a_i = \int_a^b f(t)\varphi_i(t)dt, \quad i = 1, 2, \dots \quad (8)$$

We should point out to avoid any confusion that the Fourier series (6) in this paper is assumed to be defined over finite time duration. Although, a can be $-\infty$ and b can be $+\infty$. Also, the functions $\varphi_n(t)$ are general functions and not necessarily sinusoidal harmonic functions. The expression (6) may be called as the generalized Fourier series.

In this paper we will consider only continuous functions and their Riemann integrability. We note that the continuous functions are measurable functions and the Riemann integrable functions are also Lebesgue integrable. Thus the Hilbert space theory (1-8) and the associated concepts will still remain applicable to our problems. Actually, the Lebesgue integrable functions form an equivalent class, in the sense that there exists a continuous function whose Lebesgue integral is same as the Lebesgue integral of any one of the measurable functions in that equivalent class. By the way, the Riemann integral is the one we study in our high school calculus course.

We observe from (6) that to represent a function accurately over any interval we need two sets of data: (A) An infinite set of basis functions, not necessarily orthogonal and (B) An infinite set of coefficients in the infinite series expression for the function, similar to (6). That is, these two sets completely define the information content in a mathematical function. Thus the information is not a superficial concept; it has a very meaningful, practical, and mathematical definition as mentioned in this paragraph.

Equality (6) happens only for infinite number of terms. Otherwise, the Fourier representation in (7) is only approximate for any finite number of terms. In this paper ε in (7) will be called as the measure of approximation or the accuracy estimate in representing a continuous function. The Hilbert space theory (1-8) ensures the existence of N in (7) for a given ε . The existence of such a countably infinite number of orthonormal basis functions (5) proves that the function space is an infinite dimensional vector space. This dimensionality does not depend on the length of the interval [a,b]. Even for a very small interval, like symbol time, or an infinite interval, a function is always an infinite dimensional vector. However, the context in which this vector is defined is also very important, which is, the entire function space in this case.

It is not necessary to have orthonormal basis functions for demonstrating that the function space is infinite dimensional. The collection of all polynomial functions $\{t^n, n = 1, 2, \dots\}$ is linearly independent over the interval [a,b] and their number is also countable infinity. These polynomials can be used to represent any analytic function, i.e. a function that has all derivatives. Using Taylor's series (9) we can express such a f(t) at t as:

$$f(t) = \sum_{n=0}^{\infty} \frac{f^{(n)}(c)}{n!} (t - c)^n \quad (9)$$

around the neighborhood of any point c. Thus the above polynomial set is also a basis set for the function space. Therefore using the infinite Taylor series expression (9), we prove again that a function is an infinite dimensional vector over a finite interval. Here the information is defined by the derivative coefficients and the polynomial functions.

It can be shown that a band limited function is also infinite dimensional and therefore carries infinite amount of information. Consider a band limited function f(t), with bandwidth $[-W, +W]$. Then f(t) is given by the following (10) inverse Fourier Transform (FT) [2]:

$$f(t) = \frac{1}{2\pi} \int_{-\infty}^{+\infty} F(w)e^{iwt} dw \quad (10)$$

$$= \frac{1}{2\pi} \int_{-2\pi W}^{+2\pi W} F(w)e^{iwt} dw \quad (11)$$

In (11) t is defined for all time in $(-\infty, +\infty)$, but the frequency w is defined only over $[-W, +W]$, and it can take any value: integer, rational, or irrational frequencies, within that frequency range.

The expression (11) shows that the band limited function $f(t)$ has uncountably infinite number of frequencies. Therefore $f(t)$ is an infinite dimensional vector. This is true even when we consider a small interval of time for the function $f(t)$. In that small interval the function still has all the infinite frequency components corresponding to the points in $[-W,+W]$. This is another way of showing that a band limited function is an infinite dimensional vector over a finite measurement window.

It should be pointed out here that a constant function $f(t) = C$, as an element of function space, is also an infinite dimensional vector. The only difference is that all sample values are same. In terms of Taylor series the coefficients for a constant function are $\{C,0,0,\dots\}$, which is an infinite dimensional vector. In the next subsection we discuss an all software approach for the design of digital communication systems. In the next subsection we prove infinite dimensionality in another way.

C. Finite Duration Sampling

The following is a very common way of expressing functions in mathematics. Let $f(t)$ be a continuous function defined over $L_2[a,b]$. Assume that we divide the finite time interval $[a,b]$ into $n > 1$ equal parts using equally spaced points $\{t_1, t_2, \dots, t_n, t_{n+1}\}$ where $t_1=a$ and $t_{n+1}=b$. Use the following (12) notations to represent the t -subintervals

$$\Delta t_i = \begin{cases} [t_i, t_{i+1}), & i=1,2,\dots,n-1 \\ [t_n, t_{n+1}], & i=n \end{cases} \quad (12)$$

Define the characteristic functions (13) as:

$$X_i(t) = \begin{cases} 1, & t \in \Delta t_i \\ 0, & t \notin \Delta t_i \end{cases} \quad i = 1, 2, \dots, n \quad (13)$$

In this case, the characteristic functions, $X_i(t)$ are orthogonal over the interval $[a,b]$ with respect to the inner product on $L_2[a,b]$. Because (14) given below holds.

$$X_i(t)X_j(t) = 0, \quad i \neq j, \quad \forall t \in [a, b] \quad (14)$$

Also define the simple functions (15) as

$$f_n(t) = \sum_{i=1}^n f(t_i)X_i(t) \quad \forall t \in [a, b] \quad (15)$$

Here $f(t_i)$ is the sampled value of the function $f(t)$ at $t = t_i$. It is easy to visualize that $f_n(t)$ is a sequence of discrete step functions over n . Expression (15) is an approximate Fourier series representation of $f(t)$ over $[a,b]$. This representation uses the samples of the function $f(t)$ at equal intervals, $f_n(t)$ uses n number of samples. We show that this approximate representation (15) improves and approaches $f(t)$ as we increase the number of samples, the value of n towards infinity.

Theorem 1: $f_n(t) \rightarrow f(t)$ as $n \rightarrow \infty$, $\forall t \in [a, b]$

To prove the theorem, define (16) as the error expression

$$\Delta y_n = \max_t |f(t) - f_n(t)|, \quad \forall t \in [a, b] \quad (16)$$

It is clear that $\{\Delta y_n\}$ is a monotonically decreasing sequence of n . Therefore, given any $\epsilon > 0$ we can find an N such that $\Delta y_n \leq \epsilon / \sqrt{(b-a)}$ for all $n > N$.

Starting with (17) derive the difference in norm:

$$\|f - f_n\| = \left[\int_a^b |f(t) - f_n(t)|^2 dt \right]^{1/2} \quad (17)$$

$$= \left[\int_a^b |f(t) - \sum_{i=1}^n f(t_i)X_i(t)|^2 dt \right]^{1/2} \quad (18)$$

$$= \left[\int_a^b |\sum_{i=1}^n f(t)X_i(t) - \sum_{i=1}^n f(t_i)X_i(t)|^2 dt \right]^{1/2} \quad (19)$$

$$= \left[\int_a^b [\sum_{i=1}^n (f(t) - f(t_i))X_i(t)]^2 dt \right]^{1/2} \quad (20)$$

Now performing the squaring operation, noting that equation (14) holds, expression (21) helps to further simplify the expression (20):

$$= \left[\int_a^b [\sum_{i=1}^n (f(t) - f(t_i))^2 X_i^2(t)] dt \right]^{1/2} \quad (21)$$

$$\leq \left[\int_a^b [\sum_{i=1}^n (\Delta y_n)^2 X_i^2(t)] dt \right]^{1/2} \quad (22)$$

$$= \left[\Delta y_n^2 \int_a^b (\sum_{i=1}^n X_i^2(t)) dt \right]^{1/2} \quad (23)$$

$$= [\Delta y_n^2 (b-a)]^{1/2} = \sqrt{(b-a)} \Delta y_n \leq \epsilon \quad (24)$$

Thus from (17) we see that (25) holds, $\forall n \geq N$

$$\|f(t) - \sum_{i=1}^n f(t_i)X_i(t)\| \leq \epsilon, \quad \forall t \in [a, b] \quad (25)$$

Which essentially means (26):

$$f(t) = \sum_{i=1}^{\infty} f(t_i)X_i(t), \quad \forall t \in [a, b] \quad (26)$$

This concludes the proof of Theorem 1.

Theorem 1 proves that infinite sample rate is necessary to represent a continuous function correctly over a finite time interval. Theorem 1 is similar to the one described for measurable functions in [6, pp. 185-187]. However the coefficients are not sampled values in that theorem. Another proof can be found in [7, pp. 247-257] where the Bernstein polynomial has been used instead of the characteristic function.

The above theorem confirms a very well known engineering practice. In all engineering applications, our engineers always sample a signal at more than two to four times the Nyquist rate. Theorem 1 only mathematically justifies that well known practice. We will show that this theorem also provides the analytical foundation for our new capacity theorem. Thus Theorem 1, although very simple and obvious, has a profound implication in both digital

signal processing and communication theories. Note that Theorem 1 does not depend on the bandwidth of the function $f(t)$. However ε and N , as used in (25), are dependent on the bandwidth.

Again from Theorem 1 we conclude that the function space is infinite dimensional and the information content can be represented by its infinite number of samples. This result is very important because these samples are generated by the Analog to Digital Converter (ADC) in our technology today. Thus the ADC actually produces the information content of a function.

D. Software Radio Approach

The foundation of the existing digital communication schemes is based on modulating the three parameters, amplitude A , frequency f , and phase ϕ of the sinusoidal function (27):

$$s(t) = A \sin(2\pi ft + \phi) \quad (27)$$

Most of the existing methods vary, in discrete steps, one or more of the above three parameters to represent the digital data. These methods are known as Amplitude Shift Keying (ASK), Frequency Shift Keying (FSK), and Phase Shift Keying (PSK). Collectively we call them as Shift Keying (SK) methods in this paper.

In this paper we present a modulation method for digital communication that does not use sinusoidal functions, does not use any one of the keying methods mentioned, and does not use any kind of discrete variations during the symbol intervals as well as at the inter-symbol interfaces. We show that the entire symbol stream, after concatenation, remains analytic i.e. smooth and continuous.

In the proposed method we modulate the complete function $s(t)$ or the \sin function itself. Since we are modulating the functional structure of the expression $s(t)$, we call it a function modulation (fm) method. Also, since our method does not use any discrete changes in the waveform or the function representing the symbol we call it an analog approach.

Our design approach is based on the concept of Software Radio (SWR), where we use batch data-in and batch data-out processing method as opposed to more conventional sample-in and sample-out type real time method. Of course we do this only for one symbol time which is usually millisecond or microsecond long. This SWR approach allows us to see the past, the present, and therefore the entire history of the data simultaneously, and to help extract information more effectively at the receiver. Observe that the symbol duration does not always indicate capacity or bit rate. Same symbol duration can be used for transmitting 10 bits or 20 bits of data as explained in our function modulation section. It is the number of symbols that dictates data rate or capacity. From our theory you will be able to find out that nanosecond is quite meaningful also and with our present day technology.

In this SWR method, since we are not using sinusoidal functions, we do not need to use Voltage Controlled Oscillators (VCO), Phase Lock Loops (PLL), up down converters etc., which are dependent on the concept of sinusoidal functions. We also do not need to use any linear feedback control system type concepts in this batch data processing method. Thus we avoid all the instability problems related to linear feedback theory.

This SWR design can be implemented entirely on standard off-the-shelf Digital Signal Processors (DSP) using programming concepts of time domain approaches. The advent of modern high speed DSPs enables us to take this approach. We will see that this time domain approach is more reliable and have meaningful theoretical foundation as opposed to Laplace transform or Fourier Transform (FT) based concepts that require linearity and infinite time assumptions. It should be understood that custom Application Specific Integrated Circuits (ASIC) instead of an off-the-shelf DSP can be more powerful for mass production.

Thus in our software radio approach we do not implement electronic hardware concepts using software languages. This approach allows us to implement our thought process using software languages. The thought process should not depend on the technology. The modern DSPs, high speed Analog to Digital Converters (ADC), and Digital to Analog Converters (DAC) allow us to implement our thoughts the way we think. An example of our thought process can be like this: "We want to send hundreds of symbols and our receiver should be able to detect them." We show that we have just implemented the above thought using our DSP concept.

Thus this SWR approach is not just moving the sampler near the antenna, and then implementing hardware logic using programming languages; it is all about rethinking the entire concepts using DSP, it is a paradigm shift. We do not treat things using moment by moment, like in sample by sample approaches. We treat the entire life history together, using batch data process, along with global system level, and simultaneous concept, as described later to implement our SWR. This kind of time domain approach has many advantages over conventional transform domain approaches. We know that the transform methods make infinite time and linearity assumptions. Both assumptions are not realistic in engineering problems and therefore will provide suboptimal solutions. Our approach will allow us to use mathematical techniques that we have never used before in real time, like integral equations, least square etc.

There is another very important common feature of all the existing digital communication schemes - bits of the data stream do not play any role, in the following sense, in the design of communication systems. For example, in an m -bit data stream we consider $M=2^m$ data packets. The internal bit pattern of each packet is not important. Only the number M is important. Existing methods select M waveforms to represent each one of these M packets. Any one of the

waveforms can be used to represent any one of the M data packets. Thus the link is very artificial. We could even send names of M authors, or titles of M books using these M waveforms. In the proposed method, the bits are directly embedded in the symbol i.e. there is a direct physical link between the bit pattern and the wave shape of the symbol. Thus we are sending bits also and not just symbols. Therefore Bit Error Rate (BER) is directly meaningful.

We introduce an intermediate space, called bit function space, between the data space and the symbol space. The dimension of the bit function space is m, the number of bits in the data packets. We show that fm receiver does not need to search in the symbol space; instead we can search in this newly defined bit function space. This bit function space approach reduces the number of searches. We show that, for the orthogonal bit function case, we need to search over only m bit functions instead of 2^m symbols as required by Shannon's capacity model. This is a significant reduction in the complexity of the fm receiver design and has the potentiality of providing high capacity systems.

Thus our software radio approach is dramatically different from the existing digital communication engineering. We have taken a new look to communication engineering from a global perspective and integrated the power of hardware, software, algorithm, and system level technologies. Next we extend the sampling theorem.

III. SAMPLING THEOREM

We show that when the signals are defined over finite time interval then the Nyquist rate is not enough for signal reconstruction. We must sample as fast as we can or as much the technology permits.

A. Finite Duration Case

Consider the sinusoidal function (28):

$$s(t) = A \sin(2\pi f t + \theta) \quad (28)$$

We can see from the above expression that a sinusoidal function can be completely specified by three parameters A, f, and θ . So we can use (29) to express a sine function as a three dimensional vector:

$$s = [A, f, \theta] \quad (29)$$

However (29) is very misleading. There is a major hidden assumption; that the parameters of (29) are related by the sine function. Therefore (30) can be used to give a more precise representation of (29):

$$s = [A, f, \theta, \text{"sine"}] \quad (30)$$

The word sine in (30) means the Taylor's series, which has an infinite number of coefficients. Therefore when we say (29) we really mean (30) and that the sine function (28), as usual, is really an infinite dimensional vector.

Now assume, without loss of generality, that (28) is defined over one period. That is, we have collected the signal from the display of a digital oscilloscope. We can then use the following three equations (31) to solve for the three unknown parameters, A, f, and θ :

$$\begin{aligned} s_1 &= A \sin(2\pi f t_1 + \theta) \\ s_2 &= A \sin(2\pi f t_2 + \theta) \\ s_3 &= A \sin(2\pi f t_3 + \theta) \end{aligned} \quad (31)$$

where t_1, t_2, t_3 are sample times and s_1, s_2, s_3 are corresponding three sample values. Again (32) gives a more meaningful representation in terms of samples:

$$s = [(s_1, t_1), (s_2, t_2), (s_3, t_3), \text{"sine"}] \quad (32)$$

Hence with the sinusoidal assumption, a sine function can be completely specified by only three samples. The above analysis gives a simple proof of the original sampling theorem. For band limited functions we can consider this sinusoid as the highest frequency sine wave in the signal. We can now state the well known result:

Theorem 2: A sinusoidal function, with sinusoidal assumption, can be completely specified by three non-zero samples of the function taken at any three points in its period.

From (31) we see that if we assume sinusoidality then more than three samples, or higher than Nyquist rate, will give redundant information. However without sinusoidality assumptions more sample we take more information we get, as is done in common engineering practice. It should be pointed out that Shannon's sampling theorem assumes sinusoidality. Because it is derived using the concept of bandwidth, which is defined using Fourier series or transform, which in turn uses sinusoidal functions.

Theorem 2 says that the sampling theorem should be stated as $f_s > 2f_m$ instead of $f_s \geq 2f_m$ that is, the equality should be replaced by strict inequality. Here, f_m is the signal bandwidth, and f_s is the sampling frequency. There are some engineering books [8, p. 63] that mention strict inequality.

Shannon writes about his sampling theorem [2, p. 448] in the following way: "If a function $f(t)$ contains no frequencies higher than W cps, it is completely determined by giving its ordinates at a series of points spaced $1/2W$ seconds apart." The proof [2] is very simple and runs along the following lines. See also [9, p. 271]. A band limited function $f(t)$ can be written as in (26). Substituting $t = n/(2W)$ in (26) we get the following expression (33):

$$f\left(\frac{n}{2W}\right) = \frac{1}{2\pi} \int_{-2\pi W}^{+2\pi W} F(w) e^{i w \frac{n}{2W}} dw \quad (33)$$

Then the paper [2] makes the following comments: "On the left are the values of $f(t)$ at the sampling points. The integral on the right will be recognized as essentially the nth coefficient in a Fourier-series expansion of the function

$F(w)$, taking the interval $-W$ to $+W$ as a fundamental period. This means that the values of the samples $f(n/2W)$ determine the Fourier coefficients in the series expansion of $F(W)$." It then continues "Thus they determine $F(w)$, since $F(w)$ is zero for frequencies greater than W , and for lower frequencies $F(w)$ is determined if its Fourier coefficients are determined."

Thus the idea behind his proof is that from the samples of $f(t)$ we reconstruct the unknown $F(w)$ using (33). Then from this known $F(w)$ we can find $f(t)$ using (10) for all time t . One important feature of the above proof is that it requires that the function needs to exist for infinite time, because only then you get all infinite samples from (33). We show that his proof can be extended to define functions over any finite interval with any degree of accuracy by increasing the sample rate. The idea is similar, we construct $F(w)$ from the samples of $f(t)$.

We use the principles behind the numerical inversion of Laplace transform method as described in [10, p. 359]. Let $F(w)$ be the unknown band limited Fourier transform, defined over $[-W,+W]$. Let the measurement window for the function $f(t)$ be $[0,T]$, where T is finite and not necessarily a large number. Divide the frequency interval $2W$ into K smaller equal sub-intervals of width Δw with equally spaced points $\{w_j\}$ and assume that $\{F(w_j)\}$ is constant but unknown over that i -th interval. Then we can express the integration in (33) approximately by (34):

$$f(t) \approx \frac{1}{2\pi} (\Delta w) \sum_{j=1}^K e^{itw_j} F(w_j) \quad (34)$$

The right hand side of (34) is a linear equation in $\{F(w_j)\}$, which is unknown. Now we can also divide the interval $[0,T]$ into K equal parts with equally spaced points $\{t_j\}$ and let the corresponding known sample values be $\{f(t_j)\}$. Then if we repeat the expression (34) for each sample point t_j we get K simultaneous equations in the K unknown variables $\{F(w_j)\}$ as shown below by (35):

$$\begin{bmatrix} f(t_1) \\ f(t_2) \\ \vdots \\ f(t_K) \end{bmatrix} = \frac{\Delta w}{2\pi} \begin{bmatrix} e^{it_1w_1} & e^{it_1w_2} & \dots & e^{it_1w_K} \\ e^{it_2w_1} & e^{it_2w_2} & \dots & e^{it_2w_K} \\ \vdots & \vdots & \ddots & \vdots \\ e^{it_Kw_1} & e^{it_Kw_2} & \dots & e^{it_Kw_K} \end{bmatrix} \begin{bmatrix} F(w_1) \\ F(w_2) \\ \vdots \\ F(w_K) \end{bmatrix} \quad (35)$$

These equations are independent because exponential functions in (34) are independent. Therefore we can solve them for $\{F(w_j)\}$. Theorem 1 ensures that the sets $\{F(w_j)\}$ and $\{f(t_j)\}$ can be selected to achieve any level of accuracy requirements in (34) for either $f(t)$ or $F(w)$.

For convenience we assume that the number of terms K in (34) is equal to $Tk f_s$ which is equal to $2kWT$. Here f_s is the Nyquist sample rate and $k > 1$. We state the following new sampling theorem.

Theorem 3: Let $f(t)$ be a band limited function with bandwidth restricted to $[-W,+W]$ and available over the

finite measurement window $[0,T]$. Then given any accuracy estimate $\epsilon > 0$, there exists a constant $k > 1$ such that $2kWT$ equally spaced samples of $f(t)$ over $[0,T]$ will completely specify the Fourier transform $F(w)$ of $f(t)$ with the given accuracy ϵ . This $F(w)$ can then be used to find $f(t)$ for all time t .

In a sense Shannon's sampling theorem gives a sufficient condition. That is, if we sample at twice the bandwidth rate and collect all the infinite number of samples then we can recover the function. We point out that this is not a necessary condition. That is, his theorem does not say that if T is finite then we cannot recover the function accurately by sampling it. We have confirmed this idea in the above proof of Theorem 3.

Shannon proves his sampling theorem [2] in another way. Any continuous function can be expressed using the Hilbert space based Fourier expression (6). Shannon has used the above expression for a band limited function $f(t)$, defined over infinite time interval. He has shown that if we use (36)

$$\varphi_n(t) = \frac{\sin\{\pi f_s[t-(n/f_s)]\}}{\pi f_s[t-(n/f_s)]} \quad (36)$$

Then (37) will give the coefficients of (6):

$$a_n = f(n/f_s) \quad (37)$$

Thus (38) can be used to express $f(t)$ [11, p. 58]:

$$f(t) = \sum_{n=-\infty}^{\infty} f(n/f_s) \frac{\sin\{\pi f_s[t-(n/f_s)]\}}{\pi f_s[t-(n/f_s)]} \quad (38)$$

Here $f_s \geq 2W$, where W is the finite bandwidth of the function $f(t)$. The set $\{\varphi_n\}$ in (36) is orthogonal only over $(-\infty,+\infty)$.

We make the following observations about (38):

- The representation (38) is exact only when infinite time interval and infinite terms are considered.
- If we truncate to finite time interval then the functions φ_n in (36) will no longer be orthogonal, and therefore will not form a basis set, and consequently will not be able to represent the function $f(t)$ correctly.
- If in addition we consider only finite number of terms of the series in (38) then more errors will be created because we are not considering all the basis functions. We will only be considering a subspace of the entire function space.

We prove again that, by increasing the sample rate we can get any desired approximation of $f(t)$, over any finite time

interval $[0, T]$, using the same sinc functions of (36). From calculus we know that the following (39) limit holds:

$$\lim_{x \rightarrow \infty} \frac{\sin x}{x} = 0 \quad (39)$$

Assume that f_s is the Nyquist sampling frequency, i.e. $f_s = 2W$. Let us sample the signal at k times the Nyquist rate. Here $k > 1$ is any real number. Then using (39), we can show that given any T and a small $\delta > 0$, there exists an N such that (40) as given below holds:

$$\left| \frac{\sin(\pi k f_s t)}{\pi k f_s t} \right| < \delta, \forall k > N, \forall t \geq T \quad (40)$$

Thus these orthogonal functions (36) substantially go to zero outside any finite interval $[0, T]$ for large enough sampling rate and still maintain their orthogonality property, substantially, over $[0, T]$. Thus by increasing the sample rate we squeeze many of these functions within this finite interval. The tails of these functions become substantially zero outside this interval as seen from (39). The squeezing situation is also shown in Fig. 1. Therefore for a given band limited function $f(t)$, with signal capture time limited to the finite window $[0, T]$, we can always find a high enough sample rate, $k f_s$ so that given any $\epsilon > 0$ the expression (41) will be true:

$$\left\| f(t) - \sum_{n=0}^K f\left(\frac{n}{k f_s}\right) \frac{\sin\{\pi k f_s [t - (n/k f_s)]\}}{\pi k f_s [t - (n/k f_s)]} \right\| < \epsilon \quad (41)$$

$$\forall k > N, \forall t \in [0, T]$$

Observe that from the infinite duration Fourier series (38) we have derived a finite duration Fourier series (41) merely by increasing the sample rate. Our finite duration analysis is not just about recovering the signal, but finding how many samples are necessary to correctly represent the signal. Thus our focus is different from signal reconstruction theories, which is so well known in the literature.

The number of functions in the above series (41) is now K , which is equal to the number of samples over the period $[0, T]$. Thus $K = k f_s T = 2kWT$. As k increases the number of sinc functions increases and the distance between the consecutive sinc functions reduces thus giving higher sample rate. The original proof, [12, pp. 87-88] for (36-38), which is independent of sample rate, still remains valid as we increase the sample rate. That is, the sinc functions in (36) still remain orthogonal. It can be shown using the original method that the coefficients in (37) remain valid and represent the sample values. Thus the system still satisfies the Hilbert Space theory, making the expression (41) justified over $[0, T]$. Thus we can state the following new sampling theorem.

Theorem 4: Let $f(t)$ be a band limited function with bandwidth restricted to $[-W, +W]$ and available over the finite measurement window $[0, T]$. Then given any accuracy

estimate ϵ there exists $k > 1$ such that $2kWT$ equally spaced samples of $f(t)$ over $[0, T]$ along with their sinc functions, will completely specify the function $f(t)$ for all t in $[0, T]$ at the given accuracy.

Theorems 1 and 4 are identical, because the sinc function is the FT of the characteristic function. These theorems suggest that the Nyquist rate is not enough for finite duration signals. That is, we must sample as fast as we can depending on our technology and more we sample more information we get about the function. The expression (41) shows that the information content is in the samples and in the sinc functions. We mention again that our paper is not about signal reconstruction, it is about how many samples are required for a finite duration signal.

The paper [13] gives a good summary of the developments around sampling theorem during the first thirty years after the publication of [2]. Interestingly [13] talks briefly about finite duration time functions, but the sampling theorem is presented for the frequency samples, that is, over Fourier domain which is of infinite duration on the frequency axis.

In the following subsection we give a numerical example to show how higher rate samples actually improves the function reconstruction.

B. Numerical Example

We illustrate the effect of sample rate on the reconstruction of functions. Since every function can be considered as a Fourier series of sinusoidal harmonics, we take one sine wave and analyze it. This sine function may be considered as the highest frequency component of the original band limited signal. The Nyquist rate would be twice the bandwidth, that is, in this case twice the frequency of the sine wave. We are considering only one period, and therefore the Nyquist rate will give only two samples of the signal during the finite interval of its period. We are also assuming that we do not know or cannot use the analytical expression of the sine wave that we are trying to reconstruct.

Fig. 1 shows all the graphs of this numerical result. The figure will not be very readable on a printed paper. It is quite congested also. However it will be clear if enlarged on your computer. The horizontal axis represents the time in seconds. The full scale value is 0.001 seconds, that is, one millisecond. The vertical axis is normalized to unit value of amplitude. We thought it would not be a very good idea to break it down to seven new figures.

This figure has three groups 1a, 1b, and 1c represent the group for two samples case. Similarly 2a, 2b, and 2c represent another group for three samples reconstruction process. The last group consists of 3a, 3b, and 3c and shows the six samples results. In each group of Fig. 1 we show respectively, the sinc functions, reconstructed sine wave, the error between the actual sine wave and the reconstructed graph. The graphs show that the error decreases as we

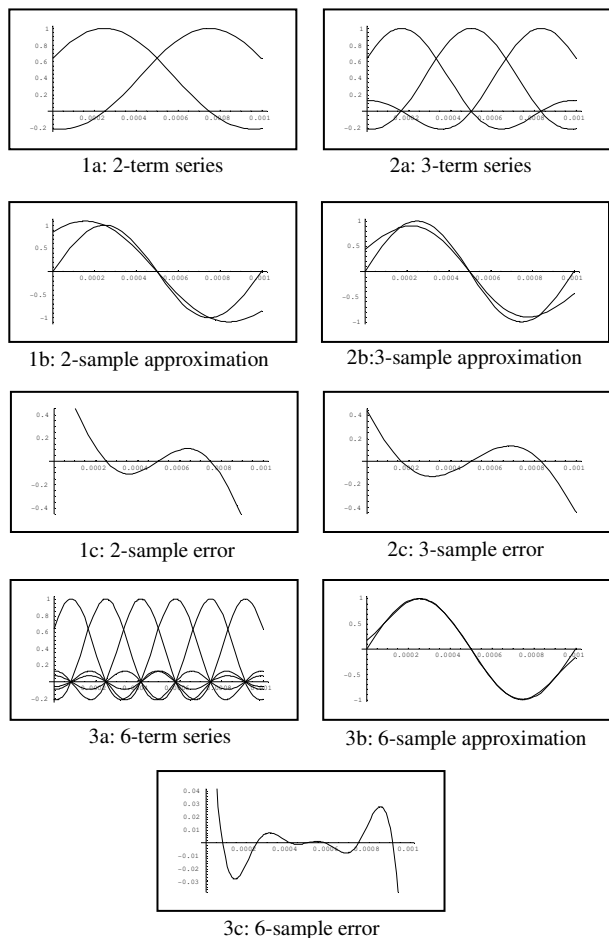


Figure 1. Signal reconstruction from samples

increase the sample rate. The middle set of graphs, 1b, 2b, and 3b, shows clearly how the signal reconstruction improves as we increase the number of samples. We have used formula (41) to reconstruct the sine waves from the sample values. A better method may give better result but our point is to show that more you sample better will be the recovery no matter what algorithm you use.

IV. FUNCTION MODULATION

A new modulation method called function modulation (fm) is discussed. We use the lower case letters fm to denote function modulation and reserve the upper case FM to represent Frequency Modulation method. We describe both transmitters and receivers of this fm scheme. The results of a practical implementation are discussed.

A. The fm Transmitter

Fig. 2 describes the design of a transmitter based on the function modulation (fm) method for digital communication system [14]. The left-hand-side vertical box represents a four bit data, as an element of data space, to be transmitted

using one symbol $s(t)$. In Fig. 2 we have assumed, the number of bits, m , to be transmitted is four, as an example, without any loss of generality.

Let $d = \{d_i, i=1..m, d_i \in \{0,1\}\}$, be a column vector, and represent a data element in the data space. Here d_i represents the i -th bit of d with 0 or 1 as its value. Let $G(t) = \{g_i(t), i=1..m, t \in [0,T]\}$, also a column vector, represent a set of analytic and independent functions defined over the symbol interval $[0,T]$. We assign the i -th function $g_i(t)$ to the i -th bit location. In Fig. 2 the arrows from the bit locations to the bit function boxes define these one-to-one assignments. These functions are referred to as bit functions. The set $G(t)$ defines the bit function space.

A set of functions $G(t)$ is called dependent if there exists constants $\{c_i, i = 1..m\}$, not all zero, such that the expression given by (42) holds:

$$g_1(t)c_1 + g_2(t)c_2 + \dots + g_m(t)c_m = 0 \tag{42}$$

for all $t \in [0,T]$. If not then it is independent [15, pp. 177-181]. The above expression is a linear combination of functions. Here the coefficients $\{c_i, i = 1..m\}$ are all real numbers.

A real valued function is analytic if all derivatives are uniformly bounded [16, p. 238]. Analytic functions are band limited [12, p. 87]. An analytic function does not have any discrete jumps; it is a smooth and continuous function. In this paper the terms analog and analytic functions are used interchangeably.

The m bit functions are combined inside the algorithm box to produce one symbol function $s(t)$. The collection of all symbols is called the symbol space. The Fig. 2 shows how we have introduced the concept of a bit function space in between the data space and the symbol space.

The algorithm is selected in such a way, so as to produce a symbol that is also an analytic function. For every bit pattern in the data space the algorithm produces one unique symbol in the symbol space using only m bit functions from the bit function space. The algorithm is an one-to-one and onto transformation, from the data space to the symbol space, ensuring that for every symbol it produces, there exists one unique bit pattern.

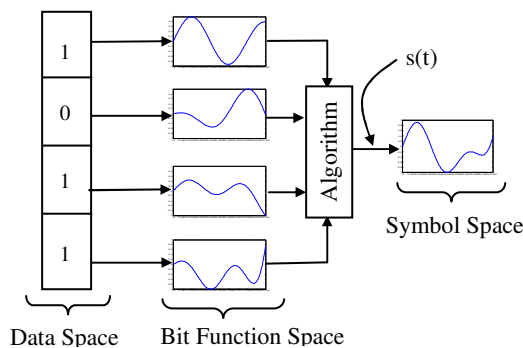


Figure 2. fm Transmitter

In general the algorithm in Fig. 2 can be represented by the following expression (43):

$$s(t) = A[G(t), d] \quad (43)$$

In (43) A is an arbitrary algorithm, operator, or transformation, which can be algebraic or dynamic, as well as, linear or non-linear. The operator A is a mapping from the product of the bit function space and the data space to the symbol space. A simple example of the operator A can be given by the expression (44):

$$\begin{aligned} s(t) &= G'(t)d \\ &= g_1(t)d_1 + g_2(t)d_2 + \dots + g_m(t)d_m \end{aligned} \quad (44)$$

The notation ' indicates the transpose of the column vector $G(t)$. Equation (44) is not a linear combination in the strict sense. The coefficients in (44) are not real numbers; they are only 0-1 integers. We will call this algorithm as a 0-1 addition algorithm. In this paper (44) will define the fm transmitter.

When all bits are zeros, expression (44) does not produce a meaningful symbol. To circumvent this problem we use a special, predefined analytic function, consistent with the technology presented here, to represent the symbol when all bits are zeros. The receiver will first test for the presence or absence of this special function, to detect the transmitted data corresponding to all zero bits, before using the standard algorithm discussed later.

We see that excepting the zero bits case the bit values are directly used to create the symbols in our fm method. In fm method the expression (44) or the general algorithm (43) physically imbeds the bit values in the symbol function. The bits directly modify the symbols as the processor creates the symbol one bit after another by adding the corresponding bit functions to the partially generated symbol. We do not arbitrarily assign the symbols to bit patterns generated by the bits in the data packets. However, these arbitrary assignments are also perfectly feasible and meaningful operation in fm case. All we are doing is that we are using analytic functions to bit patterns. We are choosing these analytic functions in such a way, as shown later, that the symbols remain analytic even at the inter-symbol interfaces.

On a side note, we observe that this 0-1 addition process has a very interesting mathematical consequence. This fm approach can be used to invert the algebraic addition process. That is, if we add two numbers, say 2 and 3 to produce 5, then given 5 we can find out which two numbers were added. Representing the integers 0 through 9 by 10 different continuous functions we can do this. Zero may be represented by zero function. This concept can generate interesting consequences in mathematical Group theory.

The fm transmitter concept may appear similar to the Orthogonal Frequency Division Multiplexing (OFDM) concept [17]. But there are some major differences. OFDM

uses one or more of the three basic modulation methods (ASK, FSK, and PSK) from the existing technology, fm does not. OFDM method configures the spectrum bandwidth into disjoint regions but fm does not. In fm every bit function spans the entire bandwidth of the channel. OFDM uses only harmonically related sinusoidal orthogonal functions; fm does not need to use any orthogonal function. fm can use non-sinusoidal orthogonal functions as well as non-orthogonal functions, OFDM cannot. However, under certain restrictive conditions OFDM is considered as a special case of fm technique. If we select only sinusoidal and harmonically related orthogonal bit functions, use only amplitude modulation with zero or full signal variation, and use 0-1 addition algorithm, then fm is same as OFDM.

B. The fm Receiver

At the receiver we will receive the symbol function $s(t)$ as generated in Fig. 2, corrupted by the noise and/or the nonlinearities of the communication channel. Our objective at the receiver will be to find out which bit functions from the bit function space $G(t)$ were used to generate the received symbol. That is, we have to decompose the received symbol into the component bit functions. The presence or absence of a bit function in the received symbol will indicate 1 or 0 value, respectively, for the bit at the corresponding bit location.

A set of bit functions $G(t)$ is orthogonal if the following integral (45) holds:

$$\int_0^T g_j(t)g_i(t)dt = 0, \quad i \neq j, \quad i, j = 1..m \quad (45)$$

Observe that we have defined orthogonality over finite time interval $[0, T]$.

All sinusoidal functions are orthogonal over infinite time interval. Only harmonically related sinusoidal functions are orthogonal over a finite time interval. It is easy to verify, using the above relation, that the two sinusoidal functions with frequencies 1000 Hz and 1100 Hz are not orthogonal over the period 1/1000 seconds or 1/1100 seconds. It is also well known [18] that there are infinitely many, band-limited, non-sinusoidal, orthogonal functions over a finite time interval. However there are only a finitely many band limited sinusoidal orthogonal functions over a given finite time interval.

The 0-1 addition formula gives the expression for the received symbol, $r(t)$, as shown below. The following (46) is a derived from (44).

$$r(t) = g_1(t)x_1 + g_2(t)x_2 + \dots + g_m(t)x_m + w(t) \quad (46)$$

Here, $w(t)$ is an Additive White Gaussian Noise (AWGN) process, $\{x_i\}$ are the bit values, unknown to the receiver but known to the transmitter and are equal to $\{d_i\}$. Thus x_i can be 0 or 1 only. If we assume that the bit functions in $G(t)$ are orthogonal then we can find x_i using the following simple relation (47):

$$x_i = \int_0^T r(t)g_i(t) dt + w_i, \quad i = 1..m \quad (47)$$

In above w_i is the projection of $w(t)$ over $g_i(t)$. We can set the bit values d_i using the relation (48) given below:

$$d_i = \begin{cases} 1, & x > 0 \\ 0, & \text{otherwise} \end{cases} \quad i = 1..m \quad (48)$$

A fm receiver design [19] that uses orthogonal functions is shown in Fig. 3.

From the above receiver figure we can also see that we are really detecting the bits. Every output line gives the values of a bit of the entire bit pattern that we have transmitted using one symbol. If we fail to detect one of the functions in the decomposition process, then we will make errors in the detection of that bit. Thus real Bit Error Rate (BER) will happen in this fm method. It is not that we are converting the symbol detection error into BER using some artificial relations.

Fig. 3 is identical to a standard figure in many communication textbooks. However it has a few significant differences also. Notice that it has only m parallel paths as opposed to 2^m parallel paths found [20, p. 135] in the existing methods. The output from each correlator is the bit value of the corresponding bit location, which is not the case in conventional methods. In conventional methods only one of the boxes produces an output indicating a symbol match in the corresponding path. You can also find a similar figure in textbooks that use orthogonal functions [20, p. 135] and that has m parallel paths. In that figure the output of each path is a real number. In Fig. 3 the outputs are only 0 or 1 integers representing the actual bit values.

Fig. 3 and equation (46) show that for the fm method, based on orthogonal functions, we need to search over only m functions in the bit function space as opposed to 2^m symbols in the symbol space. Thus the orthogonal fm method can significantly reduce the complexity of the receiver design. The introduction of the bit function space in between the symbol space and the data space helps us to achieve this interesting result. This concept indicates that the fm method has very high capacity. The dimension of the bit function space is m , because this space has m

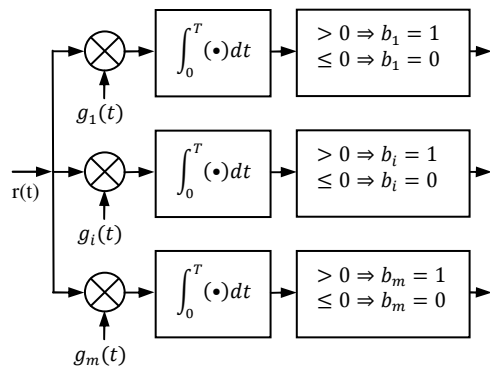


Figure 3. fm Receiver with orthogonal functions

independent functions. On the other hand the dimension of the symbol space is 2^m because it is defined by the 2^m number of independent symbols.

The receiver design for the non-orthogonal case is quite complicated and involved. The design is not unique also. In the remaining part of this section we describe one numerical algorithm or approach for the design of a fm receiver that uses 0-1 addition algorithm and non-orthogonal set $G(t)$. All the bit functions, $\{g_i(t)\}$, are in this case analytic and independent only. The set $G(t)$ is known to both the receiver and the transmitter. Given the information in (46) our problem at the receiver is, again, to solve (46) for 0-1 integer values for the unknown variables $\{x_i\}$.

Note that, in this formulation, the problem (46) is not really a classical 0-1 Integer Programming Problem (IPP). There is no optimization function associated with the equality expression (46). There is a random noise variable in (46) which is also not found in the standard IPP. Also the coefficients in (46) are not real numbers but functions of time.

There are various methods available in the scientific and engineering literature for solving the above receiver problem. In this paper we discuss only one of them. We convert the problem (46) to a least square solution problem by sampling, at fixed intervals, all the signals n times over the symbol period $[0,T]$, where n is an integer greater than or equal to m . Thus (46) can be expressed by the set of simultaneous equations (49):

$$\begin{bmatrix} r(t_1) \\ r(t_2) \\ \vdots \\ r(t_n) \end{bmatrix} = \begin{bmatrix} g_1(t_1) & g_2(t_1) & \dots & g_m(t_1) \\ g_1(t_2) & g_2(t_2) & \dots & g_m(t_2) \\ \vdots & \vdots & \ddots & \vdots \\ g_1(t_n) & g_2(t_n) & \dots & g_m(t_n) \end{bmatrix} \begin{bmatrix} x_1 \\ x_2 \\ \vdots \\ x_m \end{bmatrix} + \begin{bmatrix} w(t_1) \\ w(t_2) \\ \vdots \\ w(t_n) \end{bmatrix} \quad (49)$$

Here, $\{t_1, t_2, \dots, t_n\}$ are equally spaced sample points inside the time interval $[0,T]$. We will assume n is larger than m giving us more equations than the number of unknown variables m . Using the matrix notation the problem defined by (49) can then be rewritten as in (50).

$$r = Ax + w \quad (50)$$

Since $G(t)$ is a set of functions with analytical expressions they can be sampled any number of times. This is assured by the sampling Theorem 1. The length of the vector r can also be increased by interpolation between real samples obtained from Analog to Digital Converters (ADC). Thus the number of samples need not depend on the sample rate of the ADC or on other electronics in the receiver. This is one of the advantages of using the software radio approach discussed before. We can always get more number of equations than the number of unknowns giving us a better least square solution for (50).

In (50) r and w are n -column vectors with components consisting of n samples of the functions $r(t)$ and the AWGN process $w(t)$, respectively. A is a $n \times m$ rectangular matrix

with elements defined by (51), and x is the unknown 0-1 column vector $[x_1, x_2, \dots, x_m]'$ taken from $\{x_i\}$.

$$a_{ij} = g_j(t_i), i = 1..n, j = 1..m, t_i \in [0, T], n > m \quad (51)$$

Since the functions in the set $\{g_i(t)\}$ are independent the matrix A with elements defined by (51) is a full rank matrix. Therefore $A'A$ is non-singular and the real valued solution of (50) can be expressed using the pseudo inverse P of A [21] as given by (52):

$$x = Pr = (A'A)^{-1}A'r, \text{ where } P = (A'A)^{-1}A' \quad (52)$$

The bit values $\{d_i\}$ can then be obtained by the decision logic (53):

$$d_i = \begin{cases} 1, & x_i > \beta \\ 0, & \text{otherwise} \end{cases} \quad i = 1..m \quad (53)$$

The threshold value β is a given constant representing the channel characteristics.

The pseudo inverse gives a least square error solution of the simultaneous linear equation (50). It essentially curve fits the received symbol function $r(t)$ using the bit functions of the set $G(t)$. Note that the matrix P is constant for a given fm system, that is, when $G(t)$ is given. Therefore it is known to the receiver and can be precomputed and stored in memory. The accuracy of the fm system can be controlled by controlling the number of samples, n , for each function. The number of samples does not have to be the real samples from the ADC device. We can create an analytic function to interpolate the ADC samples and then derive as many samples as we want from the analytic expression. More details of the fm receiver with non-orthogonal functions can be found in [13].

C. Fourier Series and the fm Concept

The fm system can be considered as an implementation of the Fourier series. This interpretation will reveal many features of fm system. As we have mentioned before any continuous function defined over finite time interval can be expressed [5] by the Fourier series (54):

$$f(t) = \sum_{i=1}^{\infty} a_i \varphi_i(t), \quad \forall t \in [0, T] \quad (54)$$

Where $\{\varphi_i(t)\}$ satisfying (55)

$$\langle \varphi_i, \varphi_j \rangle = \delta_{ij} = \begin{cases} 0 & \text{if } i \neq j \\ 1 & \text{if } i = j \end{cases} \quad (55)$$

are orthonormal functions and defined over $[0, T]$. From (54) a finite term Fourier series (56) can be expressed as:

$$f(t) = \sum_{i=1}^m a_i \varphi_i(t), \quad \forall t \in [0, T] \quad (56)$$

We also know that given the orthonormal functions $\{\varphi_i(t)\}$ and the function $f(t)$ we can find the real valued coefficients $\{a_i\}$ of (56) using the following equation (57)

$$a_i = \int_0^T f(t) \varphi_i(t) dt, \quad i = 1..m \quad (57)$$

If we now assume that $\{\varphi_i(t)\}$ in (56) are the given orthonormal bit functions of the fm method, and $\{a_i\}$ are the 0-1 bit values of the data pattern, then using (56) we can generate the function $f(t)$, which can be considered as a symbol for the bits $\{a_i\}$. Thus we see that the fm transmitter of Fig. 2 actually implements a finite term Fourier series given by (56). Also we can see from (56) that there is no limit on how many bits we can transmit using orthogonal fm transmitter. Again, this explanation shows that the fm method has very high capacity.

The limit in (56) is defined by the number of band limited orthonormal functions that can be found. The paper by Slepian [18] assures that there are infinite numbers of such functions. In the later sections we show that the capacity of a digital communication channel is indeed unbounded and limited only by our technology of the receiver.

In this context we also point out that it is not necessary to use orthonormal functions in the Fourier series expression (56). The series (56) can be valid even if we use independent functions, 0-1 coefficients, and finite number of terms. We will still be able to extract the bits as shown before. Thus we have proven that the very general class of functions can be used for digital communication. Now we show how we have implemented the fm system in real life using real hardware.

D. A Real Life Implementation

The fm system has been tested [13] in a real engineering environment. In this section we briefly describe the hardware board, experimental setup, and the results of this practical real life test. We also discuss our global or system level approach to signal processing.

The block diagram of this off-the-shelf hardware boards that we found is described by Fig. 4. These are two identical TMS320C5402 DSP boards [22] from Texas Instruments (TI). Each board has a telephone line interface with a Data Access Arrangements (DAA) Integrated Circuit (IC). This DAA takes care of the voltage conditions and protection of the telephone line. The TLC320AD50 is an IC codec and contains both an Analog to Digital Converter (ADC) and a Digital to Analog Converter (DAC). This IC is the interface between the DSP and the analog world.

The board has a printer parallel port for interfacing with the computer. Via this printer port we control the boards using the TI Code Composer Studio (CCS) [23] software development tools. These boards allow us to perform the real time experiment on the Plain Old Telephone System (POTS) network.

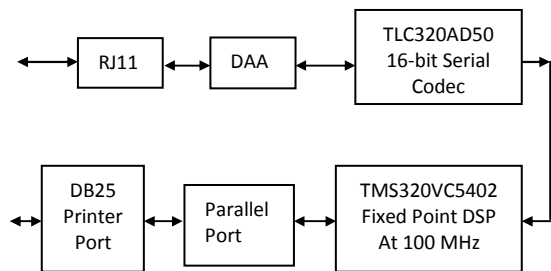


Figure 4. HW board functional block diagram

For this experiment we operate the codec for both receiver and transmitter at 16 kHz sample rate with 16-bit data resolutions. The symbol duration used was one millisecond. Only the transmission and reception of symbols via the telephone line are performed in real time using the hardware boards. The symbol creation and the symbol analysis functions are performed off line using Mathematica and Matlab software tools.

The experimental setup is shown in Fig. 5. We assemble everything, both transmitter and receiver, in one laboratory room with two telephone sockets having two different telephone numbers. The two DSP boards are connected to the telephone lines and to two computers to control them.

The bit functions shown in Fig. 6 and Fig. 7 are used to generate the symbol corresponding to the bit pattern 1011. This transmitted symbol is shown in Fig. 8. We transmit this symbol using our laboratory setup and capture the received signal, shown in Fig. 9, at the receiver end.

To synchronize the received signal we perform linear interpolation and up sampling. These two activities actually increase the resolution of the function. Synchronization is really very simple in batch data processing approach using a digital signal processor. This approach does allow you to do what you think and can visualize in your imaginary eyes. If you see the symbol on your oscilloscope, and think what you want to do to it, you can do exactly that in real time on the computer memory buffer. Remember that there are no clocks and PLL involved here. Using this method we find

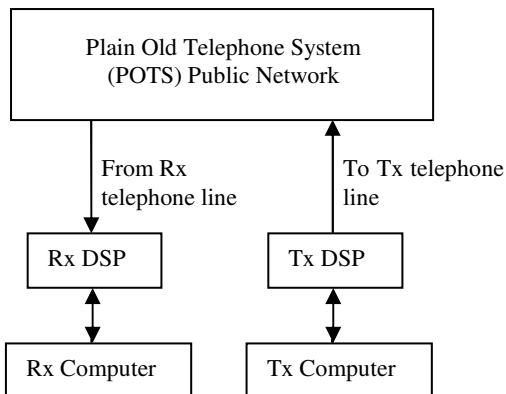


Figure 5. fm validation system

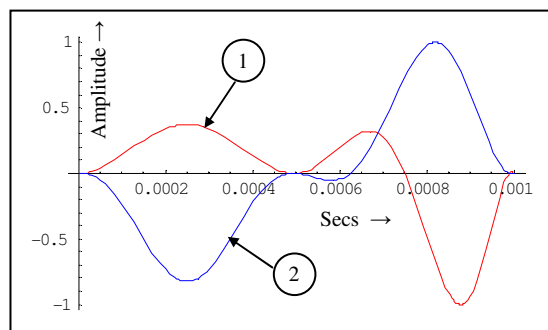


Figure 6. Bit-Functions 1 and 2

the exact zero crossing points by removing the required number of samples from both ends to make the received symbol start and end very close to the time axis. Finally we use (52) to solve for the least square curve fitting problem for 17 samples. The result is the following values for the unknown variables $\{x_i\}$:

{1.8653, 0.45037, 1.03662, 0.851587}

A threshold value of 0.5 for β in (53) gives the bit values for correct transmitted data, 1011.

Even though we encounter severe non-linear distortions we are still able to recover the bits correctly using only 17 samples. The experiment shows that the curve fitting method, using the bit functions along with the 0-1 addition algorithm, is indeed very robust. Note that it is also the availability of the entire data history that played a very important role in extracting the information.

As we can see from the figures the received signal has two positive peaks as opposed to three positive peaks in the transmitted signal. As if the second trough of the transmitted signal got folded up in the received signal.

It is clear that the conventional signal recovery methods, that use local concepts, no matter how many samples we take, cannot bring the received signal back to the transmitted form. However, a global approach or a systems approach, where we use the knowledge of the entire system can definitely help. We used the same sine wave frequencies of the transmitter, to interpolate the samples at the receiver. Here, of course, the high sample rate played an

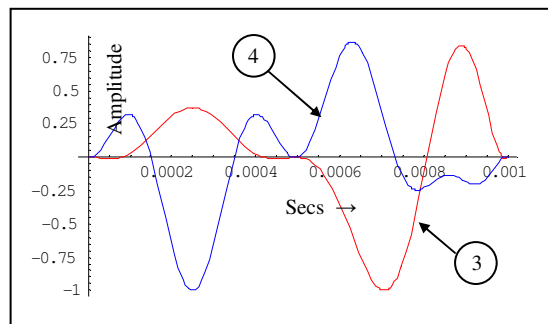


Figure 7. Bit-Functions 3 and 4

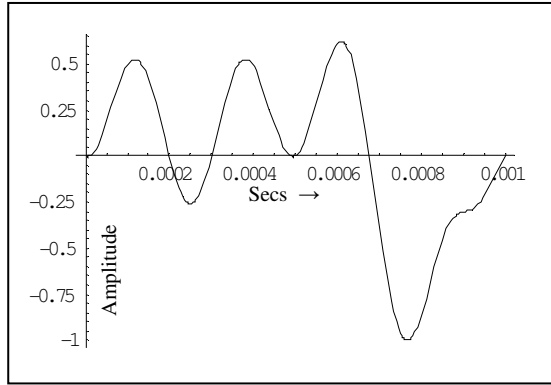


Figure 8. Transmitted fm symbol

important role in the least square interpolation method. The details of the signal processing, is quite involved, and is not given here. The large sample rate and the systems approach helped us to bring the received signal back to a shape that is very close to the transmitted signal, as shown in Fig. 10, which allowed us to detect the bits correctly. We can see that a total system level or global approach in signal processing can perform real miracles.

It should be mentioned that we performed these experiments over long period of time. During this trial and error period we developed the algorithm and the software discussed in this paper. In these lab experiments a series of concatenated symbols were transmitted using many different kinds of bit functions. In this paper we presented a specific case in a simple form for clear explanation. With a better hardware and software the algorithm presented here can be easily implemented online. Once the new hardware and the embedded environment become available we will present the results of real time high speed case. We are working on that direction now. Understandably, we are at a very early stage in terms of our real life implementation for a marketable product.

E. The fm Characteristics

The Power Spectral Density (PSD) of symbol $s(t)$ in

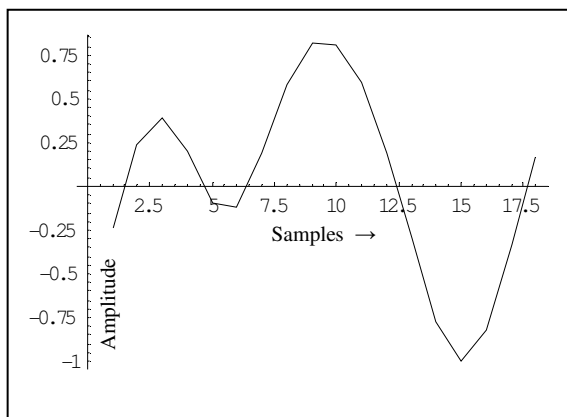


Figure 9. Received fm symbol

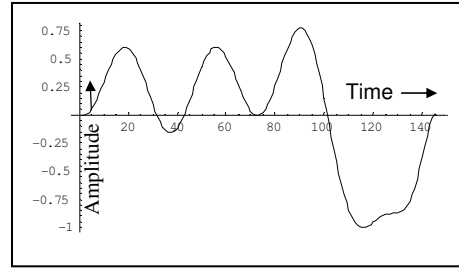


Figure 10. Best fit of the received symbol

Fig. 2 and the Bit Error Rate (BER) expressions have been derived. The BER has been derived for the case of orthogonal functions only. The PSD expression is valid for both orthogonal and non-orthogonal functions as bit functions.

The expression (58) generates the complete symbol stream $s(t)$ for the 0-1 addition algorithm and for all time t of the infinite interval:

$$s(t) = \frac{1}{m} \sum_{k=-\infty}^{\infty} \sum_{i=1}^m d_i(k) g_i(t - kT) \tag{58}$$

The factor m was introduced to normalize the amplitude of the symbol. Since each bit function is normalized, the addition of m bit functions requires renormalization by m . Note that d_i is the bit value, 0 or 1, and is not the multilevel value of the data element even though we are considering m -bit data. Also note that there is no constant pulse shaping signal associated with the symbol stream. The bit functions replaced them. It is interesting to observe that the structure of the above mathematical expression is similar to that of the standard OFDM [17, pp. 5-8].

Define the bit correlation function by (59)

$$R_{kl}(p, q) = E[d_k(p)d_l^*(q)] \tag{59}$$

and its two sided FT by (60)

$$C_{kl}(v, w) = \sum_{p=-\infty}^{\infty} \sum_{q=-\infty}^{\infty} R_{kl}(p, q) e^{-j2\pi vpT} e^{-j2\pi wqT} \tag{60}$$

Using the above two definitions and substituting $G(f)$ as the FT of $g(t)$, the PSD can be represented by (61):

$$S(f) = \frac{1}{m^2} \sum_{k=1}^m \sum_{l=1}^m C_{kl}(-f, f) G_k^*(f) G_l(f) \tag{61}$$

Although (58) is similar to OFDM, the final expression (61) for S is quite different. Here we have reused the symbol G with different meaning and we hope that the context helps to prevent confusions, if any. The absence of periodic pulses in (58) removed all discrete terms from the expression (61).

As an example of the PSD result, we use the following sinusoidal functions as defined by (62), used in Multiple Phase Shift Keying (MPSK) systems, as the bit functions in fm system:

$$g_k(t) = A \cos(2\pi f_c t + \theta_k), \quad -T/2 \leq t \leq T/2 \tag{62}$$

Substituting the above sine functions in (61) and performing some algebraic simplifications, we can arrive at the following PSD expression (63) for this case of fm scheme.

$$S_{fm}(f) = \left(\frac{AT}{2}\right)^2 \left(m \frac{\sin \pi f m T}{\pi f m T}\right)^2 \quad (63)$$

Comparing the above PSD expression with that of the MPSK [24] system, given below by (64),

$$S_{MPSK}(f) = A^2 T \left(\frac{\sin \pi f T}{\pi f T}\right)^2 \quad (64)$$

we see that the fm spectrum requirement is narrower as m increases. The PSD graphs of the two systems are plotted in Fig. 11. The graphs for fm system are plotted for four different bit data length m . If we use the band-limited orthonormal functions as designed in this paper, then the bandwidth requirements can be further reduced. It is also well known [25] that the band-limited functions do not create inter symbol interference.

We summarize the BER result here for the orthogonal case only. Consider one of the parallel paths of the orthogonal fm detection method presented in Fig. 3. The transmitted symbol $s(t)$ in fm modulation scheme using orthogonal functions can be derived from Fig. 2 and expressed by (65):

$$s(t) = \sum_{i=1}^m x_i \sqrt{E_i} g_i(t) \quad (65)$$

In the above expression we assume that x_i is -1 if the bit is zero and +1 if the bit is one, $\{g_i\}$ is the set of m orthonormal functions and $\{E_i\}$ is the energy of the orthonormal signal for bit i . Using the above expression we can show that the BER probability is given by (66):

$$P_{Bi} = Q \left(\sqrt{\frac{2E_i}{N_0}} \right) \quad (66)$$

The above result shows that the BER for the orthogonal fm receiver is same as that of the BPSK scheme. It is well known [20] that BPSK gives the lowest possible BER in all of the existing communication schemes.

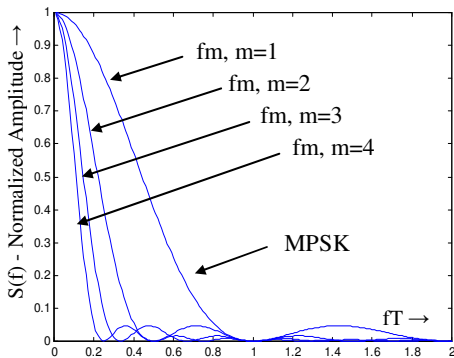


Figure 11. PSD comparison

V. CONSTRAINED GRAM SCHMIDT

It should be realized by now that the function modulation method requires a systematic approach for generating wave forms suitable for the concepts presented here. We use the words waveforms, functions, bit functions, and symbols interchangeably.

One of the major constraints that all waveforms must satisfy is the band limited property. The band limited property requires that the functions cannot have any discontinuity or sharp edges during the symbol period and also at the inter-symbol interfaces. The functions should be analytic if possible, that is, they will have smooth and continuous derivatives of all order. The orthogonality is another important requirement for the design of a simpler fm system. Otherwise all functions must be independent over the interval $[0, T]$.

In this section, we describe a very general method, called Constrained Gram Schmidt (CGS) method, for generating band-limited orthonormal functions over $[0, T]$. We qualify the method as constrained because in addition to orthogonality, the functions satisfy many constraints, appropriate for digital communication. The method can be used for constrained independent functions also.

There are many methods of generating orthogonal functions. The methods in [21] cannot produce orthogonal functions with any kind of constraints on the nature of the resulting functions. A method for generating band-limited orthogonal functions, which are orthogonal over the finite symbol time interval, has been presented in [18]. However, that method also does not allow us to control the characteristics of the orthogonal functions it produces. Reference [26] describes a modem implementation method using the orthogonal functions of [18]. Chang [25] gives a method of generating band-limited orthogonal functions, which are orthogonal over infinite time interval. Again his method also does not allow us to use constraints on the functions. In the following paragraphs, we briefly describe the CGS method. There are many possible variations of CGS, which are not explored in this paper.

Let C^1 denote the class of all real valued continuous functions, with continuous first order derivatives, defined over the finite symbol time interval $[0, T]$. Let $F(t) = \{f_i(t) \in C^1, t \in [0, T]\}$ be a set of linearly independent functions with inner product defined by (67):

$$(f_i, f_j) = \int_0^T f_i(t) f_j(t) dt \quad (67)$$

The Gram Schmidt Orthogonalization (GSO) method as described in [10] is given by the equations in (68)

$$\begin{aligned} g_1(t) &= f_1(t) \\ g_n(t) &= f_n(t) + a_{n1}f_1(t) + a_{n2}f_2(t) + \dots + a_{n-1}f_{n-1}(t), \quad n \geq 2 \end{aligned} \quad (68)$$

where the set of coefficients $\{a_i\}$ is obtained from the solution of the linear simultaneous equations (69):

$$b = Fa \quad (69)$$

Here b is a $n-1$ column vector with i -th element equal to the inner product (g_n, f_i) , a is the $n-1$ column vector of unknown coefficients $[a_1, a_2, \dots, a_{n-1}]'$, and F is a square matrix of size $n-1$ with ij -th element given by the inner product (f_i, f_j) . Our constrained approach extends the method defined by (69).

Communication channels require many different types of constraints on the symbols. Some of these requirements are stated below. The symbols (i) must join smoothly at inter-symbol boundary points, (ii) must not introduce any dc bias, and (iii) remain frequency band-limited. In addition the fm system may also need to use (iv) orthonormal functions.

Our objective is to generate a set of orthonormal functions $G(t) = \{g_i(t) \in C^1, i = 1 \dots m, t \in [0, T]\}$ from the set $F(t)$ that will satisfy the above and similar other requirements. It should be realized that it is not necessary that the elements of the function space be constrained to start with. During the process of transmission they can be dynamically adjusted to satisfy the above constraints in real time. However, the present formulation and the methodology are sufficient to keep the symbols constrained.

We express the bit functions as a linear combination of sinusoidal functions as shown in (70). Expressions (70) will ensure that the bit functions in $G(t)$ are analytic within the symbol interval $[0, T]$.

$$g_i(t) = \sum_{j=1}^{M_c} c_{ij} \sin(w_{ij}t + \phi_{ij}) \quad t \in [0, T] \quad (70)$$

In equation (70) $\{w_{ij}\}$ and $\{\phi_{ij}\}$ are some arbitrary and convenient choices for generating the functions. $\{w_{ij}\}$ must be within the channel bandwidth making sure that $G(t)$ is a band limited set. Each one of the functions in $\{g_i(t)\}$ are created using a different set of frequency parameters. Since each set of sine functions for each $g_i(t)$ are independent, their linear combinations are also independent making $G(t)$ an independent set. The value of M_c will depend on the number of constraints defined below by (71-75).

The constant coefficients $\{c_{ij}\}$ of the linear combination in (70) are selected to satisfy a series of constraints. We only mention some of the constraints that appeared to be necessary for the proper operation of the fm system as defined in this paper. Different communication channel may require different set of constraints. However the general concept presented here still covers many possibilities. The functions selected in (70) are also not the only choices. Any set of band limited and independent functions can be used to start with.

To synchronize the symbols at the receiver we make the symbols start and end at zero value (70). A sufficient condition for that is to make the bit functions behave the same way. Thus we consider the constraints (71) on $G(t)$:

$$g_i(0) = 0, \quad g_i(T) = 0, \quad i = 1 \dots m \quad (71)$$

To make the symbols join smoothly we want to impose the following derivative constraints (72) at the two ends of the bit functions.

$$\frac{d}{dt}g_i(t)|_{t=0} = \alpha, \quad \frac{d}{dt}g_i(t)|_{t=T} = \alpha, \quad i = 1 \dots m \quad (72)$$

In (15) α is any real number. In this paper we will set $\alpha=0$ merely for convenience. It is clear that if we want further smoothness at the symbol interfaces we can force the higher order derivatives to similar constraints. The constraints (71) and (72) will ensure that the entire symbol stream given by (58) is analytic. They also prevent any kind of discrete variations at the inter-symbol interfaces.

In many situations it may be necessary to avoid biasing the communication channel by a Direct Current (DC) voltage. To implement that requirement we set the integrals (73) of all bit functions to zero:

$$\int_0^T g_i(t)dt = 0, \quad i = 1 \dots m \quad (73)$$

To be able to detect the symbols properly at the receiver we may need to make the symbols pass through some predefined points. We call them way points. This property (74) may also help to synchronize the symbols properly.

$$g_i(t_k) = a_k, \quad t_k \in [0, T], \quad k = 1..K_i, \quad i = 1..m \quad (74)$$

Here, $\{K_i\}$ denotes the number of way points for the i -th bit function and $\{a_k\}$ are some known choices.

If we want to generate orthogonal functions as bit functions then we include the constraints (75):

$$\int_0^T g_i(t)g_j(t)dt = 0 \quad i, j = 1..m, \quad i \neq j \quad (75)$$

Summarizing, the method for generating the bit functions is to substitute the expression for the bit function (70) into all the constraints (71-75) defined above. This substitution will produce several linear equations, similar to (69), for the set of unknown constants $\{c_{ij}\}$. This set of simultaneous equations can then be solved for the constants. These constant coefficients will then be substituted back in (70) to get the analytical expression for each bit function. Note that for each bit function we have to solve a different set of equations like (69). The above process generates $G(t)$ as an independent set of analytic functions with specified bandwidth.

We have used the constraints (71-74) to generate four non-orthogonal bit functions. That is, we did not use the orthogonality constraints defined by (75). These bit functions are shown in Fig. 6 and Fig. 7. By including the constraint (75) we have created constrained orthogonal functions shown in Fig. 12.

Constrained Gram Schmidt (CGS) is a very powerful method of constructing orthogonal functions. The original Gram Schmidt Orthogonalization (GSO) algorithm is very

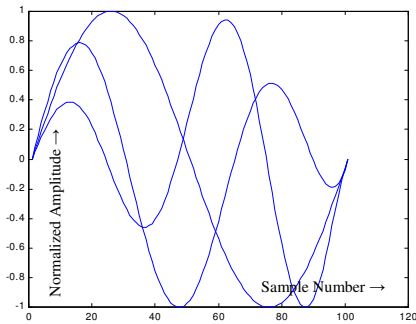


Figure 12. Constrained Orthogonal Functions

well known in literature. It is widely used for many communication problems, like Global Positioning Systems. However GSO was not enough for generating orthogonal functions with specific characteristics. We have extended GSO to CGS where you can create orthogonal functions with many additional properties. CGS will be very helpful in fm system for creating band limited orthogonal and non-orthogonal functions with desired properties.

VI. THE CAPACITY THEOREM

In this section we show that the function modulation method has higher capacity than the SHK methods. We also extend the Shannon's capacity theorem to a new higher capacity result and show that the fm method can be used to achieve such a capacity.

A. Infinity Assumption

Shannon presented his capacity theorem almost sixty years back. Lot of research has been done on this subject since then. During the early phase most of the focus was on finding alternatives [12] of sinc functions for the reconstruction of original function from the sample values. During the later phase it seems that the focus got shifted to dimensionality [27] aspect of the theorem. It appears that people have [28] assumed that T is constant and finite, which is not true. Shannon said in his paper [2] many times that T will go to infinite value in the limit. No one, it seems, has ever paid any attention to finite time issue of the engineering requirements. Recent research [29] has found that under certain assumptions ultra narrow band systems can produce capacity higher than that predicted Shannon. However the majority of research [30][31] work is now focused on comparing the performance of their systems using Shannon's theorem as a measure.

In this section we go back to the original theorem [2] and take a look at one of its core assumptions, the infinite time assumption, of the symbol duration. This subject was raised because we were sampling our symbols at a very high rate in our software radio approach. Apparently this violated the sampling theorem and the dimensionality theorem. To prove the general engineering practice of high sample rate we looked into the original theory, which eventually lead to

the capacity theorem. Both capacity and sampling theorems were presented in the same paper [2] by Shannon.

In the next few paragraphs we show how Shannon [2] used infinite time in the derivation of his capacity theorem. He used m to denote number of bits to be transmitted and M to represent the number of symbols. These two are related by the well known equation (76):

$$M = 2^m \quad (76)$$

This relationship is very important in digital communication engineering. As before, we point out that we do not transmit m bits, we transmit M symbols. From these M symbols we find out how many bits they represent using the above relation (76). Thus the focus of capacity theorem is not on the bits but on the symbols. How many symbols our receiver can detect is the main concern in the derivation of the capacity theorem.

After that, Shannon defines the capacity C using the symbol time T by (77):

$$C = \lim_{T \rightarrow \infty} \frac{\log_2 M}{T} \quad (77)$$

Thus clearly, his assumption is that T is very large and is going to go to infinity eventually. He writes near the above definition "... M different signal functions of duration T on a channel, ..". In another place he repeats, "There are 2^m such sequences, and each corresponds to a particular signal function of duration T ". Thus T is the symbol time and he assumes all his symbols are of infinite time durations.

Shannon's entire theory, derivation, and proof depend on this infinite time assumption. He writes "The transmitted signal will lie very close to the surface of the sphere of radius $\sqrt{2TW\bar{P}}$, since in a high-dimensional sphere nearly all the volume is very close to the surface". Here P is the average signal power and W is the channel bandwidth. He achieves high dimension by assuming T as very large. Thus his proof will be invalid if we assume that the symbol time T is finite and small.

An interesting observation can be derived as a result of his infinite time assumption. He writes "The quantity $TW \log(1+P/N)$ is, for large T , the number of bits that can be transmitted in time T ." This means that the bits cannot be recovered until the time T ends. Therefore bits/sec is not really meaningful here. Bits are not coming out of the system every second. He confirms "There will be, therefore, an overall delay of $2T$ seconds". Thus actually the receiver stops when T approaches infinity.

The total number of bits per symbol is infinity in Shannon's case. Because T is infinity in the expression for bits, as mentioned in the previous paragraph, $TW \log(1+P/N)$. It is true that any finite rate over infinite time will also give infinite bits. But we have shown that it is not happening here. Thus Shannon's result indicates – infinite capacity. We show that we have the same conclusion even over finite time interval.

A well explored statement in [2] is the following: “Then we can say that any function limited to the bandwidth W and the time interval T can be specified by giving 2WT numbers.” The number WT is actually infinity, because T is infinity. In the literature however, it has been presented as if it is a finite number [7, p. 93]. This finite interpretation to Shannon’s proof has generated a large volume of research papers similar to [12]. We have shown that the above finiteness interpretation violates a very well known and a fundamental mathematical theory that says all functions are infinite dimensional vectors even over finite and small time intervals and therefore cannot truly be represented by finitely many numbers. In this section we show that this infinite time assumption is not necessary.

B. The (P+N)/N Factor

Now we examine how Shannon [2] got the expression (P+N)/N in his capacity theorem. Here N is the average noise power, averaged over the symbol time T. The received signal power is P+N. The concept used in our geometric approach is actually deeply embedded in the geometric approach of [2].

Consider the ASK scenario shown in Fig. 13. The allowed amplitude levels are shown by two dashed lines. For every dashed line there is a band over which the amplitude can swing because of the noise in the channel. This band is shown by the continuous lines with width proportional to \sqrt{N} . The total number of symbols M, i.e. number of amplitudes, which can be transmitted, is then given by (78):

$$M = \frac{\text{Interval Height}}{\text{Band Height}} = \frac{OA}{BA} \tag{78}$$

Since the amplitude is proportional to the square root of power, the above expression reduces to (79):

$$M = \sqrt{\frac{P+N}{N}} \tag{79}$$

This is the maximum limit we can achieve, at this

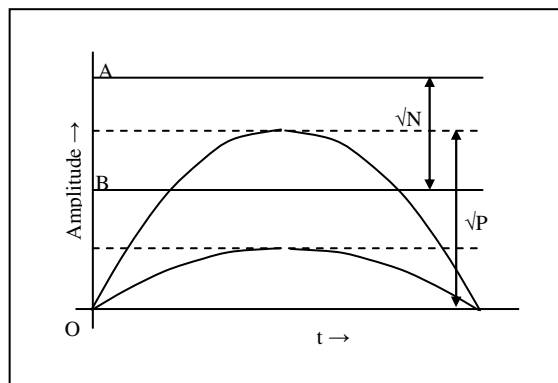


Figure 13. Discrete approach

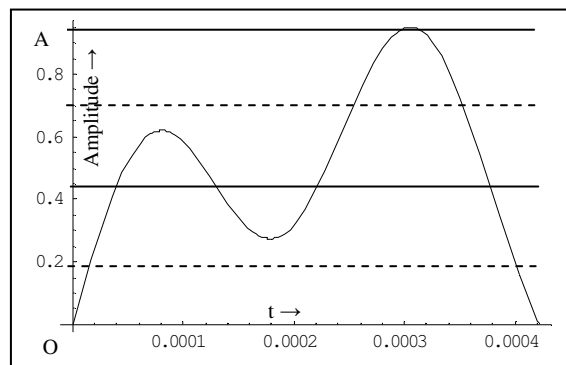


Figure 14. Analog approach

frequency for an ASK system. In a later section we consider all possible frequencies. In Fig. 13 we used: (A) Discrete bounds and (B) Sinusoidal functions. If we relax these two SHK conditions then we can significantly improve the capacity expression (79).

Consider Fig. 14 now, where we have relaxed both conditions mentioned above. In Fig. 14 we have shown only one general function. But you can imagine many such functions going up and down over the entire amplitude interval OA and crossing all bands many times. Fig. 15 shows many such allowed functions. Virtually there is no limit of the number of symbols or functions that can be transmitted or plotted and that can be distinguished also. These are the kind of functions fm uses. Thus higher capacity can be achieved by using the fm communication method as opposed to the discrete or the SHK methods.

Shannon has used such general class of functions in his derivation of capacity theorem. He wrote – “Actually, two signals can be reliably distinguished if they differ by only a small amount, provided this difference is sustained over a long period of time”.

From the above statement we can see that the noise bands can be modified to a new format as shown in Fig. 16. In this figure we show two fm symbols along with their noise bands or pipes around them. One important difference between the noise bands in fm and SHK methods is that in fm the noise band is dynamic and moves with the function and not static, discrete, or straight lines like in Fig. 13.

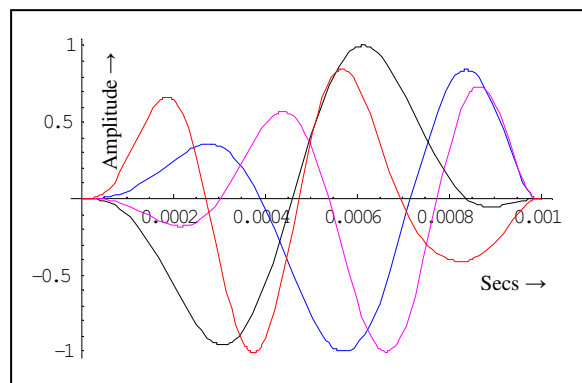


Figure 15. Bit-Functions for fm method

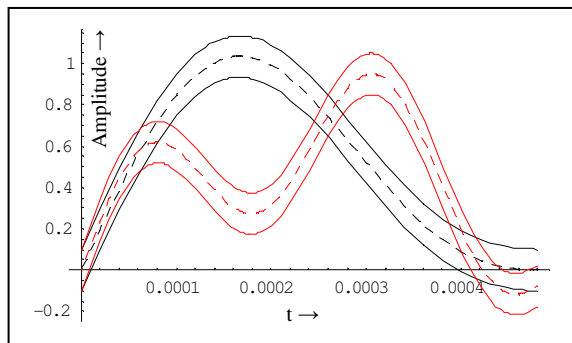


Figure 16. Noise bands

These fm bands are like transparent and flexible pipes around the functions. In fm one symbol can penetrate the noise band of another symbol. They can remain together for some duration and then get separated to distinguish themselves. This fm band is the minimum distance between two symbols. As long as the distance between two symbols is greater than this minimal distance, over only a small interval of time, the symbols will remain detectable. The important fact is that this concept of overlapping bands or flexible pipes around a function is not present in the SHK communication systems. This fact significantly increases the number of allowable symbols in the fm system.

Thus the capacity of fm method is much higher than the SHK methods and we show later that SHK cannot achieve Shannon’s limit but fm can.

C. The WT Factor

Now consider the signals used in Fig. 17 and ask the Shannon’s question [2] – “How many different signals can be distinguished at the receiving point in spite of the perturbations due to noise?” In this section we derive the same answer that he got but with the assumption that T is finite and small.

The approach is to configure the function space into small discrete rectangles, as shown in Fig. 18, and count all possible symbols that can pass through these rectangles. We

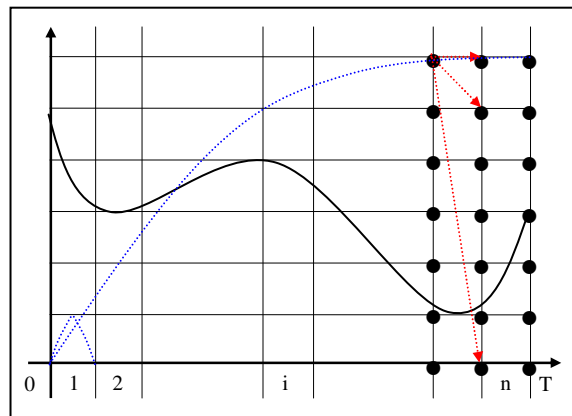


Figure 17. Nyquist sample intervals

divide the interval [0, T] on the x-axis into n equal parts. Where n is the number of samples and is equal to 2WT, because we are using the Nyquist sampling rate in this figure. The signal amplitude interval on the y-axis is $\sqrt{(P + N)}$ and is broken in to q number of y-subintervals, where $q = \sqrt{(P + N)/N}$. Thus the two dimensional plane becomes a grid of rectangular boxes. Each box can be considered to have a point through which only one detectable function can pass. Some of these points are shown, only in the last two vertical columns, to avoid too much clustering. The continuous line shows an example of a symbol function, which can pass through these dots.

We can connect any dot in one vertical column to any dot in the next or previous vertical column to create a portion of a function passing through these rectangles. The arrows in the figure show some such possible connections that the functions can take. These connection lines will not violate the bandwidth limit of the function, because the length of a t-subinterval is equal to the Nyquist length. Thus between two vertical columns there can be $qxq=q^2$ number of functions. Counting this way we can see that the total number of symbols, M, in the entire grid of Fig. 17, can be expressed by (80):

$$M = \left(\frac{\sqrt{P+N}}{N}\right) \left(\frac{\sqrt{P+N}}{N}\right) \dots \left(\frac{\sqrt{P+N}}{N}\right) \tag{80}$$

Since it has 2WT terms the above simplifies to (81):

$$M = \left(\frac{\sqrt{P+N}}{\sqrt{N}}\right)^{2WT} \tag{81}$$

This is the same factor in the capacity formula [2]. This construction process can be used to generate detectable band limited functions for the fm method proving that the fm can achieve the Shannon’s limit.

We have shown two sine functions using dashed lines in Fig. 18. One of them has the highest frequency and lowest detectable amplitude and the other one has the lowest frequency but highest possible amplitude. It is easy to see that if we use only ASK design then we can get qWT number of symbols. This is because for each frequency we get q number of amplitudes and there are WT numbers of full cycle sine functions possible over 2WT sample intervals. Although it is not known if there are any ASK system that uses these frequencies all at a time. We also see from this grid design and the graphs drawn that Fourier sine functions will not be able to cover all the grids the way general functions can. This gives a geometric proof that sinusoidal approach cannot achieve the Shannon’s capacity results.

In this subsection we provided a proof of Shannon’s theorem that did not require infinite time interval assumption. However in a small symbol time T the Nyquist rate will give very few samples and we will not be able to

recover a symbol as shown by examples in Fig. 1. Next we show how a higher sample rate enables us to detect more symbols thus increasing the capacity.

D. The Higher Sampling Rate

Assume as before that T is small and finite and we sample at k times the Nyquist rate, where k > 1. Therefore n on the x-axis of Fig. 17 is now equal to 2kWT. Since each t-subinterval is very small now, the noise energy due to N is also very small on these sub-intervals and therefore the equivalent noise band will be proportional to \sqrt{N}/k on these subintervals as shown in the Fig. 18. However, the range of total signal variation still remains $\sqrt{P+N}$ over the entire symbol time T. Thus the total number of y-axis intervals is $\sqrt{(P+N)}/(\sqrt{N}/k)$ and is equal to kq. So the grid is k times finer in both t and y axes.

In this finer grid any point on the vertical line for any t-subinterval cannot be connected to any point on the vertical line on the next or previous t-subinterval, because that will make the function rise much faster and violate the bandwidth condition. It is easy to understand, however, that a point in one t-subinterval can be connected to only q consecutive number of points in the next or previous t-subinterval without violating the bandwidth constraint.

If we consider any consecutive q rows then we can see that the situation is very similar to the Fig. 17. Since there are 2kWT numbers of columns, then the number of functions generated by any q horizontal block can be expressed by (82):

$$M = \left(\frac{\sqrt{P+N}}{\sqrt{N}}\right)^{2kWT} \tag{82}$$

This value when converted into bits/sec, using the formula (77) for capacity, will reduce to (83):

$$C > \frac{\log_2 M}{T} = kW \log_2 \left(\frac{P+N}{N}\right) \tag{83}$$

We have used greater than notation because we did not count all the functions in this finer grid. Although it is

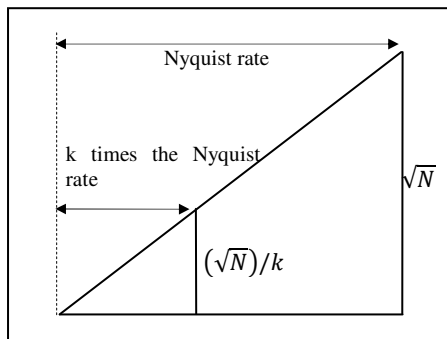


Figure 18. Noise at higher sample rate

possible to count all possible functions and get a very precise expression instead of (83). But that counting result may not lead to the well known and simple expression like (83). We are only interested in showing that the capacity depends on the sample rate and therefore theoretically can go to infinity. Expression (83) is only a lower bound. We can now state the following new capacity theorem:

Theorem 5: Assume that any arbitrary set {P, N, W, T, m} is given. Where P=signal power, N=channel noise power, W=channel bandwidth, T=finite symbol time, and m=number of bits per symbol. Then there exists a fm system, with m continuous and independent bit functions of the given bandwidth W, and a sample rate that is k times the Nyquist rate, with k > 1, which will satisfy the relation

$$m = kWT \log_2 \left(\frac{P+N}{N}\right) \tag{84}$$

Also, this resultant fm system will output m bits in every T seconds.

The statement of the above Theorem 5 is in many ways different from the original [2] statement. Most importantly it explicitly mentions the symbol time T in the statement. It should be noted that T is not infinity in our case. It is believed that the lack of such a mention of T in the original statement of Shannon created a lot of confusion in the literature. The Theorem 5 statement also describes a digital communication system for achieving such a capacity which was missing so far in the communication theory. Finally the statement essentially points out that the capacity is dependent on the technology, the sample rate.

We can see that the essential idea behind higher capacity is very similar to creating a high resolution camera. Higher the number of pixel in a digital camera better is the picture quality. In the communication case we are essentially resolving the two dimensional plane of the function space into a very high resolution grid by sampling at a very high rate.

Thus high rate sampling is equivalent to selecting a high resolution camera. This camera will allow us to see all the details of a function and thus giving the ability to detect more symbols. The result (83) is quite obvious and is expected also. Essentially we have reduced the noise by a factor of k, the sample rate, which thus produced higher capacity. In this context we should examine the definition of noise. It is actually dependent on the signal processing technology and the algorithms we use in our receiver. Thus in this sense our result is nothing new. If you can reduce the noise you can increase the capacity, which was obvious from the original Shannon's theorem. All we did is we brought out this noise factor k outside the capacity expression. However, we have also given a method, the fm method, for implementing the Shannon's theory, which was

missing so far in the literature. And finally of course the finite duration solution.

It is possible to come to the same conclusion (83), however, from another direction also. Slepian has shown [18] that there are infinitely many band limited orthogonal functions over a finite interval of time. These Slepian functions can be used in the fm method of Fig. 2 to transmit theoretically infinite number of bits. This has been described using the limit operation of the finite term Fourier series (56). We have also shown that it is not necessary to use orthonormal functions to get the same results. The series (56) can be valid for independent functions also.

Thinking philosophically, we can ask is the capacity really limited. If we look through our windows then we can see the nature outside, the blue sky, patches of clouds, mountains, trees, and plants. We can close and open our eyes and see the same view instantly. This is because our eyes and the brain working together as a receiver is immensely advanced and powerful. We have evolved over billions of years to this state of our mind, body, and soul. Thus the communication capacity of the air medium channel between the nature outside and our eyes is infinity. Assuming that is the definition of infinity, of course. The fm system presented here uses our state of the art technology. As our technology evolves we will get higher and higher capacity. The technology behind the digital camera is an example of one such step toward higher capacity. Thus it will be wrong to think that the capacity of a digital communication channel is limited and is independent of our technology.

E. Discussion

In this paper our focus is on the sampling theorem and the capacity theorem over finite duration signals. The main question we asked is how many samples we need for a finite duration signals. Our objective is not very much on how to reconstruct a finite duration signal from its samples, rather how many samples are necessary to correctly reconstruct a finite duration signal. We found that more you sample better will be your reconstruction. Or in the other words the original Nyquist rate is not good enough for recovery of signals of finite duration.

We approached the capacity theorem from the same angle. Original theory assumed that the symbols must be of infinite duration. We wanted to see what happens when symbols are of finite duration. To perform this analysis we used the finite duration sampling theorem.

Shannon's approach defines capacity as the number of symbols that a receiver can distinguish. We have also used the same concept in this paper. Thus the ability to distinguish symbols is the key issue of capacity. Clearly this then depends on what kind of symbols you are using in your system.

If we use general purpose independent functions then the ability to detect and distinguish will also depend on the computational power of the receiver. More sophisticated the

algorithm is more will be the demand on the processor power. However the demand on the ADC is not very important. We have shown that ADC does not have to be very fast. Internal sampling by interpolation can be very effectively used to increase the resolution. We have also discussed a global approach to signal processing. Thus computational power is not of immediate concern.

If we use orthogonal functions then our fm theory shows that computational burden is very low. All we have to do is to increase the number of parallel integrators in our Application Specific Integrated Circuit (ASIC). More symbols mean more integrators. Observe that in this orthogonal case, we have simplified the Shannon's approach by introducing the concept of bit functions. In orthogonal case we do not work on the symbol space but in the bit functions space which requires significantly lower number of integrators. This approach shows why capacity is higher in the orthogonal fm systems.

Because our present technology provides powerful processors, we now have very high computational capability. As a result we can revisit low bandwidth channels, like POTS, to provide high capacity data rate. The fm scheme and the algorithm presented here, based on software radio and global approach, essentially leads to that kind of direction. It is not always necessary to require high bandwidth channel to provide high capacity data rate. This fm theory can be used with all the existing theories. For example any compression algorithm can be used in conjunction with fm system to further enhance the performance. It may be possible to use many of the existing symbols in a fm scheme. It is also quite feasible to use fm symbols over a sinusoidal carrier.

The fm scheme is basically an analog approach for digital communication. All symbols in this scheme are just like continuous analog functions. No discrete concept is embedded in the symbol or in the symbol stream. Only transmitter and receivers are digital. Thus we are taking full advantage of the nature which is analog. We are not impinging any discrete disturbances in the analog world.

VII. THE SPHERE PACKING

Shannon represents [2] every symbol as a point in an n-dimensional Cartesian space. He used the entire set of Nyquist samples of a symbol as coordinates in this space. The total number of samples of a symbol is WT and increases as T increase. Thus the dimension of his space eventually increases to infinity. Since the power in each symbol is fixed all the symbols lie on the surface of a sphere of constant radius. This is because the sum of the square of the sample values is the power and is also is a measure of the distance from the origin. Thus every symbol is a point on the surface of the same sphere. Because of noise these symbols will become like a non-overlapping billiard ball centered on these points [32][33, pp. 655-659]. In this section we show another geometric representation, also in Cartesian

space, of a function using the infinite dimensionality concept of function space.

In Fig. 19 we show a function $f(t)$ taken from $C[a,b]$ space, the space of continuous functions. We consider the interval $[a,b]$ as finite and small in Fig. 19. Fig. 20 shows the corresponding representation of the function in a real n -dimensional space. Here n is any finite and fixed number, not necessarily large and is not going to infinity, its value can be two also.

We can partition the interval $[a,b]$ in many smaller subintervals as shown by marks in Fig. 19. Each such small subinterval can be sampled n times and can be represented by one point in the n -dimensional space, the same way Shannon did. Thus the interval $[a, t_1]$ of Fig. 19 is represented by the point t_1 in Fig. 20. There is no shortage of points in the function shown in Fig. 19. We have shown that infinite sample rate is meaningful because the function is infinite dimensional over any finite interval. The smaller the intervals are, larger will be the number of points in Fig. 20. If we join these points by a smooth line then we get the dashed line, which represents the function, as shown in Fig. 20.

We have also shown, by solid lines, how the noise band or pipe around the function can be represented in the same way in the n -dimensional space of Fig. 20. As mentioned, in Fig. 20 these pipes are now the symbols in the n -dimensional space. All these pipes, in the n -dimensional space, are flexible, transparent, and one pipe can penetrate or join another pipe for a period and then get separated. Contrary to sphere packing case of Shannon, where the spheres cannot overlap, in Fig. 20 we do not have that restriction. We can see now that the end points can indeed overlap and the functions will still be detectable. This flexibility of the pipes makes it possible to pack infinite number of pipes in the n -dimensional sphere. Thus proving that the capacity can be indeed infinity even when we use this n -dimensional geometric concept.

Fig. 19 and Fig. 20 are in some sense identical. Both are line graphs, one in two dimensional function space and the other one is in n -dimensional Cartesian space. Therefore it is really not necessary to go to Fig. 20 to analyze functions. It may be possible to analyze all aspects of a function using

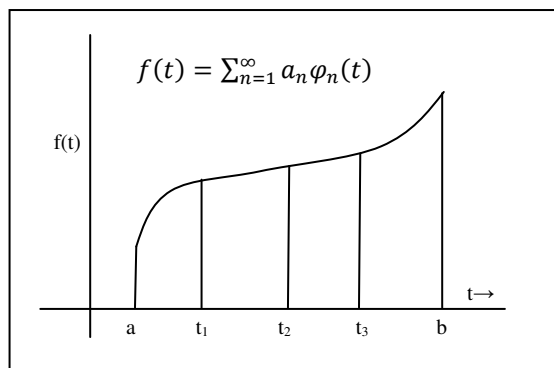


Figure 19. A function in $C[a,b]$

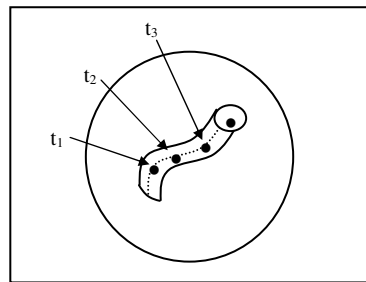


Figure 20. n -Dimensional view of a function from $C[a,b]$

Fig. 19. In some sense Fig. 19 has more information than Fig. 20. Fig. 20 represents only the coefficients of the infinite series or the sample values of the function. It does not contain the actual graph between the samples nor the orthogonal functions of the infinite Fourier series as in Fig. 19. We also point out again that the underlying concept used in this explanation is still based on infinite dimensionality property of function space.

VIII. CONCLUSION AND FUTURE WORK

In this paper we have presented an analysis of digital communication engineering using the theory of infinite dimensionality of function space. We have used non-sinusoidal symbols, finite duration theory, very high sample rate, and software radio approach to create a function modulation (fm) method. It is shown that this fm method can give much higher capacity than predicted by the original Shannon's theorem thus helping us to create a green modem.

The practical implementation of a high speed modem, based on the fm concept may require a large number of independent band limited functions. An in-depth research in that direction on a new powerful hardware is the next required milestone.

ACKNOWLEDGMENT

The first author is in many ways grateful for many suggestions and discussions with Pamela Das during the laboratory testing of the hardware implementation that helped to solve many problems. He is also deeply indebted to Hari Sankar Basak for his very careful and thorough review of the draft manuscripts at various stages of the research. It will be inappropriate not to acknowledge that the idea behind the Fig. 17 came from David Dyrnaes, a friend and colleague, during many discussions on the practical implementation of the fm concept.

REFERENCES

[1] S. Das, N. Mohanty, and A. Singh, "Capacity theorem for finite duration symbols", Proc. of IARIA International conference on networks, ICN 2009, Guadalupe, France, published by IEEE Press, 2009.

- [2] C. E. Shannon, "Communication in the presence of noise", Proc. IEEE, Vol. 86, No. 2, pp. 447-457, 1998.
- [3] S. Das, N. Mohanty, and A. Singh, "Is the Nyquist rate enough?", Proc. of IARIA Internaitoanl confercen on digital telecommunicaitons, ICDT 2008, Bucharest, Romania, published by IEEE Press, 2008.
- [4] P. A. Laplante, *Real-time systems design and analysis*, Third Edition, IEEE Press, New Jersey, 2004.
- [5] Y. Eideman, V. Milman, and A. Tzolomitis, *Functional analysis, an introduction*, Amer. Math. Soc, Providence, Rhode Island, 2004.
- [6] E. M. Vestrup, *The theory of measures and integration*, Wiley, New Jersey, 2003.
- [7] G. M. Phillips, *Interpolation and approximation by polynomials*, Can.Math.Soc., Springer, New York, 2003.
- [8] V. K. Ingle and J. G. Proakis, *Digital signal processing using Matlab*, Brooks/Cole, California, 2000.
- [9] T. M. Cover and J. A. Thomas, *Elements of information theory*, Second Edition, John Wiley, New Jersey, 2006.
- [10] R. Bellman, *Introduction to matrix analysis*, SIAM, Philadelphia, 1995.
- [11] N. Mohanty, *Signal processing*, Van Nostrand, NY, 1987.
- [12] L. W. Couch II, *Digital and analog communication systems*, Second Edition, Macmillan, NY, USA, 1987.
- [13] A. J. Jerri, "The Shannon sampling theorem, its various extensions and applications – a tutorial review", Proc. IEEE, Vol. 65, No. 11, 1977.
- [14] S. Das, N. Mohanty, and A. Singh, "A function modulation method for digital communications", Wireless telecommunications symposium, WTS 2007, Pomona, California, USA, published by IEEE Press, 2007.
- [15] J. Farlow, J. E. Hall, J. M. McDill, and B. H. West, *Differential equations linear algebra*, Prentice Hall, New Jersey, 2002.
- [16] C. C. Pugh, *Real mathematical analysis*, Springer, NY, 2002
- [17] J. Gibson, *The communication handbook*, CRC Press, Chapter 68, 2002.
- [18] D. Slepian, Some comments on Fourier analysis, uncertainty and modeling, SIAM Review, Vol. 25, pp. 378-393, Jul 1983.
- [19] S. Das and N. Mohanty, "A narrow band OFDM", IEEE vehicular technology conference, VTC Fall 2004, Los Angeles, California, USA, published by IEEE Press, 2004.
- [20] B. Sklar, *Digital communications fundamentals and applications*, Prentice Hall, NJ, USA, 1988.
- [21] G. H. Golub and C. F. Van Loan, *Matrix computation*, Third Edition, Johns Hopkins university press, pp. 236-264, 1996.
- [22] TMS320C5402 Hardware board, Texas instruments, Dallas, Texas, USA, 2001.
- [23] TMS320C5000 Code composer studio, Integrated development environment, V2.0, Texas instruments, Dallas, Texas, USA, 2001.
- [24] Fuqin Xiong, *Digital modulation techniques*, Artech House, Boston, USA, 2000.
- [25] R. W. Chang, "Synthesis of band-limited orthogonal signals for multichannel data transmission," Bell Syst. Tech. J., Vol 45, pp. 1775-1796, December 1966.
- [26] V. V. Loginov and V. A. Kochanov, "Implementing the high speed modem with multidimensional modulation using MS32c542 DSP," Spra321, Texas Instrument, September 1996.
- [27] D. Slepian, "On bandwidth", Proc. IEEE, Vol. 64, No. 3, pp. 379-393, March 1976.
- [28] A. D. Wyner and S. Shamai, "Introduction to communication in the presence of noise by C. E. Shannon", Proc. IEEE Vol.86, No.2, pp. 442-446, 1998.
- [29] F. Man and W. Lenan, "Extension to Shannon's channel capacity – The Experimental Verification", Proc. ISISPCS, Nov 2007, China, published by IEEE Press, 2007.
- [30] P. Stocia, Y. Jiang, and J. Li, "On MIMO channel capacity: an intuitive discussion", IEEE, Sign.Proc.Mag., May 2005.
- [31] Jun Wang, Shi-hua Zhu, and Lei Wang, "On the channel capacity of MJMO-OFDM systems", Proc. ISCIT 2005, published by IEEE Press, 2005.
- [32] T. D. Schneider, "Claude Shannon: biologist", IEEE Eng. Med. Bio. Mag., Feb. 2006.
- [33] B. P. Lathi, *Modern digital and analog communication systems*, Third edition, Oxford University Press, 1998.

Video Quality Assessment as Impacted by Video Content over Wireless Networks

Asiya Khan, Lingfen Sun and Emmanuel Ifeachor

Centre for Signal Processing and Multimedia Communication

School of Computing, Communications and Electronics

University of Plymouth, Plymouth PL4 8AA, UK.

e-mail: (asiya.khan, l.sun, e.ifeachor)@plymouth.ac.uk

Abstract—The primary aim of this paper is to assess video quality for all content types as affected by Quality of Service (QoS) parameters both in the application and network level. Video streaming is a promising multimedia application and is gaining popularity over wireless/mobile communications. The quality of the video depends heavily on the type of content. The contributions of this paper are threefold. First, video sequences are classified into groups representing different content types using cluster analysis based on the spatial (edges) and temporal (movement) feature extraction. Second, we conducted experiments to investigate the impact of packet loss on video contents and hence find the threshold in terms of upper, medium and lower quality boundary at which users' perception of service quality is acceptable. Finally, to identify the minimum send bitrate to meet Quality of Service (QoS) requirements (e.g. to reach communication quality with Mean Opinion Score (MOS) greater than 3.5) for the different content types over wireless networks. We tested 12 different video clips reflecting different content types. We chose Peak-Signal-to-Noise-Ratio (PSNR) and decodable frame rate (Q) as end-to-end video quality metrics and MPEG4 as the video codec. From our experiments we found that video contents with high Spatio-Temporal (ST) activity are very sensitive to packet loss compared to those with low ST-activity. Further, content providers usually send video at highest bitrate resulting in over provisioning. Through our experiments we have established that sending video beyond a certain bitrate does not add any value to improving the quality. The work should help optimizing bandwidth allocation for specific content in content delivery networks.

Keywords—QoS, MPEG4, video content classification, video quality evaluation, wireless communication

I. INTRODUCTION

The current trends in the development and convergence of wireless internet IEEE802.11 applications and mobile systems are seen as the next step in mobile/wireless broadband evolution. Multimedia services are becoming commonplace across different transmission platforms such as Wi-Max, 802.11 standards, 3G mobile, etc. Users' demand of the quality of streaming service is very much content dependent. Streaming video quality is dependent on the intrinsic attribute of the content. For example, users request high video quality for fast moving contents like sports, movies, etc. compared to slow moving like news broadcasts, etc. where to understand the content is of more importance. The future internet architecture will need to support various applications with different QoS (Quality of service) requirements [1]. QoS of multimedia

communication is affected both by the network level and application level parameters [2]. In the application level QoS is driven by factors such as resolution, frame rate, colour, video codec type, audio codec type, etc. The network level introduces impairments such as delay, cumulative inter-frame jitter, burstiness, latency, packet loss, etc.

Video quality can be evaluated either subjectively or based on objective parameters. Subjective quality is the users' perception of service quality (ITU-T P.800) [3]. The most widely used metric is the Mean Opinion Score (MOS). Subjective quality is the most reliable method however, it is time consuming and expensive and hence, the need for an objective method that produces results comparable with those of subjective testing. Objective measurements can be performed in an intrusive or non-intrusive way. Intrusive measurements require access to the source. They compare the impaired videos to the original ones. Full reference and reduced reference video quality measurements are both intrusive [4]. Quality metrics such as Peak-Signal-to-Noise-Ratio (PSNR), VQM [5] and PEVQ [6] are full reference metrics. VQM and PEVQ are commercially used and are not publicly available. Non-intrusive methods (reference-free), on the other hand do not require access to the source video. Non-intrusive methods are either signal or parameter based. More recently the Q value [7] is a non-intrusive reference free metric. Non-intrusive methods are preferred to intrusive analysis as they are more suitable for on-line quality prediction/control.

Recent work has focused on the wireless network (IEEE 802.11) performance of multimedia applications [8],[9]. In [10],[11],[12] the authors have looked at the impact of transmission errors and packet loss on video quality. In [13] authors have proposed a parametric model for estimating the quality of videophone services that can be used for application and/or network planning and monitoring, but their work is limited to videophone. Similarly, in [14] authors have taken into consideration a combination of content and network adaptation techniques to propose a fuzzy-based video transmission approach. In [15] the authors have proposed content based perceptual quality metrics for different content types, whereas, in [16],[17] video content is divided into several groups using cluster analysis [18]. In [19],[20] authors have looked at video quality assessment of low bitrate videos in multiple dimensions, e.g. frame rate, content type, etc. They have only considered parameters in the application level.

However, very little work has been done on the impact of different types of content on end-to-end video quality e.g. from slow moving (head and shoulders) to fast moving (sports) for streaming video applications under similar network conditions considering both network level and application level parameters. We have looked at the two main research questions in the network level and application level as:

(1) What is the acceptable packet error rate for all content types for streaming MPEG4 video and hence, find the threshold in terms of upper, medium and lower quality boundary at which the users' perception of quality is acceptable?

(2) What is the minimum send bitrate for all content types to meet communication quality for acceptable QoS (PSNR >27 dB) as it translates to a MOS of greater than 3.5 [21]?

To address these two questions, we first classified the video contents based on the spatial and temporal feature extraction into similar groups using cluster analysis [18]. We then carried out experiments to investigate the impact of Packet Error Rate (PER) and hence, find the threshold in terms of upper, medium and lower quality boundary above which the users' perception of quality is acceptable and identified the minimum acceptable Send Bitrate (SBR) for the content types. We chose Peak-Signal-to-Noise-Ratio (PSNR) and decodable frame rate (Q) [5] as end-to-end video quality metrics and MPEG4 as the video codec. In the presence of packet loss video quality becomes highly time-variant [20],[21]. One of the significant problems that video streaming face is the unpredictable nature of the Internet in terms of the send bitrate, and packet loss. We further investigated the impact of video quality over the entire duration of the sequence and hence observe the type of errors using objective video quality metrics such as PSNR. These could help in resource optimization and the development of QoS control mechanisms over wireless networks in the future. Our focus ranges from low resolution and low send bitrate video streaming for 3G applications to higher video send bitrate for WLAN applications depending on type of content and network conditions. The proposed test bed is based on simulated network scenarios using a network simulator (NS2) [22] with an integrated tool Evalvid [23]. It gives a lot of flexibility for evaluating different topologies and parameter settings used in this study.

The paper is organized as follows. The video quality assessment problem is formulated in section II. Section III classifies the contents. In section IV the experimental set-up is given. Section V presents the experiments conducted and analysis of results. Conclusions and areas of future work are given in section VI.

II. PROBLEM STATEMENT

In multimedia streaming services, there are several parameters that affect the visual quality as perceived by the end users of the multimedia content. These QoS parameters can be grouped under application level QoS and network level QoS parameters. Therefore, in the application level

perceptual QoS of the video bitstream can be characterized as:

$$\text{Perceptual QoS} = f(\text{Content type, SBR, frame rate, codec type, resolution,})$$

whereas, in the network level it is given by:

$$\text{Perceptual QoS} = f(\text{PER, delay, latency, jitter,})$$

It should be noted that the encoder and content dimensions are highly conceptual. In this research we chose MPEG4 as the encoder type. We further extracted spatial and temporal features of the video and classified video content accordingly. In the application level we chose send bitrate and in the network level we chose packet error rate as QoS parameters. Hence the main contributions of the paper are three-fold.

- (1) Most frequent content types are classified into three main groups by extracting temporal (movement) and spatial (blockiness, blurriness and brightness) feature using a well known tool called cluster analysis.
- (2) We define the threshold at which packet loss is acceptable for all content types and
- (3) We identify the minimum send bitrate for all content types for acceptable quality.

III. CONTENT CLASSIFICATION

The chosen video sequences ranged from very little movement, i.e. small moving region of interest on static background to fast moving sports clips. The choice of video sequences was to reflect the varying spatio-temporal activity of the content representative of typical content offered by content providers e.g. news type of content or fast moving sports content. In future, we will consider movie clips and carry out segment by segment analysis of the content features extracted. The content classification was done based on the temporal and spatial feature extraction using well known tool called cluster analysis [18].

The design of our content classification method is given in Fig. 1.

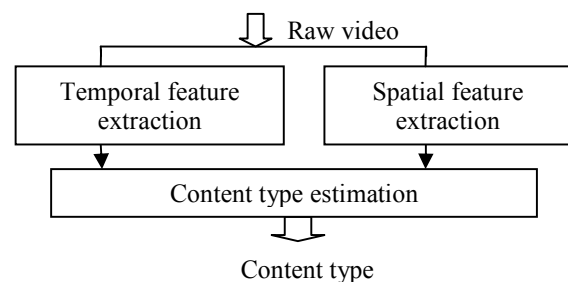


Figure 1. Content classification design

A. Temporal Feature Extraction

The motion of the temporal sequence can be captured by removing temporal-domain redundancies. The motion can be accumulated into one image that represents the activity of

the whole temporal sequence. Temporal-domain redundancy reduction techniques are well established in the video compression literature. Hybrid video compression standards employ backward and bidirectional prediction as specified by the ISO/IEC MPEG coders such as MPEG-4 part 10 [24]. On the other hand, wavelet-based video coders employ sophisticated motion-compensated temporal filtering techniques as reported in [25] and [26]. To reduce the energy of prediction error, video coders employ motion estimation and motion compensation prediction on blocks of pixels referred to as macroblocks. The outcome of the motion estimation process is a 2-D motion vector representing the relative displacement of a macroblock relative to a reference video clip. The motion compensation prediction subtracts the macroblocks of the current video clip from the best matched location of the reference video clip as indicated by the relevant motion vector. The movement in a video clip can be captured by the SAD value (Sum of Absolute Difference). In this paper, we have used the SAD values as temporal features and are computed as the pixel wise sum of the absolute differences between the two frames being compared and is given by eq. (1).

$$SAD_{n,m} = \sum_{i=1}^N \sum_{j=1}^M |B_n(i,j) - B_m(i,j)| \quad (1)$$

where B_n and B_m are the two frames of size $N \times M$, and i and j denote pixel coordinates.

B. Spatial Feature Extraction

The spatial features extracted were the blockiness, blurriness and the brightness between current and previous frames [27].

Blockiness measures the blocking effect in video sequence. For example, in contrast areas of the frame blocking is not appreciable, but in smooth areas these edges are conspicuous. The blockiness measure is calculated the visibility of a block edge determined by the contrast between the local gradient and the average gradient of the adjacent pixels [28] and is given by eq. (2).

$$Blockiness = \frac{1}{MN} \sum_{m=1}^M \sum_{n=1}^N \left\{ \frac{1}{N^2} \sum_{i=1}^N \sum_{j=1}^N [x_m^n(i,j) - \bar{x}_m^n]^2 \right\} \quad (2)$$

where $x_m^n(i,j)$ denotes the pixel value in location (i,j) of the m th block in the n th frame, \bar{x}_m^n denotes the mean of the pixel values of the m th block in the n th frame, M denotes the number of blocks per frame, and N denotes the number of frames under investigation from the video sequence.

Blurring measurement is based on the measure of local edge expansions. The vertical binary edge map is first computed with the Sobel filter. Then, the local extrema in the horizontal neighbourhood of each edge point are detected, and the distance between these extrema (x_p) is computed. Blurring is computed as the average of the edge expansions for all edge points and is given by eq. (3).

$$Blurriness = \frac{1}{N_e} \sum_{m=1}^M \sum_{n=1}^N |xp_1 - xp_2| \quad (3)$$

where N_e is the number of edge points. x_{p1} and x_{p2} are the local extrema in the horizontal neighborhood of each edge point.

Brightness (Br) is calculated as the modulus of difference between average brightness values of previous and current frames and is given by eq. (4).

$$Br_{av\{n\}} = \sum_{i=1}^N \sum_{j=1}^M |Br_{av(n)}(i,j) - Br_{av(n-1)}(i,j)| \quad (4)$$

where $Br_{av\{n\}}$ is the average brightness of n -th frame of size $N \times M$, and i and j denote pixel coordinates.

C. Cluster Analysis

We chose 12 video sequences reflecting very low spatial and temporal to very high spatial and temporal activity. Based on the table of mutual Euclidean norm in the joint temporal and spatial sense between pair of sequences, we created dendrogram on the basis of a nearest distance in a 4-dimensional Euclid-space. The dendrogram or tree diagram constructed in this way classifies the content. The features (i.e. SAD, blockiness, blurriness and brightness measurements) extracted are given in normalized form. Fig. 2 shows the obtained dendrogram (tree diagram) where the video sequences are grouped together on the basis of their mutual distances (nearest Euclid distance).

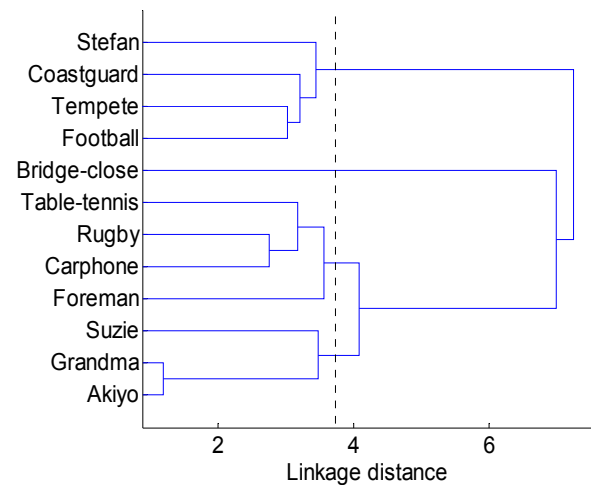


Figure 2. Tree diagram based on cluster analysis

According to Sturge's rule ($k = 1 + 3.3 \log N$), which for our data will be 5 groups. However because of the problems identified with this rule [29] we split the data (test sequences) at 38% from the maximum Euclid distance into three groups. (see the dotted line on Fig. 2) as the data contains a clear 'structure' in terms of clusters that are similar to each other at that point. Group 1 (sequences Grandma, Suzie and Akiyo) are classified as 'Slight Movement', Group 2 (sequences Carphone, Foreman, Table-tennis and Rugby) are classified as 'Gentle Walking' and Group3 (sequences Stefan and Football) are classified

as ‘Rapid Movement’. We found that the ‘news’ type of video clips were clustered in one group, however, the sports clips were put in two different categories i.e. clips of ‘stefan’ and ‘football’ were clustered together, whereas, ‘rugby’ and ‘table-tennis’ were clustered along with ‘foreman’ and ‘carphone’ which are both wide angle clips in which both the content and background are moving. Also ‘bridge-close’ can be classified on its own creating four groups instead of three. But as it is closely linked with the first group of SM we decided to put it in SM. In future, we will create more groups and compare it to our existing classification.

The cophenetic correlation coefficient, c , is used to measure the distortion of classification of data given by cluster analysis. It indicates how readily the data fits into the structure suggested by the classification. The value of c for our classification was 79.6% indicating a good classification result. The magnitude of c should be very close to 100% for a high-quality solution.

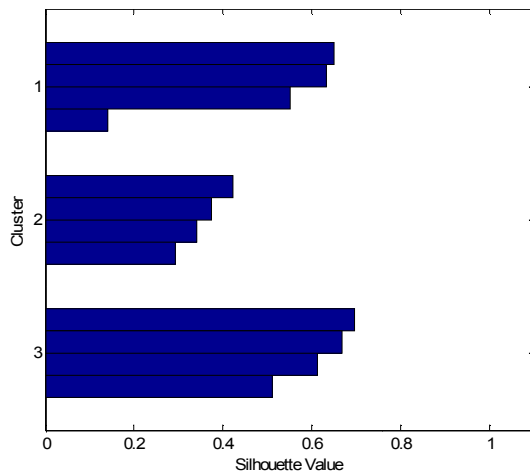


Figure 3. k-means of all contents types

To further verify the content classification from the tree diagram obtained (Fig. 2) we carried out K-means cluster analysis in which the data (video clips) is partitioned into k mutually exclusive clusters, and returns the index of the cluster to which it has assigned each observation. K-means computes cluster centroids differently for each measured distance, to minimize the sum with respect to the specified measure. We specified k to be three to define three distinct clusters. In Fig. 3 K-means cluster analysis is used to partition the data for the twelve content types. The result set of three clusters are as compact and well-separated as possible giving very different means for each cluster. Cluster 3 in Fig. 3 is very compact for the four video clips, whereas cluster 2 is reasonable compact. However, cluster 1 can be further divided into more groups. For example the video clip of bridge-close can be in a separate group. This will be looked in much detail in future work. All results were obtained using MATLAB™ 2008 functions.

The three content types are defined for the most frequent contents for mobile video streaming as follows:

1. Content type 1 – Slight Movement (SM): includes sequences with a small moving region of interest (face) on a static background. See Fig. 4.



Figure 4. Snapshots of typical ‘SM’ content

2. Content type 2 – Gentle Walking (GW): includes sequences with a contiguous scene change at the end. They are typical of a video call scenario. See Fig. 5.



Figure 5. Snapshots of typical ‘GW’ content

3. Content type 3 – Rapid Movement (RM): includes a professional wide angled sequence where the entire picture is moving uniformly e.g sports type. See Fig. 6.



Figure 6. Snapshots of typical ‘RM’ content

D. Comparison with the spatio-temporal dynamics

Video sequences are most commonly classified based on their spatio-temporal features. In order to classify video clip according to the spatial and temporal complexity of its content, a spatio-temporal grid [30] is considered and is depicted in Fig. 7.

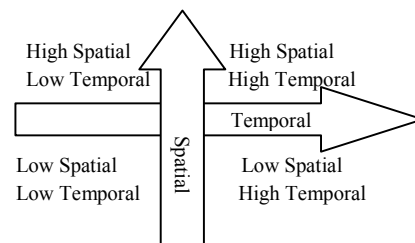


Figure 7. The spatio-temporal grid used for classifying a video sequence according to its content dynamics

From Fig. 7 the spatio-temporal grid divides each video into four categories based on its spatio-temporal features as follows:

- Low spatial – Low temporal activity: defined in the bottom left quarter in the grid.

- Low spatial – High temporal activity: defined in the bottom right quarter in the grid.
- High spatial – High temporal activity: defined in the top right quarter in the grid.
- High spatial – Low temporal activity: defined in the top left quarter in the grid.

Figure 8 shows the principal co-ordinates analysis also known as multidimensional scaling of the twelve content types. The function `cmdscale` in MATLAB™ is used to perform the principal co-ordinates analysis. `cmdscale` takes as an input a matrix of inter-point distances and creates a configuration of points. Ideally, those points are in two or three dimensions, and the Euclidean distances between them reproduce the original distance matrix. Thus, a scatter plot of the points created by `cmdscale` provides a visual representation of the original distances and produces representation of data in a small number of dimensions. In Fig. 8 the distance between each video sequence indicates the characteristics of the content, e.g. the closer they are the more similar they are in attributes.

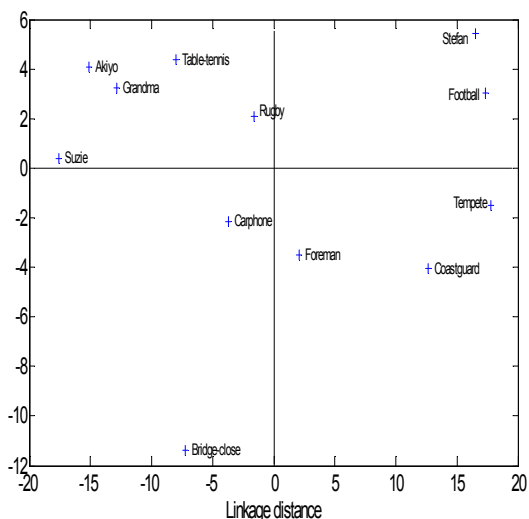


Figure 8. Principal co-ordinate analysis of all contents

Comparing Fig.7 to Fig. 8 we can see that classifying contents using feature extraction, contents of Football and Stefan are high spatial and high temporal and fit in the top right hand side, similarly contents of Bridge-close would fit in the bottom left hand side as they have low spatio-temporal features. Whereas, contents like Grandma and Suzie are in top left hand side indicating high spatial and low temporal features. Similarly, Foreman, Coastguard and Tempete are in the bottom right hand side with high temporal and low spatial features as expected. Only the video sequence of Carphone has been put in the bottom left hand side and will be investigated further.

IV. EXPERIMENTAL SET-UP

For the tests we selected twelve different video sequences of qcif resolution (176x144) as it is

recommended for low bitrate videos especially over mobile environments and encoded in MPEG4 format with an open source `ffmpeg` [31] encoder/decoder with a Group of Pictures (GOP) pattern of IBBPBBPBB. In future we will choose H.264 as it the recommended codec for low bitrates. The frame rate was fixed at 10fps. Each GOP encodes three types of frames - Intra (I) frames are encoded independently of any other type of frames, Predicted (P) frames are encoded using predictions from preceding I or P frames and Bi-directionally (B) frames are encoded using predictions from the preceding and succeeding I or P frames.

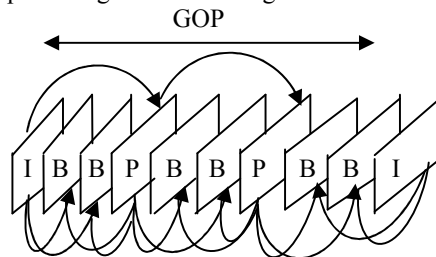


Figure 9. A sample of MPEG4 GOP (N=9, M=3)

A GOP pattern is characterized by two parameters, $GOP(N,M)$ – where N is the I-to-I frame distance and M is the I-to-P frame distance. For example, as shown in Fig.9, $G(9,3)$ means that the GOP includes one I frame two P frames, and six B frames. The second I frame marks the beginning of the next GOP. Also the arrows in Fig. 9 indicate that the B frames and P frames decoded are dependent on the preceding or succeeding I or P frames [32].

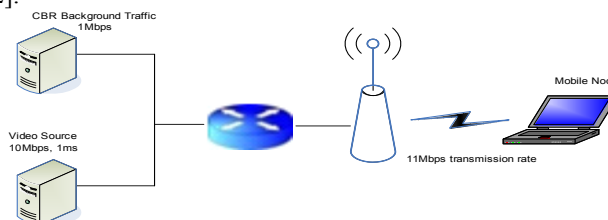


Figure 10. Simulation setup

The experimental set up is given in Fig 10. There are two sender nodes as CBR background traffic and MPEG4 video source. Both the links pass traffic at 10Mbps, 1ms over the internet. The router is connected to a wireless access point at 10Mbps, 1ms and further transmits this traffic to a mobile node at a transmission rate of 11Mbps 802.11b WLAN. No packet loss occurs in the wired segment of the video delivered path. The maximum transmission packet size is 1024 bytes. The video packets are delivered with the random uniform error model. The CBR rate is fixed to 1Mbps to give a more realistic scenario. The packet error rate is set in the range of 0.01 to 0.2 with 0.05 intervals. To account for different packet loss patterns, 10 different initial seeds for random number generation were chosen for each packet error rate. All results generated in the paper were obtained by averaging over these 10 runs.

V. EXPERIMENT AND ANALYSIS OF RESULTS

We considered both network level and application level factors and used performance metrics to evaluate video quality affected by both factors. The performance metrics used were average PSNR and decodable frame rate Q [7]. PSNR given by (1) computes the maximum possible signal energy to noise energy. PSNR measures the difference between the reconstructed video file and the original video file.

$$PSNR(s,d) = 20 \log \frac{Max}{\sqrt{MSE(s,d)}} \quad (5)$$

Max is the maximum pixel value of the image, which is 255 for 8 bit samples. Mean Square Error (MSE) is the cumulative square between compressed and the original image.

Decodable frame rate (Q) [7] is defined as the number of decodable frames over the total number of frames sent by a video source. Therefore, the larger the Q value, the better the video quality perceived by the end user. The decodable frame number is the number of decodable I/P/B frames. Considering in a GOP I frame is decodable only if all the packets that belong to the I frame are received. Similarly P frame is decodable only if preceding I or P frames are decodable and all the packets that belong to the current P frame are received well. The B frame is decodable only if the preceding and succeeding I or P frame are both decodable and all the packets that belong to the current B frame are all received.

We chose 4 different experiments as outlined in sub-sections A-D below. The motivation of these experiments was to address the two research questions raised in the Introduction section. Experiments 1-3 (sub-sections A-C) address the first question by looking at the impact of packet error rate on end-to-end quality. Whereas, experiment 4 (sub-section D) addresses the second question to identify the minimum acceptable bitrate to meet acceptable QoS.

A. Experiment 1 – Average PSNR Vs PER

Video quality is measured by taking the average PSNR over all the decoded frames across network PER from 0.01 to 0.2 (20%). All videos were encoded at a send bitrate of 256kb/s. This experiment is conducted to answer the first research question: What is the acceptable PER for maintaining the minimum QoS requirement of 27dB for the different content types ?

Fig. 11 show the average PSNR vs the PER for all 12 video clips. It shows that the average PSNR is better for slight movement compared to gentle walking which in turn is better than rapid movement which shows the dependence on content type. From our results, we found that for slight movement the video quality stays above the threshold of PSNR > 27dB (MOS >3.5) for upto 20% packet loss. However, for gentle walking and rapid movement that value drops to 10% and 6% respectively.

We observe from Fig. 11 that the drop in video quality is much higher for fast moving contents compared to that of

slow moving contents. E.g. for ‘Akiyo’ at 0.01 PER the PSNR is 44dB and at 0.2 (20%) PER it is 27.67dB. However, for ‘Football’ it is 33dB for a PER of 0.01 and 20dB for PER of 0.2. Even though the percentage drop in quality is more or less the same, 20dB is unacceptable for communication standards. This can be furthered explained by the fact that the bitrate was fixed at 256kb/s. If the bitrate is varied then the impact of packet error rate is much greater on fast moving contents.

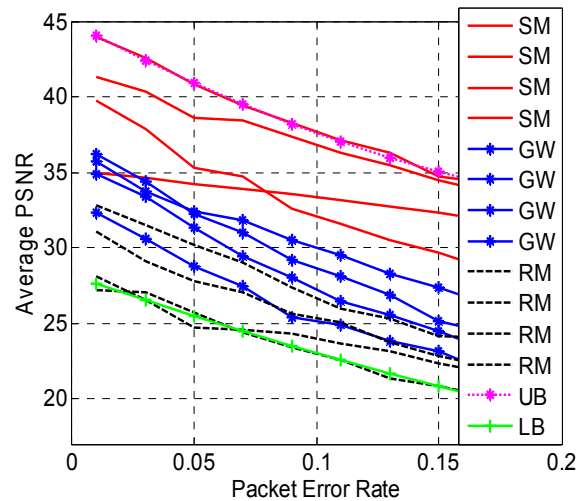


Figure 11. Packet Error Rate vs Average PSNR

Further, we derive an upper, medium and lower boundary for PSNR as a function of PER for the three content types of SM, GW and RM and hence know the threshold for acceptable quality in terms of the PSNR for the three content types with 95% confidence level and goodness of fit of 99.71% and Root Mean squared Error (RMSE) of 0.3235 is given by equations (6), (7) and (8):

$$SM: PSNR = 122.3(PER)^2 - 88.36(PER) + 42.6; PER \leq 20\% \quad (6)$$

$$GW: PSNR = 64.9(PER)^2 - 73.75(PER) + 34.43; PER \leq 10\% \quad (7)$$

$$RM: PSNR = 76.8(PER)^2 - 68.87(PER) + 31.43; PER \leq 6\% \quad (8)$$

B. Experiment 2 – Q Vs PER

The experimental set up is the same as in A but we measured Q value [7] instead of PSNR vs PER and addressed the above research question in terms of Q [7] instead of PSNR.

Fig. 12 shows the decodable frame rate (Q) of all 12 contents and shows that Q is higher when the PSNR is higher for all the video clips. In comparison to Fig 3 the decodable frame rate does not directly compare to the PSNR. However, from our results we found higher values for the average PSNR for ‘slight movement’ and it did not correspond to a higher value of Q. This is because the Q value is derived from the number of decodable frames over the total number of frames sent by a video source [5] i.e. it is sensitive to the number of frames and packets lost.

Therefore, as the content becomes more complex we would expect the video quality to degrade more for less I-frames lost compared to that of simpler contents. Hence, we conclude that for slight movement 20%, for gentle walking 10% and for rapid movement 6% packet loss is acceptable.

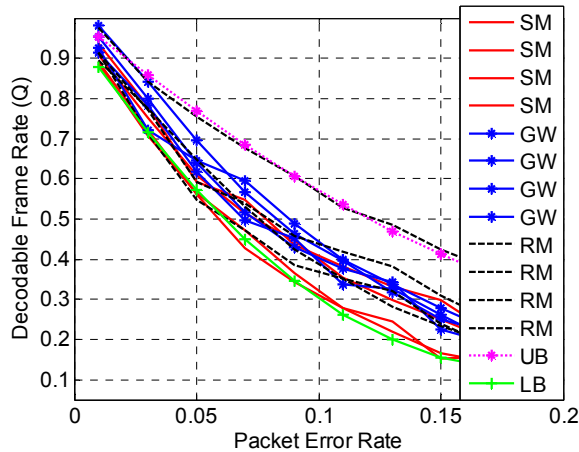


Figure 12. PER vs Q for all content types

Further, we derive an upper, medium and lower boundary for Q value as a function of PER for the three content types of SM, GW and RM and hence know the threshold for acceptable quality in terms of the Q value for the three content types with 95% confidence level and goodness of fit of 99.71% and RMSE of 0.0117 is given by the equations (9), (10) and (11):

$$SM: Q=19.89(PER)^2 - 8.03(PER) + 0.967; \quad PER \leq 20\% \quad (9)$$

$$GW: Q=18.09(PER)^2 - 7.88(PER) + 1.02; \quad PER \leq 10\% \quad (10)$$

$$RM: Q=13.84(PER)^2 - 6.5(PER) + 0.975; \quad PER \leq 6\% \quad (11)$$

Table I summarizes the findings of Figs. 11 and 12 and outlines the PSNR and Q values for acceptable quality at 20%, 10% and 6% PER for all three content types in terms of the I, P and B frames lost. We observe from Table I that for content type of SM the Q value is much lower compared to that of the PSNR. It shows that visually the quality is much lower at 20% packet loss rendering PSNR to be not a very good predictor of visual quality. For SM, Q-value outperforms the PSNR.

TABLE I
PSNR AND Q VALUES FOR THREE CONTENT TYPES @ 20%, 10% AND 6% PACKET LOSS

	I-frames lost	P-frames lost	B-frames lost	PSNR	Q-value
SM	8	14	43	27.67	0.458
GW	8	7	22	28.103	0.602
RM	8	11	12	25.57	0.615

C. Experiment3 – PSNR Vs Time

We further looked at the relationship between the PSNR over the entire duration of the sequence for all three content types.

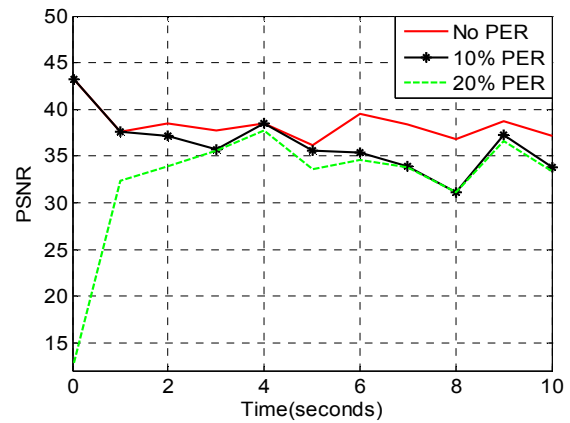


Figure 13. PER effects for SM for 32kb/s SBR

In Fig. 13 we investigate the source of effects caused by packet errors over the entire duration of the sequence. For ‘slight movement’ we compare the PSNR values for no transmission errors to 10% and 20% packet loss. The PSNR values are the same for a new I-frame over the duration of the sequence. The error occurs in the B-frames and propagates to the P-frames as expected. We observe two effects, the PSNR decreases over the entire duration and the second a more ragged response curve when packet errors of 10% and 20% are introduced. We also observe that for a send bitrate of 32kb/s the video quality is still acceptable for 20% packet loss.

Fig. 14 shows the effects of no packet loss, 10% and 20% packet loss for ‘Gentle walking’ at a send bitrate of 80kb/s. Again as previously mentioned the video quality reduces over the time duration and we observe a much bigger loss in quality as the packet loss increases to 20%.

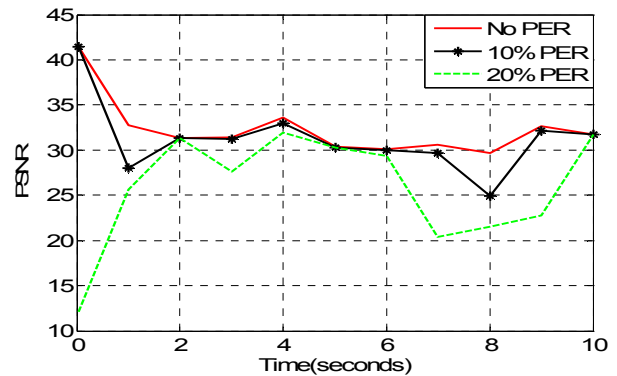


Figure 14. PER effects for GW for 80kb/s SBR

Whereas, from Fig. 15 in ‘rapid movement’ the video quality degrades fairly quickly with the increase of packet

error rate i.e. for 10% packet loss the video quality is completely unacceptable.

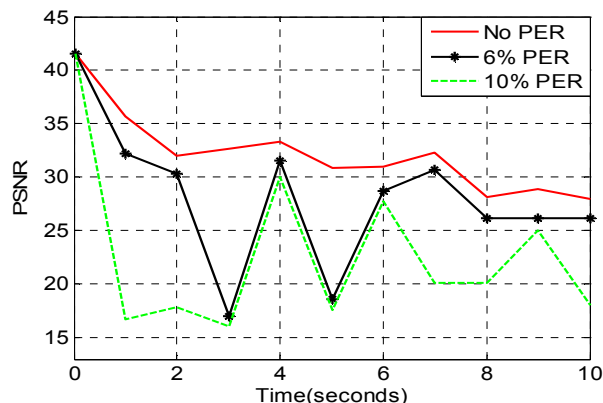


Figure 15. PER effects for RM for 256kb/s SBR

While PSNR is not a good predictor of the visual quality, it can serve as a detector of clearly visible distortions. It can be observed, however that the perceived quality degradation increases in the duration of the sequence. Due to the auto-correlation of the time series (each sample is dependent on the previous and following sample) the values are not independent. We also observed that as the scene activity in the video sequence becomes more complicated e.g. for ‘rapid movement’ at 20% packet loss the quality is completely unacceptable deteriorating at a much faster speed. All degraded video clips can be found in [33].

Fig. 16 shows that visually the quality of SM, GW and RM is unacceptable at 20%, 10% and 6% packet loss for some frames. Also from Table I we observe that even though PSNR value is acceptable (MOS>3.5) for all three content types, however, the end-to-end perceptual quality is unacceptable. From Fig. 13, the PSNR at 3.4 seconds for SM shows a value of 35dB, whereas the frames (101-103) from Fig. 16a show that the perceptual quality does not follow for those frames. Similarly, for GW at 5.2s (Fig. 14) the PSNR is 30dB and for RM at 3.2s it is 17dB. The PSNR values of GW and RM reflect the perceptual quality better compared to SM. Further from Table I it can be seen that for SM, more B-frames are lost compared to GW and RM. B-frames affect the quality least in MPEG4 GOP. I-frames take priority, then P-frames and finally B-frames. Also the values of Q correlate well with PSNR for GW and RM. However, for SM it does not. Q-value for SM actually shows that at 20% the quality is less than acceptable compared to that of PSNR. This is an area of future work to carry out substantive subjective tests to verify the results of this paper. Also it confirms previous studies [34] that PSNR is not a good indicator of perceptual quality.

D. Experiment 4 – Average PSNR Vs PER Vs SBR

The send bitrate versus PSNR curve is shown in Fig. 17 for all contents. From Fig. 17 we observe that there is a minimum send bitrate for acceptable quality (PSNR >

27dB) for all content types. For high definition IPTV applications PSNR of 32dB is recommended. Therefore, in Fig. 17 we have chosen 32dB as minimum acceptable PSNR as compared to 27dB to illustrate the point of optimizing bandwidth. A PSNR value of 35db is considered ‘good’ for streaming applications [35]. Also there is a maximum send bitrate for the three content types that gives maximum quality (PSNR > 38db). For example for the content category of SM, send bitrate of 30kbps or more gives a maximum PSNR of 38dB. However, in RM higher send bitrates are required for maximum quality i.e. > 370kb/s. From Fig. 17 it can be derived that when the send bitrate drops below a certain threshold, which is dependent on the video content, then the quality practically collapses. Moreover, the quality improvement is not significant for send bitrates higher than a specific threshold, which is also dependent on the spatial and temporal activity of the clip.

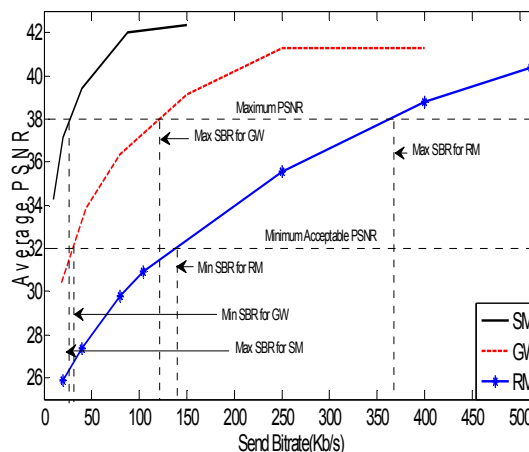


Figure 17. MOS Vs Send Bitrate for the three contents

The experimental set up is the same as in section IV, but we changed the video send bitrate to achieve the minimum send bitrate for QoS requirements and to address the research question: What is the minimum SBR for the different video content types with time variant quality acceptable for communication quality (>27dB)?

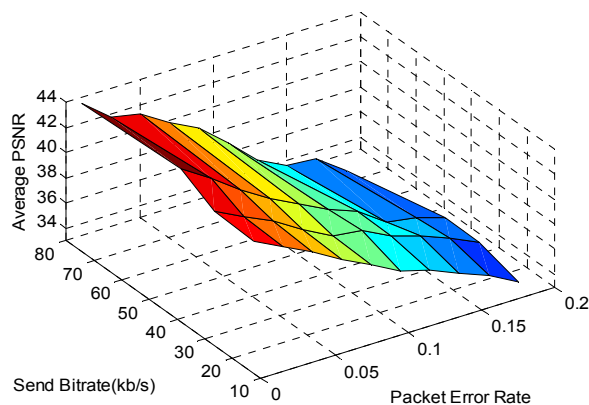


Figure 18. Average PSNR Vs PER and SBR for ‘SM’

The send bitrates ranged from 18kb/s to 384kb/s. We chose one video clip from each category. We suggest a minimum send bitrate for all three categories that achieve an average PSNR values of higher than 27dB for the video content types as it translates to a MOS of greater than 3.5 [23] which is an acceptable score for the telecommunication industry.

Fig. 18 shows the average PSNR over the video send bitrates of 18kb/s, 32kb/s, 44kb/s and 80kb/s. We found that for slow movement low bitrate of 18kb/s is acceptable as it yields an average PSNR of 30dB without any packet loss. As the send bit rate is increased to 80kb/s, average PSNR is greater than 40dB indicating that the bandwidth should be re-allocated to optimize it.

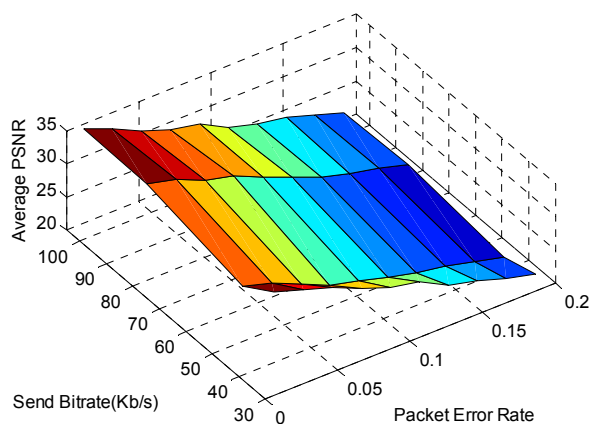


Figure 19. Average PSNR Vs PER and SBR for 'GW'

In Fig. 19 we chose send bitrates of 32kb/s, 44kb/s, 80kb/s and 104kb/s, as bitrates less than 18kb/s will give poor video quality rendering them meaningless. We suggest a send bitrate of 32kb/s for gentle walking as it gives an average PSNR value of approximately 29dB. However, with higher packet loss the quality falls below the acceptable level.

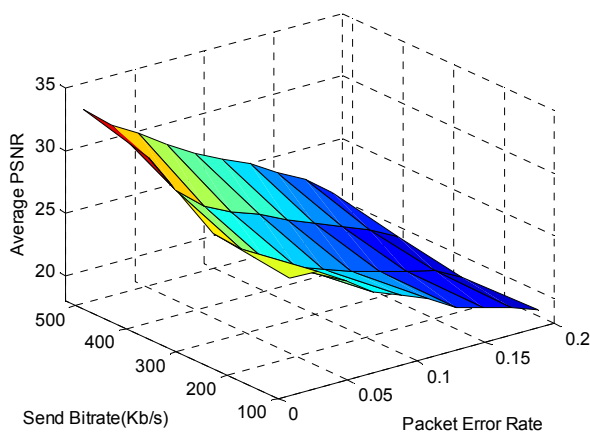


Figure 20. Average PSNR Vs PER and SBR for 'RM'

In Fig. 20 we chose bitrates of 80kb/s, 104kb/s, 256kb/s, 384kb/s and 512kb/s as bitrates less than 80kb/s gave meaningless results in terms of very low PSNR. From our results we suggest a minimum send bitrate of 256kb/s as it yields a PSNR of 30dB. Increasing the send bitrate improves the quality with no packet loss. However, increasing the send bitrate does not compensate for the higher packet loss effect of streaming video quality for fast moving content due to network congestion issues. In fact, when the network is congested the bitrate should be reduced to release congestion. However, the quality of fast moving videos reduces if the bitrate is reduced beyond a certain threshold.

Therefore, the quality of video in 'rapid movement' degrades much more rapidly with an increase in packet loss compared to that of 'slight movement' and 'gentle walking'.

VI. CONCLUSIONS

In this paper we classified the most significant content types and have established guidelines for the transmission of MPEG4 streaming video over wireless networks in terms of acceptable packet loss and minimum send bitrate. The contents were first classified using cluster analysis into three groups with good prediction accuracy. The video quality is evaluated in terms of average PSNR and decodable frame rate, Q. The acceptable PER was found to be 20%, 10% and 6% for the three content categories of SM, GW and RM respectively. We found that for content category of SM the Q value was more sensitive compared to PSNR as it gave a lower value for 20% packet loss which was more representative visually. However, for GW and RM very little difference was found between PSNR and Q.

Through the first three experiments, we established that as the ST-activity in the content increases it becomes more sensitive to network impairments such as packet loss. Although for low ST-activity videos the acceptable PER was found to be 20% in terms of the PSNR, however, visually looking at the videos, we found that quality was not acceptable at such high packet losses due to blocking and blurring effects. This also confirms previous studies that PSNR is not a good reflector of visual quality - thus addressing the first question raised in the Introduction section.

To address the second question raised in the Introduction section, through our fourth experiment we identified the minimum SBR for acceptable QoS for the three content types as 18, 32 and 256kb/s for SM, GW and RM respectively. Hence, we have established that sending video beyond a certain bitrate does not add any value to improving the end user quality.

We believe that the results would help in optimizing resource allocation for specific content in content delivery networks and the development of QoS control methods for video over mobile/wireless networks. Future direction of our work is to further investigate the more perceptual-based quality metric and adapt the video send bitrate depending on network conditions over wireless networks. Also subjective tests will be carried out to verify our results.



(a) Frames 101-103, PER @ 20% for SM encoded at 32kb/s



(b) Frames 156-158, PER @ 10% for GW encoded at 80kb/s



(a) Frames 96-98, PER @ 6% for RM encoded at 256kb/s

Figure 16. Perceptual quality comparison for the 3 content types at PER 20%, 10% and 6%

ACKNOWLEDGMENT

This paper is an invited extended version of the conference paper A.Khan, L. Sun and E. Ifeachor, "Impact of video content on video quality for video over wireless networks", published in Proc. of 5th ICAS, Valencia, Spain, 20-25 April 2009.

The work reported here is supported in part by the EU FP7 ADAMANTIUM project (contract No. 214751).

REFERENCES

[1] G. Ghinea and J. P. Thomas, "QoS impact on user perception and understanding of multimedia video clips", *Proc. Of ACM Multimedia '98*, Bristol, UK, pp. 49-54, 1998.

[2] A. Khan, Z. Li, L. Sun and E. Ifeachor, "Audiovisual quality assessment for 3G networks in support of E-healthcare", *Proc. of CIMED*, Plymouth, UK, 25-27 July 2007.

[3] ITU-T. Rec P.800, Methods for subjective determination of transmission quality, 1996.

[4] Video quality experts group, multimedia group test plan, Draft version 1.8, Dec 2005, www.vqeq.org.

[5] <http://compression.ru/video/index.htm>

[6] <http://www.pevq.org>

[7] C. Ke, C. Lin and C. Shieh, "Evaluation of delivered MPEG4 video over wireless channels", *Journal of mobile multimedia*, Vol. 3, No. 1, pp. 047-064, 2007.

[8] P. Chondros, A. Prayati, C. Koulamas and G. Papadopoulos, "802.11 performance evaluation for multimedia streaming", *Fifth*

- International Symposium on Communication Systems, Networks and Digital Signal Processing*, Patras, Greece, 19-21 July, 2006.
- [9] B. Munir, N. K. Chilamkurti and B. Soh, "A comparative study of voice over wireless networks using NS-2 simulation with an integrated error model", *International Conf. on WiCOM*, 22-24 Sept. 2006.
- [10] Y. Koucheryavy, D. Moltchanov and J. Harju, "Performance evaluation of live video streaming service in 802.11b WLAN environment under different load conditions", MIPS, Napoli, Italy, November 2003.
- [11] Z. He, H. Xiong, "Transmission distortion analysis for real-time video encoding and streaming over wireless networks", *IEEE transactions on Circuits and Systems for Video Technology*, Vol. 16, No. 9, Sept. 2006.
- [12] S. Kanumuri, P. C. Cosman, A. R. Reibman and V. A. Vaishampayan, "Modelling packet-loss visibility in MPEG2 video", *IEEE Transactions on Multimedia*, Vol. 8, No. 2, April 2006.
- [13] K. Yamagishi, T. Tominaga, T. Hayashi and A. Takahasi, "Objective quality estimation model for videophone services", *NTT Technical Review*, Vol.5, No. 6, June 2007.
- [14] V. Vassilou, P. Antoniou, I. Giannakou and A. Pitsillides "Delivering adaptive scalable video over wireless internet", *International Conference on Artificial Neural Networks (ICANN)*, Athens, Greece, September 10-14, 2006.
- [15] M. Ries, C. Crespi, O. Nemethova and M. Rupp, "Content based video quality estimation for H.264/AVC video streaming", *Proc. Of the IEEE Wireless Communication & Networking Conference*, Hong Kong, China, Mar. 2007.
- [16] Y. Suda, K. Yamori and Y. Tanaka, "Content clustering based on users' subjective evaluation", *Information and Telecommunication Technologies*, 2005. APSITT 2005 Proceedings, 6th Asia-Pacific Symposium, Pages 177-182, Nov. 2005.
- [17] A. Khan, L. Sun and E. Ifeachor, "Impact of video content on video quality for video over wireless networks", 5th ICAS, Valencia, Spain, 20-25 April 2009.
- [18] W. J. Krzanowski, "Principles of Multivariate Analysis", Clarendon press, Oxford, 1998.
- [19] G. Zhai, J. Cai, W. Lin, X. Yang, W. Zhang and M. Etoh, "Cross-dimensional perceptual quality assessment for low bitrate videos", *IEEE Transactions on Multimedia*, Vol. 10, No.7, pp. 1316-1324, Nov. 2008.
- [20] S. Winkler and F. Dufaux, "Video quality evaluation for mobile applications", *Proceedings of SPIE Visual Communications and Image Processing*, Lugano, Switzerland, 2003.
- [21] O. Nemethova, M. Ries, M. zavodsky and M. Rupp, "PSNR-based estimation of subjective time-variant video quality for mobiles", *Proc. of MESAQIN 2006*, Prag, Tschechien, June, 2006.
- [22] NS2, <http://www.isi.edu/nsnam/ns/>
- [23] J. Klaue, B. Tathke and A. Wolisz, "Evalvid – A framework for video transmission and quality evaluation", *In Proc. Of the 13th International Conference on Modelling Techniques and Tools for Computer Performance Evaluation*, pp. 255-272, Urbana, Illinois, USA, September 2003.
- [24] MPEG-4, Information Technology, Coding of Audio-Visual Objects, Part 10: Advanced Video Coding, ISO/IEC 14496-10, 2005.
- [25] P. Chen, "Fully scalable subband/wavelet coding," Ph.D. dissertation, Rensselaer Polytechnic Inst., Troy, NY, May 2003.
- [26] R. Ohm, M. Schaar, and J. Woods, "Interframe wavelet coding—Motion picture representation for universal scalability," *Signal Process. Image Commun.*, vol. 19, no. 9, pp. 877–908, Oct. 2004.
- [27] M. Al-Mualla, C. Canagarajah and D. Bull, "Video coding for mobile communications", Academy Press – An imprint of Elsevier Science, 2002.
- [28] S. Minami and A. Zakhor, "optimization approach for removing blocking effects in transform coding," *IEEE Trans. On Circuits and Systems for Video Technology*, Vol. 5, No. 7, pp. 74-82, 1995.
- [29] R. J. Hyndman, "The problem with Sturges' rule for constructing histograms", Monash University 1995.
- [30] N. Cranley and L. Murphy, "Incorporating user perception in adaptive video streaming services", in *Digital Multimedia Perception and Design* (Eds. G. Ghinea and S. Chen), published by Idea Group, Inc., May 2006. ISBN: 1-59140-860-1/1-59140-861-X.
- [31] Ffmpeg, <http://sourceforge.net/projects/ffmpeg>
- [32] J. Mitchell and W. Pennebaker, "MPEG Video: Compression Standard, Chapman and Hall, 1996, ISBN 0412087715.
- [33] www.tech.plymouth.ac.uk/spmc/staff/akhan/video_sequences/video_cpls.html
- [34] R. Feghali, F. Speranza, D. Wang and A. Vincent, "video quality metric for bit rate control via joint adjustment of quantization and frame rate", *IEEE Transactions on Broadcasting*, Vol. 53, No.1, March 2007 pp 441-446.
- [35] Telchemy application notes, "Understanding of video quality metrics", Telchemy, Feb. 2008. <http://www.telchemy.com>.

Dynamic Adaptation of Quality of Service for VoIP Communications

Nelson Costa

Instituto Superior Técnico
Lisbon, Portugal
eng.ncosta@gmail.com

Mário Serafim Nunes

IST, INESC-ID
Lisbon, Portugal
mario.nunes@inesc-id.pt

Abstract — The present work proposes an adaptive solution to provide quality of service in Voice over IP communications. This solution is based on three components that interact in order to achieve higher quality in voice communication. The first two consist in changing the codec and the transport protocol in real-time during a conversation; the third consists in using a Forward Error Correction mechanism to recover from loss packets. To demonstrate the voice quality obtained by this solution, a VoIP client application was developed, compatible with other VoIP clients, to implement the proposed quality of service algorithm and control the voice quality during a conversation. The results of the experimental measurements and simulations performed demonstrate that this solution is viable and significantly increases the voice quality of VoIP communication.

Keywords: VoIP, QoS, Codec, SIP, RTP, RTCP, FEC, MOS, E-Model

I. INTRODUCTION

In recent years Voice over IP (VoIP) has proved to be a serious competitor to Public Switched Telephone Network (PSTN), in terms of cost, efficiency, versatility and reliability. VoIP started to be used by simple applications mainly to establish voice calls between computers and then evolved to establish calls through gateways to public telephone networks. Along this evolution, VoIP made significant steps to gain the acceptance of the business community, as it provides a telephone system over IP networks just for a fraction of the cost of the traditional telephone system.

Although VoIP is a convergence solution of data and voice networks and have a large group of advantages, there are still some aspects that need to be improved, such as quality of service (QoS). Classic telephone networks that use the circuit switching service have dedicated channels for each voice session and were planned to provide a deterministic quality of voice communication. IP networks use a Best Effort service that does not provide any QoS guarantee mechanism and where all traffic is assigned the same level of priority. According to the Best Effort service, the data sent by each user is processed and forwarded through the network according with the available bandwidth. When congestion is present in the network, the packets are discarded without any distinction, not guarantying that the service is carried through successfully. Although there are

applications that are not affected by the delay, such as electronic mail, file transfer and web applications, there are some applications, as voice and video, that have stringent delay requirements, which normally are not guaranteed by the public Internet. It is imperative that interactive traffic receives a higher priority in relation to traditional traffic. There are several solutions aiming to provide some level of quality of service, such as, over-provisioning, IntServ [2], DiffServ [3] and MPLS [4], that introduce an additional complexity and cost to the network and are not yet widely deployed.

The main challenge in VoIP is to provide a high level of quality of service and being resilient to communication gaps. This challenge is still more difficult in wireless scenarios, where there is usually a high level of packet losses.

This paper presents an adaptive QoS solution to resolve the problem of the sporadic voice gaps that result from packet losses and variable delay during a conversation.

A VoIP client application was developed to test the quality of service of the proposed algorithm and control the quality of the voice provided during a conversation. This application is adaptable to the characteristics of the VoIP connection and compatible with other standard VoIP applications.

II. RELATED WORK

There are many papers that address QoS issues on VoIP, with different perspectives and applications. We selected for our analysis in particular the papers that address adaptive VoIP techniques.

In [5] is presented a method for evaluating various playout algorithms that extends the E-model by estimating user satisfaction from time varying impairments. The paper evaluates several playout algorithms and shows a correspondence between their results and those obtained via statistical loss and delay metrics.

In [6] is proposed an adaptive QoS playout algorithm based on the E-model, with dynamic retransmission in order to reduce the packet losses and in this way to increase the quality of the voice. The simulation results show improvements in the R-factor, specially for networks with low end-to-end delays, as LAN or WLANs. In the paper the authors do not considered to adapt the codec bitrate or the transport protocol.

In [7] an adaptive VoIP algorithm is proposed to improve the voice quality, based on several mechanisms, namely in the switch of the codec, FEC configuration and playout buffer size. The paper presents a theoretical analysis of the quality assessment methods and pseudo-code of the proposed algorithms, but the authors do not present an evaluation of the algorithms described, and consequently not allowing to assess the proposals presented.

In [8] an adaptive codec switching VoIP application over heterogeneous networks is presented, where the codec switching is based on the percentage of packet losses. An evaluation of the algorithm is presented, based on subjective MOS measurements, which shows that in most of the cases an increase in the voice quality is perceived when the algorithm is applied. However the proposed algorithm do not take in consideration the delay and jitter to switch the codec and consequently do not comply entirely with the E-model.

In [1] the authors of this paper present the basic concept of an adaptive VoIP algorithm fully compliant with the E-model that will be described and evaluated in detail in the following sections.

III. VOIP TECHNIQUES AND PROTOCOLS OVERVIEW

Before describing the proposed adaptive quality of service solution for VoIP communications, it is necessary to introduce some definitions, technologies and protocols that support VoIP service and that will be mentioned along the paper.

A. Voice Coding Techniques

The sound produced by human's voice is defined by the vocal system, which comprises vocal cords, lips and nose. The air passing through the vocal system causes vibrations of the vocal cords that are modeled by the positions of the tongue and lips. These vibrations are relatively slow, contributing to the predictability of the sound during the conversation. This predictability can be useful when a voice coding device named codec is applied, to minimize the quantity of data transmitted and necessary bandwidth. Codecs contain real-time compression algorithms that transform the analog signal of human voice into a bit sequence (digital signal) to be transmitted through the network, and the opposite functions at the receiver. The compression method removes the redundant and irrelevant components of the information, transmitting only what is essential to the communication. There are three types of codecs: Waveform codecs, Vocoders and Hybrid codecs. Waveform codecs try to play the original voice signal, sample by sample, based on its statistic, spectral and temporal characteristics. Vocoders codify only the important perceptual information of the voice. Hybrid codecs are a mix of the Waveform codecs and Vocoders.

One of the problems introduced when applying a voice compression system is to evaluate the voice quality. The Codec efficiency is related with the quality of the signal recovered by the destination, the used bandwidth and the algorithm complexity.

Table 1 shows the main characteristics of several codecs used in VoIP applications.

TABLE I. AUDIO CODECS COMPARISON

Codec	Algorithm	Sample Rate [KHz]	Transmission Rate [Kbit/s]	Delay [ms]
DVI4	ADPCM	8/16	32	?
G.711	PCM	8	64	0.125
G.723.1	ACELP/MP-MLQ	8	5.3/6.3	37,5
G.729	CS-ACELP	8	8	15
GSM FR	RPE-LTP	8	13	20
iLBC	LPC	8	13.33/15.2	25/40
Speex	CELP	8/16/32	[2.15-24.6][4-44.2]	30/34

B. Quality of Service Parameters and Metrics

The quality of service provided to applications is defined in terms of a Service Level Agreement (SLA), a specification that defines the QoS parameters thresholds. The more frequent QoS parameters used are: bandwidth, delay, jitter and packet loss.

- Bandwidth is the most basic QoS parameter that defines the minimum bitrate that the network needs to guarantee in order to be able to support the voice service.
- Delay represents the end-to-end delay and is calculated by the sum of all delays introduced by the equipments and the network.
- Jitter corresponds to the variation in time of data delivery, being caused by the variable delay in the network.
- Packet Loss Ratio (PER) represents the percentage of packet losses in the network.

In order to evaluate and measure permanently the quality of voice during a conversation as perceived by the user, we adopted the objective metric E-Model. The E-Model, defined in the ITU-T G.107 [9], analyses the QoS parameters and quantify the voice quality by calculating a scalar factor between 0 (worst case) and 100 (excellent), which is called the R factor. This factor represents the sum of all degradation factors in the communication, as shown in Fig. 1.

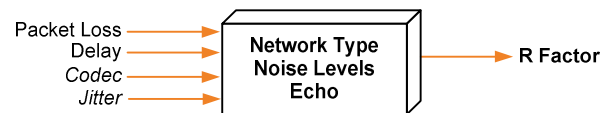


Figure 1. R factor calculation process

The E-Model R factor is obtained using the following expression:

$$R = (R_0 - I_s) - I_d - I_e + A \quad (1)$$

- Signal-to-Noise Ratio [R0], results of several types of noise, like transmission circuit noise, environment

noise both in the transmitter and receiver, and a noise ceiling corresponding to the sensitivity of the human hearing system. ITU-T G.107 specification, defined the value 94.77 for this factor.

- Simultaneous Impairment [Is], represents all the impairments that occur simultaneous with the voice signal, like the quantization distortion caused by digitizing the voice signal. ITU-T G.107 specification defined the value 1.41 for this factor.
- Delay Impairments [Id], represents the losses associated to the end-to-end delay. I_d is obtained through the following expression:

$$I_d = I_{dte} + I_{dle} - I_{dd} \quad (2)$$

I_{dte} represents the transmission losses due to echo, I_{dle} the receiver losses due to echo and I_{dd} the voice absolute delay. ITU-T G.107 specification defines the expressions to calculate each I_d component.

According to Clark [10], it is possible to obtain the I_d value through an interpolated expression of those expressions. Although, according to Lustosa [11], that expression is incorrect, because it penalize the I_d factor for $T_a \leq 175 \text{ ms}$. This may be due to a typographical error and the correct expression is presented in the following interpolated expression:

$$\begin{cases} T_a \leq 175 \text{ms} : I_d = 0,023T_a \\ T_a > 175 \text{ms} : I_d = 0,111T_a - 15,444 \end{cases} \quad (3)$$

T_a represents the system absolute delay and is obtained through the following expression:

$$T_a = T_{net} + T_{codec} + T_{buffer} \quad (4)$$

T_{net} represents the jitter, T_{codec} the codec delay and T_{buffer} the receiver buffer used for jitter compensation.

Expression 3 is represented graphically in Fig. 2.

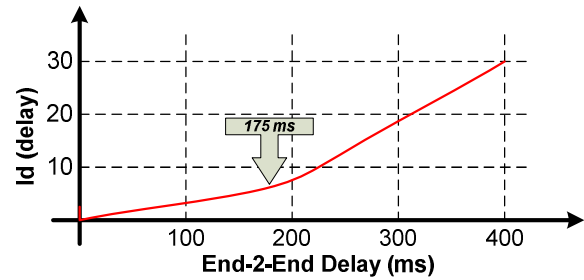


Figure 2. Relationship graphic between Id and delay

- Equipment Impairment [Ie], represents the equipment impairments caused by the codec and packet losses. ITU-T G.113 [12] defines a set of provisory values for this factor. Those values were converted to the graphics represented in Fig. 3 and Fig. 4.

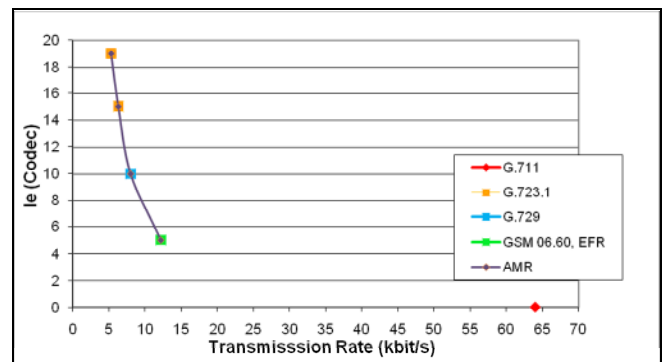


Figure 3. Ie provisory values as function of the codec

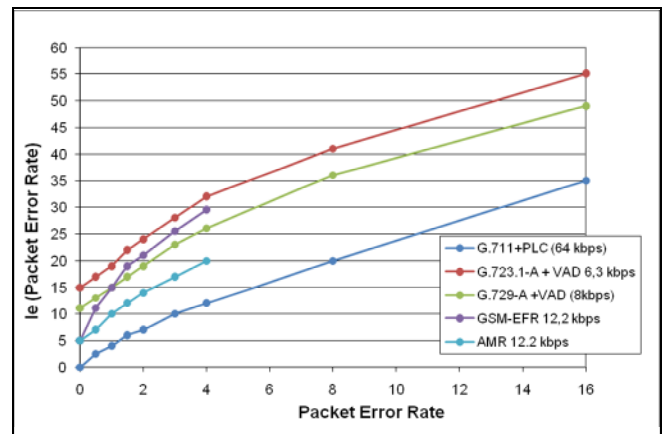


Figure 4. Ie as function of packet losses for different codecs

- Advantage Factor [A], allows for compensation of impairment factors where there are considered advantages of access to the user, e.g. mobile terminals. ITU-T G.113 specification defines $A = 0$ for fixed telephone networks.

According to these provisional and standards values, the equation 1 can be reduced to the following expression:

$$R = 93,36 - I_d - I_e(\text{codec}, PER) \quad (5)$$

To categorize the results of the R factor on the perceived call quality, it was defined five categories of values, as showed in table 2.

TABLE II. R FACTOR CATEGORY VALUES

R Factor	User Satisfaction Level
$90 \leq R < 100$	Very satisfied
$80 \leq R < 90$	Satisfied
$70 \leq R < 80$	Some users satisfied
$60 \leq R < 70$	Many users dissatisfied
$0 \leq R < 60$	Nearly all users dissatisfied

According to the limits defined in table 2, it is not recommend having an $R \leq 60$, it is desirable to obtain $R \geq 70$.

C. Forward Error Correction

The communication channel that transmits the signal containing the information could corrupt it by adding distortions and noise along the transmission. The exponential increase in the use and consumption of multimedia information through the wireless network, leads to maximize the bandwidth of the channel in order to maintain an acceptable quality of service to wireless network [13]. Since the wireless network communication channel, typically, has high error rates, caused by attenuation, dispersion and interference from other active sources, the main challenge is to provide a satisfactory service for multimedia communication on a channel with high error probability. In such cases it is imperative to use specific techniques to reduce these harmful effects and ensure a satisfactory level of voice quality in VoIP communications. In cases where selective retransmission is not possible due to stringent delay requirements, it is necessary to use redundancy mechanisms in order to recover from lost packets. This type of mechanisms is based on the transmission, in a controlled way, of redundant information that can be used in the receiver to correct possible errors that occur in the network.

Complementing the FEC technique, the receiver can also send a NAK (Negative acknowledge) when the data can not be recovered, reducing the number of retransmissions and energy consumption resulted from the retransmission of packets, since the energy consumption is higher in the transmission than in the reception.

FEC efficiency directly depends on the amount of redundant information added. Consequently it is necessary to estimate the error rate on the network to determine the amount of redundant information to be able to recover corrupt or lost packets.

D. SIP, RTP and RTCP

SIP, defined by IETF in RFC 3261 [14], is a text-based protocol, similar to the HTTP and SMTP, being designed for initiating, maintaining and terminating interactive communication sessions between users. Such sessions include voice, video, chat, interactive games, and virtual reality.

RTP, defined by IETF in RFC 3550 [15], defines a standard packet format to transport audio and video through Internet. The main reason for the definition of this protocol was to introduce temporal and sequential information that allow to identify the instants of emission and reception of data packets, as well as packet losses, information that is considered relevant when transferring real time data.

UDP is usually the transport protocol used to encapsulate the RTP packet because the applications that use RTP are more sensitive to delay than packet loss. However, UDP is a connectionless protocol that does not guarantee the delivery of packets and consequently the quality of service. However, there are situations where the use of TCP protocol could be better than UDP, namely in high packet loss environments, where the delay introduced by TCP could have lower impact in the voice quality than the delay caused the TCP retransmission mechanisms.

RTCP, defined by IETF in RFC 3550 [15], works with RTP to control the congestion and the transmitted data flows. This operation is done through the periodic transmission of control packets between the session participants. The RTCP main function is to provide information about the quality of the distribution of data to client application in order to diagnose communication faults. Although, there are five types of RTCP Packets, the most important are the Receiver Report (RR) and the Sender Report (SR). The RR packet carries statistical data related only to reception and is generated by the non-active participants in the media session. The SR packet carries the statistical data corresponding to reception and transmission for each active participant in the multimedia session.

IV. QOS PROPOSAL

In case of low traffic, Internet provides a Best Effort service where the packets are delivered with low delay and low losses. In case of network congestion packets are discarded without any service discrimination. The QoS concept in the Internet intends to reduce, for certain class of traffic, this uncertain packet delays and packet losses.

Since the main objective of this paper is to design and implement a solution to guarantee the quality of service in VoIP communication, it is convenient to analyze the main approaches available to provide QoS. Over provisioning is the simpler solution to provide quality of service in IP networks, however it is usually not suitable to WAN due to its bandwidth limitations. The IntServ model, defined by IETF, is based in resource reservations and uses the Resource Reservation Protocol (RSVP). DiffServ is another model defined by IETF that classifies marks and processes the packets according to a prioritization mechanism. MPLS

is another mechanism that uses a tag appended to IP packets, allowing to forward traffic along the network based on traffic engineering rules.

As none of the analyzed QoS approaches is widely available in the public Internet, it was decided to design a solution able to work with the Best Effort IP network and compatible with current existing VoIP implementations.

The transmission of an audio signal through a packet switching network like Internet follows the following steps: a sequence of analog audio samples is digitalized and inserted into packets that are sent through the network to a certain destination. When the packet arrives to destination, it is decoded and reproduced. Analyzing in detail how the transmission process works, we verify that there are two key points that directly influence the quality of voice during a conversation, the coding and the transport processes.

The proposed solution aims to develop an end-to-end QoS adaptive VoIP client application. This application was called NCVoIP and is responsible to control the voice quality in a conversation. To implement the control voice quality process this application uses the R factor of the objective E-model metric. This factor represents the sum of the distortion values that are transported in the RTCP messages.

In addition to implementing the basic operation of a regular VoIP client, the NCVoIP will be composed by three QoS sub solutions that complete themselves. The first two consist in switching the codec and transport protocol in real time in a conversation and the third in using a FEC mechanism.

A. Switching Codec

As discussed above, voice codecs have different characteristics, such as transmission rate and coding delay that influence the voice quality during a conversation. For instance, if the user is connected to a low bandwidth network, it is necessary to analyze if is preferable to use the 64Kbit/s G.711 codec or the 6.3 Kbit/s G.723 codec, or any other. The answer to the question "What is the best codec in a certain situation?" represents the tradeoff between the available bandwidth, the delay and the expected voice quality. Due to the IP network characteristics it is virtually impossible to define in advance the most appropriate codec for that call.

This first part of the solution intends to automate the discovery process of the more appropriate codec to use in specific network conditions.

The process of choosing the best codec for a particular application is not an easy task because it is necessary to consider several parameters that influence the quality of the voice during a conversation. Due to the IP network characteristics it is virtually impossible to define in advance the most appropriate codec for an application.

The strategy adopted to determine the more appropriate codec to use in a given moment, is based in an iterative process that dynamically switches the audio codec when the voice quality does not correspond to the minimum requirements. To determine the codec to use when the application detects that the voice quality is low, we defined

an available ordered transmission rate codec list, because as we discussed earlier, codecs with higher transmission rates have better quality. The available ordered transmission rate codec list is illustrated in Fig. 5.



Figure 5. Available ordered transmission rate codec list

As observed in Fig. 6, when a call is established between two NCVoIP applications they use the higher transmission rate codec available, usually the G.711 codec. After establishing the call, both user applications initiate their QoS control system to evaluate the call bidirectional voice quality. When the client application detects a low voice quality, it sends a request to the other application to update the VoIP call parameters and exchange the G.711 voice codec with a lower transmission rate codec. According to Fig. 5, the next codec would be the DV14. This process repeats itself until there is no more codecs in the available transmission rate codec list.

The codec switching process must be completely transparent to the user, in other words, the user should not realize that the codec has exchanged, he should only notice that the quality of voice has increased.

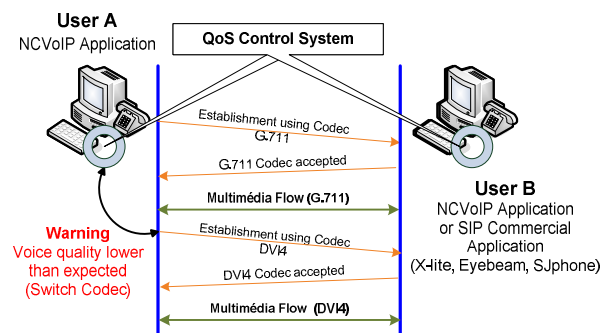


Figure 6. Real time codec switching during a VoIP call

B. Switching Transport Protocol

The end-to-end voice transport represents one of the most relevant factors to guarantee the expected QoS in VoIP communications. This way, it is necessary to define which transport protocols (UDP or TCP), fits better concerning voice quality in specific scenarios. Considering a VoIP call in a congested network, we will probably have high delay and packet losses during the call. If we are using UDP as the transport protocol, then the packet losses will be the main responsible for the quality degradation. Otherwise, if TCP is used the higher delay will be the main factor responsible for the quality reduction. This type of decision represents the tradeoff between the delay and the packet loss.

This second part of the proposed solution intends to automate the choice process of the transport protocol to use in order to optimize voice quality.

The transport protocol selection is related with the QoS parameter that we decide to minimize: delay or packet loss. In a conversation the occasional loss of one or two voice packets; although not desired, does not have a strong impact on the audio quality. The use of TCP in this case would add a considerable delay, inadmissible in media applications. Nevertheless, UDP will not always be the best option to carry voice over IP, namely in presence of a high level packet loss. In this case it is preferable to use TCP to eliminate the packet losses, at the cost of increasing delay. This tradeoff between packet loss and delay is essential to achieve a good level of quality in a conversation.

The strategy adopted to determine which transport protocol is more appropriate to carry voice in IP network, requires a permanent control of the packet loss and delay during the VoIP call. The maximum tolerable delay considered in the proposed QoS algorithm is between 100 and 200 milliseconds and the PER between 1 and 2 percent. UDP is the NCVoIP default transport protocol.

As observed in Fig. 7, when a call is established between two NCVoIP applications they use the default transport protocol, in other words UDP and both user applications initiate their monitoring system to control the call delay and the packet error rate. When the client application detects a packet error rate higher than the pre-defined, it sends a request to the other application to start using TCP.

Later if the client application detects that the call delay is higher than 200 milliseconds, it requests again the exchange of the transport protocol to UDP.

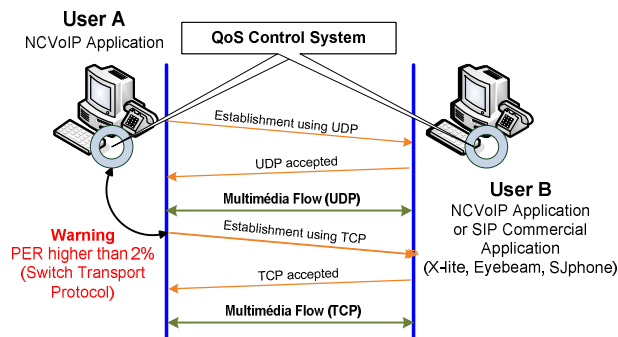


Figure 7. Real time Transport Protocol switching during a VoIP call

C. Forward Error Correction

Wireless channels, typically, have high error rates caused by attenuation, dispersion or interference from other sources. Consequently in these environments it is necessary to use an error correction technique to guarantee high voice quality. FEC emerges as the best solution to solve the problem of lost packets.

However, despite this technique is included as one of the proposed solutions in this project, it is not implemented in this version of the NCVoIP application, because further work is required to choose the most appropriate FEC mechanism and the redundant data block size.

D. Proposed Quality of Service Algorithm

The proposed QoS algorithm comprises the combination of the first two components of the solution introduced in this chapter. This algorithm is represented in Fig. 8, and seeks to discover and use automatically the more appropriate VoIP call parameters in a defined moment.

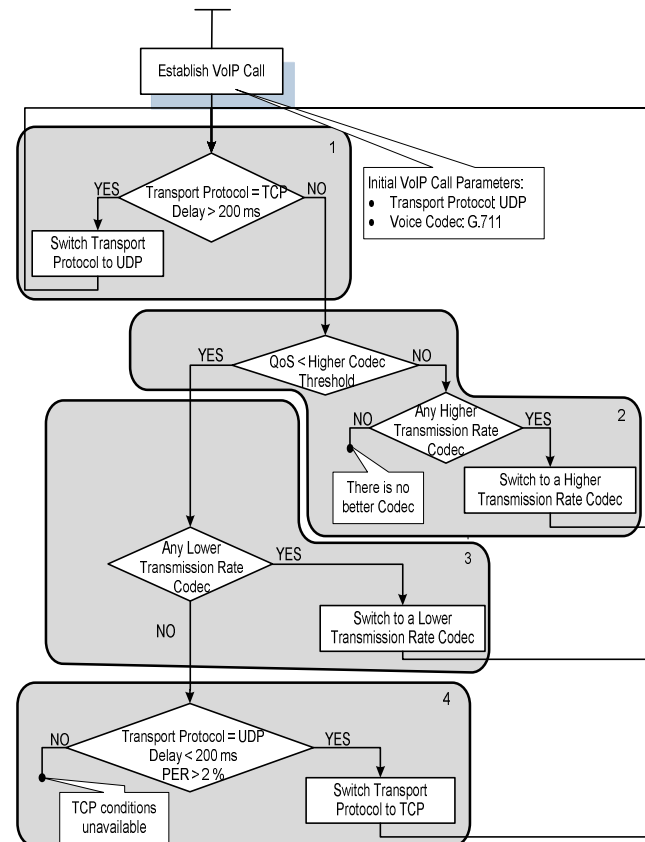


Figure 8. Quality of Service Proposed Algorithm

When a voice call is established, it starts using the UDP protocol and the highest transmission rate codec available, usually G.711. The NCVoIP application starts to regularly monitor and analyze the quality of the voice in order to assure the maximum VoIP quality. When NCVoIP detects that the quality of voice is outside the predefined values of each codec, it verifies if it is larger than the upper threshold of the Codec used, meaning that it is possible to change to a higher transmission rate Codec, if available. This process is represented in the module 2 of Fig. 8.

When the voice quality is lower than the lower threshold, the application NCVoIP checks if a lower transmission rate Codec is available and requests a Codec switch. This process takes place whenever the voice quality is lower than the expected and while there is a lower transmission rate Codec available, as exemplified in module 3 of Fig. 8.

In case there is no lower transmission rate Codec available, the delay is less than 200 ms, the PER is greater than 2% and the transport protocol used is the UDP, NCVoIP

requests to switch the transport protocol to TCP. This process is represented in the module 4 of Fig. 8. After changing to TCP protocol, it becomes necessary to periodically verify if the delay is greater than 200 ms and if the PER is less than 2%. In this case, it is necessary to switch again the transport protocol to UDP, as explained in module 1 of Fig. 8.

To avoid frequent changes of transport protocol that could cause the transmission of a high number of signaling messages, a timer is introduced after each change of transport protocol.

E. Examples of application of the proposed algorithm

Fig. 9 illustrates the application of the proposed algorithm to codec switching, using the contours of user satisfaction presented in G.109 - Amendment 1 [16]. The terminal is initially using codec G.711 at 64 Kbit/s with low delay and low losses (point A in the figure).

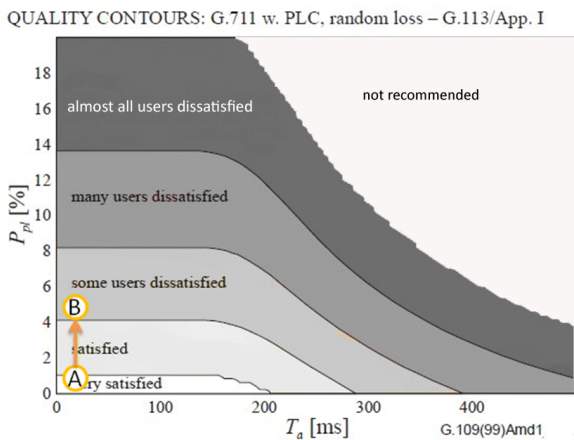


Figure 9. Initial state of the terminal with G.711 codec

If in a certain moment in time there is congestion in the network, it could cause severe packet losses in the VoIP connection (point B in the figure), degrading the VoIP quality the region “some users dissatisfied”.

As a consequence of this quality degradation, the proposed algorithm switches to the next codec with lower bitrate in order to decrease the congestion. This codec change could be done together with the activation of a FEC mechanism, in order to guarantee that the packet losses will be much lower than before.

In the example presented the new codec available is G.729A at 8 Kbit/s, which due to its much lower bitrate and the use of FEC will result in a much lower packet losses, but with higher end-to-end delay (point C in Fig. 10).

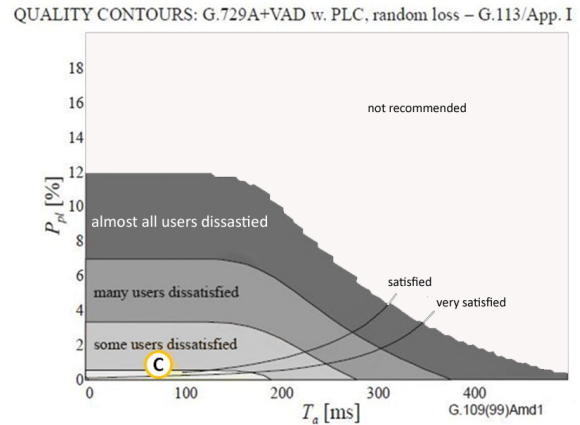


Figure 10. Terminal after switching to G.729A codec

As can be observed in Fig. 10, the terminal returned to the “very satisfied” region, what means that its quality is again very good, as desired.

Fig. 11 illustrates the application of the proposed algorithm to protocol switching. The terminal is initially at point A in this figure, as in the previous case, with low delay and low packet losses.

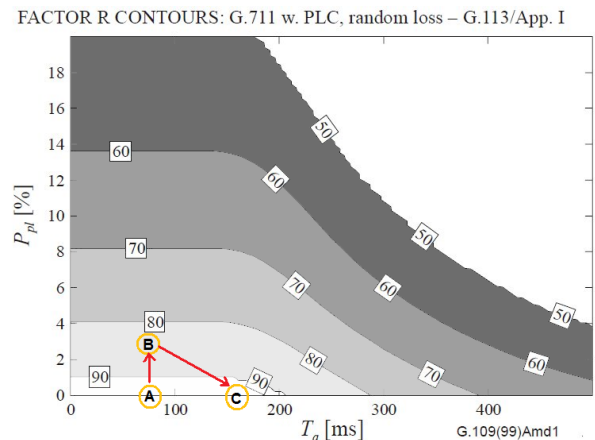


Figure 11. Transport Protocol switching sequence

If in one moment there is a sudden increase of packet losses, for instance due to noise or interference typical of wireless environments, the VoIP connection suffers high packet losses (point B in the figure).

The proposed algorithm detects this and considering that there is no other codec to switch, decides to change the protocol from UDP to TCP, in order to achieve a reliable connection, without losses. This change implies that the end-to-end delay will increase due to the occasional retransmission that happen with the TCP protocol, however if the Round Trip Time (RTT) of the TCP connection is not very high, the voice quality will still very good, since the new terminal operating point (C) will again be inside the region where the R factor is higher than 90, as can be observed in Fig. 11.

V. NCVoIP IMPLEMENTATION

Since the main objective in developing a VoIP client application was to implement and test the QoS proposed solution, it was decided to use the open source SipCommunicator Java application. This application uses the Jain-SIP v1.2 library to implement the SIP protocol and the Java Media Framework v2.1.1 library to implement the RTP and RTCP protocols.

Fig. 12 shows the architecture of the SipCommunicator client application.

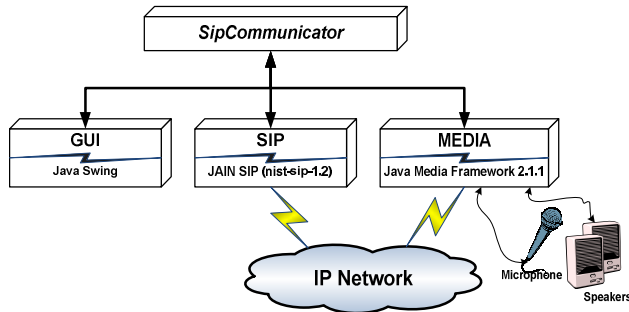


Figure 12. SipCommunicator Architecture

A. NCVoIP Components

NCVoIP architecture is shown in Fig. 13 and is structured in the five following components:

- GuiManager is responsible for the NCVoIP graphical interface presentation and its interaction with the user. This module communicates with the SipManager module when the user solicited operations that are directly related to the establishment, termination or updating of the characteristics of the call VoIP.
- SipManager, implements and manages the SIP state machine. This component creates all SIP messages that allow establishing, updating and closing a VoIP call. SipManager communicates with the MediaManager module to start, maintain and terminate the multimedia flow during a VoIP call. This module also interacts with the DoQoS module when it is necessary to change a call parameter or when it receives a request to update the characteristics of the call.
The operation to update the parameters of a VoIP call was completely implemented from scratch, since it was not included in the SIP base application. This operation was implemented using the SIP method UPDATE, defined by IETF in RFC 3311 [17]. This method allows a participant to submit a request to update the characteristics of a VoIP call in a session.
- MediaManager, generates, transmits and receives RTP and RTCP packets. This module is also

responsible for capturing and playing the multimedia data.

Upon receiving a Sender Report or Receiver Report packet, MediaManager communicates with EvalQoS in order to calculate the R factor value. MediaManager also receives indications from SipManager to start, maintain and terminate the multimedia flow during a VoIP call.

- EvalQoS is responsible for calculating periodically the E-Model R factor value based on the equations presented earlier and the values carried in RTCP packets. After calculating the R factor, this module communicates with DoQoS to evaluate and decide if it is necessary to make any change in the VoIP call parameters to increase the voice quality.
- DoQoS implements the proposed algorithm and is responsible for evaluating and deciding whether it is necessary to change any call parameter and specifies the modifications. In case it is necessary to change any call parameter, DoQoS invokes SipManager to initiate the call update process.

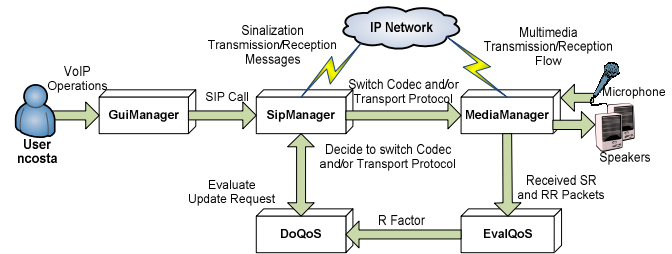


Figure 13. NCVoIP Architecture

VI. NCVoIP VOICE QUALITY MEASUREMENTS

In this chapter we present the scenarios to test, analyze and demonstrate the feasibility of the proposed solution.

The voice codecs provided by the Java Media Framework library are G.723.1, IMA/DVI4, ULAW and GSM. In order to define the order and the R factor limits associated with these codecs, it was performed a set of tests without any restriction, to measure the R factor for each codec. The duration of each test was approximately 300 seconds. Table 3 shows the results of the set of tests performed.

TABLE III. RESULTS OF ALL TESTS PERFORMED

Codec	Transmission Rate [Kbit/s]	Mean Jitter [ms]	Mean Delay [ms]	PER [%/s]	Mean R Factor
G.711	64	19,21	74,31	0	91,23
DVI4	32	19,09	74,24	0	89,00
GSM	12,2	18,60	73,73	0	86,26
G.723	6,3	17,20	72,20	0	76,55

Analyzing the values of table 3, it appears that as discussed earlier, codecs with higher transmission rate have

the highest R factor and so gradually. Therefore, the list of available codecs was ordered by its transmission rate, as shown in Fig. 14.

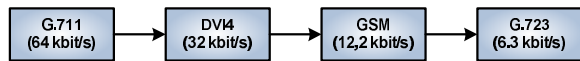


Figure 14. Ordered available JMF voice codec list

Looking again to the values of table 3, we can also determine the upper R factor limit of each codec, which will be used by the NCVoIP application to switch codec. Table 4 shows the R factor limits for each codec. This table does not include the G.711 codec, as it is the highest available voice quality codec and has no upper limit.

TABLE IV. R FACTOR CODEC HIGHER LIMITS

Codec	Higher Limit
DVI4	89
GSM	86
G.723	76

To set the lower R factor limits it was necessary to perform a set of tests using a scenario with high error rate such as the wireless network. To gather these conditions we implemented, in the NVoIP application, a mechanism to simulate packet losses in a controlled manner. It was also used the Iperf application to cause congestion and delays on the network. Therefore, using the Iperf application we were able to overload the wireless IEEE 802.11g (54 Mbit/s) with 10 Mbit/s UDP traffic.

Table 5 shows the lower R factor limits for each codec. This table does not include the G.723 codec, because it is the lower voice quality codec available.

TABLE V. R FACTOR CODEC LOWER LIMITS

Codec	Lower Limit
G.711	86
DVI4	84
GSM	74

Based on the results of table 4 and table 5 we created the table 6. This table presents the threshold limit values used for each available codec.

TABLE VI. CODEC THRESHOLD LIMITS

CODEC	Upper Limit	Lower Limit
G.711	86	-
DVI4	84	89
GSM	74	86
G.723	-	76

A. Bandwidth Limitation Test Scenario

This scenario, illustrated in Fig. 15, demonstrates how the NCVoIP voice quality behaves when there is little available bandwidth to establish a VoIP call.

To precisely limit the available bandwidth, we used the NetLimiter 2 Pro application.

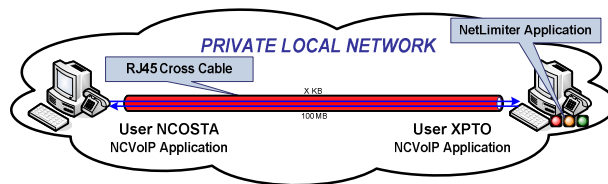


Figure 15. Bandwidth limitation test scenario

Fig. 15, illustrates the defined test scenario, which is composed by two users (NCOSTA and XPTO) that have installed the NCVoIP application to establish a VoIP call. User XPTO has also installed the NetLimiter application to limit the NCVoIP incoming bandwidth.

For each NCVoIP voice Codec available we produce two voice quality measuring tests, the first without any bandwidth limitation and the second with a pre-defined bandwidth. Every 200 seconds, user NCOSTA manually switches the voice Codec and observes its influence in the voice quality.

1) Scenario 1

In scenario 1, we defined an available bandwidth equal to 99 % of the Codec transmission rate.

TABLE VII. BANDWIDTH LIMITATION TEST SCENARIO 1

Codec	Bandwidth [Bytes]	Interval		Mean Delay	Mean PER	Mean R Factor
		Min.	Max.			
G.711	-	0	209	72.1	0.0	91.7
G.711	8110	209	399	133.6	0.4	88.7
DVI4	-	399	609	70.7	0.0	89.2
DVI4	4055	609	825	101.8	0.2	87.1
GSM	-	825	1053	69.7	0.0	86.8
GSM	1545	1053	1298	129.7	0.3	82.3
G.723	-	1298	1597	70.6	0.0	76.7
G.723	797	1597	1902	116.4	0.2	75.1

Table 7 demonstrates, as expected, that due to a packet loss increase, when we limit to 99% the available bandwidth, the R factor decreases considerably. Observing the PER values, we verify that limiting the bandwidth result in packet losses that directly influence the voice quality.

Analyzing the voice quality that resulted of the proposed QoS algorithm, we verify that in some situations it corresponds to a voice quality increase. For example, if we consider the switching process from Codec G.711 to codec DVI4, we observe that it resulted in an increase of the mean R factor from 88.76 to 89.24. On the other hand, if we consider the switching process from Codec DVI4 to GSM, we verify that it does not result in a voice quality increase, but the values are pretty close.

B. Network Congestion Test Scenario

The test scenario defined to demonstrate the voice quality achieved when two users (NCOSTA and XPTO) establish a VoIP call in a congested network is represented in Fig. 16.

User A and XPTO are connected to a 100 Mbit/s Ethernet router and user B and NCOSTA are connected to a 10 Mbit/s hub.

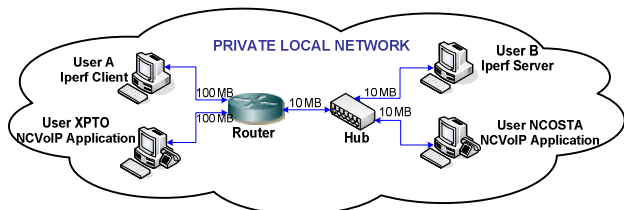


Figure 16. Network congestion test scenario

In order to simulate a network with high level of congestion we used the Iperf application to generate UDP traffic between the router and the hub. This scenario only uses the voice Codec G.711 and we switch manually the transport protocol, approximately every 300 seconds.

1) Scenario 1 – Reference Model

This first scenario represents the reference model scenario that will be used to compare the voice quality resulted by UDP and TCP protocols in the following scenarios. In this scenario, the Iperf traffic was disabled.

TABLE VIII. SCENARIO 1 TRANSPORT PROTOCOL SWITCHING SEQUENCE

Protocol	Interval		Mean Delay	Mean PER	Mean R Factor
	Min.	Max.			
UDP	0	294	73	0.0	91.7
TCP	294	603	121	0.0	90.6

Analyzing the values in table 8, we verify that the mean R factor in UDP is higher that the mean R factor in TCP, as expected.

2) Scenario 2

In this scenario we enabled the Iperf traffic and defined the Iperf client to send UDP datagram packets with a transmission rate of 8 Mbit/s.

TABLE IX. SCENARIO 2 TRANSPORT PROTOCOL SWITCHING SEQUENCE

Protocol	Interval		Mean Delay	Mean PER	Mean R Factor
	Min.	Max.			
UDP	0	295	92	0.7	89.0
TCP	295	621	130	0.0	90.2

Comparing the values in table 8 and table 9, we verify that, despite slight, the initial situation has been reversed and the TCP mean R factor is higher that UDP mean R factor.

Analyzing the values used to calculate the UDP and TCP mean R factors we verified that the UDP values are inconstant, while TCP values are constant.

3) Scenario 3

In this scenario we opted to further saturate the 10 Mbit/s connection by defining the Iperf client to send UPD datagram packets with a transmission rate of 9.5 Mbit/s.

TABLE X. SCENARIO 3 TRANSPORT PROTOCOL SWITCHING SEQUENCE

Protocol	Interval		Mean Delay	Mean PER	Mean R Factor
	Min.	Max.			
UDP	0	322	221	17.2	46.0
TCP	322	632	384	0.0	71.3

This scenario highlights even more the fact that in this situation TCP voice quality is better than UDP voice quality.

Analyzing the values in table 10, we verify that despite TCP introduces a significant delay, it is able to recover the loss packets, resulting in approximately 24 points higher than UDP.

VII. FEC EVALUATION SIMULATIONS

Since FEC was one of the solutions proposed in this paper to restore automatically the quality of voice in a VoIP call, we have done a detailed analysis to define which FEC mechanism and redundant information is the most appropriate in VoIP communications.

A. Simulation Environment

The simulation environment, represented in Fig. 17, was developed with the Simple Simulation Kernel (SSK) [18] simulator and it consists of five main blocks: TCP traffic generators, VoIP traffic generator, IP network, TCP traffic destination and VoIP traffic destination.

TCP generators simulate the best-effort traffic, VoIP generator, generate a voice G.711 packet every 20 ms. The IP network consists of two routers that have multiple queues, allowing simulating priorities and delays in packet transmission. The TCP and VoIP destinations are responsible to receive the correspondent traffic.

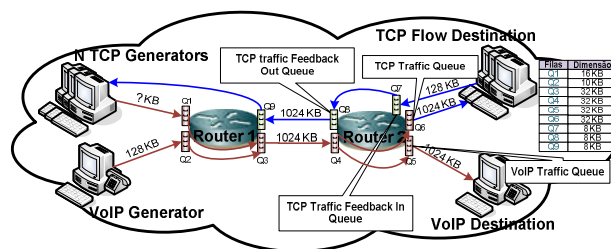


Figure 17. FEC simulation environment

B. Simulations Performed

Since we want to study the behavior of VoIP traffic in the developed simulation environment, we identified three parameters that can directly affect the performance of VoIP traffic along the path. These parameters are: size of queue Q3, number of TCP traffic generators and their respective transmission rate. The possible transmission rates are: 128 Kbit/s, 256 Kbit/s, 512 Kbit/s and 1024 Kbit/s. The TCP generators are: 1, 2, 4, 8 and 10. Each simulation has duration of 400 seconds.

In order to evaluate more accurately the influence of FEC in VoIP traffic, first we have done a set of simulations without applying the FEC technique and then repeated the

simulation with FEC. Examining the packet loss data obtained in the first phase of the simulations, we verified that the percentage of an isolated error occurrence is between 86% and 92%. Therefore, we have chosen to use a simple parity correction code FEC mechanism.

Since one of the objectives proposed in this chapter is to find the more appropriate packet block size to generate a FEC packet, we have considered the following values: 1, 2, 3, 4, 6, 8, 10, 12, 14 and 16.

Fig. 18 shows the way a FEC packet is generated from a four VoIP packet block.

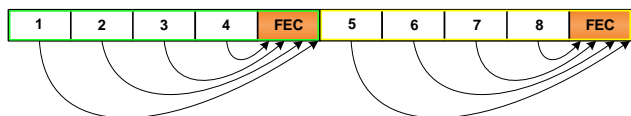


Figure 18. FEC packet generation

Since the second phase uses the first phase delay and PER values, it was necessary to correct those values due to the introduction of redundant packets in the network. The methodologies used to calculate the average values of delay and PER in this phase are explained above.

1) Mean Delay and I_d Parameter Calculation

The delay value is calculated in function of the packet block size used to generate the FEC packet. The bigger is the block size, the higher is the delay, because the receiver needs to wait for the reception of all the packets of the block until it gets the FEC packet to recover and play the missing packet.

Fig. 19 illustrates how to calculate the absolute delay when using the FEC technique to provide redundancy and be able to recover lost packets or packets with errors.

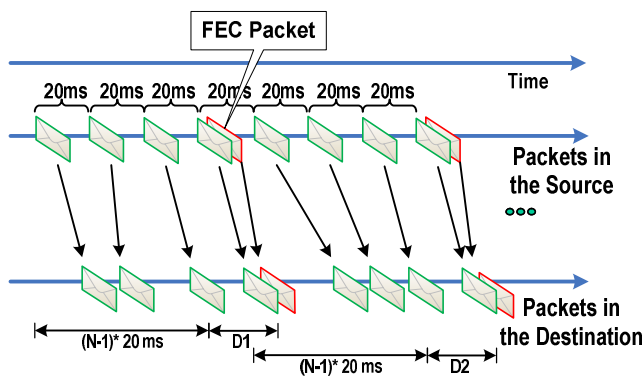


Figure 19. Absolute delay calculation

For each simulation, we grouped into blocks of N, the delay value of the VoIP packets and applied to equation 6 to obtain the new delay value.

$$newDelay = ((N - 1) \times 20 ms) + D \tag{6}$$

N represents the block size and D the delay of the last block packet. After calculated the absolute delay we used expression 3 to calculate the new I_d value.

2) Mean PER and I_e Parameter Calculation

The PER calculation process consists in grouping in blocks of N the first phase PER values and verify if there is more than one error. Using the XOR operation we can recover one packet error per block and decrease the PER value. We define PERGain as shown in equation 7.

$$PERGain = \frac{\text{number of packets recovered per second}}{\text{number of packets lost per second}} \tag{7}$$

Based on the value of the PERGain and the PER average value in the first set of simulations, it is possible to calculate the new PER average value obtained with the use of a FEC block, as illustrated in equation 8.

$$newPER = (1 - PERGain) \times PER \tag{8}$$

The I_e parameter results from the sum of I_{eloss} and I_{e0} . I_{eloss} corresponds to the equipment impairments as a function of PER. This component is directly obtained when the PER value is represented in the Fig. 4 graphic. Otherwise, I_{eloss} value is obtained through the line equation that passes between the PER adjacent points.

I_{e0} represents the overhead resulted by the introduction of the FEC packet on the IP network. To calculate this component value, we had to obtain the transmission rate correspondent to send the N + 1 packet and then use the Fig. 4 graphic.

3) VoIP over UDP and Q3 with 16 Kbyte

This first simulation group analyzes the FEC impact in VoIP traffic when router 1 has a Q3 queue of 16 Kbyte.

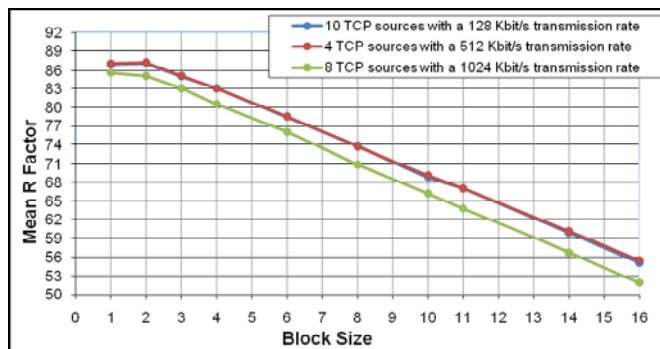


Figure 20. Simulation “VoIP over UDP and Q3 with 16 Kbyte” graphic

According to Fig. 20, in simulations of “10 TCP generators with a transmission rate of 128 Kbit/s” and “4 generators with a transmission rate of 512 Kbit/s”, it is only

efficient to use a FEC block lower than 4. In both simulations the highest R factor value happens when we have a two packet block.

4) VoIP over UDP and Q3 with 8 Kbyte

This second simulation group analyzes the FEC impact in VoIP traffic when router 1 has a Q3 queue of 8 Kbyte, as illustrated in Fig. 21.

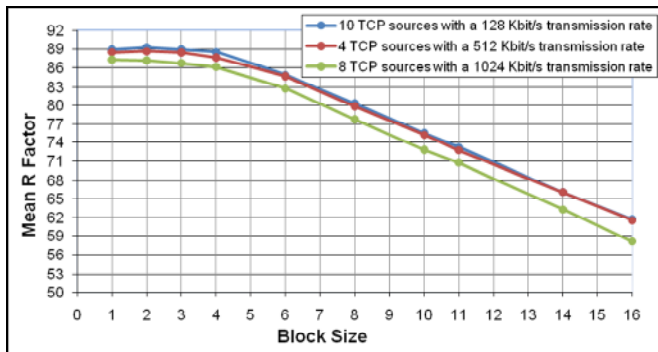


Figure 21. Simulation “VoIP over UDP and Q3 with 8 Kbyte” graphic

Analyzing the simulations “10 TCP generators with a transmission rate of 128 Kbit/s” and “4 TCP generators with transmission rate of 512 Kbit/s”, we verify that it is only efficient to use a FEC block lower than 6. In simulation “8 TCP generators with transmission rate of 1024 Kbit/s”, it is only efficient when the FEC block is lower than 8 packets.

Simulation “10 TCP generators with transmission rate of 128 Kbit/s” presents the highest R factor value when a 2 or 3 FEC block is used. Simulation “4 TCP generators with transmission rate of 512 Kbit/s” has the higher R factor value when a 2 packet FEC block is used.

VIII. CONCLUSION

This paper proposes an adaptive QoS strategy, without changing the IP network, to solve the problem of momentary drop of voice quality in a conversation and improve the overall quality of service.

To demonstrate the voice quality improvement resulting from this proposal, we developed the NCVoIP application. Based on this application, a set of voice quality measuring tests were performed. We verified that the proposed algorithm improved the quality in some scenarios, while in others there was no voice quality increase. However, based on these experimental tests, we proved that switching the voice Codec when the bandwidth is below the transmission rate of the used Codec and using TCP to encapsulate the RTP packets, when a congestion network exists, corresponds to a significant voice quality improvement. The switching of the CODEC during the communication could cause a short gap in the conversation, due to buffer re-initialization. Special care should be taken to avoid that switching of transport protocol cause losses in the audio stream.

In order to study the influence of FEC in VoIP traffic, we developed a simulation model and perform a set of

simulations. Based on these simulations we verified that it only compensate, in terms of voice quality, to use FEC when the PER is higher than 1% and that the most appropriate FEC block is two.

REFERENCES

- [1] Nelson Costa, Mário Nunes, “Adaptive Quality of Service in Voice over IP Communications”, Proceedings of the 2009 Fifth International Conference on Networking and Services (ICNS 2009), IEEE Computer Society, Valencia, Spain, April 2009, pp. 19-24.
- [2] J. Wroclawski, “The use of RSVP with IETF Integrated Services”, RFC 2210, Internet Engineering Task Force, September 1997.
- [3] S. Blake et al, “An Architecture for the Differentiated Services”, RFC2475, Internet Engineering Task Force, December 1998.
- [4] E. Rosen *et al.*, “Multiprotocol Label Switching Architecture”, IETF RFC 3031, January 2001.
- [5] M. Narbutt, A. Kelly, “Adaptive VoIP Play-out Scheduling: Assessing User Satisfaction”, IEEE, Vol. 9 N°4, July 2005.
- [6] Liang-Yi Huang Yung-Mu Chen et. Al, “Adaptive VoIP Service QoS Control based on Perceptual Speech Quality”, The 9th International Conference on Advanced Communication Technology, February 2007, Volume 2, pp. 885-890.
- [7] Wojciech Mazurczyk1, Zbigniew Kotulski, “Adaptive VoIP with Audio Watermarking for Improved Call Quality and Security”, Journal of Information Assurance and Security, September 2007, pp. 226-234.
- [8] See Leng Ng, Simon Hoh, Devinger Singh, “Effectiveness of adaptive codec switching VoIP application over heterogeneous networks”, 2nd International Conference on Mobile Technology, Applications and Systems, November 2005, pp.1-7.
- [9] ITU-T G.107, “The E-Model, a computational model for use in transmission planning”, March 2003.
- [10] A. D. Clark, “Modeling the Effects of Burst Packet Loss and Regency on Subjective Voice Quality. IP – Telephony Workshop”, 2001.
- [11] L.C.G. Lustosa, L.S.G. Carvalho, P.H.A. Rodrigues, E.S. Mota, “Using the E-Model to evaluate the quality of speech in Voice over IP communication systems”, 2004.
- [12] ITU-T G.113 Appendix I, “Provisional planning values for the equipment impairment factor I_e ”, October 2001.
- [13] Ling-Jyh Chen, Tony Sun, M. Y. Sanadidi, Mario Gerla, “Improving Wireless Link Throughput via Interleaved FEC”, UCLA, USA, 2004.
- [14] J. Rosenberg, H. Schulzrinne, G. Camarillo, A. J. Peterson, R. Sparks, M. Handley, E. Schooler, “SIP: Session Initiation Protocol”, RFC 3261, IETF, June 2002.
- [15] H. Schulzrinne, S. Casner, R. Frederick, V. Jacobson, “RTP: A Transport Protocol for Real-Time Applications”, RFC 3550, IETF, July 2003.
- [16] ITU-T G.109 Amendment 1, “The E-model based quality contours for predicting speech transmission quality and user satisfaction from time-varying transmission impairments”, January 2007.
- [17] J. Rosenberg, “The Session Initiation Protocol (SIP) UPDATE Method”, RFC 3311, IETF, September 2002
- [18] J. Azinhais, J. Jesus, “SSK – A Simple Simulation Kernel for UNIX & MS-DOS environments”, INESC, 1998

Enhancement of channel switching scenario and IGMPv3 Protocol Implementation in Multicast IPTV Networks

Benoit Hilt¹, Mounir Sarni^{1,2} and Pascal Lorenz¹

¹MIPS/GRTC
Université de Haute Alsace, France
[benoit.hilt, mounir.sarni, pascal.lorenz]@uha.fr

²Cable Departement
Vialis, France
m.sarni@calixo.net

Abstract—Nowadays, delivering television over IP technologies is increasingly used by Internet Service Providers. Having using for years the traditional TV broadcasting systems, viewers expect at least the same Quality of Experience from IPTV providers. In this paper we focus on the zapping time which is one of the most important elements for the quality experienced by the viewers. To reduce it, we propose to invert the leaving and joining operations which are traditionally used in this order. As a second step, we modify the source code of the IGMPv3 protocol implementation to leave and join IPTV channels by sending a unique message. To evaluate our solution in terms of bandwidth overhead and blackout time we conduct simulations using IGMPv2 and IGMPv3 signalling.

We show that with our proposition, in each case, the overhead stays limited in the network core. Moreover, the overhead tends to decrease when the number of the active viewers increases. Additionally, the proposed approach reduces the blackout time during a zapping process.

Keywords—component; zapping time, IGMP protocol, IPTV, bandwidth demand, channel overlapping.

I. INTRODUCTION

As the cable operator we talked about in [1], many Internet Service Providers (ISP) propose video services over IP technologies which are commonly known as IPTV (Internet Protocol Television). Unlike Internet TV [2], IPTV channels are delivered by the ISP in their own networks. An IPTV network architecture is usually set up as presented in Fig. 1. The core of the network contains an IPTV Broadband and routers. This core is connected to the clients by some active equipments which depend on the last mile technologies deployed by the ISP, such as Fiber To The Home (FTTH) technologies or Digital Subscriber Line (DSL) technologies. Finally, a Set Top Box (STB) or a Computer Software Solution allows the viewer to select and watch the channels on the TV or computer screen.

Assuming that most viewers are watching the same channels (the most popular ones), multicast streams seem to be the best way to deliver IPTV services and effectively manage the bandwidth demand of viewers. Two protocols are used to deal with multicast IPTV streams. In the core network side, a multicast routing protocol like Protocol Independent Multicast–Sparse Mode (PIM-SM) [3] is used.

It allows building distribution trees for several groups (or IPTV channels) from the source (the IPTV Broadband) to the receivers' through routers and switches. As for last mile, Internet Group Management Protocol (IGMP) [4, 5] is used by the IPTV devices to leave or join multicast IPTV streams.

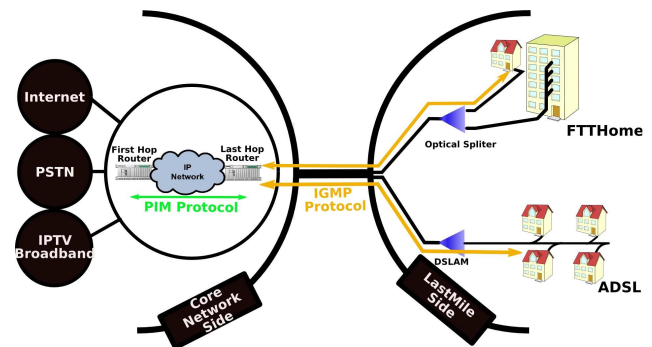


Figure 1: Typical ISP Network architecture

The use of these protocols to manage multicast streams may introduce a long network delay. This can impact the Quality of Experience (QoE) of how viewers, who have for years watched channels delivered from traditional broadcasting services (terrestrial, cable or satellite). As presented in (a) of Fig. 2, unlike the IPTV systems, in the traditional broadcasting systems, all channels are available at the user side regardless if they are requested or not. In a multicast IPTV network, only the requested channels are delivered to the viewers. So, as presented in (b) of Fig. 2 zapping delay is inevitable when viewers switch from one channel to another.

It becomes then clear that channel zapping time is one of the most important Quality of Experience parameters to be performed to deliver IPTV services in best conditions and satisfy costumers.

In the following of this section, extending the work presented in [1], we describe how we enhance channel switching scenario and IGMP protocol to efficiently switch between IPTV channels and reduce the network delay. Section II of this paper provides a background and describes some related works to reduce channel zapping time. Section

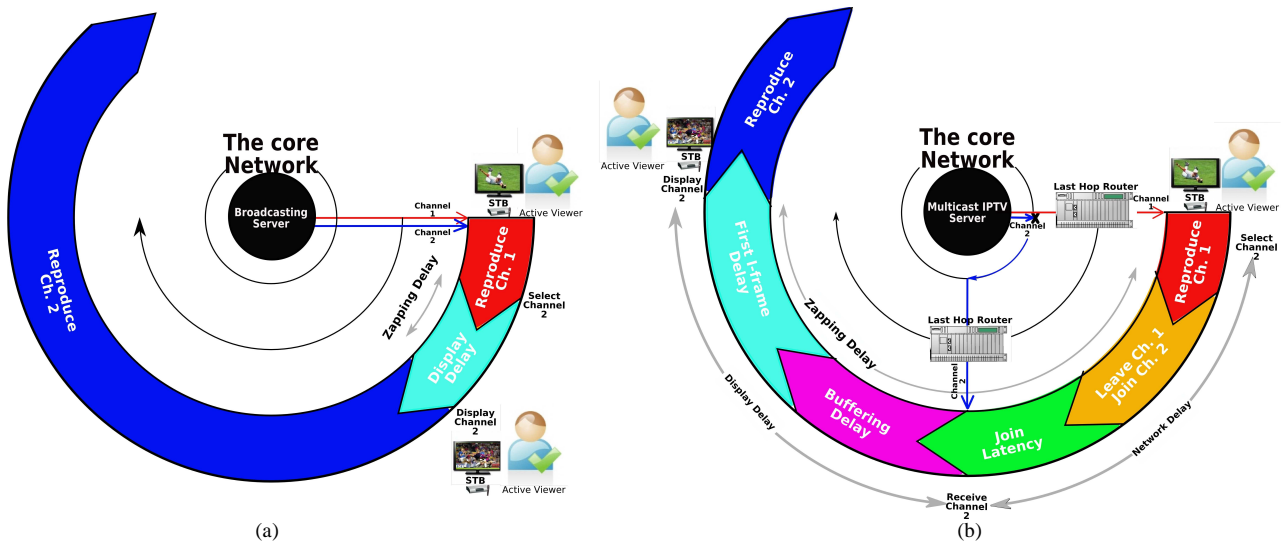


Figure 2: Broadcasting service system architecture: (a) the traditional TV broadcasting service and (b) the IPTV service

III presents our solution to improve the zapping time and section IV presents the developed multicast model with which we evaluate the bandwidth demand in the standard and the proposed approach. Section V is an overview of the IGMPv3 source code modifications made to merge the IGMP leave and IGMP join message to one and in Section VI, we show the result of our simulations. Finally, we conclude and present future work in section VII.

II. BACKGROUND AND RELATED WORK

As represented in Fig. 3, when a viewer requests a new channel, its IPTV device sends out two IGMP messages to switch between channel regardless of the IGMP version used.

When a client wants to watch a new channel he or she pushes the remote control button. After a processing delay, the IPTV device sends an IGMP-Leave message for channel being left (channel#1). When the access router receives this message, it must check, by sending an IGMP Group-Specific-Query message, if there is an IPTV receiver remaining in the network which still wants to receive channel#1. After a Last-Membership-Query-Interval which is typically set to 1 second and if the Last-Member-Query-Count is equal to 1, the access router will stop forwarding data of channel#1. If the Member-Query-Count is equal to n ($n \geq 1$), the access router will repeat the leaving process n times, as long as no response is received. The time interval between the sending of the IGMP-Leave message and the receiving of the last multicast packet of channel#1 is called the Leave Latency (LL).

After a delay we call the Channel Switch Delay (CSD), the viewer's IPTV device sends out an IGMP-Join message

for the requested channel (channel#2). If this channel is not yet available on the access router, this IGMP join message is forwarded through a PIM-Join message toward the first router having the requested channel flow available. The time interval between the sending of the IGMP-Join message and the receiving of the first multicast packet of channel#2 is called the Join Latency (JL) of channel#2.

Depending on LL , CSD , and JL values (when $LL > CSD + JL$), channel#1 could overlap with channel#2 during the Channel Overlap Delay (COD).

We can define the Network Delay (ND) as the time interval between the sending of the IGMP-Leave message for channel#1 and the receiving of the first multicast packet of channel#2. Finally, after the buffering and the decoding delay [6], the viewer can watch the requested channel on his or her computer or television screen.

This zapping scenario can be played out with version 2 of IGMP protocol which is defined in RFC 2236 [4] or with version 3 which is defined in RFC 3376 [5]. This last version has additional capabilities, but during a zapping process, the main difference with IGMPv2 is that in IGMPv3 the leave and join messages are sent to the ALL-IGMPv3-Routers multicast address (224.0.0.22) and not to the requested channel group address as in IGMPv2. This allows the router to make explicit tracking to maintain an up to date receivers and groups' lists. Therefore in the case of an IGMPv3-Leave message, if no more groups' members are registered, the router can immediately stop sending the channel data flow. This can greatly reduce the probability of having a channel overlap. However, even with IGMPv3 protocol, for code implementation reasons, two messages are still needed to achieve a zapping process.

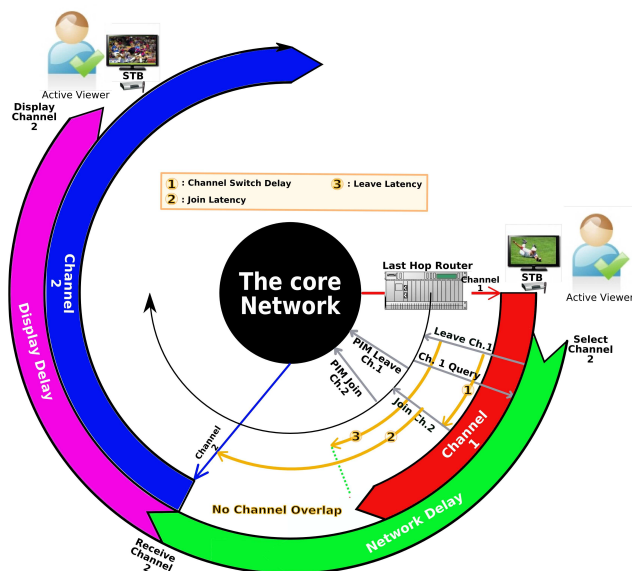


Figure 3: Standard channel switching scenario (IGMPv2, IGMPv3)

Based on the explained IPTV channel switching scenario, several ways were explored to improve channel zapping time. Some of them focused on the improvement of the Network Delay [7, 8], some others tried to reduce the zapping time by reducing the Display Delay [9, 10, 11, 12, 13, 14, 15, 16] and others tried to reduce the zapping time by predicting the behavior of the viewers during surfing [17, 18, 19, 20, 21].

A. Reduction of the Network Delay

In [7], the authors propose to reduce some IGMPv2 parameters like the General-Query-Interval (GQI) to reduce the Join Latency if the first report or join messages are lost. Over a Wavelength Division Multiplexing based Passive Optical Network (WDM-PON), they prove that when they reduce the GQI and set the Last-Membership-Query-Interval to 100 ms to quickly drop the left channel, the join delay can be reduced up to 100 ms while in the standard case it approaches 500 ms.

D. E. Smith proposes in [8] to send users unicast streams at higher than usual rates when surfing happens during commercial breaks. But even if the delay to build multicast distribution trees is avoided, the illustration of the developed model shows that this approach will highly increase the bandwidth demand by two the steady state.

B. Reduction of the Display Delay

To reduce the Display Delay by reducing the buffering delay, the authors propose in [9] to add a secondary multicast stream replicated from the main multicast stream

with a constant delay. During a zapping process the viewer's IPTV device must join both streams until the initial buffer is filled up. Then, the secondary stream is left. With a developed packet ordering rule for the secondary stream and a multiplied transmission rate r , the authors confirm a maximum reduction of 1.1 second of the zapping delay during a commercial break and a maximum zapping delay equal to 2.1 seconds.

In [10] a Multicast Assisted Zap Acceleration is presented. The aim of this method is to reduce the First I-Frame Delay (*FID*) by adding time-shifted sub-channels of the multicast mean channel. When a zapping process happens, and depending on which time the viewer requests the new channel, one of those sub-channels is considered as the main stream. Additionally, Meta-Channel that specifies the sub-channel to be chosen by the STB when a channel is requested is constantly broadcasted by the zapping accelerator. A migration solution from the sub-channel to the main IPTV channel is proposed too. Regardless of the number of the viewers, the simulations results show that this solution reduces the waiting delay of the first I-frame without requiring additional resources.

U. Jennehag and T. Zhang propose in [11] the Synchronization Frames for Channels Switching (*SFCS*) method to decrease the decoding process delay by adding a secondary stream with which resynchronization frames are sent. Viewers who want to decode the IPTV channel must join both streams. This will avoid the *FID* but will significantly increase the bandwidth utilization.

To reduce the *FID*, authors propose in [12] to change the encoding structure by adding periodically to the normal video frames additional I-frames encoded at lower bit rate. Because of these additional I-frames, the decoding process will be faster but as in [11] the bandwidth utilization is increased.

Multicast Instant Channel Change (*Multicast ICC*) method is proposed in [13]. A low bit rate multicast stream carrying only I-frames is associated to each IPTV channel. In each zapping process, the viewers must join and display first of all this secondary stream and then, when the play out buffer is filled up with the mean stream, the full quality video stream is displayed. Unlike the Unicast Instant Channel Change (*Unicast ICC*) explained in [14], this method reduces the *FID* without increasing the resource needs.

In [15], a channel control algorithm is proposed to determine the number of extra I-frames to put in the mean stream. The aim of this algorithm is to pursue an effective trade-off between the decoding delay and the bandwidth utilization.

Scalable Video Coding (SVC) was proposed in [16] to reduce the decoding delay by embedding a secondary stream in the normal stream which will reduce the bandwidth overhead compared to the MPEG coding and transport system.

C. Viewers surfing behaviors

Methods based on pre-join mechanisms are studied in [17, 18, 19]. Based on the currently watched channel, and assuming that most users use the up/down button of their remote control to surf, adjacent channels can be joined in advance [17] or sent by the IPTV Head End in low resolution [18]. In [19], the authors propose to also pre-join the most popular channels, assuming that most viewers watch only the most popular channels, but all these schemes cannot fit with each user’s preferences. In [20], a new method is proposed to reduce the channel zapping time by reflecting, for each viewer, the channel surfing behavior and the preferences, based on the pushed buttons of the remote control and the program preference of each viewers. To know the viewer’s program preferences, a personalized recommendation system for Electronic Program Guide (EPG) installed in the STBs is proposed in [21].

This analysis shows that improving channel zapping time requires several actions. Besides the pre-join methods based on viewers’ behaviors and preferences during channel surfing, solutions that reduce the Network Delay can be mixed with the propositions explained above to reduce the Buffering and the First I-frame Delay. However, all those solutions refer to the same channel switching scenario, which could be optimized.

In this paper, we propose for each version of the IGMP protocol, a novel channel switching scenario to reduce the Network Delay which stays compatible with the existing solutions presented above. With simulations, we evaluate the impact of our proposition on the network in terms of bandwidth consumption and user Quality of Experience (blackout time).

III. Proposed approach

A standard channel switching scenario consists in leaving first the currently watched channel and then joining the requested channel regardless of the IGMP protocol version used. The Network Delay is then expressed by:

$$ND_{Standard Approach} = CSD_{IPTV device} + JL_{Requested channel}$$

The Join Latency (JL) depends on several parameters like the processing capacity of the equipments used by the IPTV service provider , the number and the bit rate of the IPTV channels and the values of the IGMP protocol parameters (Last-Membership-Query-Interval, Last-

Member-Query-Count and General-Query-Interval). In [7], over a WDM-PON network, the Join Latency approaches 100 ms in the best cases.

The Channel Switch Delay (CSD) depends only on the hardware/software implementations of the used IPTV device for closing the processing of the old channel, and opening a new socket to join and start the processing of the requested channel [16]. Table I summarizes the CSD measurements of some STB from different manufacturers and some IPTV providers software solutions [22, 23]. The measured values vary from 20 ms to 200 ms. We clearly conclude that the CSD may increase the channel zapping time, especially when viewers use computer software solutions.

TABLE I
MEASURED CSD VALUES

Name	Type	Values
NetGem	Set Top Box	20 ms
Aminet110	Set Top Box	40 ms
BeePlayer	Set Top Box	50 ms
VLC0.8.6h (Linux Debian)	computer software solution	100 ms
MyFreeTV (Windows XP)	computer software solution	200 ms

To eliminate the Channel Switch Delay, we propose to modify the channel switching scenario for each version of the IGMP protocol.

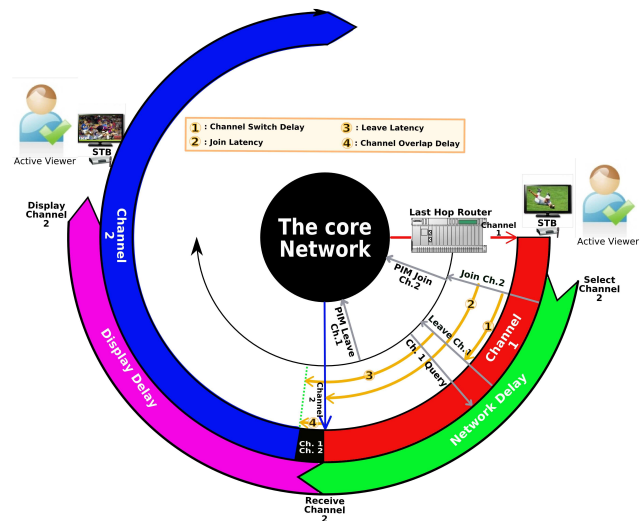


Figure 4: Proposed channel switching scenario with IGMPv2 protocol

With IGMPv2 protocol, as it’s presented in Fig. 4, we suggest to join at first the requested channel and then to leave the currently watched channel. This proposal does not need any modification of the implemented protocol but requires only modifying the embedded software of the IPTV

device. Note that in this case, unlike in the standard approach, Channel Switch Delay becomes the time interval between the sending of the IGMP-Join message and the IGMP-Leave message.

With IGMPv3 protocol, we propose to send a single message to switch between channels, as it's presented in Fig. 5. Despite the fact that IGMPv3 protocol can natively manage such a message, some code modifications are needed to make the IGMP Application Program Interface suitable to send a unique IGMP-Report message to switch between channels. These code modifications are presented in section V.

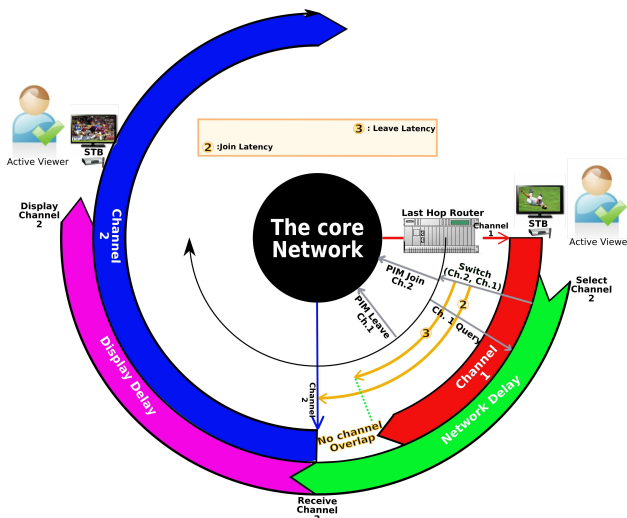


Figure 5: Proposed channel switching scenario with IGMPv3 protocol

So in both cases, regardless of the IGMP protocol version used, in light of our proposal, the Network Delay will be reduced to the Join Latency of the requested channel and therefore, can be expressed by:

$$ND_{Proposed Approach} = JL_{Requested channel}$$

If for example, as in [7], the Join Latency is equal to 100 ms, based on the values of Table I our proposal can reduce the Network Delay from 17% up to 67 %.

If we now focus on the channel overlap, as presented in Fig. 6, for the same JL , CSD and LL values, the Channel Overlap Delay may be greater in our proposed approach than in the standard approach, increasing the bandwidth consumption during surfing time.

Therefore, to evaluate the impact of our proposition in terms of bandwidth increasing during zapping times, we model the multicast IPTV service system to estimate this

increasing in different points of the network and compare it to the standard approach through simulations.

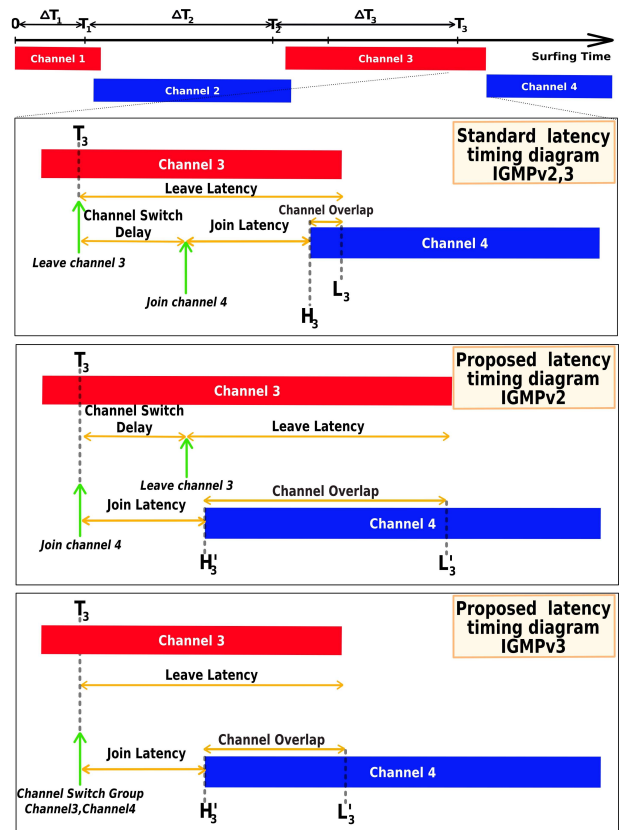


Figure 6: Channel surfing diagram

IV. MODELING IPTV SERVICE SYSTEM

Modeling of an IPTV service system takes into account several factors, including program popularity, channel definitions, viewer surfing behavior and various parameters related to the network itself. In each part of the modeling process, to finally estimate the bandwidth demand of multiple viewers, we have based our work on previous works [8, 20, 24, 25].

A. Modeling IPTV Channel Popularity

The effectiveness of the multicast model is based on how many viewers are watching the same channel at the same time. Many researches [20, 24, 25] has suggested that TV channel ranking follows a Zipf distribution. If we order the IPTV channels from the most popular to the least popular, the Zipf distribution implies that a few IPTV channels are highly ranked, whereas many are lower ranked. The Zipf distribution also known as Power Law distribution is defined by:

$$P_i = \frac{1/i^\alpha}{\sum_{c=1}^N 1/c^\alpha}$$

Where P_i is the probability that a viewer will choose the i^{th} ranked channel. N is the number of the available channels in the network and α characterizes the form of the distribution.

To set the maximum peak usage of their networks, many broadband operators apply this distribution law with a given number of viewers and broadcast channels. This allows them to calculate the blocking probability which is the probability that the bandwidth of the requested channels exceed the available bandwidth.

Fig. 7 illustrates the *Zipf* distribution law when the number of IPTV channels is equal to 40, i is equal to 1 and α varies from 0.5 to 1.5. As we can see, the number of the most popular channel tends to increase when α is going down. A study presented in [25] shows that the typical values of α goes from 0.5 to 0.95 in normal event days and could be greater than 1.5 when special event happens.

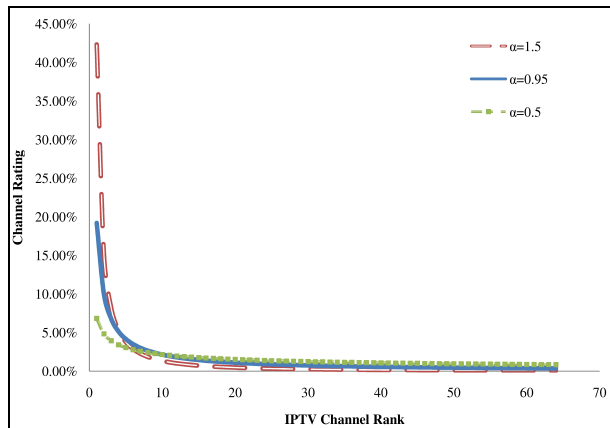


Figure 7: Channel popularity for different α values

B. Modeling Multicast Channel Surfing

The aim of modeling multicast channel surfing is to assess the maximum bandwidth usage of viewers watching multicast IPTV streams and then, to set the network load capability of the IPTV service provider to bring the blocking probability close to zero.

Basically, the total bandwidth usage at a given point of time is equal to the sum of the bit rates of the channels watched by the viewers. Therefore we will first model the bandwidth demand of a single viewer in the standard and the

proposed approach and then we will infer the total bandwidth utilization of all viewers.

B.1. Modeling the bandwidth demand of one single viewer

According to previous works [8, 20], the surfing behavior of a single viewer is represented as a Poisson distribution with an average instant of channel changing equal to λ . To take into account the difference between the two IGMP protocol versions in our proposition when a zapping happens, we first model the bandwidth demand of a single viewer when IGMPv2 protocol is used. We will then easily extrapolate to the IGMPv3 case.

Denoted by ΔT_i ($i \geq 1$) the time intervals between every channels changing. As we said earlier, ΔT_i follows a Poisson distribution. T_i ($i \geq 1$), are the times when the channel change happens, it can be described by:

$$T_i = \sum_{k=1}^i \Delta T_k$$

To define the bandwidth demand of one viewer, we will focus on IGMP messages. So at each T_i ($i \geq 1$) time, according to viewer surfing behavior, to start the channel switching process, the IPTV device will send an IGMP-Leave message in the standard case or an IGMP-Join message in our approach.

Suppose now that at time $T_0 (=0)$, the viewer is watching channel # 1. As represented in Fig. 6, in the standard case, at each time T_i ($i \geq 1$) until the end of the surfing time interval (which is in our simulation the mean duration of a commercial break), the IPTV device will send an IGMP-Leave message for channel # i and then (after the Channel Switch Delay) an IGMP-Join message for channel # $i+1$. H_i described in (1) is the first instant, after T_i in which the bandwidth demand will change. Depending on the Leave Latency (LL), the Channel Switch Delay (CSD) and the Join Latency of channel # $i+1$ (JL_{i+1}), the bandwidth demand will jump to a high state if a channel overlapping occurs or fall to zero if not. Equation (2) describes the condition for which the Channel Overlap Delay (COD) will not be equal to zero.

$$H_i = \min(LL, CSD + JL_{i+1}), i \geq 1 \quad (1)$$

$$COD_i = \begin{cases} LL - (CSD + JL_{i+1}) & \text{if } LL > CSD + JL_{i+1}, i \geq 1 \\ 0 & \text{if } LL \leq CSD + JL_{i+1}, i \geq 1 \end{cases} \quad (2)$$

Similarly, L_i described in (3) defines the instant, after $T_i + H_i$ at which the bandwidth demand will change again to be equal to the bit rate of channel # $i+1$.

$$L_i = \max(LL, CSD + JL_{i+1}), i \geq 1 \quad (3)$$

In a standard channel switching scenario, the bandwidth demand of a viewer v can therefore be expressed by:

$$B_v(t) = \begin{cases} CD_i & \text{if } t < T_i + H_i \\ 0 & \text{if } T_i + H_i \leq t < T_i + L_i \text{ and } LL < CSD + JL_{i+1}, i \geq 1 \\ CD_i + CD_{i+1} & \text{if } T_i + H_i \leq t < T_i + L_i \text{ and } LL > CSD + JL_{i+1}, i \geq 1 \\ CD_{i+1} & \text{if } T_i + L_i \leq t < T_{i+1} + H_{i+1}, i \geq 1 \end{cases} \quad (4)$$

Where CD_i is the bit rate of channel $\#i$ according to its definition (High or Simple Definition).

In the proposed channel switching scenario, when IGMPv2 protocol is used, at each T_i ($i \geq 1$) time, the IPTV device sends at first an IGMP-Join message for channel $\#i+1$ and then an IGMP-Leave message for channel $\#i$. So, we can define:

$$H'_i = \min(LL + CSD, JL_{i+1}), i \geq 1$$

$$COD'_i = \begin{cases} JL_{i+1} - (CSD + LL) & \text{if } JL_{i+1} < CSD + LL, i \geq 1 \\ 0 & \text{if } JL_{i+1} \geq CSD + LL, i \geq 1 \end{cases} \quad (5)$$

and

$$L'_i = \max(LL + CSD, JL_{i+1}), i \geq 1$$

Following the same reasoning as in the standard case, at any given point of time during the surfing, the bandwidth demand of a viewer v can be expressed by:

$$B'_v(t) = \begin{cases} CD_i & \text{if } t < T_i + H_i \\ 0 & \text{if } T_i + H_i \leq t < T_i + L_i \text{ and } LL + CSD < JL_{i+1}, i \geq 1 \\ CD_i + CD_{i+1} & \text{if } T_i + H_i \leq t < T_i + L_i \text{ and } LL + CSD > JL_{i+1}, i \geq 1 \\ CD_{i+1} & \text{if } T_i + L_i \leq t < T_{i+1} + H_{i+1}, i \geq 1 \end{cases} \quad (6)$$

In the case of using IGMPv3 protocol, the bandwidth demand has the same expression as in (6), except that when one message is sent to switch between channels instead of two, the Channel Switch Delay is equal to zero.

B.2. Modeling the bandwidth demand of m viewers.

The bandwidth demand depends on both viewers who are surfing and those who are not. To describe the bandwidth of m viewers during surfing, we must first calculate the bandwidth demand of each of them according to equation (4) or (6). Based on the bandwidth demand of each of the m viewers, the total bandwidth demand of multiple viewers can be described by:

$$B_{MV}(t) = \sum_{c=1}^n CD_c I(N_c(t) > 0)$$

Where n is the number of the channels available in the network, $N_c(t)$ is the number of the viewers who are watching channel $\#c$ and I is an indicator function.

Now that we have modeled the IPTV channel popularity and the bandwidth demand of multiple viewers, to run our simulations and estimate the bandwidth utilization based on equations (4) and (6), we need first to measure real parameters like Join Latency for a given Channel Switch Delay and Leave Latency value and that, in each approach and with each IGMP protocol version. To measure these parameters with IGMPv3 protocol when our proposition is applied, some kernel code modifications are needed to switch between channels by sending a unique message. These code modifications are presented in the following section.

V. IGMPv3 Code Modifications

The idea of switching from one IPTV channel to another with a unique message is attractive, but the current IGMPv3 Application Program Interface (API) is not suitable for this. In this section we will show how the API can be updated to make this available. When a viewer wants to join or leave a specific IPTV channel, his/her IPTV device will use the classical IP API `setsockopt()` function call with multicast options, to send a Join or a Leave IGMP message. These options are sorted in IPv4, IPv6 and IP version-independent options [26]. To illustrate our proposition we focus only in IPv4.

With the current available IGMP specific options of the `setsockopt()` function, the switching from a currently watched group (or IPTV channel) to a new one needs two successive calls. All tested software/hardware solutions send first an IGMP-Leave message and then an IGMP-Join message. These requests are expressed at the socket layer by successive `setsockopt(socket, IPPROTO_IP, ACTION, imr, sizeof(imr))` calls, where "ACTION" is first set to "IP_DROP_MEMBERSHIP" to drop the left multicast channel and then to "IP_ADD_MEMBERSHIP" to join the new one. `imr` is an `ip_mreq` structure containing the multicast address and the device on which the group will be joined or left.

Branches 1 and 2 of Fig. 8 represent the IGMP functions called to switch between channels in the standard case. When the viewer's IPTV device calls the `setsockopt()` function to join or leave an IPTV channel, the corresponding `do_ip_setsockopt()` (line 402: `ip_sockglue.c`) [27] function in the kernel space is called. Depending on the "ACTION" parameter the program goes to the join or to the leave part.

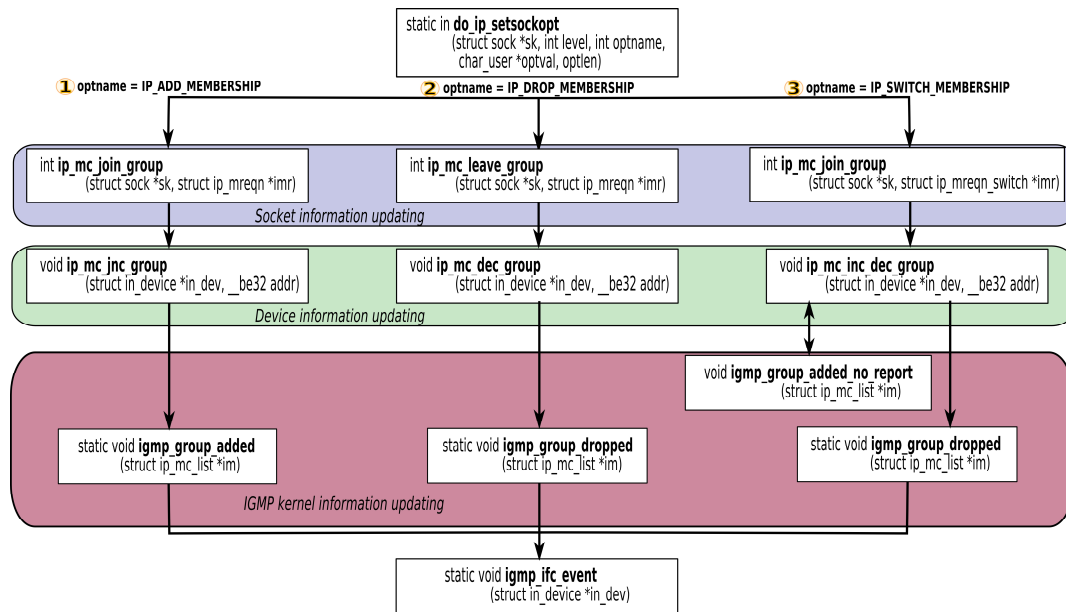


Figure 8: Flowchart of the called functions to switch between channels

The behavior is similar in both cases and follows these steps:

1. Firstly, in the *ip_mc_join_group()* (line 1720:*igmp.c*) or *ip_mc_leave_group()* (line 1792:*igmp.c*) function, the elements of the current socket are updated by adding the multicast group to be joined or deleting the multicast group to be left,
2. Secondly a call to the *ip_mc_inc_group()* (line 1198:*igmp.c*) or *ip_mc_dec_group()* (line 1257:*igmp.c*) updates the elements of the physical device on which the socket is connected. This is done by adding the multicast group to join or by deleting the multicast group to leave. Additionally the elements like IGMPv3 timers and filter modes are set [5],
3. Thirdly, the *igmp_group_added()* (line 1159:*igmp.c*) or *igmp_group_dropped()* (line 1122:*igmp.c*) function is called to mainly deal with the active version of IGMP (version 2 or version 3).
4. Finally, the *igmp_ifc_event()* (line 716:*igmp.c*) function is called to trigger the IGMP-Report message to join or to leave the IPV channel.

As indicated earlier, depending on the value of the IGMP Robustness Variable, these steps could be repeated.

According to our proposition made in section III, we define a new “ACTION” option called

“IP_SWITCH_MEMBERSHIP”, which can be used in the *setsockopt()* function . Its goal is to produce a single message carrying both *Join and Leave* information.

A. The new “IP_SWITCH_MEMBERSHIP” option in the IGMP host part

To make the new “IP_SWITCH_MEMBERSHIP” option available for *setsockopt()* calls, we modified the source code [27] and added a new case in the *do_ip_setsockopt()* function code. Branch 3 of Fig 8 summarizes the sequences of the called functions to finally send a unique message to switch between multicast channels.

Unlike the “IP_ADD_MEMBERSHIP” and the “IP_DROP_MEMBERSHIP” options, the new “IP_SWITCH_MEMBERSHIP” option needs simultaneous information about the joined and the left groups. Therefore we created a new *ip_mreqn* structure called *ip_mreqn_switch* carrying two address fields called *imr_joinaddr* and *imr_leaveaddr* instead if the one which is called *imr_multiaddr* in the standard case. The rest of the structure stays similar to the standard case.

```

struct ip_mreqn_switch {
    struct in_addr imr_joinaddr; /* group to join */
    struct in_addr imr_leaveaddr; /* group to leave */
    struct in_addr imr_interface; /* interface to join on */
}
    
```

Like the joining/leaving sequences presented in branch 1 and 2 of Fig. 8, the `do_ip_setsockopt()` function calls a new `ip_mc_switch_group()` function. This function is the merge of the `ip_mc_join_group()` (line 1614:igmp.c) and the `ip_mc_leave_group()` (line 1692:igmp.c) functions. The goal of this new function is to update the structure of the properties of the socket in use. So the `imr_joinaddr` address is inserted at the beginning of the multicast groups list and the `imr_leaveaddr` address is removed from this group list. Additionally, the `ip_mc_inc_group()` (line 1659:igmp.c) and the `ip_mc_dec_group()` (line 1717:igmp.c) functions of the branch 1 and 2 of Fig. 8 are replaced by a new `ip_mc_inc_dec_group()` function. This function is used to update the elements of the physical device used by the current socket. It is the merging of `ip_mc_inc_group()` and `ip_mc_dec_group()` functions. The difference with the original functions is that this function needs to receive the two groups' information simultaneously.

Finally, the `igmp_group_added()` function of the standard case is replaced by a new `igmp_group_added_no_report()` function. In the original `igmp_group_added()` function, in addition to the settings of the IGMP protocol variables and timers there is a call to the `igmp_ifc_event()` (line 1091:igmp.c) function. This call triggers an IGMP-Report message. To avoid this and allow the further message to be sent as a 2 in 1 message, we create a new function called `igmp_group_added_no_report()` in which the `igmp_ifc_event()` is suppressed. The rest of the merged functions remains unchanged. That's it, at the end of the `ip_mc_inc_dec_group()` function a call to the `igmp_ifc_event()` function triggers an IGMP-Report message. This message will then contain both the new added group in the form of a (`group_to_join:change_to_include_mode`) group record and the deleted group in the form of a (`group_to_leave:change_to_exclude_mode`) group record.

As shown in Fig. 9, in the standard approach, the switching method from group 239.1.1.1 to group 239.1.1.2 made with the multimedia player VLC is expressed with IGMPv3 by two redundant messages. IGMP protocol

robustness requires that each message is repeated twice. This requirement leads to a mixed Leave/Join message at the end of the switching process. Delta time are displayed in the "Time" column, we can see that the CSD is equal to 152 ms in this try.

The frames capture of Fig. 10 show the result of a `setsockopt()` call with the new defined "IP_SWITCH_MEMBERSHIP" option for a switching from group 239.1.1.2 to group 239.1.1.1. As in Fig. 9, the robustness variable value (equal to 2) makes that the message is repeated twice. The comparison of Fig. 9 and Fig. 10 shows us that now, only one messages is sent to switch from one group to another.

B. The new "IP_SWITCH_MEMBERSHIP" option in the IGMP router part

Because the version 3 of the IGMP protocol is designed to take into account IGMP-Report messages carrying several records of IGMP-Join/Leave information, there is no need to any modification in order to take into account this new option.

C. Backward compatibility

If we force the IGMP version of multicast hosts to version 2 by setting the kernel `force_igmp_version` parameter to 2 and run zapping tests with code using the "IP_SWITCH_MEMBERSHIP" option, we notice that our new implemented option stay compatible with version 2 of IGMP and two messages will be sent to switch between channels.

VI. SIMULATION AND RESULTS

As indicated at the end of section IV, to run our simulation based on equations (4) and (6) we went through two steps. In a real network, we started by measuring the Join Latency (JL) of IPTV channels for a given values of LL

Time	Source	Destination	Info
0.000000	172.16.179.132	224.0.0.22	v3 Membership Report / Join group 239.1.1.1 for any sources
0.786027	172.16.179.132	224.0.0.22	v3 Membership Report / Join group 239.1.1.1 for any sources
6.758307	172.16.179.132	224.0.0.22	v3 Membership Report / Leave group 239.1.1.1
0.152416	172.16.179.132	224.0.0.22	v3 Membership Report / Join group 239.1.1.2 for any sources
0.589402	172.16.179.132	224.0.0.22	v3 Membership Report / Leave group 239.1.1.1 / Join group 239.1.1.2 for any sources

Figure 9: Whireshark screenshot of the channel switching scenario in the standard case when IGMPv3 is used

Time	Source	Destination	Info
0.000000	172.16.179.132	224.0.0.22	v3 Membership Report / Join group 239.1.1.2 for any sources
4.087784	172.16.179.132	224.0.0.22	v3 Membership Report / Join group 239.1.1.2 for any sources
3.199888	172.16.179.132	224.0.0.22	v3 Membership Report / Leave group 239.1.1.2 / Join group 239.1.1.1 for any sources
2.452044	172.16.179.132	224.0.0.22	v3 Membership Report / Leave group 239.1.1.2 / Join group 239.1.1.1 for any sources

Figure 10: Whireshark screenshot of the channel switching scenario in the proposed case when IGMPv3 is used

before running our simulations.

A. Measurement of the Join Latency in a real network

Vialis [28] is a small ISP based in Colmar (France) offering a triple play service over a Cable, FTTH-PON (FTTH-Passive Optical Network) and FTTH-P2P (FTTH-Point To Point) networks. In [1] we already measured the Join Latency and evaluated the bandwidth demand in Vialis PON network where only IGMPv2 was used. In this paper, to run additional simulations, we have chosen the FTTH-P2P Vialis network in which we measured the Join Latency, and so the Network Delay, in the standard and the proposed approach with each IGMP protocol version.

As presented in Fig. 11, Vialis IPTV network is based on 1 IPTV Broadband, 4 multicast routers, one Ethernet switch and two optical switches (one in the Head End and another in the last mile side). Each optical switch has 24 optical ports and all active equipments run IGMP Proxy function.

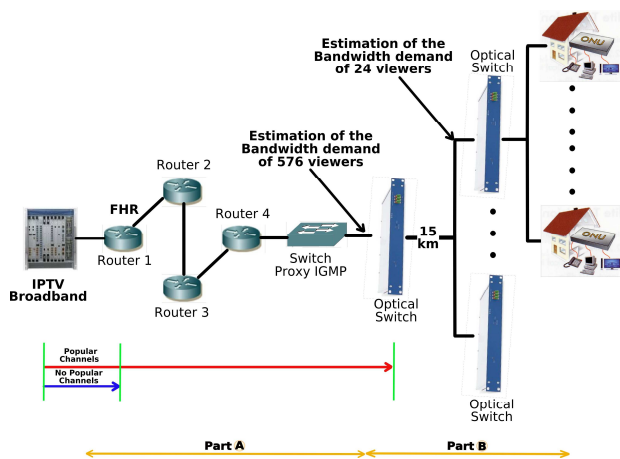


Figure 11: Vialis FTTH-P2P network

According to previous work [11], the most popular channels are directly available at the optical switch in the Head End while all others must be required further in the network. According to [7], we set the Leave Latency equal to 100ms (Max Response Time = 100ms, Robustness Variable =1).

We modified the software code of the IPTV device to test our proposed approach with IGMPv2 and IGMPv3. When IGMPv2 is used with our proposition, the Channel Switch Delay was measured equal to 10 ms. This value may be reduced when the software code modification is optimized

The time to setup a branch end to end between an IPTV device and the IPTV Broadband was measured equal to 125ms. For each version of IGMP protocol, this value is

composed of 10 ms from the IPTV device to the optical switch in the Head End (branch A in Fig. 11) and, in accordance with [29], 115 ms from this optical switch to the IPTV Broadband through the 4 routers and the Ethernet switch (branch B in Fig. 11). To simplify our illustration, we assume that at any place of the network, the Join Latency does not vary with the network traffic load.

Table II summarizes the values of the parameters used in our simulation, 10% of the available channels are HD channels and 60 % of the users have STB to watch IPTV channels, the rest uses software solutions.

TABLE II
PARAMETERS VALUES OF OUR EXAMPLE

Symbol	Definition	Values
λ	Mean of Poisson distribution	5
T_{surf}	Channel surfing duration	300 seconds
n	Number of available channels	500 channels
α	Zipf exponent value	0.95
SD	Bit stream of Simple Definition channel	4 Mbps
HD	Bit stream of High Definition channel	15 Mbps
LL	Leave Latency	100 ms
CSD_1	Channel Switch Delay of STB (in the Standard Approach)	20 ms
CSD_2	Channel Switch Delay of computer software solution (in the Standard Approach)	200 ms
CSD_3	Channel Switch Delay (in the Proposed Approach)	10 ms
JL_1	Join latency of the 10 most popular channels	10 ms
JL_2	Join Latency of all channels except the 10 most popular one	125 ms

Now that we have the values of the simulation parameters, we will estimate, as a second step, the bandwidth demand and the maximum channels requested for a given number of viewers and channels during a commercial break with Scilab, a software for numerical computations [30].

B. Estimation of the bandwidth demand of 24 active viewers

At T=0, suppose that all active viewers are watching IPTV channels according to their popularity. The first simulation conducted with Scilab shows us in Fig. 12 that for a branch of 24 active viewers, the bandwidth demand varies from 51 Mbps to 175 Mbps both in the standard and the proposed approach. The big gap between the minimum and the maximum value of the bandwidth demand is caused by the number of the requested channels according to their popularity, and the channel overlapping when it happens. This means that, as we did, the channel switching scenario

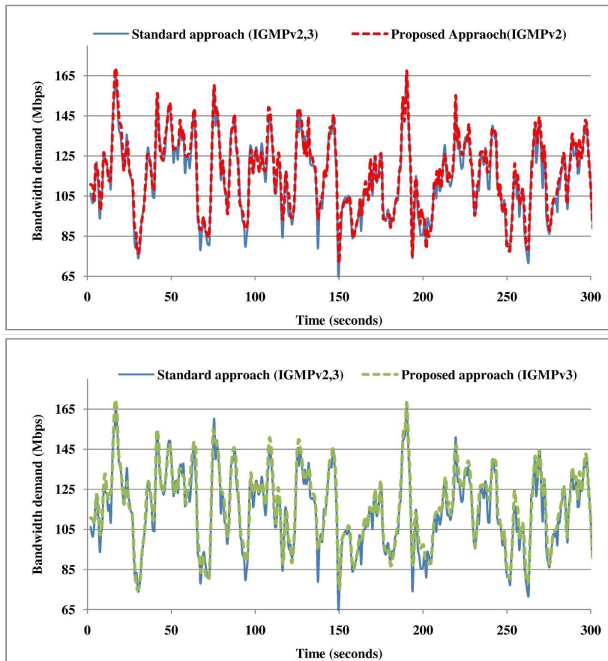


Figure 12: 3-moving average of bandwidth demand

must be taken into account to model the bandwidth demand of multicast streams.

Fig. 13 shows over a short period of time the difference between the bandwidth demand in the standard and the proposed approach for each version of IGMP protocol. We

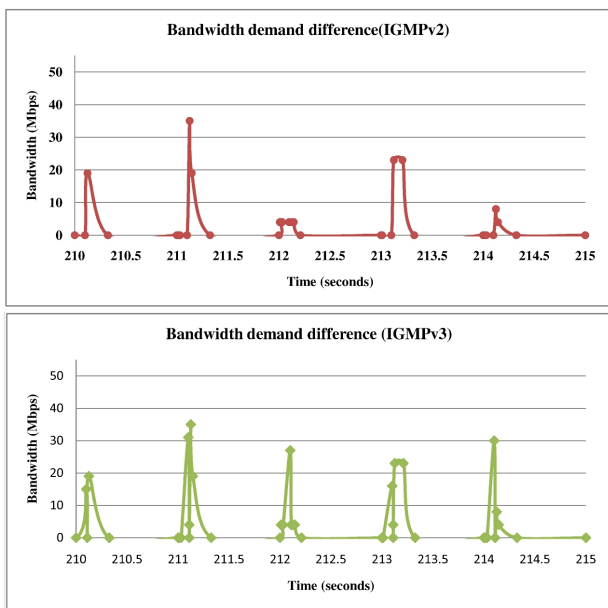


Figure 13: Bandwidth demand difference

can see that our solution increases the bandwidth demand only during overlap periods.

Unlike the estimation of the maximum number of the requested channels at the same time, illustrating a real time bandwidth demand is not a good indicator to dimension multicast IPTV networks and know, at the top, how many channels will be requested at the same time.

C. Estimation of the maximum number of the requested channels by the active viewers

To evaluate the maximum number of channels requested at the same time in the multicast IPTV network, we use Monte Carlo approach [25]. Keeping the same parameter values of Table II, we vary the number of active viewers from 24 to 576 (24*24) and the number of available channels from 250 to 500. For each of those parameters value, we repeat the process 1,000 times. At first we do not vary the value of the Zipf exponent α and set it to 0.95.

As we can see in Fig. 14, for 24 active viewers in a single FTTH-P2P branch, our approach will not increase the maximum number of the requested channels regardless of the number of available channels in the network and the IGMP protocol version used. For each approach, the maximum number of the requested channel varies from 23 to 27 if 250 channels are available and from 24 to 28 if 500 channels are available. In 1000 runs, 24 and 25 are the numbers of the maximum channels which occurs the most if respectively 250 channels and 500 channels are available.

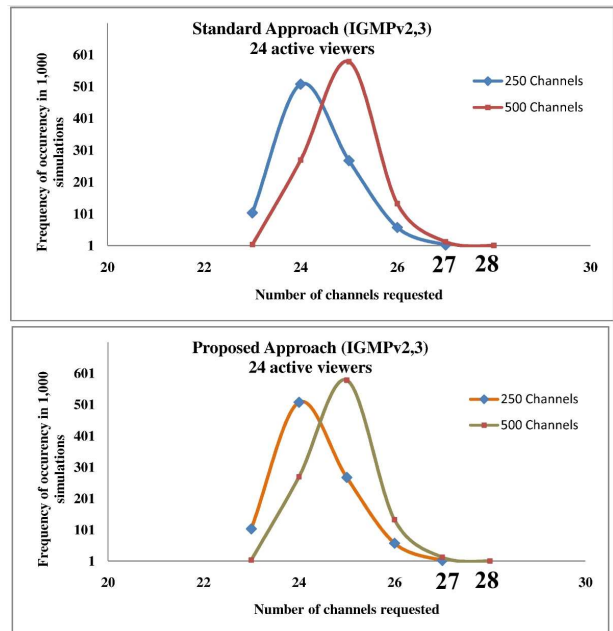


Figure 14: Maximum channels requested by 24 active viewers

However, to set the network load capability and bring the blocking probability close to zero, an IPTV service provider must estimate the maximum peak rate in the core network.

Since the 10 most popular channels are available at the optical switch in the Head End, to estimate the maximum number of the requested channels between the optical switch and the upper router, these channels will be taken into account regardless of viewer behavior in both approaches. At this point of the network, based on the values in Table II, the Join latency is equal to 115 ms ($JL_2 - JL_1$).

Fig 15 makes it clear that globally, as in the FTTH-PON network [1], for the chosen parameters values of Table II, our approach does not increase the bandwidth demand compared to the standard approach. In other terms, the multicast bandwidth necessary to provide IPTV service is the same in both standard and proposed channel switching scenario. This is due to the fact that, as it's showed in Table III, when the Join Latency is equal to 115 ms, the Channel Overlay Delay (COD) is equal to zero based on equation (2) and (5), in each approach, regardless of the IGMP protocol version.

The COD is not null in a branch of 24 users only when the popular channels are requested.

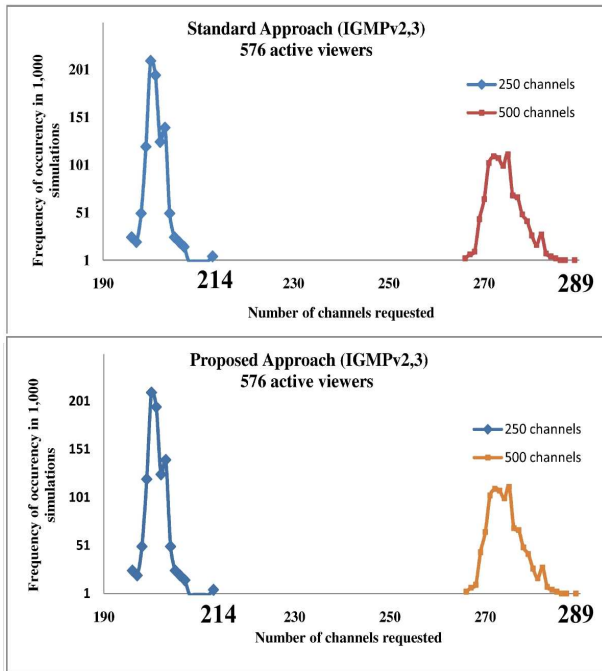


Figure 15: Maximum channels requested by 576 active viewers

TABLE III
VALUES OF THE CHANNEL OVERLAP DELAY (1)

Cases	Leave Latency (ms)	Channel Switch Delay (ms)	Join Latency (ms)	Channel Overlay Delay (ms)	Part in Fig. 11
Standard IGMPv2,3	100	20	10	70	B
	100	20	115	0	A
	100	20	125	0	A+B
	100	200	10	0	B
	100	200	115	0	A
	100	200	125	0	A+B
Proposed IGMPv2	100	10	10	100	B
	100	10	115	0	A
	100	10	125	0	A+B
Proposed IGMPv3	100	0	10	90	B
	100	0	115	0	A
	100	0	125	0	A+B

To see what happens if the Channel Overlay Delay exists in our approach, the Join Latency must be reduced to satisfy the following condition:

$$JL < CSD + LL$$

Therefore, only one multicast router in the Head End was necessary to remove to reduce the Join Latency and make channels overlap in the proposed approach. Table IV summarizes those new measured Join Latency values in each part of the network presented in Fig. 11. We will then compare our approach when channels overlap during a zapping process with a standard case in which channels don't overlap in the core network.

TABLE IV
VALUES OF THE CHANNEL OVERLAP DELAY (2)

Cases	Leave Latency (ms)	Channel Switch Delay (ms)	Join Latency (ms)	Channel Overlay Delay (ms)	Part in Fig. 11
Standard IGMPv2,3	100	20	10	70	B
	100	20	85	0	A
	100	20	95	0	A+B
	100	200	10	0	B
	100	200	85	0	A
	100	200	95	0	A+B
Proposed IGMPv2	100	10	10	100	B
	100	10	85	25	A
	100	10	95	15	A+B
Proposed IGMPv3	100	0	10	90	B
	100	0	85	15	A
	100	0	95	5	A+B

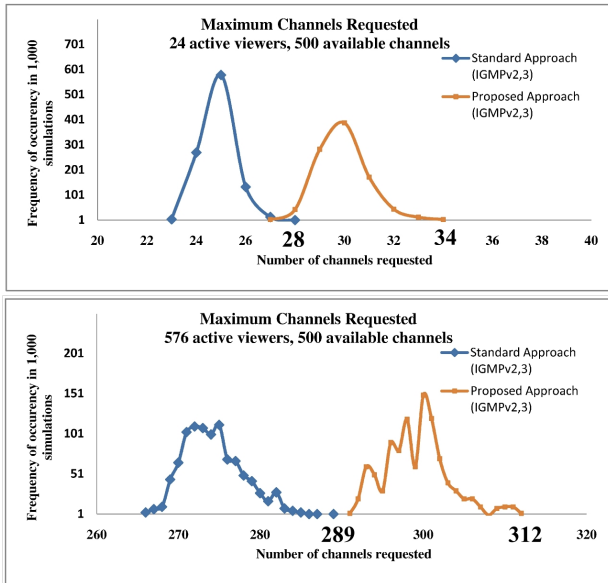


Figure 16: Maximum channels requested if channels overlap

As showed in Fig. 16, compared to the standard approach, our proposition may increase the maximum number of the requested channels when channels overlap during a zapping process. In our approach, if 500 channels are available in a branch of 24 active viewers, the maximum number of the requested channels varies from 27 to 34 with a mean of 30 channels. Compared to the standard approach, this increase is about 21%. In the network core when 576 viewers are active, the number of the maximum channels requested at the same time varies from 290 to 312 channels in our approach, which is an increasing of 8% compared to the standard approach.

Of course, depending on the values of the Zipf exponent, for a given number of active viewers, the maximum number of the requested channels may not be the same in each approach. Therefore, we evaluate the impact of channel popularity in Fig. 17 and Fig. 18 for a branch of 24 active viewers and then, for 576 active viewers.

Fig. 17 shows us, based on the values in Table IV, the maximum number of the requested channels in a branch of 24 active viewers for 3 different α values. As we can see, in the standard approach, this number goes from 21 channels, if we have special events ($\alpha=1.5$), to 28 channels if the raking values of the most popular channel are small ($\alpha=0.5$). In the proposed approach, the maximum number of the requested channels varies from 27 to 39. Also, compared to the standard approach, our approach increases in each branch of the FTTH-P2P network, the maximum number of the requested channels from 9% to 32% depending on α value.

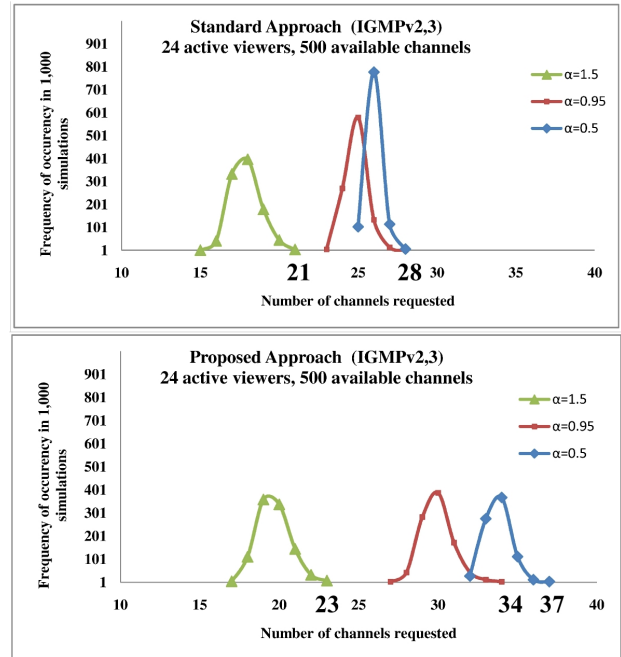


Figure 17: Maximum channels requested depending on α value

Fig. 18 shows us that in a multicast IPTV network of 576 active viewers our proposition increases the maximum number of the requested channel only by 8% the standard approach, regardless of the IPTV programs popularity and the IGMP protocol version used. This is because of the big number of active viewers who request generally the same IPTV channels during the surfing.

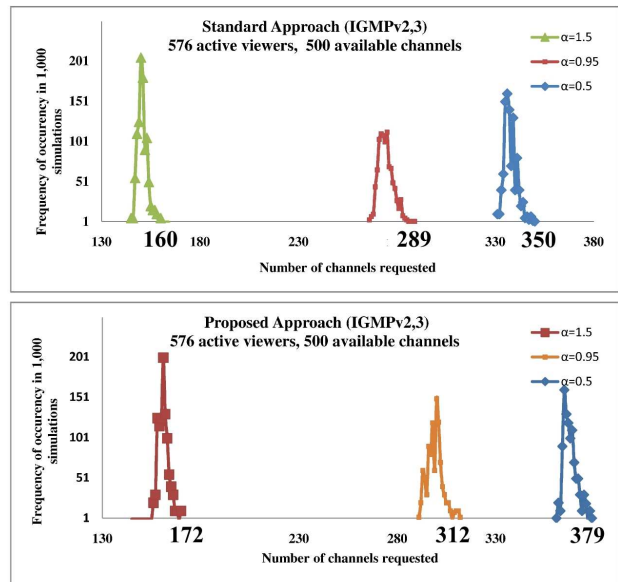


Figure 18: Maximum channels requested depending on α value

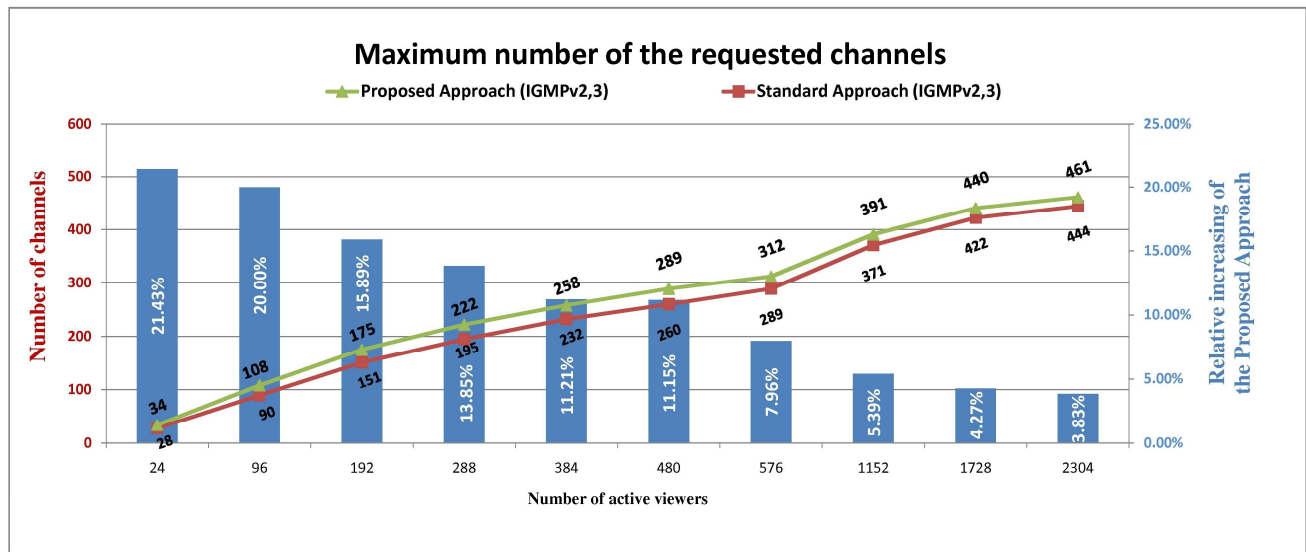


Figure 19: Maximum number of the requested channels

Our last simulations show that, compared to the standard approach, the relative increasing caused by our approach when channels overlap, is reduced when the number of viewers increases. As it's presented in Fig. 19, when $\alpha=0.95$ and 500 channels are available, the impact of the channel overlapping has less effect when the number of active viewer is increasing. The biggest difference value of the maximum requested channels was measured when 480 viewer are active, this value decreased to be equal to 17 channels when 2304 active viewers are in the network.

D. Reduction of the Blackout time in the proposed approach

When a viewer requests a new channel, a blackout appears during the switching time. This is due to the decoding process delay and the time between the last packet of the currently watched channel and the first packet of the requested one.

Depending on the network parameter values (Leave Latency, Join Latency and Channel Switching Delay), our approach may introduce a channel overlapping. In the previous section, we showed that this may increase a little the bandwidth demand in the network core, but the good point is that it can also reduce the blackout time increasing the quality experienced by the viewer.

Based on the parameter values of Table II, during a period of 300 seconds, we summed, according to (4) and (6), the time interval in which the bandwidth demand is equal to zero. In a branch of 24 active viewers, the average of the measured value was measured equal to 6.5 seconds per viewer in the standard approach while in our approach, this value goes down to 0.6 second per viewer when IGMPv2 is

used and 1 second when IGMPv3 is used to switch between channels.

VII. CONCLUSION AND FUTURE WORK

To reduce the zapping time, many solutions were proposed based on the same channel switching scenario, this standard scenario could be more optimized. Therefore, we proposed in this paper a novel scenario which stays working with the previous solutions. Unlike the standard approach, to switch between two channels, the solution we proposed consists in sending an IGMP-Join message for the requested channel before leaving the currently watched channel by sending an IGMP-Leave message. Our solution improves channel zapping time, especially when users are using computer software solution. However, it may create short overlaps period between channels during a zapping process increasing briefly the bandwidth demand.

We showed then that with some source code modifications, IGMPv3 becomes suitable for switching between channels with a unique message

To estimate the impact of the channel overlapping in terms of bandwidth consumption, we modeled the multicast bandwidth demand of viewers surfing during a commercial break and we prove that globally, depending on network parameters values and regardless of the used IGMP version protocol, our solution increase by 8% the maximum number of the requested channel in a core network where 500 channels are available and 576 viewers are active during a zapping process. Moreover, this relative increasing tends to decrease when the number of the active viewer becomes bigger.

We finally measured that the blackout time is reduced bringing an additional improvement of the viewer experience.

In this work, we acted mainly at the first step of the zapping process which is the network processing part. In further work, we will focus on the second step of the zapping process. For the same aim, we will propose some mechanisms to send secondary streams, based on the mean streams and the moment of the zapping, to reduce the Buffering Delay and the First I-Frame Delay at the same time.

REFERENCES

- [1] M. Sarni, B. Hilt and P. Lorenz, "A Novel Channel Switching Scenario in Multicast IPTV Networks", The Fifth International Conference on Networking and Services (ICNS 2009), April 2009.
- [2] "Assuring Quality of Experience for IPTV", HeavyReading Whitepaper, July 2006.
- [3] Estrin D., Farinacci D., Helmy A., Thaler D., Deering S., Handley M., Jacobson V., Liu C., Sharma P., and L. Wei, "Protocol Independent Multicast-Sparse Mode (PIM-SM): Protocol Specification", 4601, August 2006.
- [4] W. Fenner, "Internet Group Management Protocol, version 2", RFC 2236, November 1997.
- [5] B. Cain, S. Deering, I. Kouvelas, B. Fenner, A. Thyagarajan, "Internet Group Management Protocol, version 3", RFC 3376, October 2002.
- [6] L. Hart, "Introduction to MPEG; MPEG-1, MPEG-2 and MPEG-4", Althos Publishing, August 2006.
- [7] J. Kim, H. Yun, M. Kang, T. Kim, and J. Yoo, "Performance evaluation of channel zapping protocol in broadcasting services over hybrid WDM-PON", International Conference on Advanced Communication Technology, vol. 2, pp. 1152-1155, Feb. 2005.
- [8] D. E. Smith, "IP TV Bandwidth Demande : Multicast and Channel Surfing", International Conference on Computer Communications, vol. 26, pp. 2546 -2550, 2007.
- [9] C. Saraki, A. Tagami, T. Hasengawa and S. ANO, "Rapid Channel Zapping for IPTV Broadcasting with Additional Multicast Stream," International Conference on Communication, October 2008.
- [10] Y. Berjerano and P. V. Koppol, "Improving Zap Response Time for IPTV", International Conference on Computer Communication, March 2009.
- [11] U. Jennehag and T. Zhang, "Increasing bandwidth utilization in next generation IPTV networks", International Conference on Image Processing, vol. 3, pp. 335-340, July 2002.
- [12] J. M. Boyce and A. M. Tourapis, "Fast efficient channel change [set-top-box applications]", International Conference on Computers in Education Digest of Technical Papers, pp. 1-2, Jan. 2005.
- [13] D. Banodkar, K. K. Ramakrshmann, S. Kalyanaraman, A. Gerber and O. Spatscheck, "Multicast Instant Channel Change in IPTV Systems", 3rd International Conference on Communication Systems Software and Middleware, January 2008.
- [14] Cisco System, "Optimizing Video Transport in Your IP Triple Play Network", WhitePaper, 2006.
- [15] H. Joo, H. Song, D. B. Lee, and I. Lee, "An effective IPTV channel control algorithm considering channel zapping time and network utilization", in IEEE Transactions on Broadcasting, vol. 51, pp. 208-216, 2008.
- [16] P. Sieber, T. N. M. Van Caenegem and M. Wagner, "Analysis and Improvements of Zapping Time in IPTV Systems", IEEE Transaction on Broadcasting, p. 404-418, vol.55, n.2, June 2009.
- [17] C. Cho, I. Han, Y. Jun and H. Lee, "Improvement of channel zapping time in IPTV services using the adjacent groups join-leave method", International Conference on Advanced Communication Technology, vol. 2, pp. 971-975, 2004.
- [18] S. M. Mandal, M. MBuru, "Intelligent Pre-fetching to Reduce Channel Switching Delay in IPTV Systems", department technical report, Texas A & M University.
- [19] J. Lee, G. Lee, S. Seok, B. Chung, "Advanced scheme to reduce IPTV channel zapping time", in LNCS 4773, pp. 235-243, 2007.
- [20] Y. Kim, J. K. Park, H. J. Choa, S. Lee, H. Park, J. Kim, Z. Lee and K. Ko, "Reducing IPTV channel zapping time based on viewer's surfing behavior and preference", International Symposium on Broadband Multimedia Systems and Broadcasting, 2008.
- [21] S. H. Hsu, M. Wen, H. Lin, C. C. Lee, and C. H. Lee, "AIMED – A personalized TV Recommendation system", in LNCS 4471, pp. 166-174, 2007.
- [22] VLC, <http://www.videolan.org/>.
- [23] MyFreeTV, <http://myfreetv.sourceforge.net//>
- [24] D. T. vanVeen, M. K. Weldon, C. C. Bahr, and E. E. Harstead, "An Analysis of the Technical and Economical Essentials for Providing Video over Fiber-to-the-Premises Network", Bell Labs Tech J., vol. 10, no. 1, pp. 181-200, 2005.
- [25] J. Gong, D. A. Vivanco and J. Martin "Simulation Study of the Spectral Capacity Requirements of Switched Digital Broadcast", Fourth International Conference on Broadband Communications, Networks and Systems, September 2007.
- [26] W.R Stevens, B. Fenner, A. M Rudoff, "Unix Network Programming", Addison Wesley, Nov. 21, 2003.
- [27] IPv4 API, <http://www.isovarvas.com/lxr/http/source/net/ipv4>.
- [28] Vialis website, www.calixo.net.
- [29] V. Lucas, J. J. Pansiot, M. Hoerdet "Influence du temps d'adhésion sur le contrôle de congestion multicast", French symposium on engineering protocols, 2006.
- [30] Scilab software, <http://www.scilab.org/>.

Efficient Packet Scheduling Schemes with Built-in Fairness Control for Multiantenna Packet Radio Systems

Stanislav Nonchev and Mikko Valkama

Tampere University of Technology
 Department of Communications Engineering
 P.O. Box 553, FI-33101, Tampere, FINLAND
 Email: stanislav.nonchev@tut.fi, mikko.e.valkama@tut.fi

Abstract – In this article, we propose fairness-oriented dual stream multiple-input multiple-output (MIMO) packet scheduling schemes with efficient utilization of channel quality indicator (CQI) feedback for emerging multiantenna packet radio systems. In general, multiuser multiantenna transmission schemes allow users to be scheduled on different parallel streams on the same time-frequency resource. Based on that, implementations of more intelligent scheduling schemes that are aware of the instantaneous state of the radio channel require utilization of time, frequency and spatial domain resources in an efficient manner. Stemming from the earlier advanced proportional fair (PF) scheduler studies, we extend the developments to dual stream MIMO packet radios with fairness-oriented scheduling metric and practical feedback reporting mechanisms, including the effects of mobile measurement and estimation errors, reporting delays, and CQI quantization and compression. Furthermore, we investigate the resulting fairness distribution among users together with the achievable radio system performance in terms of throughput and coverage, by simulating practical OFDMA cellular system environment with MIMO functionality in Micro and Macro cell scenarios. As a concrete example, we demonstrate that by using the proposed fairness-oriented multiuser scheduling schemes, significant coverage improvements in the order of 40% can be obtained at the expense of only 16% throughput loss for all feedback reporting schemes. Furthermore, the user fairness is also greatly increased, by more than 30%, when measured using Jain’s fairness index.

Keywords - radio resource management; packet scheduling; proportional fair; channel quality feedback; fairness; coverage; throughput; multiantenna

I. INTRODUCTION

The advancement of new radio technologies for beyond third generation (3G) cellular systems continues steadily. This includes, e.g., third generation partnership project (3GPP) long term evolution (LTE) [2], worldwide interoperability for microwave access (WiMAX) [3] and the work in various research projects, like WINNER [4]. Some common elements in most of these developments are orthogonal frequency division multiple access (OFDMA) based air interface, operating bandwidths of at least 10-20 MHz, and the exploitation of multiple-input multiple-output

(MIMO) techniques and advanced channel-aware packet scheduling principles [2]. MIMO in terms of *spatial multiplexing* (SM), possibly combined with pre-coding, is considered as one core physical layer technology towards increased link spectral efficiencies compared to existing radio systems. In addition, it also provides the packet scheduler (PS) with an extra degree of freedom (spatial domain), by offering a possibility to multiplex multiple data streams of one or more users on the same physical time-frequency resource. The two principal concepts widely analyzed in literature (see, e.g., [5]-[6] and the references therein) in this context are single user (SU) and multiuser (MU) MIMO. The SU-MIMO approach allows only the streams of one individual UE to be scheduled at the same time-frequency resource block (RB), while MU-MIMO provides additional flexibility so that streams of multiple users can be scheduled over the same time-frequency RB. Assuming relatively accurate channel state feedback in terms of channel quality indicator (CQI) reports from mobile stations (MS) to base station (BS), together with fast link adaptation mechanisms, advanced channel-aware packet scheduling schemes have major impact on the system-level performance optimization in terms of, e.g., throughput and coverage. Practical CQI reporting mechanisms in this context are described, e.g., in [7]-[13]. Another important feature of multiuser radio systems related to scheduling, in addition to throughput and coverage, is fairness, implying that also users with less favorable channel conditions should anyway be given some reasonable access to the radio spectrum. This is especially important in serving users at, e.g., cell edges in cellular networks.

Recently, multiantenna oriented packet scheduling principles have started to be investigated in the literature, see, e.g., [14]-[19]. New scheduling algorithms have been proposed and their performance been evaluated in different simulator environments in [1], [16]-[19]. In this article, we concentrate on the proportional fair (PF) principle, which in general offers an attractive balance between cell throughput and user fairness, and extend it with spatial domain functionality for the needs of SU- and MU-MIMO operation. More specifically, we extend our earlier studies

in [1], [18]-[19] on algorithm development by deploying SM functionality to frequency domain (FD) PF scheduling schemes that can efficiently utilize the provided feedback information from all the user equipments (UEs), in terms of quantized CQI reports. A new packet scheduler is proposed, called MIMO modified PF (MMPF), with built-in fairness control in its scheduling metric, which is shown to improve the system performance considerably, in terms of cell-edge coverage and overall scheduling fairness, when compared to existing reference schedulers. For practicality, all the performance evaluations are carried out in 3GPP LTE system context, covering both Micro and Macro Cell scenarios, and conforming to the 3GPP evaluation criteria [2]. The used radio system performance measures are cell throughput distribution, average throughput, cell-edge coverage and Jain's fairness index [21].

In general, while the increased flexibility of channel-aware scheduling can offer great performance enhancements, compared to fixed resource allocation, it also has some practical disadvantages. This includes, e.g., relatively higher scheduling complexity, in terms of scheduling metric calculations and increased signaling overhead to facilitate CQI reporting. Keeping these at reasonable levels requires thus some constraints on the scheduling algorithm, so for simplicity we assume here that only one MIMO mode (SU or MU) and fixed modulation and coding scheme (MCS) is allowed per user within one time-frequency scheduling element (RB). For simplicity, we also assume that the BS as well as all the UE's are equipped with 2 antennas (dual antenna TX and RX).

The rest of the article is organised as follows: Section II describes the MIMO channel-aware scheduling principles and the proposed fairness-oriented scheduling scheme. Section III, in turn, gives an overview of different feedback reporting schemes in packet scheduling context. The overall radio system model and simulation assumptions are then presented and discussed in Section IV. The corresponding simulation results and analysis are presented in Section V, while the conclusions are drawn in Section VI.

II. CHANNEL-AWARE MIMO SCHEDULING

In general, the task of the packet scheduler is to select the most suitable users to access the overall radio resources at any given time window, based on some selected priority metric calculations. Typically the scheduler also interacts with other radio resource management (RRM) units such as *link adaptation* (LA) and *Hybrid ARQ* (HARQ) manager as shown in Figure 1. The scheduling decision is based on received users' signaling information in terms of acknowledgements (ACK/NACK) and channel state information (CQI reports) per given transmission time interval (TTI) [9] and per frequency domain physical resource block (PRB). More specifically, in this article in multiantenna radio system context, we assume that both

single stream and dual stream CQIs are reported to BS by each UE. Depending on the selected CQI reporting scheme, the accuracy and resolution of the channel quality information can then easily differ considerably [7], [8], [11], [12], as will be explained in Section III. Moreover, the CQI information is not necessarily available for all the individual subcarriers but more likely for certain groups of subcarriers only [13], [22], [23]. Based on this information, the BS scheduler then decides whether the particular time-frequency resource is used for (i) transmitting only one stream to a specific UE, (ii) two streams for a specific UE (SU-MIMO) or (iii) two streams to two different UEs (MU-MIMO, one stream per UE).

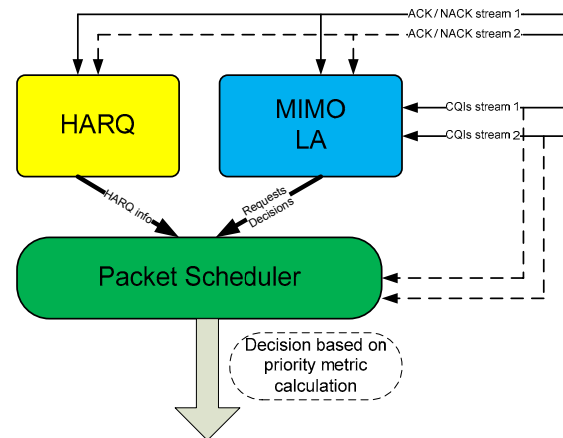


Figure 1: Joint time- and frequency-domain scheduling process.

A. Proposed Scheduler at Principal Level

In general, we use the well-known two-step PF approach with extended functionality in extra spatial dimension to enable MIMO operation [1], [5], [18]-[19]. The first step is time-domain (TD) scheduling in which the scheduler selects a sub-group of users in each TTI, called scheduling candidate set, based on the full bandwidth channel state information. More specifically, the TD step selects those I_{BUFF} UE's (out of the total number of UE's, say I_{TOT}) whose total instantaneous throughput, per TTI, calculated over the full bandwidth is highest [20]. In this stage, we also take the different spatial multiplexing possibilities (single stream, dual stream SU, dual stream MU) into account, in calculating all the possible full bandwidth reference throughputs.

The second step is then frequency-domain (FD) / spatial-domain (SD) scheduling in which the scheduler first reserves the needed PRB's for pending re-transmissions (on one stream-basis only for simplicity) and the rest available PRB's are allocated to the selected UE's of the scheduling candidate set obtained from the TD step. The actual metric in FD/SD allocation is based on the PRB-level and stream-wise channel state information, and the corresponding

throughput calculations, as will be explained in more details below.

B. Exact Scheduling Metrics

Here we describe the actual scheduling metrics used in ranking users in the TD scheduling step as well as mapping the users to FD/SD resources in the second step. First a multistream extension of “ordinary” PF is described in sub-section II.B.1, used as a reference in the performance simulations, and then the actual proposed modified metric with increased fairness-control is described in sub-section II.B.2.

1) Multistream Proportional Fair:

For the PF scheduler, scheduling decision per TTI is based on the following priority metric

$$\gamma_{i,k,s} = \arg \max_i \left\{ \frac{R_{i,k,s}(n)}{T_i(n)} \right\} \quad (1)$$

in which $R_{i,k,s}(n)$ is the estimated instantaneous throughput of user i at sub-band k on stream s for the time instant (TTI) n (calculated based on the CQI reports through, e.g., EESM mapping [1]). $T_i(n)$, in turn, is the average delivered throughput to the UE i during the recent past and is calculated by

$$T_i(n) = \left(1 - \frac{1}{t_c} \right) T_i(n-1) + \frac{1}{t_c} R_i(n-1) \quad (2)$$

Here t_c controls the averaging window length over which the average delivered throughput is calculated [11]-[15] and $R_i(n-1)$ is the actually delivered throughput to user i at previous TTI $n-1$, calculated over all sub-bands k and possible streams s . In general, $1/t_c$ is also called the forgetting factor.

Considering the previous TD and FD/SD steps described earlier in Section II.A, the above metrics are used as follows:

a) *TD*: Metric (1) is evaluated over the full bandwidth and for different stream options to rank the I_{TOT} UE's. Out of these, $I_{BUFF} < I_{TOT}$ UE's with highest metric are picked to the following FD/SD stage. In the following, this subset is called scheduling candidate set (SCS), and is denoted by $\Omega(n)$.

b) *FD/SD*: The access to individual PRB and stream(s) is granted for the user(s) belonging to the above SCS with the highest metric (1) evaluated for the particular PRB and stream at hand.

2) Modified Multistream Proportional Fair (MMPF):

Stemming from the earlier work in [1], [11], the following modified multistream PF metric is proposed:

$$\bar{\gamma}_{i,k,s} = \arg \max_i \left\{ \left(\frac{CQI_{i,k,s}(n)}{CQI_i^{ave}(n)} \right)^{\alpha_1} \left(\frac{T_i(n)}{T_{tot}(n)} \right)^{-\alpha_2} \right\} \quad (3)$$

Here, α_1 and α_2 are scheduler optimization parameters ranging basically from 0 to infinity, $CQI_{i,k,s}$ is the CQI of user i at PRB k and stream s , and CQI_i^{ave} is the average CQI of user i calculated using

$$CQI_i^{avg}(n) = \left(1 - \frac{1}{t_c} \right) CQI_i^{avg}(n-1) + \frac{1}{t_c} \frac{1}{K_{TOT}} \frac{1}{S_{TOT}} \sum_{s=1}^{S_{TOT}} \sum_{k=1}^{K_{TOT}} CQI_{i,k,s}(n) \quad (4)$$

In above, K_{TOT} is the total number of available PRB's while S_{TOT} denotes the maximum number of streams which is here two (max two streams). In (3), $T_{tot}(n)$ is the average delivered throughput (during the recent past) to all I_{BUFF} users served by the BS and is calculated as

$$T_{tot}(n) = \left(1 - \frac{1}{t_c} \right) T_{tot}(n-1) + \frac{1}{t_c} \frac{1}{I_{BUFF}} \sum_{i \in \Omega(n-1)} T_i(n-1) \quad (5)$$

Intuitively, the proposed scheduling metric in (3) is composed of two elements affecting the overall scheduling decisions. The first dimension measures in a stream-wise manner the relative instantaneous quality of the individual user's radio channels against their own average channel qualities while the second dimension is related to measuring the achievable throughput of individual UE's against the corresponding average throughput of scheduled users. In this way, and by understanding the power coefficients α_1 and α_2 as additional adjustable parameters, the exact scheduler statistics can be tuned and controlled to obtain a desired balance between the throughput and fairness. This will be demonstrated later using radio system simulations. Considering finally the actual TD and FD/SD steps described at general level in Section II.A, the same approach as in sub-section II.B.1 is deployed but the metrics (1)-(2) are of course here replaced by the metrics in (3)-(5).

III. FEEDBACK REPORTING PROCESS

The overall channel state reporting process between UE's and BS is illustrated in Figure 2. Within each time window of length t_r , each mobile sends channel quality indicator (CQI) reports to BS, formatted and possibly compressed, with a reporting delay of t_d seconds [7], [8], [11], [12]. Each report is naturally subject to errors due to imperfect decoding of the received signal. In general, the CQI reporting frequency-resolution has a direct impact on the achievable multiuser frequency diversity and thereon to

the overall system performance and the efficiency of radio resource management, as described in general, e.g., in [12]. In our studies here, the starting point (reference case) is that the CQI reports are quantized SINR measurements across the entire bandwidth (wideband CQI reporting), to take advantage of the time and frequency variations of the radio channels for the different users. Then also alternative reduced feedback schemes are described and evaluated, as discussed below.

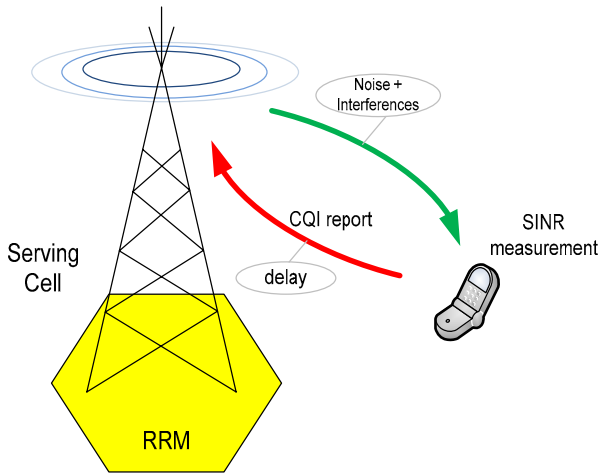


Figure 2: Reporting mechanism between UE and BS.

A. Full CQI Reporting

In a general OFDMA radio system, the overall system bandwidth is assumed to be divided into v CQI measurement blocks. Then quantizing the CQI values to say q bits, the overall full CQI report size is

$$S_{full} = q \times v \quad (6)$$

bits which is reported by every UE for each TTI [2]-[4], [12]. In case of LTE, with 10 MHz system bandwidth and grouping 2 physical resource blocks into 1 measurement block, it follows that $v = 25$. Assuming further that quantization is carried with $q = 5$ bits, then each UE is sending $25 \times 5 = 125$ bits for every 1ms (TTI length).

B. Best- m CQI Reporting

One simple approach to reduce the reporting and feedback signaling is obtained as follows. The method is based on selecting only $m < v$ different CQI measurements and reporting them together with their frequency positions to the serving cell [9], [12]. We assume here that the evaluation criteria for choosing those m sub-bands for reporting is based on the highest SINR values (hence the name *Best- m*). The resulting report size in bits is then given by

$$S_{best-m} = q \times m + \left\lceil \log_2 \left(\frac{v!}{m!(v-m)!} \right) \right\rceil \quad (7)$$

As an example, with $v = 25$, $q = 5$ bits and $m = 10$, it follows that $S_{best-m} = 72$ bits, while $S_{full} = 125$ bits. Furthermore, on the scheduler side, we assume that the PRBs which are not reported by the UE are allocated a CQI value equal to the lowest reported one.

C. Threshold based CQI Reporting

This reporting scheme is a further simplification and relies on providing information on only the average CQI value above certain threshold together with the corresponding location (sub-band index) information. First the highest CQI value is identified within the full bandwidth, which sets an upper bound of the used threshold window. All CQI values within the threshold window are then averaged and only this information is sent to the BS together with the corresponding sub-band indexes. On the scheduler side, the missing CQI values can then be treated, e.g., as the reported averaged CQI value minus a given dB offset (e.g., 5 dB; the exact number is again a design parameter). The number of bits needed for reporting is therefore only

$$S_{threshold} = q + v \quad (8)$$

As an example, with $v = 25$ and $q = 5$ bits (as above), it follows that $S_{threshold} = 30$ bits, while $S_{best-m} = 72$ bits and $S_{full} = 125$ bits. The threshold-based scheme is illustrated graphically in Figure 3 [11].

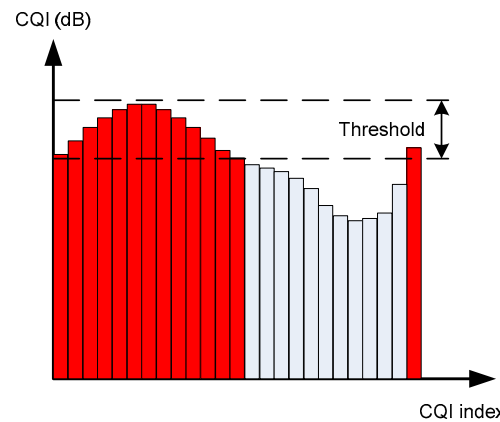


Figure 3: Basic principle of threshold-based CQI reporting.

IV. QUASI-STATIC RADIO SYSTEM SIMULATOR

A. Basic Features

System-level performance of the proposed scheduling scheme is evaluated based on a quasi-static radio system

simulator for LTE downlink, providing traffic modeling, multiuser packet scheduling and link adaptation [2]. As a practical example, the 10 MHz system bandwidth case of LTE is assumed, meaning that there are 50 physical resource blocks each consisting of 12 sub-carriers with sub-carrier spacing of 15 kHz. This sets also the basic resolution in FD/SD UE multiplexing (scheduling), i.e., the allocated individual UE bandwidths are multiples of the PRB bandwidth. The actual reported CQI's are based on received signal-to-interference-and-noise ratios (SINR), calculated by the UE's for each PRB. Here the UE's are assumed to deploy dual antenna linear MMSE (LMMSE) receiver principle, and utilize in the SINR calculations the actual radio channel response, the received noise level, and the structure of the detector (like described in more details below). Furthermore, like mentioned already earlier, the UE's always report single stream as well as both SU and MU dual stream SINR's (at the corresponding detector output).

In a single simulation run, mobile stations are randomly dropped or positioned over each sector and cell. Then based on the individual distances between the mobile and the serving base station, the path losses for individual links are directly determined, while the actual fading characteristics of the radio channels depend on the assumed mobility and power delay profile. In updating the fading statistics, the time resolution in our simulator is set to one TTI (1ms). In general, a standard hexagonal cellular layout is utilized with altogether 19 cell sites each having 3 sectors in Macro case and 1 sector in Micro case as show in Figure 4. In the performance evaluations, statistics are collected only from the central cell site while the others simply act as sources of inter-cell interference.

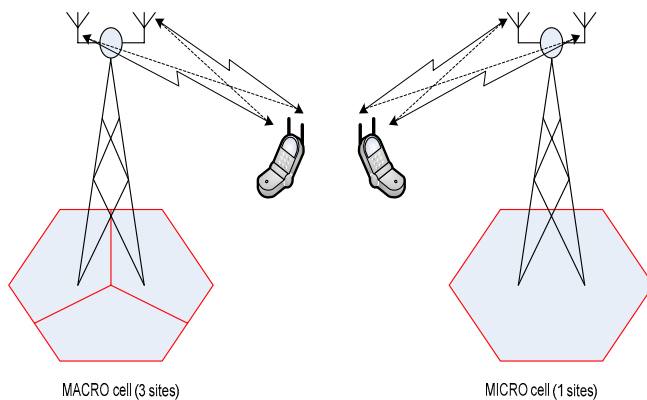


Figure 4: Macro and Micro cell scenarios.

The main simulation parameters and assumptions are generally summarized in TABLE 1 for both Macro and Micro cell scenarios, following again the LTE working assumptions. The used MIMO scheme is *per-antenna rate control* (PARC) with two transmit antennas at the BS and two receive antennas at the UE's and the receivers are

equipped with LMMSE detectors. As illustrated in Figure 1, the RRM functionalities are controlled by the packet scheduler together with link adaptation and HARQ mechanisms. Notice that the maximum number of simultaneously multiplexed users (I_{BUFF}) is set to 10 here while the total number of UE's (I_{TOT}) is 15. In general, we assume that the BS transmission power is equally distributed among all PRB's. In the basic simulations, 15 UE's are uniformly dropped within each cell and experience inter-cell interferences from the surrounding cells, in addition to path loss and fading. The UE velocities are 3km/h, and the typical urban (TU) channel model standardized by ITU is assumed in modeling the power-delay spread of the radio channels. Infinite buffer traffic model is applied in the simulations, i.e. every user has data to transmit (when scheduled) for the entire duration of a simulation cycle. Exponential effective SINR mapping (EESM) is used for link-to-system level mapping (throughput calculations), as described in [2]. The length of a single simulation run is set to 5 seconds which is then repeated for 10 times to collect reliable statistics.

Considering MIMO functionality, every UE has an individual HARQ entry per stream, which operates the physical layer re-transmission functionalities. It is based on the stop-and-wait (SAW) protocol and for simplicity, the number of entries per UE is fixed to six. HARQ retransmissions are always transmitted with the same MCS and on the same PRB's (if scheduled) as the first transmissions in a single stream mode. The supported modulation schemes are QPSK, 16QAM and 64QAM with variable rates for the encoder as shown in TABLE 1.

Link adaptation handles the received UE reports containing the channel quality information for each PRB based on single and dual stream MIMO modes. The implemented link adaptation mechanism consists of two separate elements – the inner loop (ILLA) and outer loop (OLLA) LA's – and are used for removing CQI imperfections and estimating supported data rates and MCS. It is assumed that the CQI reporting errors are log-normal distributed with 1dB standard deviation.

B. Detectors and SINR Modeling

The actual effective SINR calculations rely on subcarrier-wise complex channel gains (estimated using reference symbols in practice) and depend in general also on the assumed receiver (detector) topology. Here we assume that the LMMSE detector, properly tailored for the transmission mode (1-stream SU, 2-stream SU or 2-stream MU) is deployed. The detector structures and SINR modeling for different transmission modes are described in detail below.

TABLE 1. Basic simulation parameters.

Parameter	Assumption
Cellular layout	Hexagonal grid, 19 cell sites, 3 sectors per site for Macro / 1 sector per site for Micro
Inter-site distance	500 m - Macro / 1732 m - Micro
Carrier frequency / Bandwidth	2000 MHz / 10 MHz
Number of active sub-carriers	600
Sub-carrier spacing	15 kHz
Sub-frame duration	0.5 ms
Channel estimation	Ideal
PDP	ITU Typical Urban 20 paths
Minimum distance between UE and cell	>= 35 meters - Macro >= 10 meters - Micro
Average number of UE's per sector	15
Max. number of frequency multiplexed UEs (I_{BUFF})	10
UE receiver type	LMMSE
Shadowing standard deviation	8 dB
UE speed	3km/h
Total BS TX power (P_{total})	46 dBm
Traffic model	Full Buffer
Fast fading model	Jakes Spectrum
CQI reporting schemes	Full CQI, Best - m (with m=10), Threshold based (with 5dB threshold)
CQI log-normal error std.	1 dB
CQI reporting time	5 TTI
CQI delay	2 TTIs
CQI quantization	1 dB
CQI std error	1 dB
MCS rates	QPSK (1/3, 1/2, 2/3), 16QAM (1/2, 2/3, 4/5), 64QAM (1/2, 2/3, 4/5)
ACK/NACK delay	2 ms
Number of SAW channels	6
Maximum number of retransmissions	3
HARQ model	Ideal chase combining (CC)
1 st transmission BLER target	20%
Scheduler forgetting factor	0.0025
Scheduling schemes used	Ordinary PF Modified PF (proposed)
Simulation duration (one drop)	5 seconds
Number of drops	10

1) Single Stream SU Case

In this case, only one of the two BS transmit antennas is used to transmit one stream. At individual time instant (time-index dropped here), the received spatial 2x1 signal vector of UE i at sub-carrier c is of the form

$$\mathbf{y}_{i,c} = \mathbf{h}_{i,c}x_{i,c} + \mathbf{n}_{i,c} + \mathbf{z}_{i,c} \quad (9)$$

where $x_{i,c}$, $\mathbf{h}_{i,c}$, $\mathbf{n}_{i,c}$ and $\mathbf{z}_{i,c}$ denote the transmit symbol, 2x1 channel vector, 2x1 received noise vector and 2x1 inter-cell interference vector, respectively. Then the LMMSE detector $\hat{x}_{i,c} = \mathbf{w}_{i,c}^H \mathbf{y}_{i,c}$ is given by

$$\mathbf{w}_{i,c} = \sigma_{x,i}^2 (\mathbf{h}_{i,c}^H \sigma_{x,i}^2 \mathbf{h}_{i,c} + \Sigma_{n,i} + \Sigma_{z,i})^{-1} \mathbf{h}_{i,c} \quad (10)$$

where $\sigma_{x,i}^2$, $\Sigma_{n,i}$ and $\Sigma_{z,i}$ denote the transmit power (per the used antenna), noise covariance matrix and inter-cell interference covariance matrix, respectively. Now the SINR is given by

$$\gamma_{i,c} = \frac{|\mathbf{w}_{i,c}^H \mathbf{h}_{i,c}|^2 \sigma_{x,i}^2}{\mathbf{w}_{i,c}^H \Sigma_{n,i} \mathbf{w}_{i,c} + \mathbf{w}_{i,c}^H \Sigma_{z,i} \mathbf{w}_{i,c}} \quad (11)$$

The noise variables at different receiver antennas are assumed uncorrelated (diagonal $\Sigma_{n,i}$) while the more detailed modeling of inter-cell interference (structure of $\Sigma_{z,i}$) takes into account the distances and channels from neighboring base stations (for more details, see, e.g., [19]).

2) Dual Stream SU Case

In this case, both of the two BS transmit antennas are used for transmission, on one stream per antenna basis. At individual time instant, the received spatial 2x1 signal vector of UE i at sub-carrier c is now given by

$$\mathbf{y}_{i,c} = \mathbf{H}_{i,c} \mathbf{x}_{i,c} + \mathbf{n}_{i,c} + \mathbf{z}_{i,c} \quad (12)$$

where $\mathbf{x}_{i,c}$ and $\mathbf{H}_{i,c} = [\mathbf{h}_{i,c,1}, \mathbf{h}_{i,c,2}]$ denote the 2x1 transmit symbol vector and 2x2 channel matrix, respectively. Now the LMMSE detector $\hat{\mathbf{x}}_{i,c} = \mathbf{W}_{i,c} \mathbf{y}_{i,c}$ is given by

$$\begin{aligned} \mathbf{W}_{i,c} &= \Sigma_{x,i} \mathbf{H}_{i,c}^H (\mathbf{H}_{i,c} \Sigma_{x,i} \mathbf{H}_{i,c}^H + \Sigma_{n,i} + \Sigma_{z,i})^{-1} \\ &= \begin{bmatrix} \mathbf{w}_{i,c,1}^H \\ \mathbf{w}_{i,c,2}^H \end{bmatrix} \end{aligned} \quad (13)$$

where $\Sigma_{x,i} = \text{diag}\{\sigma_{x,i,1}^2, \sigma_{x,i,2}^2\} = \text{diag}\{\sigma_{x,i}^2/2, \sigma_{x,i}^2/2\}$ denotes the 2x2 covariance matrix (assumed diagonal) of the transmit symbols. Note that compared to single stream case, the overall BS transmit power is now divided between the two antennas, as indicated above. Then the SINR's for the two transmit symbols are given by

$$\begin{aligned} \gamma_{i,c,1} &= \frac{|\mathbf{w}_{i,c,1}^H \mathbf{h}_{i,c,1}|^2 \sigma_{x,i,1}^2}{|\mathbf{w}_{i,c,1}^H \mathbf{h}_{i,c,2}|^2 \sigma_{x,i,2}^2 + \mathbf{w}_{i,c,1}^H \Sigma_{n,i} \mathbf{w}_{i,c,1} + \mathbf{w}_{i,c,1}^H \Sigma_{z,i} \mathbf{w}_{i,c,1}} \end{aligned} \quad (14)$$

$$\begin{aligned} \gamma_{i,c,2} &= \frac{|\mathbf{w}_{i,c,2}^H \mathbf{h}_{i,c,2}|^2 \sigma_{x,i,2}^2}{|\mathbf{w}_{i,c,2}^H \mathbf{h}_{i,c,1}|^2 \sigma_{x,i,1}^2 + \mathbf{w}_{i,c,2}^H \Sigma_{n,i} \mathbf{w}_{i,c,2} + \mathbf{w}_{i,c,2}^H \Sigma_{z,i} \mathbf{w}_{i,c,2}} \end{aligned}$$

3) Dual Stream MU Case

In this case, the transmission principle and SINR modeling are similar to subsection 2) above, but the two spatially multiplexed streams belong now to two different UE's, say i and i' . Thus the SINR's in (14) are interpreted accordingly.

Finally, for link-to-system level mapping purposes, the exponential effective SINR mapping (EESM), as described in [2-4], is deployed.

V. NUMERICAL RESULTS

In this section, we present the results obtained from the quasi-static radio system simulations using the PS algorithms described in the article. The system-level performance is generally measured and evaluated in terms of:

- Throughput* – the total number of successfully delivered bits per unit time. Usually measured either in kbps or Mbps.
- Coverage* – the experienced data rate per UE at the 95% coverage probability (5% throughput CDF point).
- Fairness* – measures the resource allocation fairness among all UE's from the average throughput point of view. Evaluated using Jain's fairness index [21] which is calculated here as

$$fairness = \frac{\left(\sum_{i=1}^{I_{TOT}} \bar{\mu}_i \right)^2}{I_{TOT} \sum_{i=1}^{I_{TOT}} \bar{\mu}_i^2} \quad (15)$$

where $\bar{\mu}_i$ denotes the average throughput value of user i across different simulation realizations (here ten). In single simulation run, the corresponding throughput of user i is given by

$$\mu_i = \frac{1}{N_{TTI}} \sum_{n=1}^{N_{TTI}} R_i(n) \quad (16)$$

where N_{TTI} denotes the length of a single simulation run in TTI's while $R_i(n)$ is the actually delivered throughput to user i at individual TTI n .

In the following, we illustrate the behavior of the proposed MMPF scheduler with using different power coefficients α_1 and α_2 as shown in TABLE 2. To focus mostly on the role of the channel quality reporting in the priority metric calculation in equation (3), α_2 is fixed here to

1 and different values are then demonstrated for α_1 . More specifically, with large α_2 values, the effect of second term in priority metric calculation based on throughput estimation would be emphasized and the scheduling algorithm would behave like maximum throughput scheduler, which in turn would imply reduced fairness distribution. Consequently, the impact of the different CQI reporting schemes is seen now more clearly. For the cases of *Best-m* and *Threshold* based CQI reporting schemes, we fix the value of m equal to 10 and threshold to 5 dB, respectively. Similar example values have also been used by other authors in the literature earlier, see, e.g., [12]. Complete performance statistics are gathered for both Macro cell and Micro cell case scenarios.

A. Macro Cell Case

Figure 5 (left column) illustrates the average user throughput and coverage for the different schedulers. The power coefficient values from TABLE 2 are presented as index M, where M1 represents the first couple, etc. The obtained results are compared with the reference PF scheduler described also in Section II. By using the first term (M1) of the new metric calculation for MMPF, in combination with full CQI reporting scheme, we achieve coverage gain in the order of 63% at the expense of 20% throughput loss as shown in Figure 5 (a) and (b). This sets the basic reference for comparisons in the other cases. In the case of *Best-m* and *Threshold* based reporting schemes presented in Figure 5 (c) and (d), and Figure 5 (e) and (f), we have coverage increases by 69% and 74% with throughput losses of 15% and 20%, correspondingly.

Continuing on the evaluation of relative system performance using the proposed scheduler, we clearly see a trade-off between average cell throughput and coverage for different power coefficient cases. Furthermore, the remaining power coefficient values shown in TABLE 2 are used for tuning the overall system behavior together with the choice of the CQI reporting scheme. In the case of full CQI feedback and coefficient α_1 varying between 2 and 8 (M2 –M5) the cell throughput loss is decreased to around 7%, while the coverage gain is reduced to around 21%. Similar results are obtained for the other feedback reporting schemes as well. Consequently, an obvious trade-off between average cell throughput and coverage is clearly seen. In order to preserve the average sector throughput and still to gain from the coverage increase, coefficient values should thus be properly chosen. The exact percentage values for the coverage gains and throughput losses are stated in TABLE 3 at the end of the article.

Further illustrations on the obtainable system performance are presented in Figure 5 (right column) in terms of the statistics of individual UE data rates for the applied simulation scenarios. The slope of the CDF reflects generally the fairness of the algorithms. Therefore we aim

to achieve steeper slope corresponding to algorithm fairness. This type of slope change behavior can clearly be established for each simulation scenario. Clearly, at 5% (coverage) point of the throughput CDF curves, corresponding to users typically situated at the cell edges, we observe significant data rate increases indicated by shift to the right for all CQI feedback schemes when the coefficient α_1 is changed in the proposed metric. This indicates improved overall cell coverage at the expense of slight total throughput loss.

Figure 6 (left column) shows the modulation and coding scheme (MCS) distributions for different schedulers and with applied feedback reporting schemes. The negligible decrease in higher order modulation usage (less than 3%) leads to the increase in the lower (more robust) ones for improving the cell coverage. In all the simulated cases, the MCS distribution behavior has a relatively similar trend following the choice of the power coefficients in the proposed packet scheduling. In general, the use of higher-order modulations is affected mostly in the case of *Best-m* and *Threshold* based reporting schemes.

Figure 6 (right column) illustrates the HARQ distributions for the different scheduler scenarios and reporting schemes. Clearly, the 20% BLER target rate is achieved in all simulated cases. Moreover, the MMPF scheduler provides slight increase in probability of successful first transmission of around 2% for the *Best-m* and *Threshold* based feedback cases.

TABLE 2. DIFFERENT POWER COEFFICIENT COMBINATIONS

Coefficient	Value				
	1	2	4	6	8
α_1	1	2	4	6	8
α_2	1	1	1	1	1

B. Micro Cell Case

The performance statistics obtained for Micro cell case demonstrate similar trends, as in the previous Macro case, as shown in Figure 7. Starting from the primary case M1, with full CQI, we obtain a 17% loss in throughput and 92% coverage improvement. For the reduced feedback reporting schemes – *Best-m* and *Threshold* based – we have 21% and 19% throughput losses and 100% and 96% coverage gains, respectively. Furthermore, similar behavior is observed in the CDF's of individual UE throughputs, as well as MCS and HARQ distributions. The exact percentage values read from the figures are again stated in table format in TABLE 4 at the end of the article.

C. Jain's Fairness Index

Figure 8 illustrates the Jain's fairness index per scheduling scheme for Micro and Macro cell scenarios, calculated over all the $I_{TOT} = 15$ UE's. The value on the x axis corresponds to used scheduler type, where 1 refers to the reference PF scheduler, 2 refers to MMPF with index M1, etc. The value of Jain's fairness index is generally in the range of [0,1], where value of 1 corresponds to all users having the same amount of resources. Clearly, the fairness distribution with MMPF outperforms the used reference PF scheduler for both cases. The received fairness gains are in range of 13%-37% with *full* CQI feedback, 15-32% with *Best-m* CQI feedback and 17-35% with *Threshold* based CQI feedback in the Macro case scenario. The corresponding fairness gains in Micro case scenario are 25-46%, 32-41% and 34-43% for *full* CQI, *Best -m* and *Threshold* based reporting schemes, correspondingly. The exact percentage values read from the figures are again stated in table format in Table 5 in the end of the article.

VI. CONCLUSIONS

In this article, we have studied the potential of advanced multiuser packet scheduling algorithms in OFDMA type radio system context, using UTRAN long term evolution (LTE) downlink in Macro and Micro cell environment as practical example cases. New multistream proportional fair scheduler metric covering time-, frequency- and spatial domains was proposed that takes into account both the instantaneous channel qualities (CQI's) as well as resource allocation fairness. Also different practical CQI reporting schemes were discussed, and used in the system level performance evaluations of the proposed scheduler. Overall, the achieved throughput performance together with coverage and fairness statistics were assessed, by using extensive radio system simulations, and compared against more traditional proportional fair scheduling with multiantenna spatial multiplexing functionality. In the case of fixed coverage requirements and based on the optimal parameter choice for CQI reporting schemes, the proposed scheduling metric calculations based on UE channel feedback offers better control over the ratio between the achievable cell/UE throughput and coverage increase, as well as increased UE fairness. As a practical example, even with limited CQI feedback, the fairness in resource allocation together with cell coverage can be increased significantly (more than 40%) by allowing a small decrease (in the order of only 10-15%) in the cell throughput.

ACKNOWLEDGMENT

The authors would like to thank Markku Kuusela, Nokia Devices, Helsinki, Finland, and Dr. Toni Huovinen, Tampere University of Technology, Tampere, Finland, for fruitful discussions.

REFERENCES

- [1] S. Nonchev and M. Valkama, "Efficient packet scheduling schemes for multiantenna packet radio downlink," in Proc. Fifth Advanced Int. Conf. Telecommunications (AICT-2009), Venice, Italy, May 2009.
- [2] "Physical Layer Aspects for Evolved UTRA", 3GPP Technical Report TR 25.814, ver. 7.1.0, Oct. 2006.
- [3] WiMAX Forum™, <http://www.wimaxforum.org>, Aug. 2006.
- [4] "Wireless World Initiative New Radio (WINNER)," IST-507581, European Information Society Technologies, Technical Report, Dec. 2006.
- [5] N. Wei, B. Talha, T. B. Sørensen, T. E. Kolding, and P. E. Mogensen, "Spectral efficiency of closed-loop transmit diversity with limited feedback for UTRA Long Term Evolution," in Proc. IEEE Int. Symp. Personal, Indoor and Mobile Radio Communications (PIMRC-2006), Helsinki, Sept. 2006.
- [6] R. W. Heath, M. Airy, and A. Paulraj, "Multiuser diversity for MIMO wireless systems with linear receivers," in Proc. Asilomar Conf. Signals, Systems and Computers, Pacific Grove, CA, 2001.
- [7] E. Dahlman et al., 3G Evolution: HSPA and LTE for Mobile Broadband, Academic Press, 2007.
- [8] Y. Sun et al., "Multi-user scheduling for OFDMA downlink with limited feedback for evolved UTRA," in Proc. IEEE Vehicular Technology Conf. (VTC-2006 Fall), Montreal, Canada, Sept. 2006.
- [9] S. Yoon, C. Suh, Y. Cho, D. Park, "Orthogonal frequency division multiple access with an aggregated sub-channel structure and statistical channel quality measurements," in Proc. IEEE Vehicular Technology Conf. (VTC-2004 Fall), Los Angeles, CA, Sept. 2004.
- [10] I. Toufik and H. Kim, "MIMO-OFDMA opportunistic beamforming with partial channel state information," in Proc. IEEE Int. Conf. Communications (ICC-2006), Istanbul, Turkey, June 2006.
- [11] T.E. Kolding, F. Frederiksen, A. Pokhariyal, "Low-bandwidth channel quality indication for OFDMA frequency domain packet scheduling," in Proc. IEEE Int. Symp. Wireless Communication Systems (ISWCS-2006), Valencia, Spain, Sept. 2006.
- [12] K.I. Pedersen, G. Monghal, I.Z. Kovacs, T.E. Kolding, A. Pokhariyal, F. Frederiksen, P. Mogensen, "Frequency domain scheduling for OFDMA with limited and noisy channel feedback," in Proc. IEEE Vehicular Technology Conf. (VTC-2007 Fall), Baltimore, MD, Sept. 2007.
- [13] P. Svedman, D. Hammarwall, B. Ottersten, "Sub-carrier SNR estimation at the transmitter for reduced feedback OFDMA," in Proc. European Signal Processing Conf., Florence, Italy, Sept. 2006.
- [14] C. Wengerter, J. Ohlhorst, and A.G.E Von Elbwert, "Fairness and Throughput Analysis for Generalized Proportional Fair Frequency Scheduling in OFDMA," in Proc. IEEE Vehicular Technology Conf. (VTC-2005 Spring), Stockholm, Sweden, May 2005.
- [15] T. E. Kolding, "Link and system performance aspects of proportional fair scheduling in WCDMA/HSDPA," in Proc. IEEE Vehicular Technology Conf. (VTC-2003 Fall), Orlando, FL, USA, Oct. 2003.
- [16] P. Svedman, S.K.Wilson, L.J. Cimini, and B. Ottersten, "A simplified opportunistic feedback and scheduling scheme for OFDMA," in Proc. IEEE Vehicular Technology Conf. (VTC-2004 Spring), Milan, Italy, May 2004.
- [17] I. Z. Kovács et al, "Effects of non-ideal channel feedback on dual-stream MIMO OFDMA system performance," in Proc. IEEE Vehicular Technology Conf. (VTC-2007 Fall), Baltimore, MD, Oct. 2007.
- [18] S. Nonchev, J. Venäläinen and M. Valkama, "New frequency domain packet scheduling schemes for UTRAN LTE downlink," in Proc. ICT-MobileSummit, Stockholm, Sweden, 2008.
- [19] S. Nonchev and M. Valkama, "A new fairness-oriented packet scheduling scheme with reduced channel feedback for OFDMA packet radio systems," Int. Journal of Communications, Network and System Sciences (IJNS), vol. 2, No. 7, Oct. 2009.
- [20] N. Wei, et al., "Performance of MIMO with frequency domain packet scheduling," in Proc. IEEE Vehicular Technology Conf. (VTC-2007 Spring), Dublin, Ireland, May 2007.
- [21] D. Chui and R. Jain, "Analysis of the increase and decrease algorithms for congestion avoidance in computer networks," Computer Networks and ISDN Systems, 1989.
- [22] P. Svedman, L.J. Cimini, B. Ottersten, "Using unclaimed sub-carriers in opportunistic OFDMA systems," in Proc. IEEE Vehicular Technology Conf. (VTC-2006 Fall), Montreal, Canada, September 2006.
- [23] S. Sanayei, A. Nosratinia, N. Aldhahir, "Opportunistic dynamic sub-channel allocation in multiuser OFDM networks with limited feedback," in Proc IEEE. Information Theory Workshop, San Antonio, TX, October 2004, pp. 182-186.

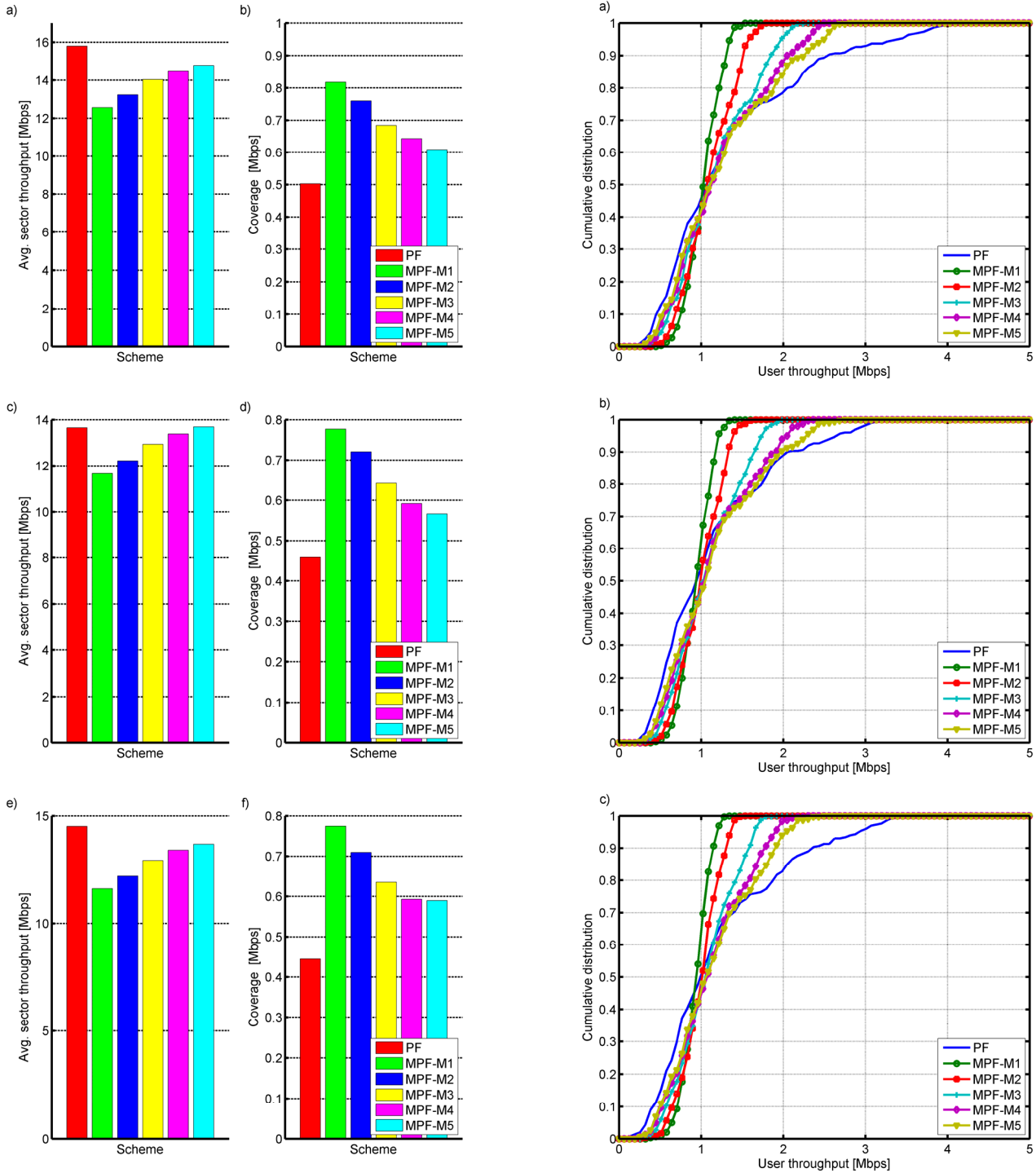


Figure 5: Left column: Average sector throughput and coverage for different scheduling schemes for Macro cell scenario with *full* CQI feedback (a, b), *Best-m* CQI feedback (c, d) and *Threshold* based CQI feedback (e, f). M1-M5 refer to the proposed scheduler with power coefficient values as given in TABLE 2. Right column: CDF's of individual UE throughputs for different scheduling schemes for Macro cell scenario with *full* CQI feedback (a), *Best-m* CQI feedback (b) and *Threshold* based CQI feedback (c).

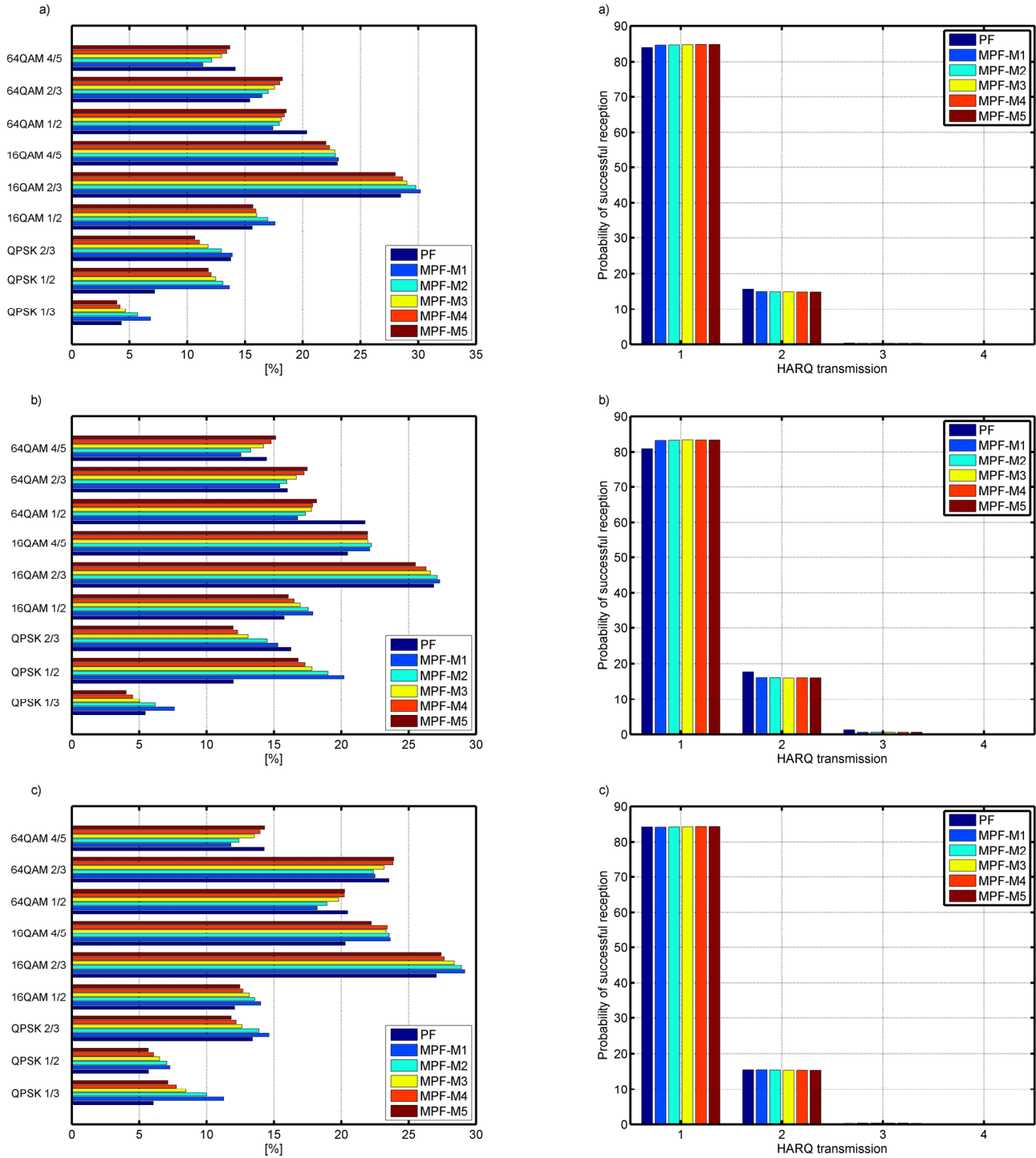


Figure 6: Left column: MCS distributions [%] for different scheduling principles for Macro cell scenario with *full* CQI feedback (a), *Best - m* CQI feedback (b) and *Threshold* based CQI feedback (c). Right column: HARQ distributions for different scheduling schemes for Macro cell scenario with *full* CQI feedback (a), *Best - m* CQI feedback (b) and *Threshold* based CQI feedback (c).

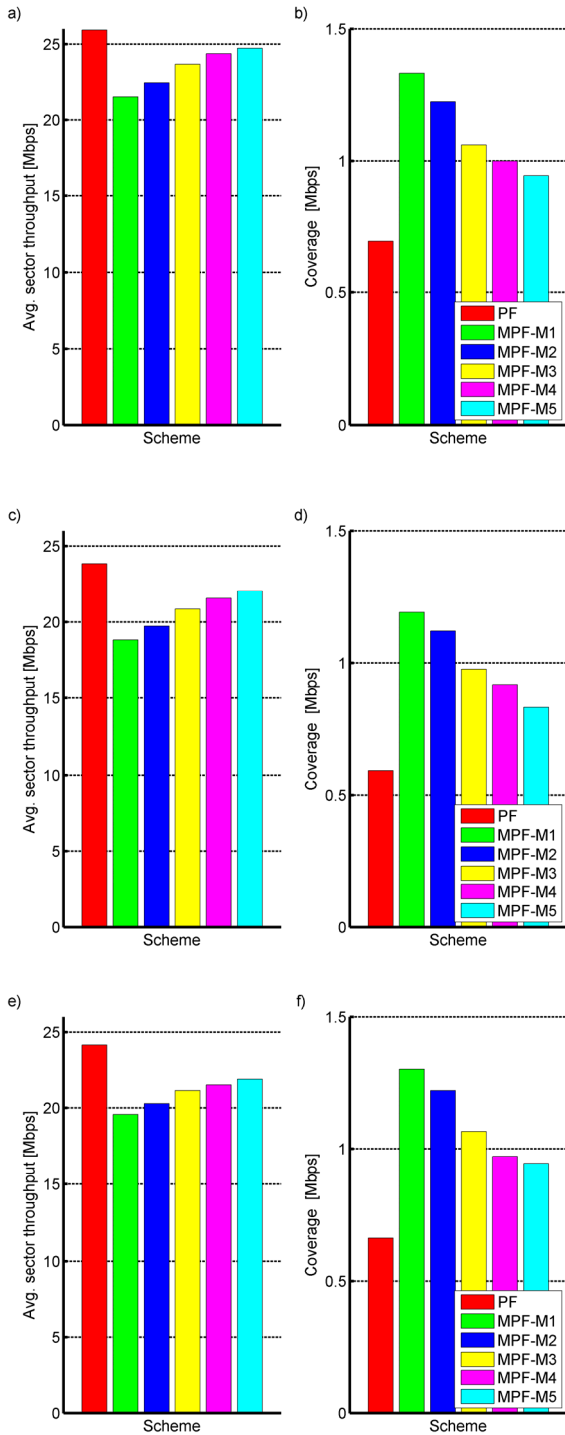


Figure 7: Average cell throughput and coverage gain over the reference PF scheduling scheme for Micro cell simulation scenario. The schemes M1-M5 refer to the new proposed scheduler with power coefficient values as given in TABLE 2.

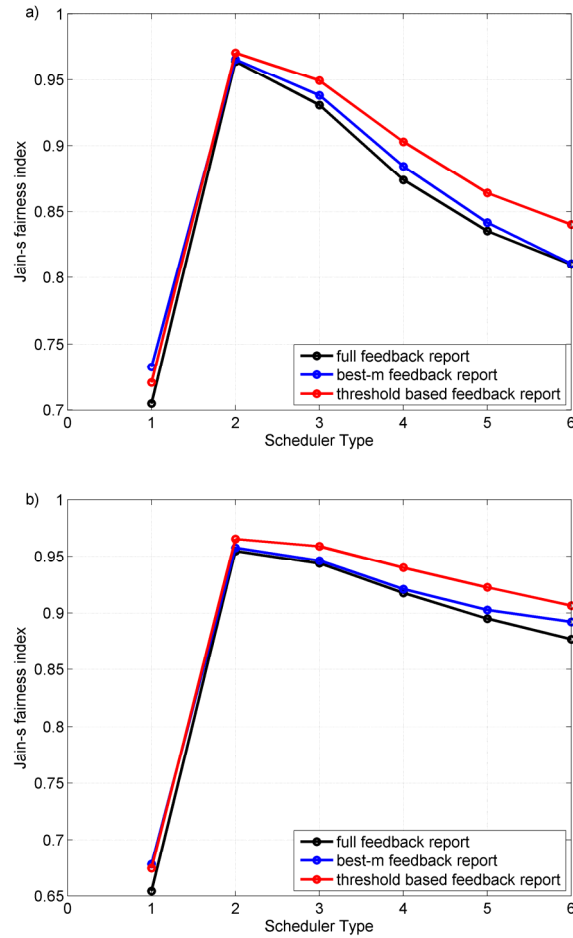


Figure 8: Jain's fairness index per feedback reporting scheme for the different simulation scenarios – Macro cell (a) and Micro cell (b). Scheduler type 1 means ordinary PF, while 2-6 means proposed modified PF with power coefficients as described in TABLE 2.

TABLE 3.

OBTAINED PERFORMANCE STATISTICS COMPARED TO ORDINARY PF SCHEDULER WITH DIFFERENT CQI REPORTING SCHEMES AND DIFFERENT POWER COEFFICIENTS (M1-M5) FOR THE PROPOSED SCHEDULER. MACRO CELL CASE SCENARIO.

	Coverage Gain [%]			Throughput Loss [%]		
	full	best-m	threshold	full	best-m	threshold
M1	63	69	74	20	15	20
M2	51	57	60	16	11	16
M3	36	40	43	13	6	12
M4	28	29	33	9	2	8
M5	21	24	32	7	0	6

TABLE 4.

OBTAINED PERFORMANCE STATISTICS COMPARED TO ORDINARY PF SCHEDULER WITH DIFFERENT CQI REPORTING SCHEMES AND DIFFERENT POWER COEFFICIENTS (M1-M5) FOR THE PROPOSED SCHEDULER. MICRO CELL CASE SCENARIO.

	Coverage Gain [%]			Throughput Loss [%]		
	full	best-m	threshold	full	best-m	threshold
M1	92	100	96	17	21	19
M2	76	88	84	13	17	16
M3	53	64	60	9	14	14
M4	44	54	46	6	11	12
M5	36	40	42	5	8	10

TABLE 5.

OBTAINED JAIN'S FAIRNESS INDEXES COMPARED TO ORDINARY PF SCHEDULER WITH DIFFERENT CQI REPORTING SCHEMES AND DIFFERENT POWER COEFFICIENTS (M1-M5) FOR THE PROPOSED SCHEDULER. MACRO AND MICRO CELL CASE SCENARIOS.

	Macro case Fairness Gain [%]			Micro case Fairness Gain [%]		
	full	best-m	threshold	full	best-m	threshold
M1	37	32	35	46	41	43
M2	32	28	32	44	40	42
M3	19	21	25	29	36	39
M4	16	15	20	27	33	37
M5	13	15	17	25	32	34

SLS Management Validation for End to End QoS Management in a Multidomain Testbed Environment

Șerban Georgică Obreja, *Member IEEE*

University Politehnica Bucharest
Bucharest, Romania
e-mail: serban@radio.pub.ro

Eugen Borcoci, *Member IEEE*

University Politehnica Bucharest
Bucharest, Romania
e-mail: eugen.borcoci@elcom.pub.ro

Radu Lupu, *Member IEEE*

University Politehnica Bucharest
Bucharest, Romania
e-mail: rlupu@elcom.pub.ro

Silviu Ciocchină, *Member IEEE*

University Politehnica Bucharest
Bucharest, Romania
e-mail: silviu@comm.pub.ro

Abstract — This paper presents the validation of an end-to-end QoS integrated management system in a multidomain test-bed environment. The integrated management system was designed and implemented in the framework of the ENTHRONE European project. This paper focuses on the network service management validation at both the Service Provider and Network Provider. The Network Service Management is based on the SLS management: in the core network the pSLS management is used to deal with users aggregated services, while cSLS management is used to deal with individual users services. Both functionality and scalability tests for SLS management are presented

Keywords-SLS, end to end QoS Management, testbed, functional and scalability tests.

I. INTRODUCTION

Today's high speed networks together with enhanced coding techniques for audio and video have made the real time delivery of multimedia services over internet possible. These real time multimedia services raise new challenges for the network regarding the quality of services (QoS) control in order to ensure the proper delivery of the services from content provider (source) to content consumer (destination). An integrated management system should exist, capable of managing the high level services with E2E (end to end) QoS guarantees, while preserving the independency of each network domain to be administrated autonomously in terms of its resources. This management system should also be capable to accommodate heterogeneous network technologies utilized today in the Internet.

An integrated end to end QoS management system has been designed, implemented and validated in the framework of ENTHRONE project (FP6 IST-507637 European project) [3][4][5][6][7]. The ENTHRONE Integrated Management Supervisor (EIMS) [5][6] is the main management entity designed according to the MPEG-21 standard, sitting at the top of a heterogeneous network infrastructure. The EIMS

offers a unified management framework in the audio-visual distribution chain. It assures E2E QoS provisioning using service management based on Service Level Agreements/ Specifications (SLA/SLS) concepts. The QoS approach includes the content adaptation, i.e., the adjustment of the application to the network and terminal capabilities and/or to compensate for the deficiencies of the network.

Several works exist, dealing with end to end QoS management. The IMS solution for 3G mobile network has been standardized by the 3GPP consortium [13]. Also, for the IP world the TISPAN IMS architecture was proposed by NGN group [12]. Both are based on Integrated Services (Intserv) approach for QoS management. A separate signaling path-coupled session, crossing IP core domains, e.g., based on RSVP or NSIS approach, is run for each individual call. Such a solution could raise scalability problems.

The European projects CADENUS, TEQUILA, MESCAL and EuQoS [9][10][11], have also been dedicated to the E2E QoS issues. The projects have developed solutions to provision IP premium services. Efficient solutions have been proposed for services and resources management in single domain networks, while extension over multi-domain heterogeneous networking infrastructure is still an open issue.

CADENUS focused especially on service management. It did not get into details of how static and dynamic resource management is achieved. TEQUILA [11] and MESCAL [10] basically focused on QoS aware IP connectivity network services, intra-domain and inter-domain respectively. The MESCAL did not consider the end-user services or service creation, i.e., the process of (automated) service definition and service offering by the SPs, and the business-related aspects of high-level service offerings and the different roles of stakeholders. The EuQoS project developed and integrated an E2E QoS system to support QoS aware applications, but uses per-individual flow signaling for resource provisioning thus having scalability problems.

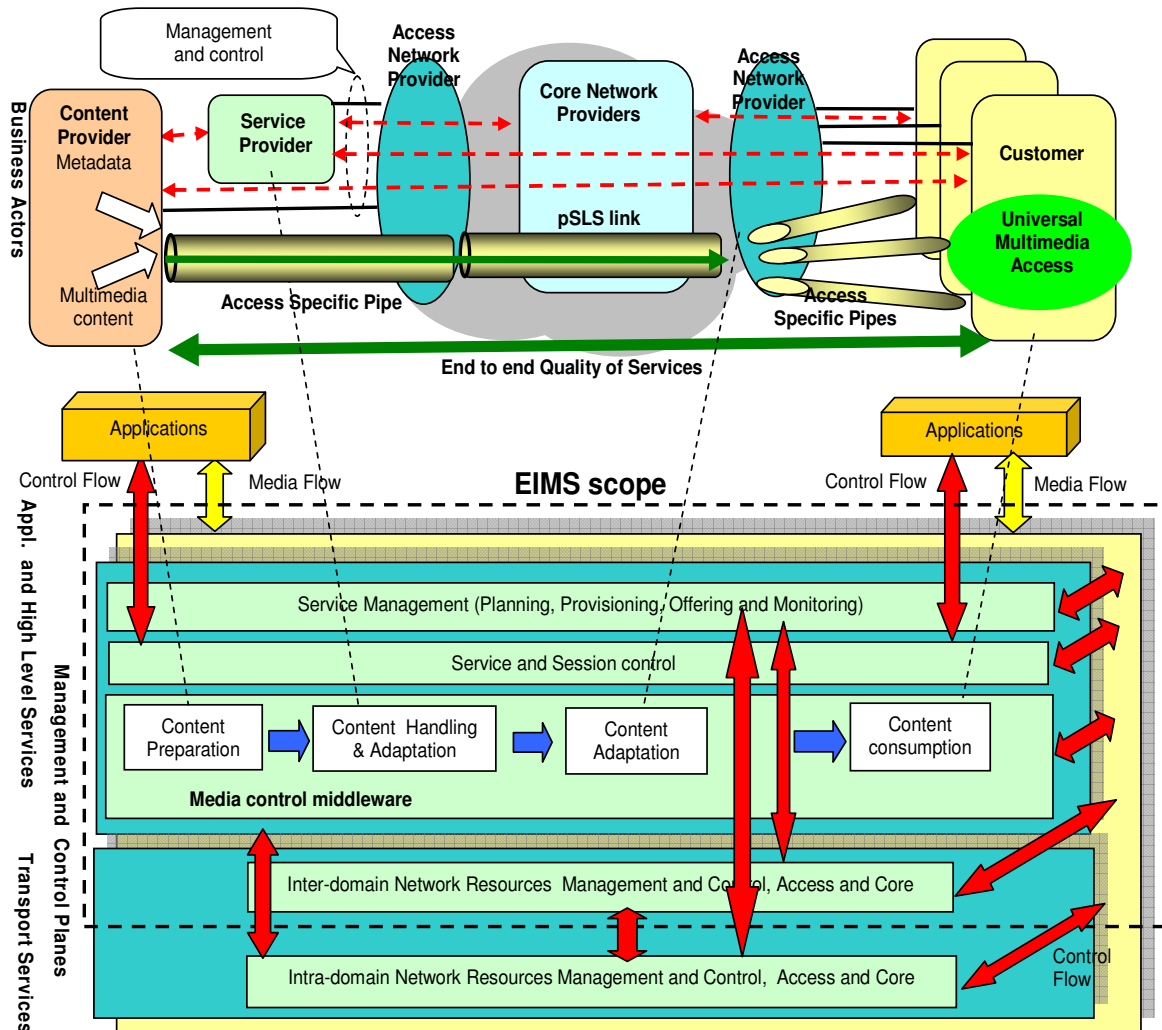


Figure 1. Multiple plane high level view of the ENTHRONE architecture

ENTHRONE architecture deals with both service level and resource management. Its EIMS is independent of network technology and harmonizes the inter-domain functioning while the network domains are autonomic in terms of resource management.

The ENTHRONE EIMS supports different business models and entities having their own resources and capabilities, but cooperating to offer value-added services for end-users. These business entities are: Service Providers (SP), Content Providers (CP)-owning Content Servers (CS), Network Providers (NP), Content Consumers (CC), Access Network Providers (ANP), Brokers/Resellers, etc., [3][4][5][6][7][8]. The SP provides high level services to the end-users, while the NPs manage their autonomous network domains. The ANPs manage the Access Networks.

ENTHRONE testbeds are set-up in several countries, that are interconnected in order to build an international pilot. Each testbed consists of a networking infrastructure (core IP domains, various access networks) and hosts having installed the relevant software components, corresponding to the

business entities (SP, NP, ANP, CC, CP/CS). The testbeds are aimed at several objectives to be fulfilled: the development and validation of the software components to be integrated in the management and control system; validation of the transport services management (or IP level network services) in both access and core IP part of the network; validation and deployment of the high level services. Both functional (i.e. correctness) and scalability aspects are targeted in the test campaigns. Appropriate scenarios are specified for each kind of test.

This paper presents the implementation and infrastructure of a complex multiple domain testbed developed at University "Politehnica" of Bucharest (UPB), based on the ENTHRONE architecture. Examples are given of functional validation results.

The paper is organized as follows. Section 2 shortly presents the ENTHRONE network service management framework. Section 3 describes the Pilot set up at University "Politehnica" of Bucharest. Section 4 presents samples of scenarios for functional and performance level testing.

Section 5 presents the test results and Section 6 contains the conclusions.

II. ENTHRONE ARCHITECTURE AND NETWORK SERVICE MANAGEMENT SUMMARY

ENTHRONE has defined an E2E QoS multi-domain *ENTHRONE Integrated Management Supervisor (EIMS)*. The service management (SM) is a part of the EIMS. It considers all actors mentioned above and their contractual service related relationships, *Service Level Agreements (SLA)* and *Service Level Specifications (SLS)*, as defined in [3][4][5][6][7][8]. The SM is independent on particular management systems used by different NPs in their domains. The SM entities should cooperate to realize the E2E chain. They are present in different amounts in SP, CP, NP CC entities, depending on the entity role in the E2E chain. The SM located in NPs should cooperate with each domain manager and also with other actors in the E2E chain.

The QoS control is accomplished at the service level by logical QoS enabled aggregated pipes, built through the domains crossed by the path from source to destination, and logical QoS enabled individual pipes, built for each user in the access network. Several individual QoS enabled pipes are included in an aggregated pipe at the core network level.

The pSLS is a contract performed at the Management Plane, and established by horizontal negotiation signaling between two peer managers, e.g., SM@NP, in which the requested NP agrees or does not agree to offer to the requester the QoS-enabled service (in the terms of QoS enabled pipes). Negotiations are required to establish an end-to-end pipe.

The EIMS architecture at NP (EIMS@NP) contains four functional planes (Figure 1): the *Service Plane (SPI)* establishes appropriate SLAs/SLSs among the operators/providers/customers. The *Management Plane (MPI)* performs long term actions related to resource and traffic management. The *Control Plane (CPI)* performs the short term actions for resource and traffic engineering and control, including routing. In a multi-domain environment the *MPI* and *CPI* are logically divided in two sub-planes: inter-domain and intra-domain. Therefore, each domain may have its own management and control policies and mechanisms. The *Data Plane (DPI)* is responsible to transfer the multimedia data and to set the DiffServ traffic control mechanisms to assure the desired level of QoS.

The main task of the EIMS@NP is to find, negotiate and establish a QoS enabled pipe, from a Content Server (CS), belonging to a Content Provider, to a region where potential clients are located. This unidirectional pipe is referred as pSLS pipe, and it could cross multiple domains. Each pipe is established and identified by a chain of pSLS agreements between successive NP managers. The forwarded cascaded model is used to build the pSLS pipes [7]. The pipes are unidirectional ones. An end to end negotiation protocol is

used to negotiate the pSLS pipe construction across multiple network domains [7].

The process of establishing a pSLS-link/pipe is triggered by the SP. It decides, based on market analyses and users recorded requirements, to build a set of QoS enabled pipes, with QoS parameters described by a pSLS agreement. It starts a new negotiation session for each pSLS pipe establishment. It sends a pSLS Subscribe request to the EIMS@NP manager of the Content Consumer network domain. The EIMS@NP manager performs the QoS specific tasks such as admission control (AC), routing and service provisioning. To this aim, it splits the pSLS request into intra-domain respectively inter-domain pSLS request. It also performs intra-domain routing, to find the intra-domain route for the requested pSLS, and then it performs intra-domain AC. If these actions are successfully accomplished, and if the pSLS pipe is an inter-domain one, then the manager uses the routing agent to find the ingress point in the next domain, does inter-domain Admission Control and then send a pSLS Subscribe request towards the next domain. This negotiation is continued in the chain up to the destination domain, i.e., the domain of the CC access network. If the negotiation ends successfully, the QoS enabled pipe is considered logically established along the path from source to destination.

The Network Service Management (NSM) is the EIMS subsystem offering network connectivity service to the applications. The NSM manages the services and network resources by using an overlay based approach. This means that a network domain is abstracted with a virtual domain and the services and domain resources management is performed based on the virtual domain information. Each domain has its own local manager, called Intra-domain Resource Manager, which is in charge with the local domain management. Also it applies the decisions taken at the virtual level in the managed domain [7][15].

The network connectivity service is first built at the overlay level. This is done during the pSLS Subscription phase, which is performed using pSLS negotiation between the SP and the NP of the first domain and between the successive NPs along the service path. The negotiation result is an aggregated pipe built for the service traffic between the content source and the destination access network. During the pSLS Invocation phase, the pSLS pipe is installed on the network equipments of each domain, crossed by the aggregated pipe, by the associated Intra-domain Resource Managers. The pSLS pipe resources could be invoked totally or partially, depending on the amount of traffic estimated for the pSLS associated services in the following time period.

With the pSLS pipe built, the SP can now offer the service to the users by allocating pSLS pipe slices, cSLS pipes, to the individual users' calls. These cSLS pipes are built at the access network level. In this way the ENTHRONE solution avoid per flow signaling in the core domain.

III. ROMANIAN PILOT TOPOLOGY

The Romania Pilot island (RPI) general infrastructure consists of three sections:

- Core IP – The Core IP network consists of three autonomous domains, each managed by the ENTHRONE EIMS at Network Provider subsystem. The Core network is linked via GEANT with the other ENTHRONE pilots;
- Access Networks – We have implemented several type access technologies i.e., IP/Ethernet; wireless - WiMAX 802.16d, and DVB-T. For the WiMAX access based network we have developed, in ENTHRONE project, a WiMAX Resource Manager which is integrated with the ENTHRONE EIMS. It is capable of cSLS management inside the WiMAX network;
- ENTHRONE Terminals with wired or wireless access based on WLAN-802.11b/g. They are supporting the ENTHRONE signaling via the Terminal Device Manager, which is used to connect the terminal to the ENTHRONE EIMS system.

This infrastructure allows experimentations of full ENTHRONE scenarios locally, but can be interconnected to other countries' pilots too. The terminals can be fixed or mobile, with single mode or hybrid mode access. The ENTHRONE business entities supported are CC, CP, SP, NP. The relevant EIMS entities are located in: Core IP; Access (Aggregation) Networks; User Terminals; Content Providers hosts.

The UPB pilot was focused on the SLS management validation, both pSLS and cSLS management. In Figure 9 the simplified version of the pilot topology, showing only the components involved in the validation tests, is presented. There are three core IP network domains NP1, NP2 and NP3, each one managed by its own *NetSrvMngr@NP* (in the current implementation it includes also the Inter-domain Network Resource Manager). The Intra-domain Resource Manager (*IntraResMngr@NP*) manages the resources at the local domain level. In particular, the access network technology used in our example is IEEE 802.16d/WiMAX, [5]. The AN is managed by its Resource Manager (*ResMngr@ANP*), which reserves resources on the WiMAX links at SP requests.

The structure of the core network is detailed: the allocated IP addresses, the name of the border routers and the applications installed on the testbed. The core routers are implemented using the Linux machines and the resource control in the data plane is done using the Linux Traffic Control application. The network management modules are communicating using the Web Services technology, the interfaces between them are defined using the WSDL description language [7][18][19].

The NP1 domain has four border routers (*border_an*, *border_elcom*, *border_as1as2* and *border_as1as3*). The *border_elcom* router is connected through the GEANT backbone with other ENTHRONE pilots. The AN connected to *border_an* router contains the EIMS SP machines and also

the CP machines. The EIMS SP and CP machines are implemented using virtual machines.

The NP2 domain has two border routers (*border_as2as1*, *border_an103*). The WiMAX AN is connected to the *border_an103*. In this network we have the ENTHRONE terminal and player. The NP3 domain contains only one machine, with a simulated virtual domain containing three border routers (*border_as3as1*, *border_as3as2*, *border_an105*).

The main ENTHRONE components and their placement are shown in Figure 9. In red are highlighted the modules involved in the network service management: Network Service Manager at Service Provider and Network Provider (*NetSrvMngr*), the Intra-domain Network Resource Manager at Network Provider and the WiMAX Resource Manager at Access Network. A detailed description of the ENTHRONE modules could be found in [3][5][7][16]. The main task of the Network Service Manager is to find, negotiate and establish a QoS enabled pipe from a Content Server to a Content Consumer. The following components are installed at each IP domain:

- Network Service Manager at Network Provider
- Intra-domain Resource Manager: specific blocks of NP for resource management and traffic engineering
- Node monitoring and Network Monitoring

The assembly of these components provides the service and resource management for support of the network connectivity in the core network.

The overall goal of the UPB testbed was the deployment, validation and demo for a subset of the ENTHRONE general functionalities. Specifically, we targeted to test and validate the network IP connectivity QoS enabled services over several core IP domains and heterogeneous access networks (ANs), in unicast and multicast mode.

Appropriate scenarios have been defined to provide the necessary framework for functional and performance system validation. Each scenario defines the test environment and a sequence of actions (inputs, internal actions and expected outputs) to perform. We define *Operational Scenarios* (in terms of functionality), technically-oriented (correctness, scalability, stability, etc.), and usability-oriented (cost/benefit to provider and end-user) relatively to a given subsystem to be tested; *High level services Scenarios*- oriented towards services like VoD, streaming, E-learning, etc., aimed to measure the related performance and benefits seen from user perspective [20].

IV. SCENARIOS FOR NETWORK CONNECTIVITY SERVICES FUNCTIONAL VALIDATION

In this section we will present samples of operational scenarios to validate the inter-domain negotiation signaling and processing for the pSLS-links (in core IP domains) and cSLS-links (in AN) installation in the network.

These tests are aimed at validating the correctness of the EIMS Network Service Manager (NSM) implementation behavior, relative to p/cSLS subscription and invocation, in a multi-domain environment for unicast case.

The Figure 2 shows an example of a message sequence launched by SP in order to install in the networks (three IP domains) a pSLS-link. The pSLS-link invocation phase is considered. It is supposed that the pSLS-link has been already subscribed, through a similar sequence of actions. The EQoS-pSLS negotiation protocol has the task to transport the negotiation messages between entities [6][8]. This protocol has been implemented as Web Services, [7][18][19]. The pSLS subscription invocation scenario main phases are described below. The modification and deletion scenarios derive from this one.

1 The SP administrator decides, based on current needs data, to invoke, partially or totally, a previously subscribed pSLS-link. It configures the pSLS parameters in the web management interface and then it triggers the subscription of a new pSLS link. See action 0 on Figure 2. The SLS parameters specify among others, the bandwidth required, delay, and class of services associated to this request.

2 The *NetSrvMngr@SP* starts an invocation signaling session. So, it sends the pSLS invocation request, using the EQoS client, to the first *NetSrvMngr@NP*(action 1).

3 The negotiation is carried in cascaded forwarding mode between the *NetSrvMngrs@NPs*, down to the last core IP domain where the potential CCs are located. See actions 2, 3.

4. It is assumed a successful scenario where all resource checks are successful, therefore vertical commands are given by each *NetSrvMngr@NP* to its *IntraResMngr@NP* in order to install the pipe in the network (actually configuration of the Diffserv LINUX Traffic Control for the associated QoS class is done). See (4,5; 7,8; 10,11) actions.

5. Responses are returned to the upstream *NetSrvMngr@NPs*, (6, 9, 12) and then, finally, to SP Admin.

The Figure 3 shows a scenario in which a client (CC) browses a website (which can be based on a Digital Item Description -DID) which offers the latest Digital Items for consumption. The module Customer Service Manager (*CustSrvMngr*) is in charge with the high level service management. It is the main subsystem which coordinates all

the other subsystems of the Service Provider. Then the following message sequence is performed in order to allow users access to the ENTHRONE services:

1 The CC chooses a specific DI and sends a request for it to *Service Provider Frontend* (SP-FE)

2 The SP-FE forwards it to *CustSrvMngr*. The parameters are: the content ID, class of service, the initial (i.e., the static) usage environment (UED) of the client (Terminal Capabilities, User Characteristics/ Preferences, Natural Environment Characteristics and Network Characteristics), IP address of the client.

3. *CustSrvMngr@SP* selects a content variation list (in cooperation with other EIMS blocks not shown here)

4. The *CustSrvMngr@SP* queries the *NetSrvMngr@SP* about the available pSLS(s) between each content variation and the CC. Then (4.1, 4.2) *NetSrvMngr@SP* queries the repository to obtain a list of the appropriate pSLSes

5. *NetSrvMngr@SP* returns a list with available pSLSs, between the content sources and the access network, to the *CustSrvMngr*

6. After getting pSLS status, the *CustSrvMngr* performs other actions. Among others, it selects an appropriate pSLS link.

7. *CustSrvMngr@SP* requests cSLS subscription to *NetSrvMngr@SP*. Then a sequence of actions denoted with 7.1-7.6 follows: *NetSrvMngr@SP* checks for available resources on the pSLS link, then negotiate with the access network resource manager (*ResMngr@ANP*) to reserve resources for the cSLS link in the access network. If all these actions are successfully accomplished, then the *NetSrvMngr@SP* updates the resources status and records the cSLS agreement.

8. *NetSrvMngr@SP* responds to *CustSrvMngr@SP* with the new cSLS subscription data. Other actions may be performed by the *CustSrvMngr@SP*- not detailed here.

9. 10 *CustSrvMngr@SP* responds to the CC, via *SP-FE*, about the success of the DI selection.

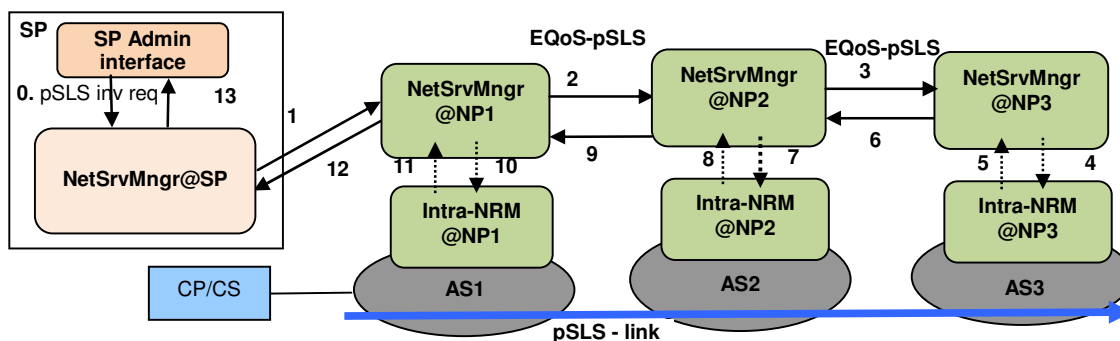


Figure 2. Basic pSLS invocation chain of signalling (3 IP domains).

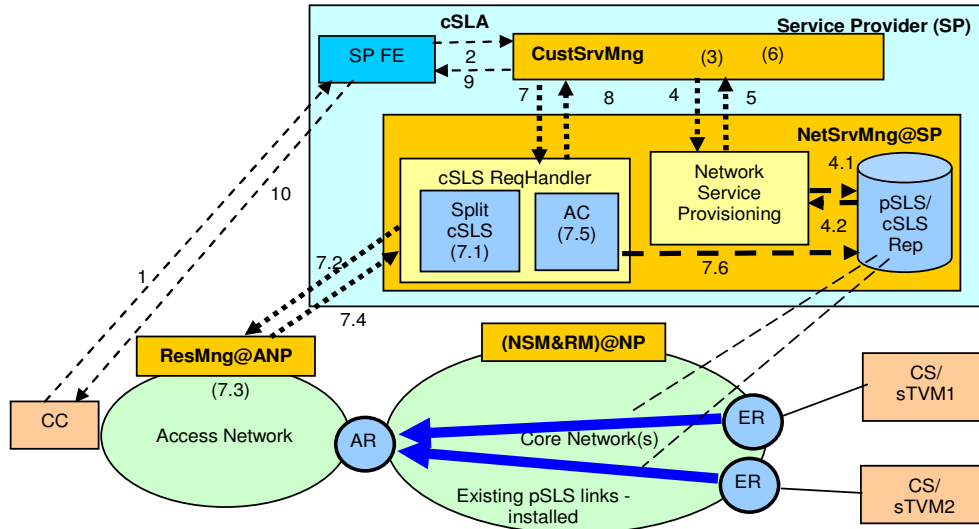


Figure 3. Message Sequence showing the pSLS status query and cSLS subscription related actions

The Figure 9 shows, in graphical form, on the testbed diagram, the results for the two scenarios above, aiming to construct a pSLS-link in the NP1 and NP2 IP domains and complete it with a cSLS-link, as a last mile installed in the WiMAX AN network. The pSLS link is subscribed spanning from *Border_an* up to *Border_an103*. The concatenated pipes at the left side (subscription phase) represent the pSLS-link subscribed. This is done at EIMS overlay level in each domain; EIMS knows only the ingress and egress points in each domain and the inter-domain links. The inter-domain route selection [21] is not the subject of this paper. The actual path established in invocation phase within each IP domain is different from the overlay one; e.g., in NP1 the path is A1, E4 and E3. The arrows 1, 2, 3, 4 represent the horizontal signaling actions between *NetSrvMngr@SP* and *NetSrvMngr@NPs* for pSLS subscription. The arrows 5,6,7,8 represent the similar actions for pSLS invocation. The arrows 6' and 7' represent the vertical commands given by the *IntraNetResMngr@NP* to routers in order to install the pipes (i.e. Traffic Control parameters configuration). The arrows 9, 10 and 11, 12 represent respectively the signaling actions between the *NetSrvMngr@SP* and *ResMngr@AN* to subscribe and invoke the cSLS-link in the WiMAX segment. The arrow 11' represents the command given to the WiMAX Base Station (BS) to install the associate service flow between BS and Subscriber Station (SS). The thick line in the Figure 9 represents the path of the future media flow through the domains, form CP up to the CC. A lot of experiments for other different scenarios are reported in [17].

V. TESTS PERFORMED IN THE UPB TESTBED

The testbed focused on validating the SLS management as standalone functionality and also integrated with the overall ENTHRONE end to end QoS management system. Functionality and scalability tests were done for the SLS management [1][2][16][17].

A. Functionality tests

1) pSLS management

In this section there are presented some functionality tests performed. The complete description of tests suit performed in UPB testbed can be found in [16].

The first suit of functionality tests refers to the pSLS subscription. The pSLS subscription request is triggered by the Service Provider's Network Service Manager in order to reserve resources, at the overlay (virtual domain) level, in the core network. As a result of the pSLS subscription a logical pipe, pSLS pipe, is built in the core network. We made tests for intra-domain and inter-domain pSLS subscription and invocation.

As an example, for intra-domain case it was built a pSLS pipe between the *border_an* and *border_elcom* border routers (Figure 9). For inter-domain case a pSLS pipe was subscribed between the *border_an* machine (on NP1 domain) and *border_an103* machine (on NP2 domain). The *border_an* machine is the border router for the Content Server access network, and *border_an103* is the border router for the access network containing the ENTHRONE terminal. The pSLSSubscribe operation was triggered from the *NetSrvMngr@SP* installed on the SP virtual machines. In the negotiation were involved the *NetSrvMngr@NP1* and *NetSrvMngr@NP2*.

In Figure 4 there are presented the messages exchanged between the *NetSrvMngr@SP* and the *NetSrvMngr@NPs* for the inter-domain pSLS subscription case. For the *NetSrvMngr@NP1*, the messages exchanged between the main modules involved in pSLS management are also detailed: pSLS provisioning, pSLS split and pSLS admission control. For the second domain a similar suit of messages will be exchanged in order to fulfill the request.

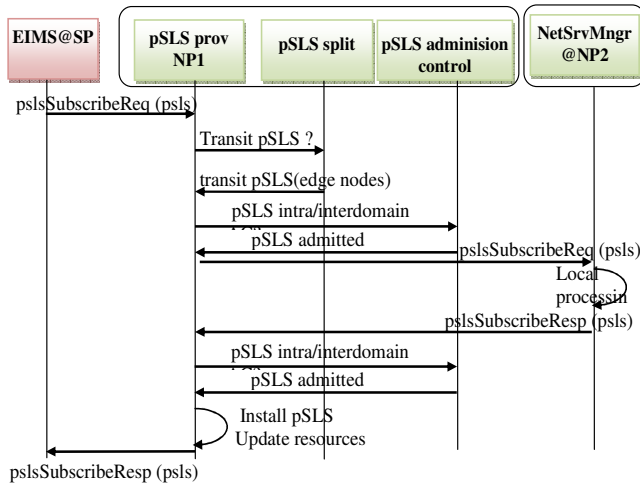


Figure 4. MSC for the inter-domain pSLS

For the pSLS pipe subscribed it has also tested the invocation phase. Both the invocation for intra and inter-domain case were considered.

There were triggered invocation requests from the *NetSrvMgr@SP*. In the negotiation phase, the following entities were involved: the *NetSrvMgr@NP1*, *Intra-domainResMgr@NP1* modules for intra-domain and *NetSrvMgr@NP1/NP2*, *Intra-domainResMgr@NP1/NP2* for inter-domain pSLS invocation. As a result the pSLS pipe resources were reserved on the Linux routers along the path. The bandwidth resources were reserved in the Linux router using the Traffic Control application. The reservation was performed successfully. The system was able to prioritize the pSLS traffic against a noise traffic generated in order to test the invocation result.

In Figure 10 one can see a screen capture with two movies, one whose stream is treated as best effort traffic, while the packets for the second one are transmitted through the pSLS pipe in the core network. One can see that the second movie's quality is much better than for the first movie. The traffic classes created by Traffic Control application, for best effort and for the pSLS pipe, and the noise traffic generated with Iperf application are also shown.

The operations for modifying and closing the Invocation and for closing the pSLS subscription were also performed successfully.

2) cSLS management

For the cSLS management it was performed both standalone tests, using a Customer Service Manager test module used to trigger cSLS subscription and invocation requests, and tests using the whole ENTHRONE end to end QoS management system. In this section we will present the whole ENTHRONE signaling mechanism with focus on the cSLS management.

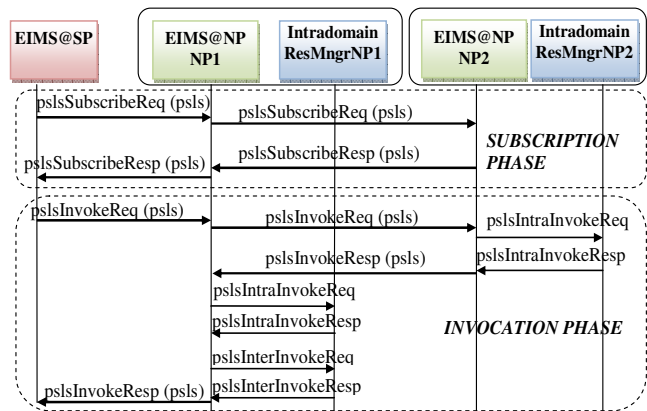


Figure 5. The MSC for pSLS subscription and invocation

After the pSLS subscription and invocation phases, a pSLS pipe will be established in the UPB testbed. The pSLS pipe, which is crossing both the NP1 and NP2 domains, is built from the 192.168.202.200 server to the 10.242.103.0 access network. The 192.168.202.200 server has the Adaptation TVM installed on it. In the 10.242.103.0 access network we have an ENTHRONE terminal with the ENTHRONE Player and Terminal Device Manager Client installed on it. After the pSLS pipe was built between the aTVM content server and the access network containing the ENTHRONE Terminal, the ENTHRONE end to end scenario can be run. The cSLS pipes requested by the users will be associated with the pSLS inter-domain pipe. In the 10.242.103.0 access network we have a WiMAX based network, managed by an ENTHRONE Resource Manager at Access Network Provider (*WimaxMgr@ANP*), installed on *border_an103* machine. We will be able to test the subscription and invocation phases, for the cSLS pipes, at the access network level.

After the ENTHRONE end to end overall scenario will be run, the cSLS/pSLS pipes will be installed in the access network. At the WiMAX access network level the cSLS pipe is installed as a service flow on the BS-SS WiMAX link.

The traffic streamed from the Adaptation Terminal towards the ENTHRONE Terminal will be inserted in the pSLS pipe, while crossing the NP1 and NP2 domains, and in the Service Flow associated with the cSLS pipe, while crossing the access network. In NP1 domain and in the access network the links crossed by the user's traffic were flooded with some noise traffic from a traffic generator. As a result of the resource reservations performed during the invocation phases, the users are able to see the movie with a good quality (Figure 10).

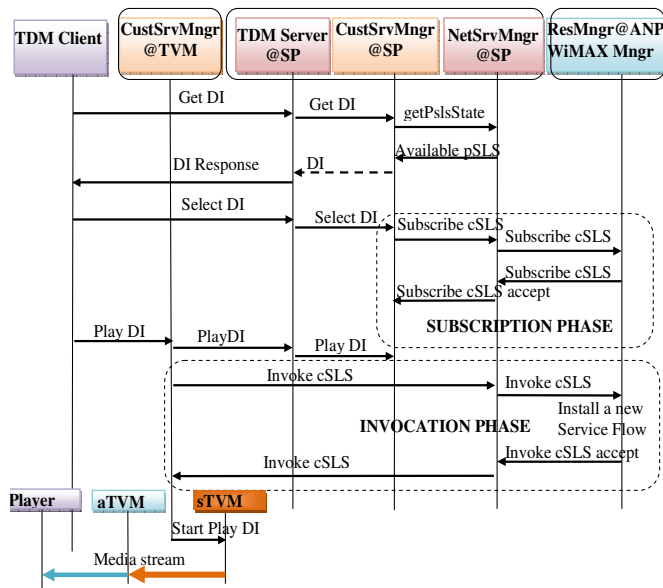


Figure 6. cSLS invocation and subscription phase in the overall end to end ENTHRONE scenario

In Figure 6 the messages exchanged during the overall end to end QoS management scenario are shown. The cSLS subscription and invocation phases' placement in the message sequence is also shown.

In Figure 6, by DI we noted Digital Item which is defined in the MPEG 21 standard; by CustSrvMngr we refer the Customer Service Manager either Service Provider or at TVM and by TDM the Terminal Device Manager [3][5][6][7][16] [17].

B. Scalability tests

Besides the functionality tests, which were used to validate the ENTHRONE functional architecture, the correct behavior of the ENTHRONE modules, we have tried to determine the scalability of the ENTHRONE Network Service Manager's modules. Because the Service Provider has to deal with user's requests, which are greater in number than the requests for pSLS pipe establishment triggered by the Service Provider before the service offering, we have considered that scalability problems could be generated by the Network Service Manager at the Service Provider module, when it should answer to the cSLS subscription and invocation requests.

In order to test the scalability for the NetSrvMngr@SP module we have used a CustSrvMngr test module to generate cSLS subscription and invocation requests. The test module was used on a terminal situated outside the university campus. In order to connect to the testbed we have used a VPN connection. So, the requests have to travel initially through the Internet before reaching the UPB testbed, simulating in this way the real case where the users connects to the Service Provider via Internet.

Several successive requests were generated and the time required to fulfill all the requests was measured. The following cases were considered:

- Several cSLS subscription requests (Figure 7)
- Several groups of cSLS subscription and invocation requests (Figure 8). In this case, because the number of the cSLS invocation is large, we have used a dummy WiMAX manager module which did not install the service flows on the WiMAX equipment, but just returned a positive answer.
- Several groups of cSLS subscription, invocation and invocation close requests (Figure 8). In this case we have used the real WiMAX manager, because in this case, after the service flow is installed, it is also removed afterwards.

From the picture one can see that the NetSrvMngr@SP could serve 200 requests suites cSLS subscription, cSLS invocation, cSLS invocation close in less than 20 seconds. Taking into account that the cSLS requests are for video on demand services, we believe that serving speed is satisfactory. We didn't perform yet tests with the case when the requests are coming from different machines.

VI. CONCLUSION AND FUTURE WORK

A testbed for an integrated E2E QoS management system validation, developed in the framework of the ENTHRONE Project, is briefly described. Several tests were presented, both functionality and scalability tests, aimed to validate the SLS management and the ENTHRONE overall system.

Scalability tests are in progress. Some basic scalability tests for the pSLS/cSLS negotiation were done. Further tests have to be done for the scalability in the case of requests coming from different hosts. Also we should do tests in order to measure the scalability for the entire system, with all the ENTHRONE modules integrated.

The tests have proved that ENTHRONE is a functional, flexible, feasible solution for E2E QoS management for multimedia streams delivery. While functionality test were successfully, a difficult part is to prove its scalability. Some tests in this direction were started, but there is still lot of work in this direction. We stressed the system with some automatically generated requests and the serving rate was acceptable.

The ENTHRONE system is designed for multimedia delivery, but it has no support for VoIP services and for audio/video conferencing/chat. Because of the long term nature of the pSLS aggregated pipes they are not well suited for the dynamic and diversity of these interactive services. Future work will be done to enhance the ENTHRONE system and also to adapt it to some new services link requiring QoS, like VoIP and videoconferencing.

ACKNOWLEDGMENT

This work was supported by the FP6 project ENTHRONE project IST 507637 (continued with ENTHRONE II, IST 038463).

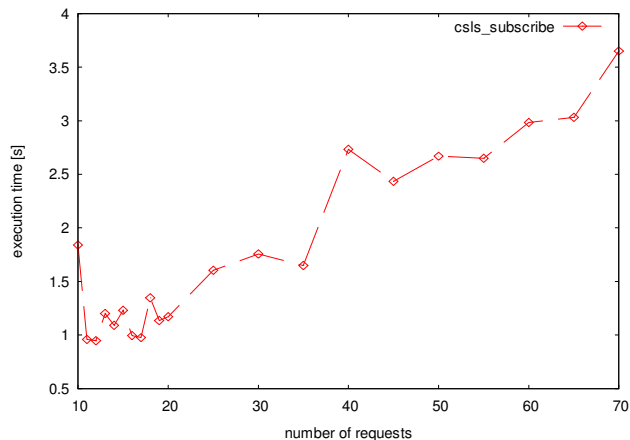


Figure 7. The execution time for cSLS requests

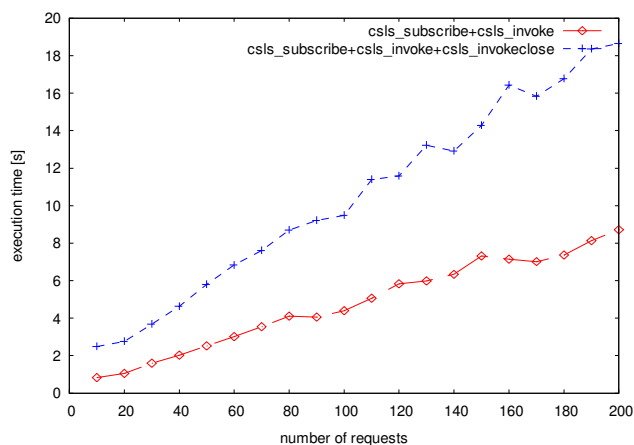


Figure 8. The execution time for cSLS subscribe, cSLS invocation suite and for cSLS subscribe, cSLS invocation, cSLS invocation close suite

REFERENCES

[1] S. Obreja, E. Borcoci, R. Lupu, M. Stanciu and S. Ciocina: *Functionality and scalability validation for an end to end QoS management system*, The Fifth Advanced International Conference on Telecommunications, AICT 2009, pp.142-147, Venice/Mestre, Italy.

[2] E. Borcoci, Ș. G. Obreja and R. Lupu: *Overlay Management of Network Services for Multimedia Flows Transport over Multiple Domains - Testbed Validation*, The Fifth Advanced International Conference on Telecommunications, AICT 2009, pp.136-141, Venice/Mestre, Italy.

[3] Brétilion, P. (ed) et al.: ENTHRONE II Deliverable D01, *Overall System Architecture*, February 2007.

[4] P. Sommer (ed.) et al.: ENTHRONE II Deliverable D02, *Pilot Architecture and Services Definition*, February 2007.

[5] P. Souto and M. Ransburg, (eds.) et al.: ENTHRONE II Deliverable D03, *EIMS for ENTHRONE II*, February 2008.

[6] M. Sidibé and A. Mehaoua, (eds.) et al., ENTHRONE II Deliverable D06, *Service management and monitoring*, Febr. 2008.

[7] E.Borcoci and S. Obreja (eds.) et al., ENTHRONE II Deliverable D18, *Service management and QoS provisioning*, June 2007.

[8] M.Stier, (ed.) et al., *End-to-End QoS Signalling Protocols and All-IP Approach*, ENTHRONE II Deliverable D22F, March 2007, <http://www.ist-ENTHRONE.org>

[9] T.Engel, et al, *AQUILA: Adaptive Resource Control for QoS Using an IP-Based Layered Architecture*, IEEE Communications Magazine, January 2003, pp. 46-53.

[10] P. Morand, et. al., *Final specification of protocols and algorithms, for inter-domain SLS management and traffic, engineering for QoS-based IP service delivery*, MESCAL IST Project Public Deliverable, D1.3, July 2005.

[11] T. Damilatis, et.al., *Final Architecture, Protocol and Algorithm Specification*, TEQUILA IST Project Public Deliverable, D3.4 Part B, Oct. 2002.

[12] ETSI RES 282 001: *Telecommunications and Internet converged Services and Protocols for Advanced Networking (TISPAN)*, NGN Functional Architecture Release 2, March 2007

[13] 3GPP TS 23.228: *IP Multimedia (IM) Subsystem; Stage 2 (Release 8)*, December 2007.

[14] T.Ahmed, A.Asgari, A.Mehaoua, E.Borcoci, L.Berti-Équille and G.Kormentzas *End-to-End QoS Provisioning through an Integrated Management System for Multimedia Content Delivery*, Computer Communication Journal, May 2005.

[15] E.Borcoci, A.Asgari, N.Butler, T.Ahmed, A.Mehaoua, G.Kourmentzas and S.Eccles *Service Management for End-to-End QoS Multimedia Content Delivery in Heterogeneous Environment*, AICT Conference, July 2005, Lisbon.

[16] T. Ahmed, (ed.) et al., ENTHRONE II Deliverable D27 *Pilot and services integration and tests*, March 2008

[17] ENTHRONE II Deliverable D28 *Trials and evaluation*, November 2008

[18] S.Obreja, E.Borcoci, R.Lupu and R.Iorga, *Web-service solution for inter-domain QoS negotiation*, Int'l Conference on Communication Theory, Reliability, and Quality of Service CTRQ July 2008, Bucharest, Romania.

[19] S. Obreja, E. Borcoci, R. Lupu and M. Stanciu, *Web-service based implementation of a Network Service Manager at Network Provider*, IEEE Int'l Conference on Automation, Quality and Testing, Robotics AQTR 2008 - THETA 16th edition, May 22-25 2008, Cluj-Napoca, Romania.

[20] E. Borcoci, A. Asgari, S. Ciocina and S. Obreja, *The Methodology for Testbed Validation and Performance Assessment of Network/Service Management Systems*, IEEE Int'l Conference on Automation, Quality and Testing, Robotics AQTR 2008 - THETA 16th edition - May 22-25, 2008, Cluj-Napoca, Romania.

[21] S. Obreja, E. Borcoci, *Finding inter-domain Qos enabled routes using an overlay topology approach*, International Journal On Advances in Telecommunications, issn 1942-2601, vol. 2, no. 1, year 2009, pp.16-26, <http://www.ariajournals.org/telecommunications/>.

LEGEND FOR FIGURE 9:

- TVM – Multimedia TV processor (source TVM and adaptation TVM),
- EIMS@SP- ENTHRONE Integrated Management System at Service Provider,
- NetSrvMngr@SP/NP – Network Service Manager at SP/NP,
- IntraResMngr@NP – Intra-domain Resource Manager at NP,
- WiMAXmngr – Resource Manager at AN for the WiMAX access network

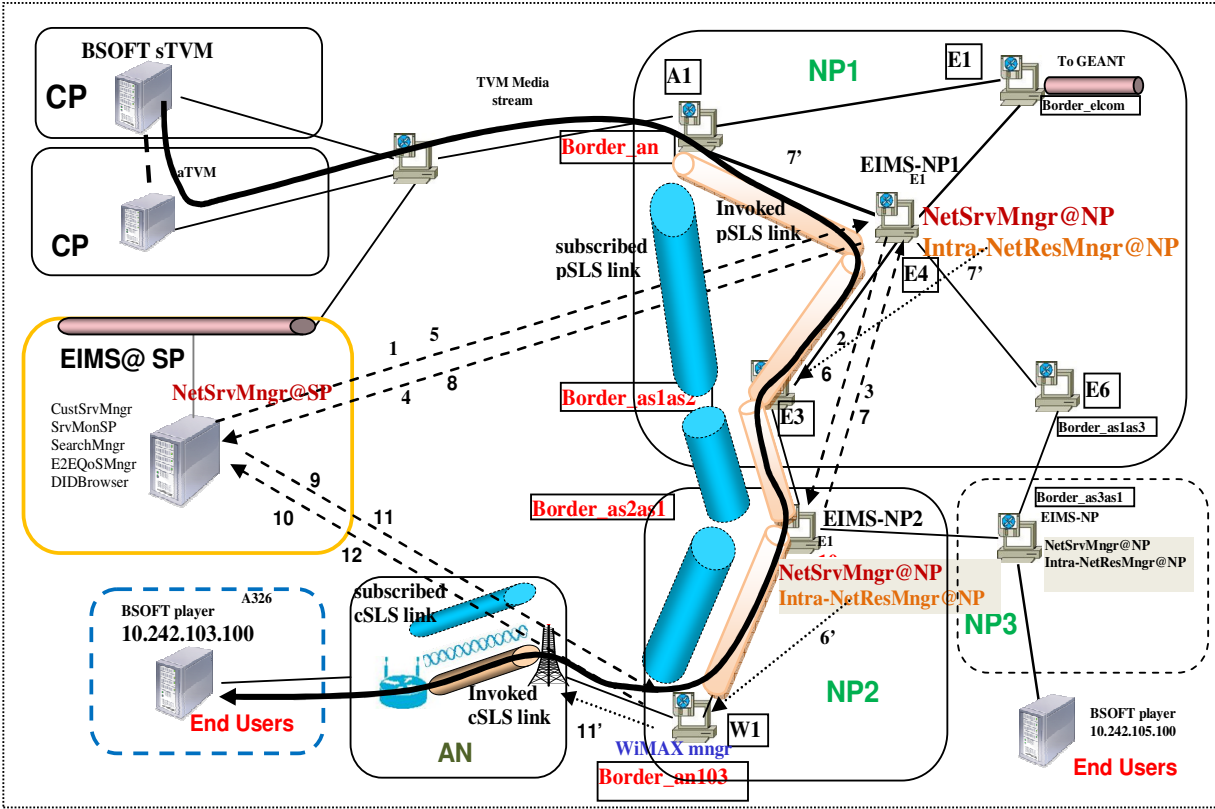


Figure 9. UPB testbed infrastructure: installation of pSLS link and cSLS link in NP1, NP2 and in WiMAX Access Network.

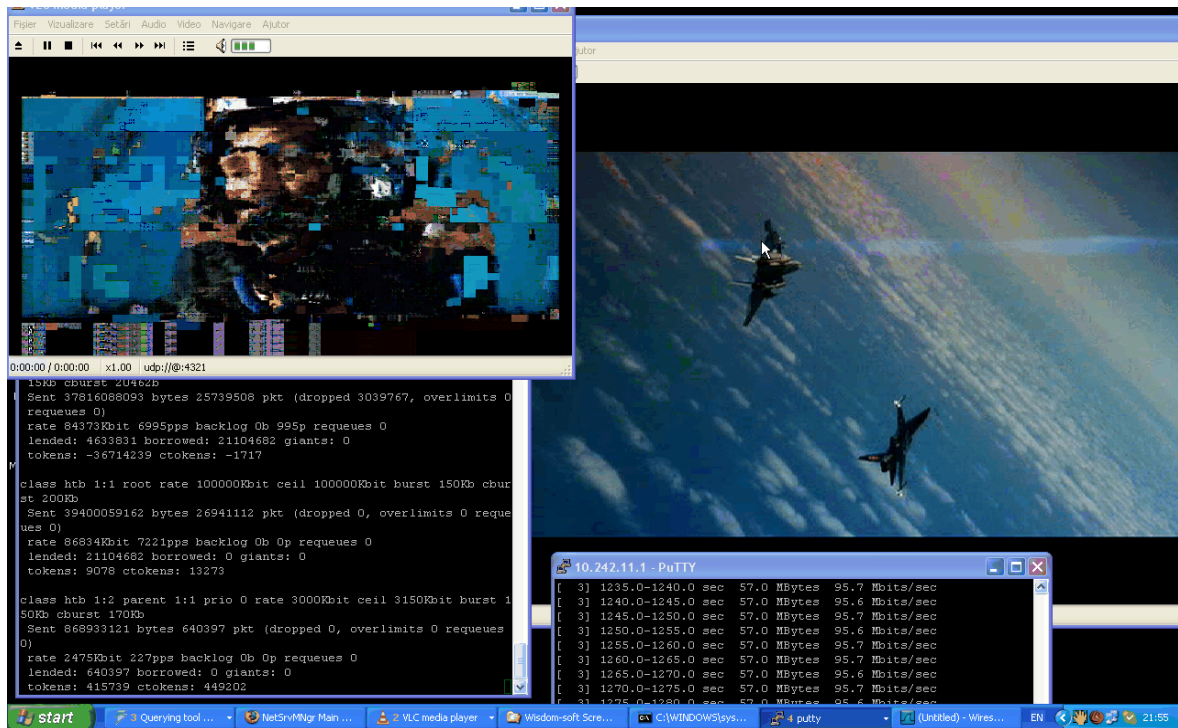


Figure 10. The result of the cSLS/pSLS invocation.

Diffusion Approximation Models for Transient States and their Application to Priority Queues

Tadeusz Czachórski

IITiS PAN

Polish Academy of Sciences

44-100 Gliwice, ul. Baltycka 5, Poland

tadek@iitis.gliwice.pl

Tomasz Nycz

Centrum Komputerowe

Politechnika Slaska

44-100 Gliwice, ul. Akademicka 16, Poland

tomasz.nycz@polsl.pl

Ferhan Pekergin

LIPN

Université Paris-Nord

93430 Villetaneuse, France

pekergin@lipn.univ-paris13.fr

Abstract—The article presents a diffusion approximation model applied to investigate the behavior of priority queues. We discuss the use of the diffusion approximation in transient analysis of queueing models in the case of a single station and of a queueing network presenting the solutions. We emphasize the numerical aspect of the solution and analyze the errors. In classical queueing theory, the analysis of transient states is complex and practically does not go far beyond M/M/1 queue and its modifications. However, the time dependent flows in computer networks and especially in Internet focus our interest on transient-state analysis, which is necessary to investigate the dynamics of TCP flows cooperating with active queue management or to see the changes of priority queues which assure the differentiated QoS. With the use of G/G/1/N and G/G/1/N/PRIOR models, we present the potentials of the diffusion approximation and in conclusions we compare it with alternative methods: Markovian queues solved numerically, fluid-flow approximation and simulation. Diffusion approximation allows us to include fairly general assumptions in queueing models. Besides the transient state analysis, it gives us a tool to consider input streams with general interarrival time distributions and servers with general service time distributions. Single server models can be easily incorporated into the network of queues. Here we apply the diffusion approximation formalism to study transient and steady-state behavior of G/G/1 and G/G/1/N priority preemptive models. The models can be easily converted to non-preemptive queueing discipline. The introduction of self-similar traffic is possible as well. The models can be useful in performance evaluation of mechanisms to differentiate the quality of service e.g. in IP routers, WiMAX, metro networks, etc.

Index terms — diffusion approximation, transient states, priority queues.

I. INTRODUCTION

The paper extends results presented earlier in [11]. Classical queueing models of priority queues are practically limited to steady-state analysis of M/G/1 queues with non-preemptive or preemptive resume priorities, see e.g. [18], [23], [19]. It is not enough to analyze today mechanisms to ensure the quality of service inside e.g. IP routers or in access networks where the load is changing dynamically and the traffic is entirely different from Poisson streams. Therefore we adapt the method of diffusion to consider transient states in the case of priority queues. The method is based on Gelenbe's model of G/G/1 and G/G/1/N queue supplemented with our approach [5] to solve transient states using this model. The single server models are summarized in Section II, in Section III they are extended to open network queueing models. We tested this approach

several times in other non-priority models, considering e.g. the dynamics of FIFO queues in ATM routers [1], the dynamics of queues in ATM multiplexers in the case of self-similar traffic [6], the stability of TCP connections in the presence of AQM (RED queues) inside IP routers [8], investigating transmission time in ad-hoc networks [9] or modeling traffic control by leaky-bucket algorithm [10]. Section IV presents diffusion approximations of busy periods distributions which are important for priority queues presented in Section V.

II. DIFFUSION APPROXIMATION OF A FIFO STATION

Let $A(x)$, $B(x)$ denote the interarrival and service time distributions at a service station and $a(x)$ and $b(x)$ be their density functions. The distributions are general but not specified, the method requires only the knowledge of their first two moments. The means are denoted as $E[A] = 1/\lambda$, $E[B] = 1/\mu$ and variances are $\text{Var}[A] = \sigma_A^2$, $\text{Var}[B] = \sigma_B^2$. Denote also squared coefficients of variation $C_A^2 = \sigma_A^2 \lambda^2$, $C_B^2 = \sigma_B^2 \mu^2$. $N(t)$ represents the number of customers present in the system at time t .

Diffusion approximation replaces the process $N(t)$ by a continuous diffusion process $X(t)$, e.g. [25], the incremental changes $dX(t) = X(t+dt) - X(t)$ of which are normally distributed with the mean βdt and variance αdt , where β , α are coefficients of the diffusion equation

$$\frac{\partial f(x, t; x_0)}{\partial t} = \frac{\alpha}{2} \frac{\partial^2 f(x, t; x_0)}{\partial x^2} - \beta \frac{\partial f(x, t; x_0)}{\partial x}. \quad (1)$$

This equation defines the conditional pdf of $X(t)$:

$$f(x, t; x_0) dx = P[x \leq X(t) < x + dx \mid X(0) = x_0].$$

The density of the diffusion process approximates the distribution of $N(t)$: $p(n, t; n_0) \approx f(n, t; n_0)$, and in steady state $p(n) \approx f(n)$.

Both processes $X(t)$ and $N(t)$ have normally distributed changes; the choice $\beta = \lambda - \mu$, $\alpha = \sigma_A^2 \lambda^3 + \sigma_B^2 \mu^3 = C_A^2 \lambda + C_B^2 \mu$ ensures that the parameters of these distributions grow at the same rate with the length of the observation period.

More formal justification of the use of diffusion approximation lies in limit theorems for G/G/1 system given e.g. in [17]. If \hat{N}_n is a series of random variables derived from $N(t)$:

$$\hat{N}_n = \frac{N(nt) - (\lambda - \mu)nt}{(\sigma_A^2 \lambda^3 + \sigma_B^2 \mu^3) \sqrt{n}},$$

then this series is weakly convergent (in the sense of distribution) to ξ , where $\xi(t)$ is a standard Wiener process provided that the system is overloaded and never attains equilibrium.

A. Unlimited queue: G/G/1 station, transient solution

The process $N(t)$ is never negative, hence $X(t)$ should be also restrained to $x \geq 0$. A simple solution is to put a *reflecting barrier* at $x = 0$, see [22]. In this case

$$\int_0^\infty f(x, t; x_0) dx = 1,$$

and

$$\frac{\partial}{\partial t} \int_0^\infty f(x, t; x_0) dx = \int_0^\infty \frac{\partial f(x, t; x_0)}{\partial t} dx = 0.$$

Replacing $\partial f(x, t; x_0)/\partial t$ in the above integral by the right side of the diffusion equation we obtain the boundary condition corresponding to the reflecting barrier at zero:

$$\lim_{x \rightarrow 0} \left[\frac{\alpha}{2} \frac{\partial f(x, t; x_0)}{\partial x} - \beta f(x, t; x_0) \right] = 0. \tag{2}$$

The solution of Eq. (1) with conditions (2) is, cf. [22]

$$f(x, t; x_0) = \frac{\partial}{\partial x} \left[\Phi \left(\frac{x - x_0 - \beta t}{\alpha t} \right) - e^{\frac{2\beta x}{\alpha}} \Phi \left(\frac{x + x_0 + \beta t}{\alpha t} \right) \right]$$

where $\Phi(x) = \int_{-\infty}^x \frac{1}{\sqrt{2\pi}} e^{-t^2/2} dt$ is the PDF of standard normal distribution.

The reflecting barrier excludes the zero value of the process: the process is immediately reflected. Therefore, this version of diffusion process is a heavy-load approximation: it gives reasonable results if the utilization of the investigated station is close to 1, i.e. probability $p(0)$ of the empty system is negligible.

This inconvenience can be removed by the introduction of another limit condition at $x = 0$: *a barrier with instantaneous (elementary) jumps* [14]. When the diffusion process comes to $x = 0$, it remains there for a time exponentially distributed with a parameter λ_0 and then returns to $x = 1$. The time when the process is at $x = 0$ corresponds to the idle time of the system.

The diffusion equation becomes

$$\begin{aligned} \frac{\partial f(x, t; x_0)}{\partial t} &= \frac{\alpha}{2} \frac{\partial^2 f(x, t; x_0)}{\partial x^2} - \beta \frac{\partial f(x, t; x_0)}{\partial x} + \lambda p_0(t) \delta(x - 1), \\ \frac{dp_0(t)}{dt} &= \lim_{x \rightarrow 0} \left[\frac{\alpha}{2} \frac{\partial f(x, t; x_0)}{\partial x} - \beta f(x, t; x_0) \right] - \lambda p_0(t), \end{aligned}$$

where $p_0(t) = P[X(t) = 0]$. The term $\lambda p_0(t) \delta(x - 1)$ gives the probability density that the process is started at point $x = 1$ at the moment t because of the jump from the barrier. The second equation makes the balance of the $p_0(t)$: the term $\lim_{x \rightarrow 0} \left[\frac{\alpha}{2} \frac{\partial f(x, t; x_0)}{\partial x} - \beta f(x, t; x_0) \right]$ gives the probability flow *into* the barrier and the term $\lambda p_0(t)$ represents the probability flow *out* of the barrier.

Our approach, see [5], to obtain the function $f(x, t; x_0)$ of the process with jumps from the barrier is to express it with the use of another pdf $\phi(x, t; x_0)$ for the diffusion process with the absorbing barrier at $x = 0$. This process starts at

$t = 0$ from $x = x_0$ and ends when it attains the barrier. Its probability density function is easier to determine and has the following form [4],

$$\phi(x, t; x_0) = \frac{e^{\frac{\beta}{\alpha}(x-x_0) - \frac{\beta^2}{2\alpha}t}}{\sqrt{2\pi\alpha t}} \left[e^{-\frac{(x-x_0)^2}{2\alpha t}} - e^{-\frac{(x+x_0)^2}{2\alpha t}} \right]. \tag{3}$$

The density function of the first passage time from $x = x_0$ to $x = 0$ is

$$\begin{aligned} \gamma_{x_0,0}(t) &= \lim_{x \rightarrow 0} \left[\frac{\alpha}{2} \frac{\partial}{\partial x} \phi(x, t; x_0) - \beta \phi(x, t; x_0) \right] = \\ &= \frac{x_0}{\sqrt{2\pi\alpha t^3}} e^{-\frac{(\beta t + 1)^2}{2\alpha t}}. \end{aligned} \tag{4}$$

Suppose that the process starts at $t = 0$ at a point x with density $\psi(x)$ and every time it comes to the barrier it stays there for a time given by a density function $l_0(x)$ and then reappears at $x = 1$. The total stream $\gamma_0(t)$ of probability mass that enters the barrier is

$$\begin{aligned} \gamma_0(t) &= p_0(0)\delta(t) + [1 - p_0(0)]\gamma_{\psi,0}(t) + \\ &\int_0^t g_1(\tau)\gamma_{1,0}(t - \tau)d\tau \end{aligned} \tag{5}$$

where

$$\begin{aligned} \gamma_{\psi,0}(t) &= \int_0^\infty \gamma_{\xi,0}(t)\psi(\xi)d\xi, \\ g_1(\tau) &= \int_0^\tau \gamma_0(t)l_0(\tau - t)dt. \end{aligned}$$

The density function of the diffusion process with instantaneous returns is

$$f(x, t; x_0) = \phi(x, t; \psi) + \int_0^t g_1(\tau)\phi(x, t - \tau; 1)d\tau. \tag{6}$$

For Laplace transforms of these equations we have

$$\begin{aligned} \bar{\gamma}_0(s) &= p_0(0) + [1 - p_0(0)]\bar{\gamma}_{\psi,0}(s) + \bar{g}_1(s)\bar{\gamma}_{1,0}(s), \\ \bar{g}_1(s) &= \bar{\gamma}_0(s)\bar{l}_0(s) \end{aligned} \tag{7}$$

where

$$\bar{\gamma}_{x_0,0}(s) = e^{-x_0 \frac{\beta + A(s)}{\alpha}}, \quad \bar{\gamma}_{\psi,0}(s) = \int_0^\infty \bar{\gamma}_{\xi,0}(s)\psi(\xi)d\xi,$$

and then

$$\bar{g}_1(s) = \left[p_0(0) + [1 - p_0(0)]\bar{\gamma}_{\psi,0}(s) \right] \frac{\bar{l}_0(s)}{1 - \bar{l}_0(s)\bar{\gamma}_{1,0}(s)}. \tag{8}$$

Equation (6) in terms of Laplace transform becomes

$$\bar{f}(x, s; x_0) = \bar{\phi}(x, s; \psi) + \bar{g}_1(s)\bar{\phi}(x, s; 1),$$

where

$$\begin{aligned} \bar{\phi}(x, s; x_0) &= \frac{e^{\frac{\beta(x-x_0)}{\alpha}}}{A(s)} \left[e^{-|x-x_0| \frac{A(s)}{\alpha}} - e^{-|x+x_0| \frac{A(s)}{\alpha}} \right], \\ \bar{\phi}(x, s; \psi) &= \int_0^\infty \bar{\phi}(x, s; \xi)\psi(\xi)d\xi, \quad A(s) = \sqrt{\beta^2 + 2\alpha s}. \end{aligned}$$

The inverse transforms of these functions could only be found numerically. For this purpose we use the Stehfest's algorithm

[28]: for any fixed argument t , the function $f(t)$ is obtained from its transform $\bar{f}(s)$ as

$$f(t) = \frac{\ln 2}{2} \sum_{i=1}^N V_i \bar{f}\left(\frac{\ln 2}{t} i\right), \quad (9)$$

where

$$V_i = (-1)^{N/2+i} \sum_{k=\lfloor \frac{i+1}{2} \rfloor}^{\min(i, N/2)} \frac{k^{N/2+1} (2k)!}{(N/2 - k)! k! (k-1)! (i-k)! (2k-i)!}.$$

N is an even integer and its choice depends on a computer precision; we used $N = 12 - 40$.

The above transient solution of $G/G/1$ model assumes that the parameters of this model are constant. If they are evolving, we should define the time-periods where they can be considered constant and solve diffusion equation within these intervals separately. A transient solution obtained at the end of an interval serves as the initial condition for the next interval.

B. Limited queue: $G/G/1/N$ station, transient solution

In the case of $G/G/1/N$ station, the second barrier should be placed at $x = N$. When the process comes to this barrier, it stays there for a time corresponding to the period when the queue is full and incoming customers are lost and then, after the completion of the current service, the process jumps to $x = N - 1$.

The model equations become [14]

$$\begin{aligned} \frac{\partial f(x, t; x_0)}{\partial t} &= \frac{\alpha}{2} \frac{\partial^2 f(x, t; x_0)}{\partial x^2} - \beta \frac{\partial f(x, t; x_0)}{\partial x} + \\ &\quad + \lambda_0 p_0(t) \delta(x-1) + \lambda_N p_N(t) \delta(x-N+1), \\ \frac{dp_0(t)}{dt} &= \lim_{x \rightarrow 0} \left[\frac{\alpha}{2} \frac{\partial f(x, t; x_0)}{\partial x} - \beta f(x, t; x_0) \right] - \lambda_0 p_0(t), \\ \frac{dp_N(t)}{dt} &= \lim_{x \rightarrow N} \left[-\frac{\alpha}{2} \frac{\partial f(x, t; x_0)}{\partial x} + \beta f(x, t; x_0) \right] - \\ &\quad \lambda_N p_N(t), \end{aligned} \quad (10)$$

where $\delta(x)$ is Dirac delta function.

The density function $f(x, t; x_0)$ is obtained in the similar way as previously. First we obtain the density $\phi(x, t; x_0)$ of the diffusion process with two absorbing barriers at $x = 0$ and $x = N$, started at $t = 0$ from $x = x_0$, cf. [4]

$$\phi(x, t; x_0) = \frac{1}{\sqrt{2\pi\alpha t}} \sum_{n=-\infty}^{\infty} (a_n - b_n)$$

where

$$\begin{aligned} a_n &= \exp \left[\frac{\beta x'_n}{\alpha} - \frac{(x - x_0 - x'_n - \beta t)^2}{2\alpha t} \right] \\ b_n &= \exp \left[\frac{\beta x''_n}{\alpha} - \frac{(x - x_0 - x''_n - \beta t)^2}{2\alpha t} \right] \end{aligned}$$

and $x'_n = 2nN$, $x''_n = -2x_0 - x'_n$.

If the initial condition is defined by a function $\psi(x)$, $x \in (0, N)$, $\lim_{x \rightarrow 0} \psi(x) = \lim_{x \rightarrow N} \psi(x) = 0$, then the pdf of the process has the form $\phi(x, t; \psi) = \int_0^N \phi(x, t; \xi) \psi(\xi) d\xi$.

Then the pdf $f(x, t; \psi)$ of the diffusion process with elementary returns from both barriers is expressed as

$$\begin{aligned} f(x, t; \psi) &= \phi(x, t; \psi) + \int_0^t g_1(\tau) \phi(x, t - \tau; 1) d\tau + \\ &\quad \int_0^t g_{N-1}(\tau) \phi(x, t - \tau; N-1) d\tau. \end{aligned}$$

Densities $\gamma_0(t)$, $\gamma_N(t)$ of the probability that at time t the process enters to $x = 0$ or $x = N$ are

$$\begin{aligned} \gamma_0(t) &= p_0(0) \delta(t) + [1 - p_0(0) - p_N(0)] \gamma_{\psi,0}(t) + \\ &\quad + \int_0^t g_1(\tau) \gamma_{1,0}(t - \tau) d\tau + \\ &\quad + \int_0^t g_{N-1}(\tau) \gamma_{N-1,0}(t - \tau) d\tau, \\ \gamma_N(t) &= p_N(0) \delta(t) + [1 - p_0(0) - p_N(0)] \gamma_{\psi,N}(t) + \\ &\quad + \int_0^t g_1(\tau) \gamma_{1,N}(t - \tau) d\tau + \\ &\quad + \int_0^t g_{N-1}(\tau) \gamma_{N-1,N}(t - \tau) d\tau, \end{aligned}$$

where $\gamma_{1,0}(t)$, $\gamma_{1,N}(t)$, $\gamma_{N-1,0}(t)$, $\gamma_{N-1,N}(t)$ are the densities of the first passage times between corresponding points, e.g.

$$\gamma_{1,0}(t) = \lim_{x \rightarrow 0} \left[\frac{\alpha}{2} \frac{\partial \phi(x, t; 1)}{\partial x} - \beta \phi(x, t; 1) \right]. \quad (11)$$

The functions $\gamma_{\psi,0}(t)$, $\gamma_{\psi,N}(t)$ denote densities of the probabilities that the initial process, started at $t = 0$ at the point ξ with density $\psi(\xi)$, will end at time t by entering respectively $x = 0$ or $x = N$.

Finally, we can express $g_1(t)$ and $g_N(t)$ with the use of functions $\gamma_0(t)$ and $\gamma_N(t)$:

$$\begin{aligned} g_1(\tau) &= \int_0^\tau \gamma_0(t) l_0(\tau - t) dt, \\ g_{N-1}(\tau) &= \int_0^\tau \gamma_N(t) l_N(\tau - t) dt, \end{aligned}$$

where $l_0(x)$, $l_N(x)$ are the densities of sojourn times in $x = 0$ and $x = N$; the distributions of these times are not restricted to exponential ones.

The presented transient solutions tend as $t \rightarrow \infty$ to the known steady-state solutions, given by [14]:

$$f(x) = \begin{cases} \frac{\lambda p_0}{-\beta} (1 - e^{zx}) & \text{for } 0 < x \leq 1, \\ \frac{\lambda p_0}{-\beta} (e^{-z} - 1) e^{zx} & \text{for } 1 \leq x \leq N - 1, \\ \frac{\mu p_N}{-\beta} (e^{z(x-N)} - 1) & \text{for } N - 1 \leq x < N, \end{cases} \quad (12)$$

where $z = \frac{2\beta}{\alpha}$ and p_0, p_N are determined through normalization

$$\begin{aligned} p_0 &= \lim_{t \rightarrow \infty} p_0(t) = \left\{ 1 + \varrho e^{z(N-1)} + \frac{\varrho}{1 - \varrho} [1 - e^{z(N-1)}] \right\}^{-1}, \\ p_N &= \lim_{t \rightarrow \infty} p_N(t) = \varrho p_0 e^{z(N-1)}. \end{aligned}$$

Customer classes. As proposed in [15], the input stream λ can be composed of K classes of customers and $\lambda = \sum_{k=1}^K \lambda^{(k)}$ (all parameters concerning class k have an upper index with brackets) then the joint service time pdf is defined as

$$b(x) = \sum_{k=1}^K \frac{\lambda^{(k)}}{\lambda} b^{(k)}(x),$$

hence

$$\frac{1}{\mu} = \sum_{k=1}^K \frac{\lambda^{(k)}}{\lambda} \frac{1}{\mu^{(k)}},$$

and

$$C_B^2 = \mu^2 \sum_{k=1}^K \frac{\lambda^{(k)}}{\lambda} \frac{1}{\mu^{(k)^2}} (C_B^{(k)^2} + 1) - 1.$$

We assume that the input streams of different class customers are mutually independent, the number of class k customers that arrived within sufficiently long period of time is normally distributed with variance $\lambda^{(k)} C_A^{(k)^2}$; the sum of independent randomly distributed variables also has normal distribution with variance which is the sum of composing variances, hence

$$C_A^2 = \sum_{k=1}^K \frac{\lambda^{(k)}}{\lambda} C_A^{(k)^2}. \quad (13)$$

The above parameters yield α, β of the diffusion equation; function $f(x)$ approximates the distribution $p(n)$ of customers of all classes present in the queue: $p(n) \approx f(n)$ and the probability that there are $n^{(k)}$ customers of class k is

$$\begin{aligned} p_k(n^{(k)}) &= \\ &= \sum_{n=n^{(k)}}^N \left[p(n) \binom{n}{n^{(k)}} \left(\frac{\lambda^{(k)}}{\lambda} \right)^{n^{(k)}} \left(1 - \frac{\lambda^{(k)}}{\lambda} \right)^{n-n^{(k)}} \right], \\ k &= 1, \dots, K. \end{aligned}$$

Numerical examples. We consider a G/G/1/30 queue (in fact, it is M/M/1/30 queue, as we assume $C_A^2 = C_B^2 = 1$). In Example 1 the input rate $\lambda(t)$ is varying in time as presented in Fig. 1. It represents a typical TCP flow with additive increases and multiplicative decreases in the case of packet losses, the range of time is $[0,100]$ time units. In computations, the values of diffusion parameters are changed each 0.5 time unit. Figs. 2 - 5 present the main results of the diffusion model compared with the simulation results (in the latter case it is the average of 500 000 independent runs).

In Figs. 2 and 3 display the same numerical results concerning the values of the mean queue. Fig. 2 displays them in linear scale and Fig. 3 does it in logarithmic scale, to see better the errors of the diffusion approximation: they become visible for very small mean queue values, i.e. less than 0.001 at this model. Next figures present the probability $p(0, t)$ of the empty queue as a function of time, following time-dependent

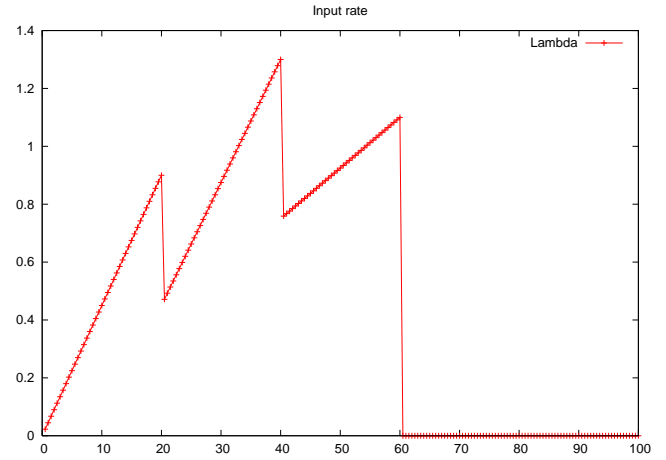


Fig. 1. Example 1: Input traffic intensity $\lambda(t)$.

input, Fig. 4, and the probability $p(N, t)$ that the queue is full, i.e. saturated, and rejects the arriving customers, Fig. 5.

In Example 2 the input rate is periodically varying between values 0.25 and 5. Figs. 6, 7, 8 display the same kind of results as previously: the mean number of customers, the probability of the empty and the probability of the saturated queue as a function of time. All results prove an almost perfect match of diffusion and simulation results. All simulations in the article have been performed with the use of OMNET++ [26].

III. OPEN NETWORK OF G/G/1/N QUEUES

The diffusion steady state model of an open network of G/G/1 or G/G/1/N queues was presented in [15]. Below we present its short summary. Let M be the number of stations, the throughput of station i is, as usual, obtained from traffic equations

$$\lambda_i = \lambda_{0i} + \sum_{j=1}^M \lambda_j r_{ji}, \quad i = 1, \dots, M, \quad (14)$$

where r_{ji} is routing probability between station j and station i ; λ_{0i} is external flow of customers coming from outside of network.

The second moment of interarrival time distribution is obtained from two systems of equations; the first defines C_{Di}^2 , the squared coefficient of variation of interdeparture times distribution at station i , as a function of C_{Ai}^2 and C_{Bi}^2 ; the second defines C_{Aj}^2 as another function of $C_{D1}^2, \dots, C_{DM}^2$:

1) The formula (15) defining the density function $d_i(x)$ of interdeparture times at station i is exact for M/G/1, M/G/1/N stations and is approximate in the case of non-Poisson input [3]

$$d_i(x) = \varrho_i b_x(t) + (1 - \varrho_i) a_i(x) * b_i(x), \quad i = 1, \dots, M, \quad (15)$$

where $*$ denotes the convolution operation. From (15) we get

$$C_{Di}^2 = \varrho_i^2 C_{Bi}^2 + C_{Ai}^2 (1 - \varrho_i) + \varrho_i (1 - \varrho_i). \quad (16)$$

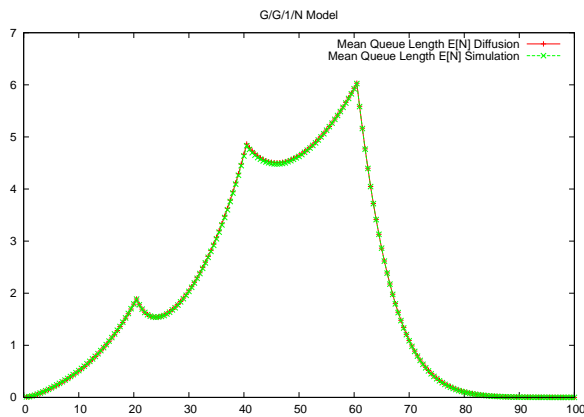


Fig. 2. Example 1: The mean number of customers as a function of time; diffusion approximation and simulation results. .

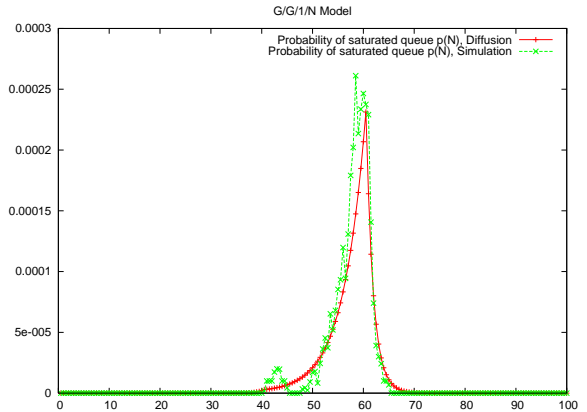


Fig. 5. Example 1: The probability $p(N, t)$ of the saturated queue, diffusion approximation and simulation results.

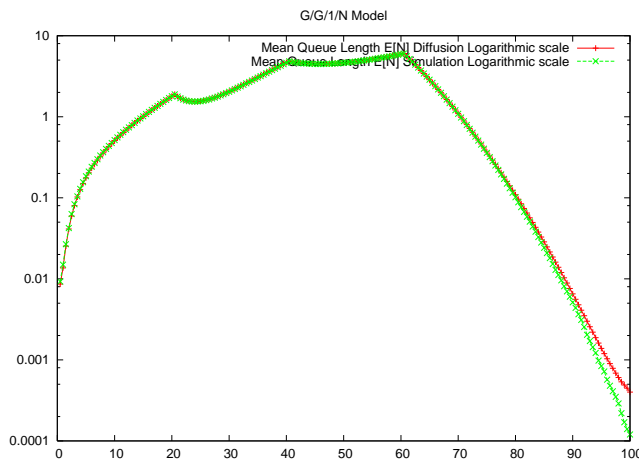


Fig. 3. Example 1: The mean number of customers (logarithmic scale) as a function of time; diffusion approximation and simulation results. .

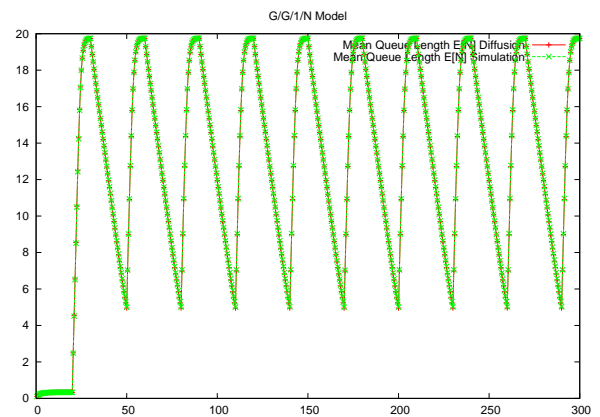


Fig. 6. Example 2: The mean number of customers as a function of time; diffusion approximation and simulation results. .

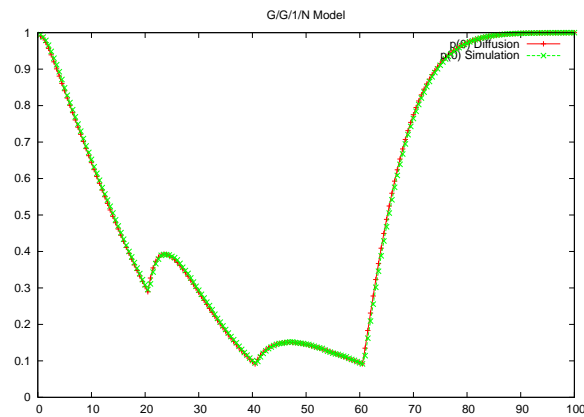


Fig. 4. Example 1: The probability $p(0, t)$ of the empty queue, diffusion approximation and simulation results.

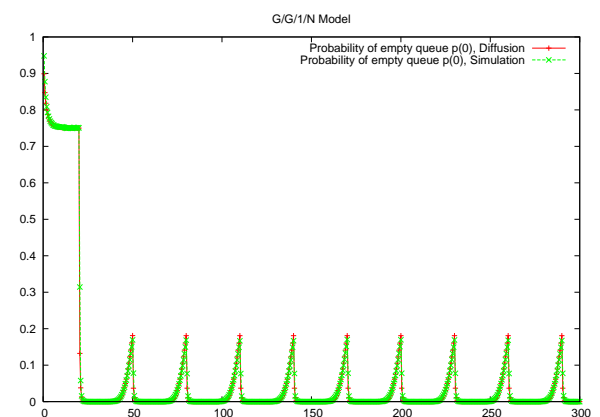


Fig. 7. Example 2: The probability $p(0, t)$ of the empty queue, diffusion approximation and simulation results.

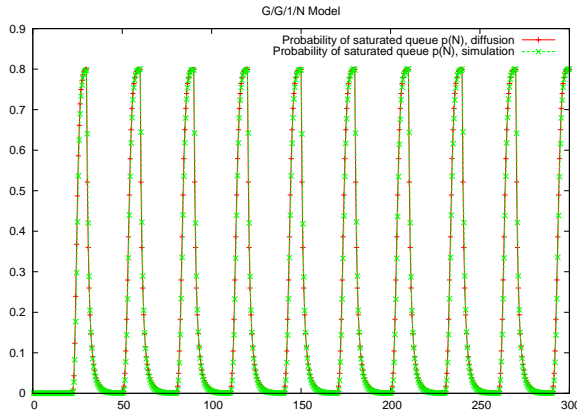


Fig. 8. Example 2: The probability $p(N, t)$ of the saturated queue, diffusion approximation and simulation results.

2) Customers leaving station i choose station j with probability r_{ij} : intervals between customers passing this way have the pdf $d_{ij}(x)$

$$d_{ij}(x) = d_i(x)r_{ij} + d_i(x) * d_i(x)(1 - r_{ij})r_{ij} + d_i(x) * d_i(x) * d_i(x)(1 - r_{ij})^2 r_{ij} + \dots$$

or, after Laplace transform,

$$\bar{d}_{ij}(s) = \bar{d}_i(s)r_{ij} + \bar{d}_i(s)^2(1 - r_{ij})r_{ij} + \bar{d}_i(s)^3(1 - r_{ij})^2 r_{ij} + \dots = \frac{r_{ij}\bar{d}_i(s)}{1 - (1 - r_{ij})\bar{d}_i(s)},$$

hence

$$E[D_{ij}] = \frac{1}{\lambda_i r_{ij}}, \quad C_{D_{ij}}^2 = r_{ij}(C_{D_i}^2 - 1) + 1. \quad (17)$$

$E[D_{ij}]$, $C_{D_{ij}}^2$ refer to interdeparture times; the number of customers passing from station i to j in a time interval t has approximately normal distribution with mean $\lambda_i r_{ij} t$ and variation $C_{D_{ij}}^2 \lambda_i r_{ij} t$. The sum of streams entering station j has normal distribution with mean

$$\lambda_j t = \left[\sum_{i=1}^M \lambda_i r_{ij} + \lambda_{0j} \right] t$$

and variance

$$\sigma_{A_j}^2 t = \left\{ \sum_{i=1}^M C_{D_{ij}}^2 \lambda_i r_{ij} + C_{0j}^2 \lambda_{0j} \right\} t,$$

hence

$$C_{A_j}^2 = \frac{1}{\lambda_j} \sum_{i=1}^M r_{ij} \lambda_i [(C_{D_i}^2 - 1)r_{ij} + 1] + \frac{C_{0j}^2 \lambda_{0j}}{\lambda_j}. \quad (18)$$

Parameters λ_{0j} , C_{0j}^2 represent the external stream of customers.

For K classes of customers with routing probabilities $r_{ij}^{(k)}$ (let us assume for the sake of simplicity that the customers do not change their classes) we have

$$\lambda_i^{(k)} = \lambda_{0i}^{(k)} + \sum_{j=1}^M \lambda_j^{(k)} r_{ji}^{(k)}, \quad i = 1, \dots, M; \quad k = 1, \dots, K, \quad (19)$$

and

$$C_{D_i}^2 = \lambda_i \sum_{k=1}^K \frac{\lambda_i^{(k)}}{\mu_i^{(k)^2} [C_{B_i}^{(k)^2} + 1]} + 2\rho_i(1 - \rho_i) + (C_{A_i}^2 + 1)(1 - \rho_i) - 1. \quad (20)$$

A customer in the stream leaving station i belongs to class k with probability $\lambda_i^{(k)}/\lambda_i$ and we can determine $C_{D_i}^{(k)^2}$ in the similar way as it has been done in Eqs. (17-18), replacing r_{ij} by $\lambda_i^{(k)}/\lambda_i$:

$$C_{D_i}^{(k)^2} = \frac{\lambda_i^{(k)}}{\lambda_i} (C_{D_i}^2 - 1) + 1; \quad (21)$$

then

$$C_{A_j}^2 = \frac{1}{\lambda_j} \sum_{l=1}^K \sum_{k=1}^K r_{lj}^{(k)} \lambda_l \left[\left(\frac{\lambda_l^{(k)}}{\lambda_l} (C_{D_l}^2 - 1) \right) r_{lj}^{(k)} + 1 \right] + \sum_{k=1}^K \frac{C_{0j}^{(k)^2} \lambda_{0j}^{(k)}}{\lambda_j}. \quad (22)$$

Eqs. (16), (18) or (20), (22) form a linear system of equations and allow us to determine $C_{A_i}^2$ and, in consequence, parameters β_i , α_i for each station.

In the case of transient analysis, the time axis is divided into small intervals (equal e.g. to the smallest mean service time) and at the beginning of each interval the Eqs. (14), (16), (18) are used to determine the input parameters of each station based on the values of $\rho_i(t)$ obtained at the end of the precedent interval. A software tool was prepared and the examples below, concerning 2 network topologies, see Fig. 9 a,b, are computed with its use.

Example 3. The network is composed of the source and three stations in tandem, Fig. 9a. The source parameters are: $\lambda = 0.1$ $t \in [0, 10]$, $\lambda = 4.0$ $t \in [10, 20]$. Parameters of all stations are the same: $N_i = 10$, $\mu_i = 2$, $C_{B_i}^2 = 1$, $i = 1, 2, 3$.

Fig. 10a presents mean queue lengths of stations in Model 1 as a function of time. Diffusion approximation is compared with simulation.

Example 4. The network topology is as in Fig. 9b. The characteristics of three sources and of one station are changing with time in the following pattern:

source A: $\lambda_A = 0.1$ for $t \in [0, 10]$, $\lambda_A = 4.0$ for $t \in [10, 21]$, $\lambda_A = 0.1$ for $t \in [21, 40]$,

source B: $\lambda_B = 0.1$ for $t \in [0, 11]$, $\lambda_B = 4.0$ for $t \in [11, 20]$, $\lambda_B = 0.1$ for $t \in [20, 40]$,

source C: $\lambda_C = 0.1$ for $t \in [0, 15]$, $\lambda_C = 2.0$ for $t \in [15, 22]$, $\lambda_C = 4.0$ for $t \in [22, 30]$, $\lambda_C = 2.0$ for $t \in [30, 31]$, $\lambda_C = 0.1$ for $t \in [31, 40]$.

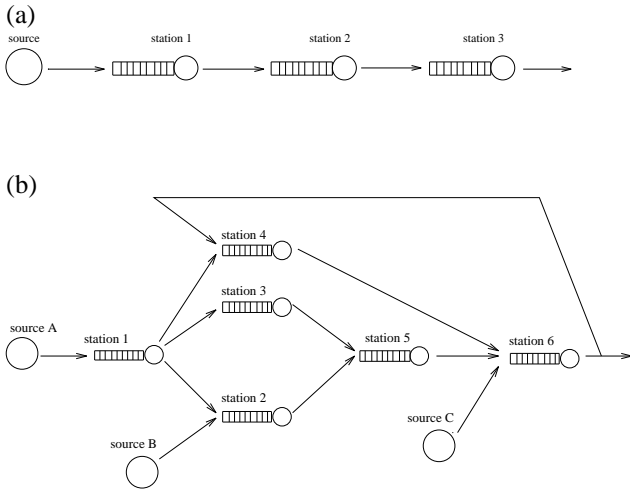


Fig. 9. Example 3 and 4 network topologies

Station 6: $\mu_6 = 2$ for $t \in [10, 15]$ and $t \in [31, 40]$; $\mu_6 = 4$ for $t \in [15, 31]$.

Other parameters are constant: maximum queue lengths $N_1 = N_4 = 10$, $N_3 = 5$, $N_2 = N_6 = 20$, $\mu_1 = \dots = \mu_5 = 2$. Routing probabilities are: $r_{12} = r_{13} = r_{14} = 1/3$, $r_{64} = 0.8$. Initial state: $N_1(0) = 5$, $N_1(0) = 5$, $N_2(0) = 10$, $N_3(0) = 10$, $N_4(0) = 5$, $N_5(0) = 5$, $N_6(0) = 10$. The results in the form of mean queue lengths are presented and compared with simulation in Figs. 10, 11.

We observe that the output of queueing network models is not as good as in the case of single station models, but still reasonable.

IV. DIFFUSION APPROXIMATION OF THE G/G/1 AND G/G/1/N BUSY PERIODS

Busy periods play an important role in the description of priority queues. During a busy period of higher priority customers, the server is not available for lower priorities.

A. G/G/1 station

Let $\Gamma(t)$ and $\gamma(t)$ denote PDF and pdf of the busy period duration; for the M/M/1 system the function $\gamma(t)$ is known explicitly [19]

$$\gamma(t) = \frac{1}{t\sqrt{\rho}} e^{(\lambda+\mu)t} I_1(2t\mu\sqrt{\rho})$$

where $I_1(x) = \sum_{k=0}^{\infty} \frac{1}{k!(k+1)!} \left(\frac{x}{2}\right)^{2k}$ is the modified Bessel function of the first kind and of order one. For M/G/1 system, a functional equation,

$$\bar{\gamma}(s) = \bar{B}(s + \lambda + \lambda\bar{\gamma}(s))$$

where $\bar{\gamma}(s) = \int_0^{\infty} e^{-st}\gamma(t)dt$, $\bar{B}(s) = \int_0^{\infty} e^{-st}b(t)dt$ are the Laplace transforms of $\gamma(t)$, $b(t)$, although impossible to invert in most cases, enables us to compute the moments of $\gamma(t)$, e.g.

$$E[\gamma] = -\frac{d}{ds}\bar{\gamma}(s)_{s=0} = \frac{1/\mu}{1-\rho} \quad (23)$$

$$E[\gamma^2] = \frac{d^2}{ds^2}\bar{\gamma}(s)_{s=0} = \frac{E[b^2]}{(1-\rho)^3} \quad (24)$$

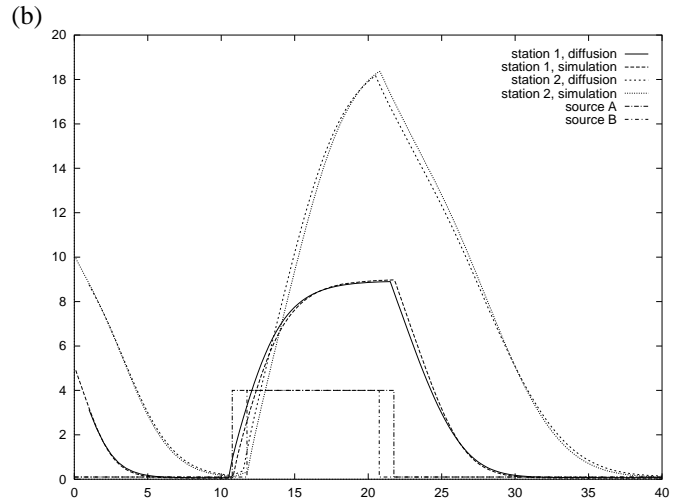
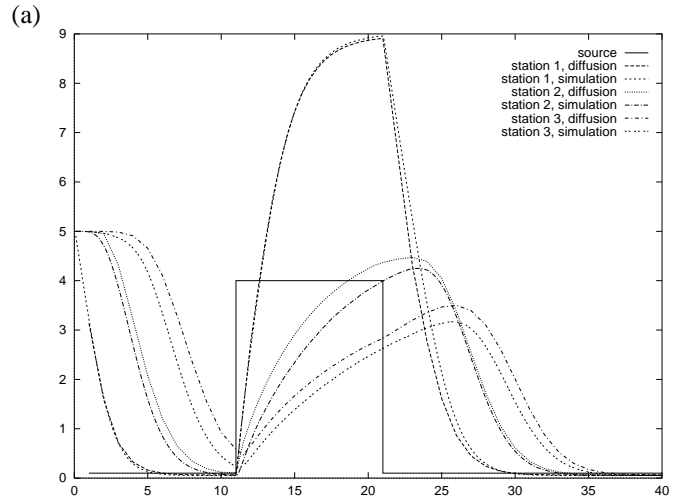


Fig. 10. (a) Example 3: The mean queue lengths of station1, station2 and station3 as a function of time — diffusion and simulation (100 000 repetitions) results; the source intensity $\lambda(t)$ is indicated. (b) Example 4: The mean queue lengths of station1 and station2 as a function of time — diffusion and simulation (100 000 repetitions) results; the source intensities $\lambda_A(t)$, $\lambda_B(t)$ are indicated.

The expression

$$\Gamma(t) = \int_0^t \sum_{n=1}^{\infty} e^{-\lambda t} \frac{(\lambda t)^{n-1}}{n!} b^{*n}(t) dt$$

where $b^{*n}(t)$ is the n -fold convolution of $b(t)$ with itself, could be helpful in numerical evaluation of the busy time distribution for the M/G/1 queue [19]. We know virtually nothing about $\Gamma(t)$, $\gamma(t)$ for the G/G/1 system. In the diffusion approximation, the busy period has a simple interpretation. In the case of G/G/1 system, it is just the first passage time from $x = 1$ to the absorbing barrier at $x = 0$, its pdf is given by Eq. (4) that yields

$$E[\gamma_{dif}] = \frac{1}{-\beta}, \quad E[\gamma_{dif}^2] = -\frac{\alpha}{\beta^3} + \frac{1}{\beta^2}$$

which are exact results in the case of M/M/1 and M/G/1 systems.

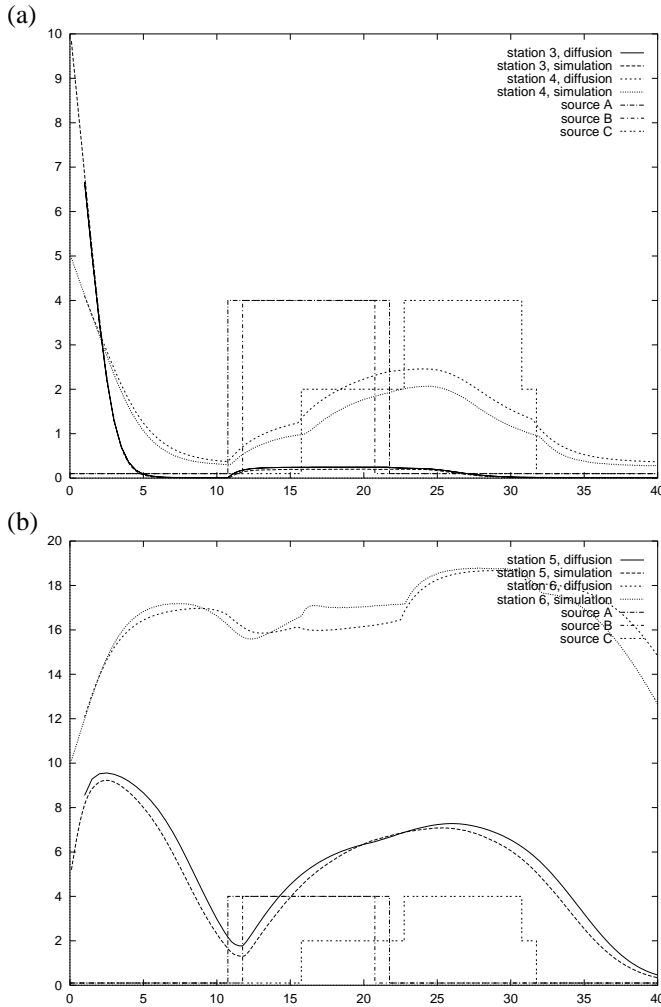


Fig. 11. Example 4: The mean queue lengths of station3 and station4 (a) and of station5 and station6 (b)

B. Busy period at G/G/1/N

As the process starting at $x = 1$ may visit the barrier at $x = N$ an unlimited number of times before coming to $x = 0$, the density function of the busy period is, preserving the previously used notation

$$\gamma(t) = \gamma_{1,0}(t) + \gamma_{1,N}(t) * l_N(t) * \gamma_{N-1,0}(t) + \gamma_{1,N}(t) * l_N(t) * \gamma_{N-1,N}(t) * l_N(t) * \gamma_{N-1,0}(t) + \dots \quad (25)$$

where * denotes the convolution operator, or

$$\begin{aligned} \bar{\gamma}(s) &= \bar{\gamma}_{1,0}(s) + \bar{\gamma}_{1,N}(s)l_N(s)\bar{\gamma}_{N-1,0}(s) + \\ &+ \bar{\gamma}_{1,N}(s)\bar{l}_N(s)\bar{\gamma}_{N-1,N}(s)\bar{l}_N(s)\bar{\gamma}_{N-1,0}(s) + \dots \\ &= \bar{\gamma}_{1,0}(s) + \frac{\bar{\gamma}_{1,N}(s)l_N(s)\bar{\gamma}_{N-1,0}(s)}{1 - \bar{\gamma}_{1,N}(s)l_N(s)}. \end{aligned} \quad (26)$$

Fig. 12 presents the comparison of busy period pdf given by diffusion approximation and simulation.

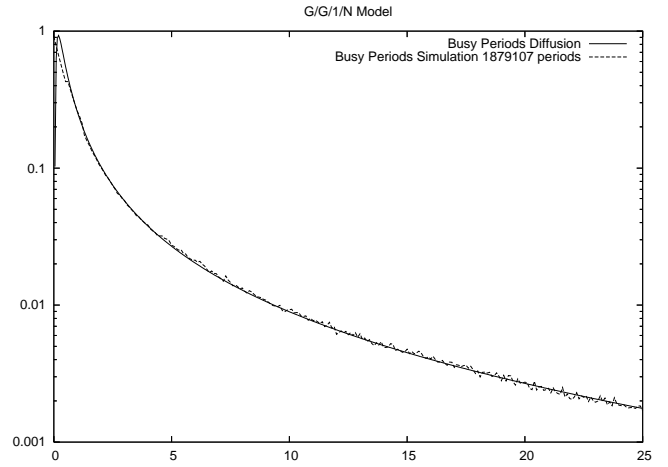


Fig. 12. M/M/1/20 queue, $\rho = 0.75$, busy period diffusion approximation compared with simulation (histogram of over 1.8 million samples).

V. DIFFUSION APPROXIMATION OF PREEMPTIVE - RESUME PRIORITY SYSTEM

This paragraph introduces a diffusion model of a single server with priority preemptive - resume queuing discipline. Customers arriving to the system are divided into a certain number, say K , of classes. Each class is distinguished by its index k , $k = 1, \dots, K$, and has its own priority. The lower the number of the index, the higher the priority of the class. When a customer of class k is being served and a customer of class l , $l < k$ arrives, the current service is suspended and the service of the newcomer begins. After the completion of this service and the service of other, more privileged than class k customers, who have arrived meanwhile, the interrupted service is resumed at the point of suspension. Customers of the same priority class are served in the order of arrival. The presence of lower class customers is transparent to customers of a given class. We assume that interarrival times in the particular stream are characterized by parameters $\lambda^{(k)}$, $\sigma_A^{(k)^2}$ having the same meaning as λ , σ_A^2 in the case of one-class system. The service time of customers of class k has mean value $1/\mu^{(k)}$ and variance $\sigma_B^{(k)^2}$.

Following exactly the same procedure as for the FIFO system, we define: input process $E^{(K)}(t)$ as the total number of customers of all K classes who arrived to the system during the time period $[0, t]$, and the output process $H^{(K)}(t)$ as the number of customers of all K classes who left the system in $[0, t]$. Applying the central limit theorem and using the same arguments as for the first-come-first-served discipline, we can prove that these processes have approximately normal distributions if the period $[0, t]$ is sufficiently long and within a busy period of the server. The input process $E^{(K)}(t)$ consists of separate input processes $\varepsilon^{(k)}(t)$ for each class of customers:

$$E^{(K)}(t) = \sum_{k=1}^K \varepsilon^{(k)}(t)$$

The output process $H^{(K)}(t)$ can be described as

$$\begin{aligned} H^{(K)}(t) &= \sum_{k=1}^K \eta^{(k)}(t) \frac{\varrho^{(k)}}{1 - R^{(k-1)}} (1 - R^{(k-1)}) \frac{1}{R^{(k)}} \\ &= \sum_{k=1}^K \frac{\varrho^{(k)}}{R^{(k)}} \eta^{(k)}(t) \end{aligned} \quad (27)$$

where $\eta^{(k)}(t)$ is the output process for the k -priority stream in the absence of other classes, $R^{(k)} = \sum_{l=1}^{(k)} \varrho^{(l)}$ and $\varrho^{(l)} = \lambda^{(l)} / \mu^{(l)}$. $R^{(k)}$ denotes the probability that the busy period for customers of classes 1, ..., k taken altogether is in progress, $\frac{\varrho^{(k)}}{1 - R^{(k)}}$ denotes the probability that a customer of class k is present in the system. Class k has the $1 - R^{(k-1)}$ part of the server time at its disposal. $1 - R^{(k-1)}$ denotes the probability that there are no customers of priority higher than k present in the system. The total number of customers of classes 1, ..., K present in the system

$$N^{(K)}(t) = E^{(K)}(t) - H^{(K)}(t)$$

is changing and its changes during the time period $[0, t]$ have the mean $\beta^{(K)}t$ and the variance $\alpha^{(K)}t$,

$$\begin{aligned} \beta^{(K)} &= \sum_{k=1}^K \lambda^{(k)} - \sum_{k=1}^K \frac{\varrho^{(k)}}{R^{(k)}} \mu^{(k)}, \\ \alpha^{(K)} &= \sum_{k=1}^K \lambda^{(k)} C_A^{(k)2} + \sum_{k=1}^K \frac{\varrho^{(k)}}{R^{(k)}} \mu^{(k)} C_B^{(k)2}, \\ C_A^{(k)2} &= \lambda^{(k)2} \sigma_A^{(k)2}, \quad C_B^{(k)2} = \mu^{(k)2} \sigma_B^{(k)2} \end{aligned}$$

and are approximately normally distributed. We replace the discrete-state process $N^{(K)}(t)$ by the continuous-state process $X^{(K)}(t)$ whose infinitesimal changes have normal distribution with the mean $\beta^K dt$ and the variance $\alpha^K dt$. Solving the diffusion equation with the same type of boundary conditions as defined earlier with the intensity of jumps from $x = 0$: $\Lambda^{(K)} = \sum_{k=1}^K \lambda^{(k)}$ we obtain the density function $f^{(K)}(x, t; x_0)$ for all classes considered together.

Let $v^{(K)}(n)$ denote the probability that n customers of class K are present in the system and $p^{(K-1)}(N - n)$ denote the probability that $N - n$ customers of all other classes are present in the system. Obviously,

$$p^{(K)}(N) = \sum_{n=0}^N p^{(K-1)}(N - n) v^{(K)}(n)$$

and similarly,

$$p^{(k)}(n) = \sum_{\nu=0}^n p^{(k-1)}(n - \nu) v^{(k)}(\nu), \quad k = 2, \dots, K$$

or

$$v^k(n) = \frac{p^{(k)}(n) - \sum_{\nu=0}^{n-1} p^{(k-1)}(n - \nu) v^{(k)}(\nu)}{p^{(k-1)}(0)}, \quad k = 2, \dots, K.$$

For the highest priority class

$$v^{(1)}(n) = p^{(1)}(n).$$

Thus, we know the distribution $v^k(n)$, the mean number of customers present in the system

$$E[n^{(k)}] = \sum_{\nu=0}^{\infty} v^{(k)}(\nu) \nu$$

and, by Little's result, the mean time they spend in the system

$$E[T^{(k)}] = \frac{E[n^{(k)}]}{\lambda^{(k)}} \quad k = 1, \dots, K$$

for each class of customers.

The inconvenience of this approach is the propagation of errors of the method. An alternative approach is to study the diffusion processes corresponding to the number of each class customers separately and to see the influence of higher classes on the queues of lower classes through the probability that the system is occupied by higher classes and thus is not able to serve the lower ones.

For example, if we take two classes, the first diffusion process corresponding to the priority class has parameters $\beta^{(1)} = \lambda^{(1)} - \mu^{(1)}$ and $\alpha^{(1)} = \sigma_A^{(1)2} \lambda^{(1)3} + \sigma_B^{(1)2} \mu^{(1)3}$ and the second one, corresponding to the lower class which is served only in absence of the higher class, has the parameters

$$\begin{aligned} \beta^{(2)} &= \lambda^{(2)} - \mu^{(2)} p^{(1)}(0, t) \\ \alpha^{(2)} &= \sigma_A^{(2)2} \lambda^{(2)3} + \sigma_A^{(2)2} \lambda^{(2)3} + \sigma_B^{(2)2} \mu^{(2)3} p^{(1)}(0, t) + \\ &\quad + \sigma_B^{(1)2} \mu^{(1)3}. \end{aligned}$$

Before the waiting time can be considered, we have to define the distribution of the completion time. The completion time is the time period between the beginning and the end of the service of any customer. On the highest priority level the completion time is equal to the service time, for the other classes it additionally includes the breaks caused by the service of more privileged customers. Let T be the service time of a customer of class k . If n customers of classes 1, ..., $k - 1$ arrive during the time T , the service will be interrupted n times, n has approximately normal distribution with the mean $\Lambda^{(k-1)}$ and the variance $\sum_{l=1}^{k-1} \lambda^{(l)} C_A^{(l)2} T$.

The duration of any of n breaks is distributed like the busy period $\gamma^{(k-1)}$ of the system serving customers of classes 1, ..., $k - 1$. The total time of breaks in T has the pdf

$$\varphi^{(k)}(t | T) = \sum_{n=0}^{\infty} p_{n|T} \gamma^{(k-1)(*n)}(t)$$

where $p_{n|T}$ is the probability of n breaks in T , $\gamma^{(k-1)(*n)}(t)$ is the n -fold convolution of $\gamma^{(k-1)}(t)$ with itself. Thus the pdf $c^{(k)}(t)$ of the completion time is

$$c^{(k)}(t) = \int_0^{\infty} b^{(k)}(t) \varphi^{(k)}(t - T | T) \mathbf{1}(t - T) dT,$$

where $\mathbf{1}(t) = 0$ for $t < 0$ and $\mathbf{1}(t) = 1$ for $t \geq 0$, and from its Laplace transform

$$c^{(k)}(s) = \int_0^{\infty} b^{(k)}(T) e^{-sT} \sum_{n=0}^{\infty} \{p_{n|T} [\bar{\gamma}^{(k)}(s)]^n\} dT$$

we obtain its moments $E = [c^{(k)}]$ and $E[(c^{(k)})^2]$:

$$E = [c^{(k)}] = -\frac{d}{ds}c^{(k)}(s)_{s=0} = \{E[\gamma^{(k-1)}]\Lambda^{(k-1)} + 1\} \frac{1}{\mu^{(k)}},$$

$$E[(c^{(k)})^2] = \frac{d^2}{ds^2}c^{(k)}(s)_{s=0} =$$

$$= E[\gamma^{(k-1)}]^2 \left[\left(\sum_{l=1}^{(k-1)} \lambda^{(l)} C_A^{(l)2} \right) \frac{1}{\mu^{(k)}} + \right.$$

$$\left. - \Lambda^{(k-1)} \frac{1}{\mu^{(k)}} \right] + E[(\gamma^{(k-1)})^2] \Lambda^{(k-1)} \frac{1}{\mu^{(k)}} +$$

$$+ E[\gamma^{(k-1)}] E[(b^{(k)})^2] \Lambda^{(k)} \cdot$$

$$\cdot \{E[\gamma^{(k-1)}] \Lambda^{(k-1)} + 2\} + E[(b^{(k)})^2].$$

When all input streams are Poisson, i.e. $C_A^{(l)2} = 1, l = 1, \dots, k$ the results are identical to the exact formula given for this case in [18]. Finally, we can define the mean waiting time for every priority level as

$$E[w^{(k)}] = \frac{E[n^{(k)}]}{\lambda^{(k)}} - E[c^{(k)}].$$

If we intend to consider a network of servers, we are obliged to determine the output stream of each server. In the case of priority queues we extend the approach used previously for a network of G/G/1/N stations, see Eqs. (16), (18) or (20), (22).

Let us denote $d^{(k)}(t)$ the pdf of interdeparture times in the stream of class k customers, it can be expressed as

$$d^{(k)}(t) = \frac{\varrho^{(k)}}{1 - R^{(k-1)}} c^{(k)}(t) + \left(1 - \frac{\varrho^{(k)}}{1 - R^{(k-1)}} \right)$$

$$\times [(1 - R^{(k-1)}) a^{(k)}(t) * c^{(k)}(t)$$

$$+ R^{(k-1)} a^{(k)}(t) * \gamma^{(k-1)}(t) * c^{(k)}(t)]. \quad (28)$$

The components of this expression correspond to three situations, possible after the departure of any customer of class k :

- the next customer of the class k is in the system (it occurs with probability $\frac{\varrho^{(k)}}{1 - R^{(k-1)}}$) and will leave it after its completion time,
- there are no customers of this class in the system and we shall wait the time described by $a^{(k)}(t)$, the interarrival time pdf (when the input is non-Poisson it is merely an approximation) until it appears and enters the server,
- no customer of class k is present in the system and a customer of higher class comes before him, so the busy period $\gamma^{(k-1)}$ must be terminated first.

The mean interdeparture time is obviously the same as the mean interarrival time and from the above (28), where in turn the densities of busy periods at each priority level are given by expressions of the type (25) and their moments are obtained from (26), we calculate the squared coefficient of the variation of interdeparture times at each priority customers, needed to integrate a single priority station into a network of such stations. The final formula is as follows:

$$C_D^{(k)2} = \sum_{l=1}^k h^{(k,l)} C_A^{(l)2} + \psi^{(k)} \quad (29)$$

where

$$h^{(k,l)} = \begin{cases} \left(\zeta^{(k,l)} + \frac{1 - R^{(k)}}{1 - R^{(k-1)}} R^{(k-1)} g^{(k-1,l)} \right) (\lambda^{(k)})^2, & l < k, \\ \frac{1 - R^{(k)}}{1 - R^{(k-1)}}, & l = k, \end{cases}$$

and

$$\zeta^{(k,l)} = \frac{\lambda^{(l)}}{\mu^{(k)} (\beta^{(k-1)})^2} + g^{(k-1,l)} \frac{\Lambda^{(k-1)}}{\mu^{(k)}},$$

$$g^{(k,l)} = \frac{1}{(\beta^{(k)})^3},$$

$$\psi^{(k)} = \chi^{(k)} (\lambda^{(k)})^2 + \frac{1 - R^{(k)}}{1 - R^{(k-1)}} \left\{ 1 + R^{(k-1)} e^{(k-1)} (\lambda^{(k)})^2 \right.$$

$$+ 2\varrho^{(k)} \left(1 - \frac{\Lambda^{(k-1)}}{\beta^{(k-1)}} \right) +$$

$$\left. - \frac{\lambda^{(k)} R^{(k-1)}}{\beta^{(k-1)}} \left[1 + 2\varrho^{(k)} \left(1 - \frac{\Lambda^{(k-1)}}{\beta^{(k-1)}} \right) \right] \right\} - 1,$$

$$\chi^{(k)} = \frac{C_B^{(k)2} + 1}{(\mu^{(k)})^2} \frac{\Lambda^{(k-1)}}{\beta^{(k-1)}} \left(\frac{\Lambda^{(k-1)}}{\beta^{(k-1)}} - 2 \right) -$$

$$\frac{\Lambda^{(k-1)}}{(\beta^{(k-1)})^2 \mu^{(k)}} + e^{(k-1)} \frac{\Lambda^{(k)}}{\mu^{(k)}} \frac{C_B^{(k)2} + 1}{(\mu^{(k)})^2},$$

$$e^{(k)} = \frac{1}{(\beta^{(k)})^2} - \frac{1}{(\beta^{(k)})^3} \sum_{l=1}^k \frac{\varrho^{(l)}}{R^{(k)}} \mu^{(l)} C_B^{(l)2}.$$

The equation (29) corresponds to (16): it defines how the variation of the interdeparture times of the class- k customers depends on the variations of the interarrival times of all classes that may influence the output of this class. The parameters of service time distributions are hidden in the coefficients of the equation. Similarly, the extension of the equation (18) defining the squared coefficient of variation of interarrival times in the flow of class- l customers coming to station j has the following form

$$C_{A_j}^{(l)2} = \frac{1}{\lambda_j^{(l)}} \sum_{i=1}^M \sum_{k=1}^K r_{ij}^{(kl)} \lambda_i^{(k)} [(C_{D_i}^{(k)2} - 1) r_{ij}^{(kl)} + 1] + \frac{C_{0j}^{(l)2} \lambda_{0j}^{(l)}}{\lambda_j^{(l)}}, \quad (30)$$

where $r_{ij}^{(kl)}$ is the probability that a class- k customer leaving station i goes directly to station j having there class- l priority. Equations (29) and (30) taken together determine the input flow parameters for each class and each station, allowing us to analyze each station separately. As usual, in the case of transient states, all parameters should be considered constant at small intervals and all model equations should be solved for these parameters to define conditions at the beginning of the next interval.

Numerical examples Consider a server with two priority levels. In Example 5, the priority customers come with intensity $\lambda^{(1)} = 0.4$ during intervals $t \in [0, 10], [20, 30], [40, 50]$, etc. Otherwise $\lambda^{(1)} = 0$. The intensity of non-priority customers is constant, $\lambda^{(2)} = 0.4$. In Example 6 the server utilization is higher and the bursts of priority input stream are longer, $\lambda^{(1)} = 1.2$ during intervals $t \in [0, 20], [40, 60], [80, 100]$,

and $\lambda^{(1)} = 0$ between these intervals while the second class intensity is constant, $\lambda^{(2)} = 0.5$.

The queue capacities are in both cases limited: $N^{(1)} = N^{(2)} = 20$. To validate the diffusion model by the comparison of its results with the exact ones obtained with Markov chain model solved numerically, we assume Poisson input streams and exponential service time distributions for both types of customers, $\mu^{(1)} = \mu^{(2)} = 1$. Figs. 13, 14 refer to the Example 5. Fig. 13 displays the mean number of customers of each class as a function of time, given by diffusion model and by the corresponding Markov model. Fig. 14 compares the total number of customers of both classes.

Figs. 15, 16 give the same results for the Example 6.

Of course, diffusion approximation gives not only the mean values but also the queue distributions; e.g. Fig. 17 presents, for Example 5, exact and estimated probabilities $p^{(1)}(0, t)$, $p^{(2)}(0, t)$ that the queues of class 1 or class 2 are empty. Fig. 18 presents for Example 6 exact and estimated probabilities $p^{(1)}(N^{(1)}, t)$, $p^{(2)}(N^{(2)}, t)$ that the queues of class 1 or class 2 are saturated. For all computations we considered constant parameters inside subintervals of the 0.1 time unit length. In all cases the errors observed for priority queues are smaller than for non-priority ones. It is natural, the errors of the second class queue accumulate the errors of both classes.

VI. CONCLUSIONS

The article presents an adaptation of the diffusion approximation model with absorbing barriers to the analysis of transient states of queueing models. The method was applied previously to G/G/1/N service stations, here we also present the case of preemptive-resume priority queues.

In the article, we demonstrate how the diffusion approximation formalism is applied to study transient and behavior of G/G/1 and G/G/1/N non-priority and preemptive-priority models. The way we switch from one model to another demonstrates the flexibility of the method. Also the preemptive discipline can be easily converted to non-preemptive queueing discipline. Also the introduction of self-similar traffic is possible: as we change the diffusion parameters each small time-interval, we can modulate them to reflect self-similarity and long-term correlation of the traffic. Some other applications may be considered: recently we have used the diffusion approximation to estimate transfer times inside a sensor network [9], to model the performance of leaky-bucket algorithm as well as to study the work of call centers [10], and to investigate the stability of TCP connections with IP routers having AQM queues [8]. In the first case the diffusion process reflects the distance defined as the number of hops between the transmitted packet and its destination (sink). Owing to the introduction of the transient state analysis, the model captures more parameters (time-dependent and heterogeneous transmission, the presence of losses specific to each hop) of a sensor network transmission time than the already existing models of this type, also based on the diffusion approximation [16]. It also gives more detailed results: the density function of a packet travel time instead of its mean value. In the second

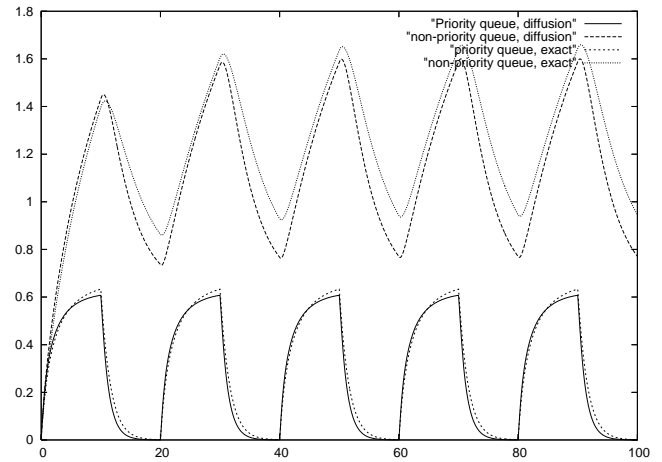


Fig. 13. Example 5: Mean number of customers as a function of time for the first and second priority levels, diffusion approximation and exact results

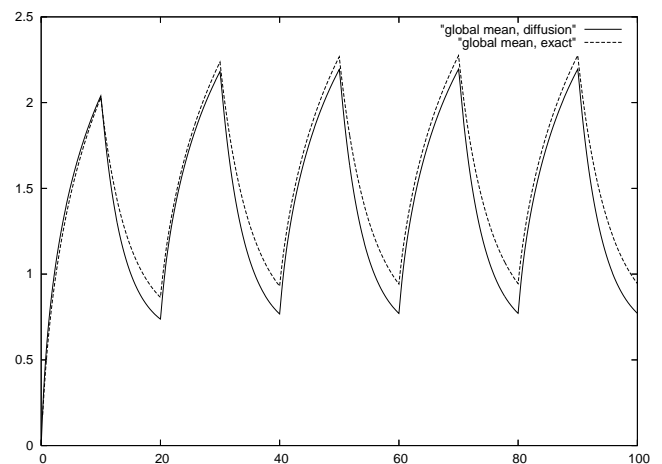


Fig. 14. Example 5: Global mean number of customers as a function of time, diffusion approximation and exact results.

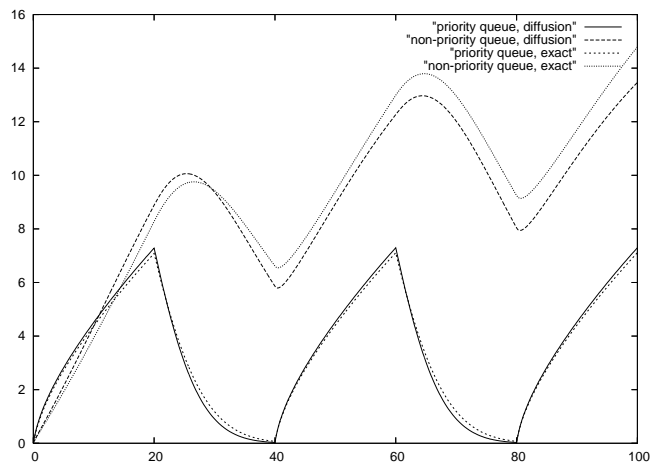


Fig. 15. Example 6: The mean number of customers as a function of time for the first and second priority levels, diffusion approximation and exact results.

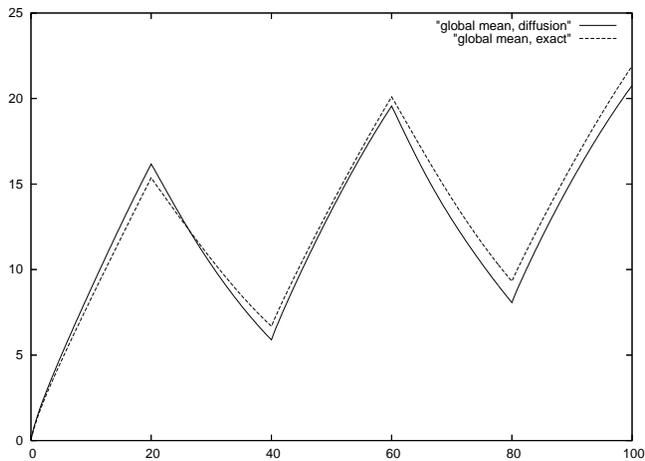


Fig. 16. Example 6: Global mean number of customers as a function of time, diffusion approximation and exact results.

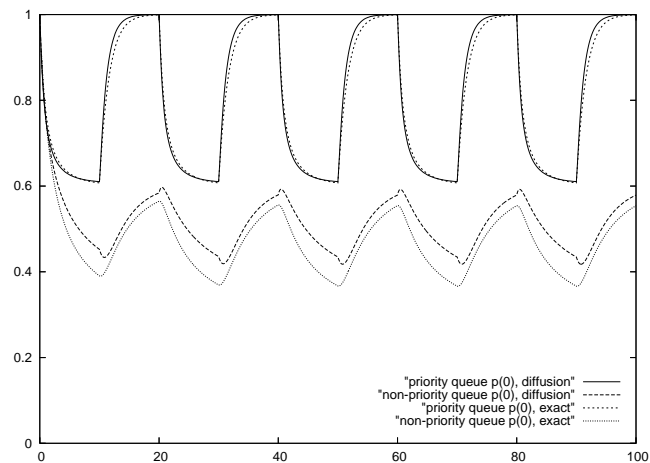


Fig. 17. Example 5: Probabilities $p^{(1)}(0, t)$, $p^{(2)}(0, t)$ that the queues of class 1 or class 2 are empty, diffusion approximation and exact results.

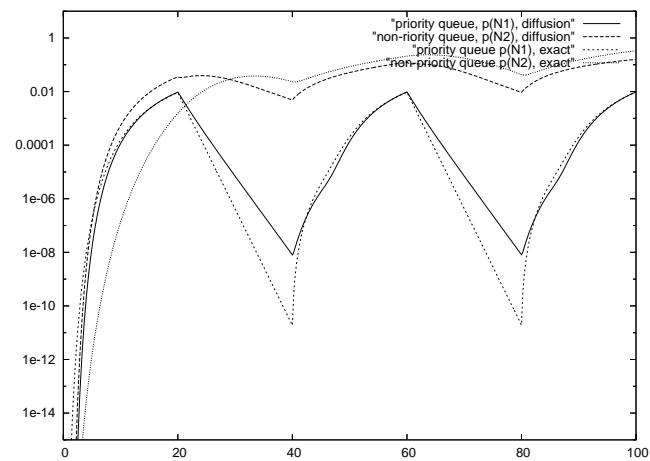


Fig. 18. Example 6: Probabilities $p^{(1)}(N^{(1)}, t)$, $p^{(2)}(N^{(2)}, t)$ that the queues of class 1 or class 2 are saturated, diffusion approximation and exact results. Logarithmic scale is chosen for better presentation of very small probabilities.

case, the introduction of state-dependent diffusion coefficients enables us to study transient states of parallel stations of G/G/N/N type. The third position proposes a diffusion model of a queue with RED (Random Early Detection) mechanism and considers the dynamics of TCP connections having RED queue in the congested router. Also the application of diffusion approximation to model wireless networks based on IEEE 802.11 standard gives promising results, [12].

Numerical examples, where the quantitative results of diffusion approximations are compared with simulations or the numerical solutions of corresponding Markov chain models, indicate acceptable level of errors of the proposed approach.

Of course, there are several ways we can analyze transient states in queueing models. In recent years we have put a considerable effort to master their use as efficient tools that give sound numerical results. Each of them has its advantages and disadvantages. Firstly, we can use simulation models. In this purpose we have developed an extension of OMNET++ (a popular simulation tool written in C++, [26]) allowing the simulation of transient state models. In particular, random generators were modified to make the changes of their parameters as a function of time possible, a new software was added to collect the statistics of multiple runs and to aggregate it. We used this module to validate the diffusion approximation results. Basically, the simulation run in a transient state investigation should be repeated sufficient number of times (e.g. 500 000 in our examples) and the results for a fixed time should be averaged. As the number of repetitions is high, the estimation of errors is easy (confidence interval) on the basis of normal distribution. However, the number of repetitions is related to the value of the investigated probabilities and in the case of rare events should be high and it increases the simulation time (typically in some of our examples, 5 minutes of computations for a diffusion model are compared to 24 hours of simulations, on a standard PC station).

The other way to model transient states is to create a Markov chain model and to solve it numerically. This approach, also combined with the use of stochastic Petri nets, gained already a considerable attention of researches, e.g. [13], [30], [27] and a number of software tools, e.g. SHARP, PEPSY, SNMP, MOSES [2] or XMARCA [20] was implemented. The numerical problems of solving very large systems of equations related to Markov models were thoroughly studied, e.g. [21]. This effort concerned mainly steady-state models. For several years we have developed a software to construct and to solve very large (having millions of states) Markov chains relating to queueing models and we have adopted suitable numerical methods and distributed algorithms. In the case of transient states, the implementation is based on the reduction of state space due to Arnoldi's orthogonal projection into the Krylov subspace [29]. We have also used Markov model to evaluate the errors in the case of the priority model presented here. Naturally, the usability of the approach depends on the size of the considered model, and it is relatively easy to go beyond the limit number, i.e. some tens of millions, of tractable states. We are still working on more powerful Markovian modules using

distributed algorithms and run on a cluster architecture.

Another well-known approach of modeling is the fluid-flow approximation where only the mean values of traffic intensity and service intensity are considered. Compared to the diffusion approximation, the model is simple: instead of partial differential equations of second order, the ordinary first-order linear differential equations are used. Due to its simplicity, it gained much interest in the analysis of transient states in Internet and in investigation of stability of its connections, e.g. [24]. However, as we tested in [7], the errors of the fluid-flow approximation in modeling queues dynamics are considerably larger than in the case of diffusion approximation which is a second-order approximation, where not only the mean values but also the variances of flow changes and of service times are considered.

Therefore we consider the diffusion approximation as a very convenient tool in the analysis of transient states queueing models in performance evaluation of computer and communication networks.

VII. ACKNOWLEDGEMENTS

This research was partially financed by the Polish Ministry of Science and Education grant N517 025 31/2997. The Authors thank the Referees for their valuable remarks.

REFERENCES

- [1] T. Atmaca, T. Czachórski, F. Pekergin, "A Diffusion Model of the Dynamic Effects of Closed-Loop Feedback Control Mechanisms in ATM Networks", 3rd IFIP Workshop on Performance Modelling and Evaluation of ATM Networks, Ilkley, UK, 4-7th July 1995.
- [2] G. Bolch, S. Greiner, H. de Meer, K. S. Trivedi, "Queueing networks and Markov chains: modeling and performance evaluation with computer science applications", Wiley-Interscience, New York, 1998.
- [3] P.J. Burke, The Output of a Queueing System, Operations Research, vol. 4, no. 6, pp. 699-704.
- [4] R. P. Cox, H. D. Miller, The Theory of Stochastic Processes, Chapman and Hall, London (1965).
- [5] T. Czachórski, "A method to solve diffusion equation with instantaneous return processes acting as boundary conditions", Bulletin of Polish Academy of Sciences, Technical Sciences vol. 41 (1993), no. 4.
- [6] T. Czachórski, F. Pekergin, "Transient diffusion analysis of cell losses and ATM multiplexer behaviour under correlated traffic", 5th IFIP Workshop on Performance Modelling and Evaluation of ATM Networks, Ilkley, UK, 21-23 July 1997.
- [7] T. Czachórski, J. M. Fourneau, F. Pekergin, "The Dynamics of Cell Flow and Cell Losses in ATM Networks Modelled by a Diffusion Process", Bulletin of Polish Academy of Sciences, Technical Sciences vol. 43, no. 4, pp. 538-548, 1995.
- [8] T. Czachórski, K. Grochla, F. Pekergin, "Stability and Dynamics of TCP-NCR(DCR) Protocol", LNCS no. 4396, Wireless Systems and Mobility in Next Generation Internet, Springer-Verlag 2007.
- [9] T. Czachórski, K. Grochla, F. Pekergin, "Un modèle d'approximation de diffusion pour la distribution du temps d'acheminement des paquets dans les réseaux de senseurs" Proc. of CFIP'2008, Les Arcs, 25-28 mars 2008, proceedings, edition électronique <http://hal.archives-ouvertes.fr/CFIP2008>.
- [10] T. Czachórski, J.-M. Fourneau, T. Nycz, F. Pekergin, "Diffusion approximation model of multiserver stations with losses", Proc. of Third International Workshop on Practical Applications of Stochastic Modelling PASM'2008, Palma de Mallorca, 23rd September 2008, to appear also as an issue of Elsevier's ENTCS (Electronic Notes in Theoretical Computer Science).
- [11] T. Czachórski, T. Nycz, F. Pekergin, "Transient states of priority queues – a diffusion approximation study", Proc. of The Fifth Advanced International Conference on Telecommunications AICT 2009 May 24-28, 2009 - Venice/Mestre, Italy.
- [12] T. Czachórski, K. Grochla, T. Nycz, F. Pekergin, "A diffusion approximation model for wireless networks based on IEEE 802.11 standard" submitted to COMCOM Special Journal Issue on Heterogeneous Networks: Traffic Engineering and Performance Evaluation of Computer Communications.
- [13] J. B. Dugan, K. S. Trivedi, R. Geist, V. F. Nicola, "Extended Stochastic Petri Nets: Applications and Analysis", in: E. Gelenbe(Hrsg.), Performance, North-Holland, 1984.
- [14] E. Gelenbe, "On Approximate Computer Systems Models", J. ACM, vol. 22, no. 2, (1975).
- [15] E. Gelenbe, G. Pujolle, "The Behaviour of a Single Queue in a General Queueing Network", Acta Informatica, Vol. 7, Fasc. 2, pp.123-136, 1976.
- [16] E. Gelenbe, "Travel delay in a large wireless ad hoc network", 2nd Workshop on Spatial Stochastic Models of Wireless Networks (SPASWIN), Boston, 7th April (2006).
- [17] D. Iglehart, "Weak Convergence in Queueing Theory", Advances in Applied Probability, vol. 5, pp. 570-594, 1973.
- [18] K. N. Jaiswal, Priority Queues, Academic Press, New York 1968.
- [19] L. Kleinrock, "Queueing Systems", vol. I: Theory, vol. II: Computer Applications, Wiley, New York 1975, 1976.
- [20] R. L. Klevans, W. J. Stewart, From queueing networks to Markov chains: the XMARCA interface", Performance Evaluation, vol. 24, no. 1-2, pp. 23-46, 1995.
- [21] W. Knottenbelt, "Distributed task-based solution techniques for large Markov models", Proc. of NSMC '99 Zaragoza, Spain, 1999.
- [22] H. Kobayashi, "Modeling and Analysis: An Introduction to System Performance Evaluation Methodology", Addison Wesley, Reading, Massachusetts 1978.
- [23] S. S. Lavenberg, "Computer Performance Modeling Handbook", Academic Press, New York 1983.
- [24] V. Misra, W.-B. Gong, D. Towsley: Fluid-based Analysis of a Network of AQM Routers Supporting TCP Flows with an Application to RED, ACM SIGCOMM 2000.
- [25] G. F. Newell, Applications of Queueing Theory, Chapman and Hall, London 1971.
- [26] OMNET++ Community Site www.omnetpp.org.
- [27] R. A. Sahner, K. S. Trivedi, A. Puliafito, "Performance and Reliability Analysis of Computer Systems: An Example-Based Approach Using the Sharpe Software Package", Kluwer 1996.
- [28] H. Stehfest, "Algorithm 368: Numeric inversion of Laplace transform", Comm. of ACM, vol. 13, no. 1, p. 47-49 (1970).
- [29] W. Stewart, Introduction to the Numerical Solution of Markov Chains, Princeton University Press, Chichester, West Sussex 1994.
- [30] K. S. Trivedi, A. Puliafito, D. Logothetis, "From Stochastic Petri Nets to Markov Regenerative Stochastic Petri Nets", in: P. W. Dowd (Hrsg.), E. Gelenbe, (Hrsg.): Proc. of MASCOTS, IEEE Computer Society, 1995.



www.iariajournals.org

International Journal On Advances in Intelligent Systems

✦ ICAS, ACHI, ICCGI, UBICOMM, ADVCOMP, CENTRIC, GEOProcessing, SEMAPRO, BIOSYSCOM, BIOINFO, BIOTECHNO, FUTURE COMPUTING, SERVICE COMPUTATION, COGNITIVE, ADAPTIVE, CONTENT, PATTERNS

✦ issn: 1942-2679

International Journal On Advances in Internet Technology

✦ ICDS, ICIW, CTRQ, UBICOMM, ICSNC, AFIN, INTERNET, AP2PS, EMERGING

✦ issn: 1942-2652

International Journal On Advances in Life Sciences

✦ eTELEMED, eKNOW, eL&mL, BIODIV, BIOENVIRONMENT, BIOGREEN, BIOSYSCOM, BIOINFO, BIOTECHNO

✦ issn: 1942-2660

International Journal On Advances in Networks and Services

✦ ICN, ICNS, ICIW, ICWMC, SENSORCOMM, MESH, CENTRIC, MMEDIA, SERVICE COMPUTATION

✦ issn: 1942-2644

International Journal On Advances in Security

✦ ICQNM, SECURWARE, MESH, DEPEND, INTERNET, CYBERLAWS

✦ issn: 1942-2636

International Journal On Advances in Software

✦ ICSEA, ICCGI, ADVCOMP, GEOProcessing, DBKDA, INTENSIVE, VALID, SIMUL, FUTURE COMPUTING, SERVICE COMPUTATION, COGNITIVE, ADAPTIVE, CONTENT, PATTERNS

✦ issn: 1942-2628

International Journal On Advances in Systems and Measurements

✦ ICQNM, ICONS, ICIMP, SENSORCOMM, CENICS, VALID, SIMUL

✦ issn: 1942-261x

International Journal On Advances in Telecommunications

✦ AICT, ICDT, ICWMC, ICSNC, CTRQ, SPACOMM, MMEDIA

✦ issn: 1942-2601